Università degli Studi della Basilicata

Dottorato di Ricerca in

"INGEGNERIA PER L'INNOVAZIONE E LO SVILUPPO SOSTENIBILE"

TITOLO DELLA TESI

"Tecniche ed approcci alternativi per il miglioramento delle prestazioni sismiche di tamponature in laterizio"

_____

"Alternative techniques and approaches for improving the seismic performance of masonry infills"

Settore Scientifico-Disciplinare

"ICAR-09"

Coordinatore del Dottorato

Prof.ssa Aurelia **SOLE**

Tutor

Prof. Ing. Donatello **CARDONE**

Dottorando

Dott. Ing. **VIGGIANI** Luciano Rocco Salvatore

Ciclo **XXXV**

"Una delle più grandi scoperte che un uomo può fare, una delle sue grandi soprese, è scoprire che può fare ciò che temeva di non poter fare"

Henry Ford

A Sabrina,
il mio porto sicuro,
per il suo amore ed il suo costante supporto.

TABLE OF CONTENTS

LIST OF FIGURES

LIST OF TABLES

AKNOWLWGDMENTS

I would like to express my gratitude to my supervisor, Prof. Donatello Cardone, whose expertise, understanding, and patience, added considerably to my graduate experience. I appreciate his vast knowledge and skill in many areas, and his constant assistance in writing papers, reports and this thesis.

I would also like to acknowledge to ReLuis consortium: second part of this work was developed within the activities of the ReLuis-DPC 2019-2021 research program, funded by the Italian Dept. of Civil Protection.

A very special thanks goes out to Prof. Christoph Butenweg and his research team from RWTH Aachen University (Aachen, Germany), whose contributed to the development of the third phase of the work.

I am grateful to my colleagues Amedeo Flora, Nadia Conte, Gianluca Auletta, Alessio Telesca and Vito Possidente for the fruitful discussions, and for their genuine encouragement.

A very special thanks goes to Giuseppe Gesualdi and Giuseppe Perrone for their technical and human support.

Also thanks to "cumma" Mariangela for her moral support.

Finally, I would like to thank my family for everything they have done for me. First to my parents, Michele e Margherita, who made sure I always had everything I ever needed.

Most of all, I wish to thank my wife Sabrina for giving me the strength and inspiration. Your love, patience, and continuous support gives me the power to always go further in life. Thank you very much for your understanding, for all the beautiful moments we shared and most importantly, for your love.

In conclusion, I recognize that this research would not have been possible without the financial assistance of University of Basilicata - School of Engineering and Region of Basilicata and I express my gratitude to these agencies.

DISCLAIMER

Part of the content of this thesis has been already published on research journals, as reported in the list below.

1. Gesualdi, G., ***Viggiani, L.R.S***. & Cardone, D. Seismic performance of RC frame buildings accounting for the out-of-plane behavior of masonry infills. *Bull Earthquake Eng* **18**, 5343–5381 (2020). https://doi.org/10.1007/s10518-020-00904-1
2. Donatello Cardone, Amedeo Flora, Giuseppe Perrone, ***Luciano R.S. Viggiani*** (2021) Risk-Target-Based Design of Base-Isolated Buildings, Book Reliability-Based Analysis and Design of Structures and Infrastructure Chapter 13 - CRC Press DOI https://doi.org/10.1201/9781003194613
3. F. Micozzi, A. Flora, ***L.R.S. Viggiani***, D. Cardone, L. Ragni & A. Dall'Asta (2022) Risk Assessment of Reinforced Concrete Buildings with Rubber Isolation Systems Designed by the Italian Seismic Code, Journal of Earthquake Engineering, 26:14, 7245-7275, DOI: 10.1080/13632469.2021.1961937
4. D. Cardone, ***L.R.S. Viggiani***, G. Perrone, A. Telesca, A. Di Cesare, F.C. Ponzo, L. Ragni, F. Micozzi, A. Dall'Asta, M. Furinghetti & A. Pavese (2022) Modelling and Seismic Response Analysis of Existing Italian Residential RC Buildings Retrofitted by Seismic Isolation, Journal of Earthquake Engineering, DOI: 10.1080/13632469.2022.2036271
5. I. Iervolino, R. Baraschino, A. Belleri, D. Cardone, G. Della Corte, P. Franchin, S. Lagomarsino, G. Magliulo, A. Marchi, A. Penna, ***L. R.S. Viggiani*** and A. Zona (2021). Seismic fragility of Italian code conforming buildings by multi-stripe dynamic analysis of three-dimensional structural models. Journal of Earthquake Engineering
6. Cardone D., ***Viggiani L.R.S***., Milijaš A., Šakić B., Marinković M., Butenweg C. (2022) Seismic Perfomance of Rc Frame Buildings with Decoupled Infills. Journal of Building Engineering *(submitted)*

ABSTRACT

This doctoral dissertation aims to report on the research work carried out in the field of alternative techniques and approaches for improving the seismic performance of masonry infills.

An aspect often overlooked in the design and/or verification of Reinforced Concrete (RC) frame buildings it is the one related to the so-called "non-structural" elements, that are elements without a main structural function, but capable of causing damage to things and people during the seismic action. A typical example of non-structural elements are the external infills of RC frame buildings, which often have masses and stiffnesses able to significantly modify the behavior and response of the structure during the seismic action. Typically, the UnReinforced Masonry (URM) infill walls are made of single or double facing hollow bricks placed inside the meshes of RC frames. The main damage mechanisms observed in URM infill walls during seismic events include in the plane (IP) or out of the plane (OOP) damage mechanisms, both characterized by degradation of strength, stiffness and low energy dissipation.

In this doctoral dissertation, the analysis of the influence of the in-plane and out-of-plane behavior of UnReinforced Masonry infill walls on global seismic performances of different RC frame buildings is presented. The research mainly focuses on: i) numerical investigation of the in- plane / out-of-plane interaction in order to evaluate its entity and severity pointing out the correct description of the damage scenarios; ii) identification of alternative intervention solutions, aimed at mitigating the phenomenon of overturning of the infill panels; iii) estimate of the expected economic losses.

Rough cost-benefit analyses have been carried out in order to compare the sustainability of alternative seismic rehabilitation techniques, thus providing a rational base and objective criteria that can be used in the design and/or preliminary screening phase by insurance companies, to reduce the seismic risk and the impact of earthquakes on a community.

.

APPENDIX

APD = Average Percentage of Damage

BF= Bare Frame

CLS = Collapse prevention Limit State

CMS = Conditional Mean Spectra

D/C = Demand/Capacity

DLS = Damage Limit State

FC = Fragility Curves

FPS = Friction Pendulum Sliders

FSB = Flat Sliding Bearings

GC = Global Collapse

GLD = Gravity Load Design buildings

GMPE = Ground-motion prediction equation

HDRB = High Damping Rubber Bearings

HSD = High Seismic Design buildings

IDR = Intersorey Drift Ratio

IF= Infilled Frame

IF-I = Infilled Frame with decoupled infills

IM = Intensity Measures

IML = Intensity Measures Level

INGV = Italian Institute of Geophysics and Vulcanology

INODIS = Innovative Decoupled Infill System

IP = In-Plane

LLS = Life-safety Limit State

LS = Life Safety

LSD = Low Seismic Design buildings

MD = Modern standard Design buildings

MNS = Multi Normal Spring

NR(IP) = Not-Repairable IP damage

NTC = Norme Tecniche per le Costruzioni (CS.LL.PP., 2008, 2018)

NTHA = Non - Linear Time History Analysis

NTHA = Non-Linear Time History Analysis

OLS = Operability Limit State

OOP = Out-Of-Plane

PL = Performance Level

POA = Push-Over Analysis

RC = Reinforced Concrete

RINTC = Rischio Implicito delle strutture progettate secondo le NTC

SDOF = Single Degree Of Freedom

SLE = serviceability limit states

SLU = ultimate limit states

SSD = Substandard Design buildings

Tr = Return Period

UPD = Usability Preventing Damage

URM infills = UnReinforced Masonry infills

ZL = zero-length

INTRODUCTION

Masonry infills can have contrasting effects on the seismic response of RC structures; a regular distribution of infill walls in the frame provides an extra stiffness and strength to the structure during an earthquake, reduce the global displacement demand and increase the energy dissipation capacity. However, the stiffness increase leads to the increase of the seismic demand on the structure. Conversely, an irregular distribution in plan and/or elevation of the infills leads to a strongly irregular structure, consequently more susceptible to damage and even to collapse.

In most modern design guidelines, infills are considered non-structural elements; for this reason, they are often excluded from computational models in current professional practice. Furthermore, a further complication concerns the complexity of including them in numeral models. However, neglecting the infill walls in the non-linear analysis of building structures leads to a considerable inaccuracy in predicting the lateral stiffness, strength and ductility of the structures, as well as a significant underestimation of the level of damage expected after the earthquake and of the seismic demand.

Indeed, in many recent earthquakes, infill walls have usually been the first elements to be damaged. Most of the damage is observed on the infill walls due to failure mechanisms caused by the sequential or combined in- and out-of-plane loading. Additionally, RC elements can be significantly damaged due to frame-infill interaction. All of this can cause high economic losses or even lead to human deaths and casualties.

The aim of this research is to compare technical alternatives and approaches to improve the seismic performance of URM infill walls in realistic RC frame structures by monitoring the development of cracks and collapses induced by the combination of In-Plane (IP) and Out-Of-Plane (OOP) actions.

The first step is related to the study of the state of the art concerning the out-of-plane behavior of URM infills and the IP/OOP interaction. Next, a macro-element, able to capture the IP stiffness and strength reduction due to the OOP displacement demand (and vice-versa) is implemented. The model is calibrated with experimental results already available relevant to brick infill walls which are frequent in Italian construction. This preliminary study allowed to confirm the importance of correctly modeling the non-structural elements, in order to correctly evaluate the seismic response of infilled buildings.

After having identified the complexity and importance of the topic, two different strategies were then examined in detail: (i) the seismic base isolation system and (ii) an innovative typology of infills, equipped with a decoupling system.

Among the different structural types required by the codes, in the recent years, an increasing interest has been showed for isolated structures, especially after the destructive seismic events occurring in Italy. In fact, base isolation is one of the most common and effective techniques used for seismic protection of buildings and their equipment.

Currently the isolation device (industrial) production is dominated by two main typologies: high damping elastomeric bearings (HDRBs) and friction pendulum sliders (FPSs). Recently, the use of hybrid systems obtained by combining elastomeric devices (HDRBs) and flat surface sliders (FSBs), is increasing. As a matter of fact, the aforesaid configuration is able to guarantee a suitable deformability of the isolation system without compromising the restoring capability and torsional stiffness of the system and prevent uplift phenomena in the sliding bearings.

An alternative technique to base-isolation system that can successfully reduce the seismic damage in masonry infill walls is the use of decoupled infills such as those based on the innovative INODIS system. This system is made of soft elastomeric material to decouple masonry infills from the surrounding RC frame. It is designed to delay the activation of masonry infills under in-plane loading and to withstand the OOP loads at the same time. The effectiveness of the INODIS system have been already investigated through full-scale experimental tests on 1-storey 1-bay infilled frames. In this work the first investigation to confirm the effectiveness of the INODIS system on a building level is carried out.

The thesis is organized in 4 sections, outlining the main steps of the research.

Section 1 serves as an overview on the scientific literature relevant to this study and as a general framework of Out-Of-Plane behaviour of masonry infills. The most relevant computational modelling proposals are reported, focusing on the macro-modelling approaches. The main objective of this section is to investigate the seismic performance of RC frame buildings accounting for the interaction between IP and OOP behavior of masonry infills. To this end, a suitable nonlinear model, able to capture the IP stiffness and strength reduction due to the OOP displacement demand (and vice-versa) is implemented. The selected model incorporates a routine that removes infills from the structural model when either IP or OOP collapse occurs. Different building models, representative of typical residential buildings, realized in Italy (and

other European countries) from '50s to '90s, are examined through Nonlinear response-Time History Analysis (NTHA) at different earthquake intensity levels, with return period ranging from 30 to 5000 years. Two alternative infill configurations (single layer and double layer with inner cavity) are considered, in accordance with the construction practice of the time.

The comparison between the models with and without IP/OOP interaction points out the relevance of the OOP behavior towards an accurate evaluation of the seismic performance of RC frame buildings. A set of fragility curves is proposed, for different building performance levels, ranging from immediate occupancy to life safety.

Section 2 is dedicated to seismic performance of masonry infills in base isolated buildings.

The present section was developed within the DPC/RELUIS 2019-2021 project (available at http://www.reluis.it) regarding the "implicit risk" (RINTC) assessment of existing RC frame buildings seismically retrofitted by base isolation. The RINTC project is a large research project aimed at assessing the seismic structural reliability, expressed in terms of annual failure rate, of code-conforming and pre-code structures in Italy.

This section describes the nonlinear analyses carried out on existing RC buildings retrofitted using the seismic isolation technique. Different performance levels ranging from immediate occupancy to collapse prevention conditions have been examined. In particular, in this study, the isolation system adopted at the base level of the selected case study buildings is a hybrid isolation system composed by High Damping Rubber Bearings (HDRBs) and Flat Sliding Bearings (FSBs). Six archetype residential RC buildings, differing for construction period (50s-60s, 70s, 80s-90s) and design approach have been considered. Three of them were designed for gravity loads only (GLD buildings, located in Naples) and the other three were seismically designed based on old technical standards (SLD buildings, located in L'Aquila)

All the isolation systems have been designed to avoid any damage of the superstructure up to the Life Safety limit State, in accordance with the current Italian Seismic Code. One of the most advanced numerical models currently available for the description of the nonlinear cyclic behaviour of HDRBs (namely the Kikuchi Bearing element implemented in OpenSees) has been used in the analyses, due to its capability of simulating the behaviour of HDRBs under large displacements and high axial loads. The model parameters have been calibrated against experimental results of an extensive experimental investigation. The macro-model implemented for masonry infill walls is even more refined than the one proposed in the previous section; in this study, in fact, the local effects of masonry infills on the surrounding frame have

been also considered. As known, the lateral force transmitted by the infill to the top of adjacent RC columns may trigger premature brittle shear failure of such structural elements. This is particularly relevant for older RC frame buildings, designed for gravity loads only or featuring substandard seismic details.

Two different performance levels are examined, namely: Global collapse prevention and Usability preventing damage. Seismic performance is assessed by multi-stripe nonlinear time-history analysis, considering earthquake intensity levels with return period ranging from 10 to 100000 years. Results point out that seismic isolation works effectively in limiting damage well beyond the design limit state level while it shows a limited margin with respect to collapse beyond the design limit state level.

Section 3 relates to investigation of seismic performance of RC frame building, where the infills are decoupled using the INODIS system. In order to compare the behaviour of traditional double-layer infills with the behaviour of modern single-layer infills with the INODIS system, numerical simulations are performed with Opensees. One of the six buildings presented in the previous section (SLD 80-90 located in L'Aquila) is used as a case-study. The IP and OOP behaviour of the decoupled infills with INODIS system is modelled by fitting available experimental and numerical results. Modal, pushover and NTHA analyses were carried out considering three different earthquake intensity levels, with return periods equal to 50, 500 and 2500 years. A total of 20 pairs of bidirectional records are selected for each seismic intensity. Results of NTHA show that the INODIS system can successfully prevent dangerous OOP failure modes caused by the IP-OOP interaction. The application of the INODIS system significantly improves the seismic performance of masonry infilled RC frame buildings. The reduced damage to non-structural elements leads to the smaller need for the wall repairment after the earthquakes, which shows the high economic benefits when using cost-efficient INODIS system.

Section 4, serves as a general summary of the study, it derives preliminary conclusions and presents recommendations for future research work. In particular, a comparison (for a specific case-study building) is carried out in terms of performance and economic losses using (i) traditional infills in a fixed-based building, (ii) traditional infills in a base isolated building and (iii) innovative infills with decoupling system.

SECTION 1:
OUT OF PLANE BEHAVIOR OF MASONRY INFILLS

1.1. INTRODUCTION

UnReinforced Masonry (URM) infills are widely used in Reinforced Concrete (RC) frame buildings as internal partitions and exterior enclosure walls, because of their reliability against fire and moisture, good thermal and acoustic insulation, and low construction costs.

Typical configurations of URM walls include single or double layers of hollow clay bricks inserted in, and rigidly connected to, the RC frame. URM infills are usually considered as non-structural elements and are then neglected in the seismic design of the building. However, the presence of URM infills can significantly modify the global seismic response of the buildings, inducing both positive and negative effects (Fardis and Panagiotakos 1997). In principle, a regular distribution of the URM infills can considerably increases the peak strength and initial lateral stiffness of the structure (Dolšek and Fajfar 2008). Masonry infills can also increase the energy dissipation capacity of RC buildings, thus reducing the displacement demand imposed by the earthquake (Ozkaynak et al. 2013). On the other hand, infill walls can strongly interact with the surrounding RC frame, triggering the brittle shear failure of RC columns, thus strongly affecting the overall performance of the RC building (Furtado et al. 2015a).

Generally speaking, masonry infills feature two different brittle failure mechanisms, in the following referred to as In-Plane (IP) (see Figure 1a)and Out-Of-Plane (OOP) (see Figure 1b) collapse mechanism, both characterized by degradation of strength, stiffness and low energy dissipation (El-Dakhakhni et al. 2003).

In recent years, several strong earthquakes have repeatedly pointed out the high vulnerability of URM infills (Braga et al. 2011, Vincente et al. 2012, Varum et al. 2018), especially of those realized between ‘50s and ‘70s, featuring two thin layers (high height/thickness ratio) of hollow clay bricks with an inner cavity.

The damage scenario typically observed for masonry infills after strong earthquakes includes extensive diagonal cracking, corner crushing (De Luca et al 2014), and sometimes the overturning of entire infill walls, usually located at the low-to-middle storeys of the building (Ricci et al 2011, Masi et al. 2019). As argued by Morandi et al (2013), the OOP collapse of the infill walls located at the low-to-middle storeys of the building indicates that they underwent a significant reduction of their out-of-plane resistance (compared to the infill walls at the upper storeys) due to the larger interstory drift demand previously sustained.

(a) (b)

Figure 1 Infill masonry walls earthquake damage in L'Aquila: a) in-plane diagonal cracking, b) out-of-plane collapse (Furtado et al. (2016), Marinković (2019))

Extensive damage to masonry infills can jeopardize the usability of a building after an earthquake with obvious important socio-economic consequences (Braga et al. 2011, Taghavi and Miranda 2002), including large economic losses for building repairing (Cardone and Perrone 2017). Moreover, the OOP collapse of URM walls might seriously threaten human life either inside or outside the building.

In current practice, the safety verification of OOP collapse mechanisms of infill walls is carried out following force-based pseudostatic approaches. A number of recommendations and semi-empirical relationships are proposed in modern seismic codes (FEMA306 1998, CEN 2005, NZSEE 2006) for the estimation of the OOP strength of URM infills, which in some cases also take into account the OOP strength reduction due to previous IP damage.

For all the above reasons, in these last decades, efforts have been made to develop analytical tools and computational models able to describe the seismic behavior of masonry infills and

their interaction with RC frames. Micro-models and macro-models are the two alternative modeling strategies investigated by various authors (see Asteris et al. 2013 for a comprehensive state-of-the-art on this subject). Despite their accuracy, the use of micro-models is very complex, requiring long computational efforts and time, being based on non-linear finite elements modeling both RC frame, infill panels and the interface between RC frame and infill wall. Macro-models are much simpler than micro-models. Indeed, they are implemented through single- or multiple mono-dimensional elements described by a limited number of numerical parameters that can be calibrated from experimental results (Lam et al. 2003), in order to simulate the overall force–displacement behavior of the infill with low computational efforts.

The development of macro-models for the description of the in-plane behavior of URM infills took place before and independently with respect to the development of analytical models for the out of plane behavior of infills.

Based on experimental tests carried out by Polyakov (1960), Holmes (1961) and Stafford-Smith (1962) first proposed a simple and low time-consuming macro-model, based on the assumption of an equivalent "strut", for the simulation of the IP behavior of masonry infills subjected to seismic loading. In particular, Polyakov (1960) described experiments performed on a three-bay, three-storey model steel frame infilled with masonry. Further on, Holmes (1961 and 1963), showed test results of steel frames with concrete infills, while observations of the tests carried out by Stafford Smith (1962 and 1966) led to the conclusion that, the wall could be replaced by an equivalent diagonal "strut".

Mainstone (1971) derived a semi-empirical equation for the calculation of the equivalent strut width. Subsequently, many authors proposed further improvements and developments to the equivalent strut model, in order to simulate the overall inelastic response under monotonic and cyclic loading (Mehrabi and Shing 1997; El-Dakhakhni et al. 2003; Panagiotakos and Fardis 1996), considering different IP failure mechanisms that may occur in masonry infills (Decanini et al. 2004; Sassun et al. 2016).

Generally speaking, according to El-Dakhakhni et al. 2003, the behaviour of masonry infills for in-plane loads can be described by four failure modes of infill panel: compression failure in the corners (i) or in the middle of the infill (ii), shear failure in the middle of the wall along a mortar joint (iii) and diagonal tensile failure (iv).

Some of these specifications have been also included in international guidelines and standards for the seismic analysis and rehabilitation of buildings (FEMA 274 1997; CEN 2005).

The equivalent diagonal strut approach can model the global force-displacement behaviour of the infilled frame, but model of the infill wall with just one single strut element is not capable of properly taking into account the change in the bending moment and shear diagram along the column length due to the presence of the panel and therefore it is ineffective in modelling the complex behaviour of infilled frames.

To overpass this limit, in the last years, a series of multi-strut models (see Figure 2), differing in the number and layout of diagonal struts, have been proposed (Crisafulli and Carr 2007; Smyrou et al. 2011) to capture the in-plane interaction between masonry infills and RC frame.

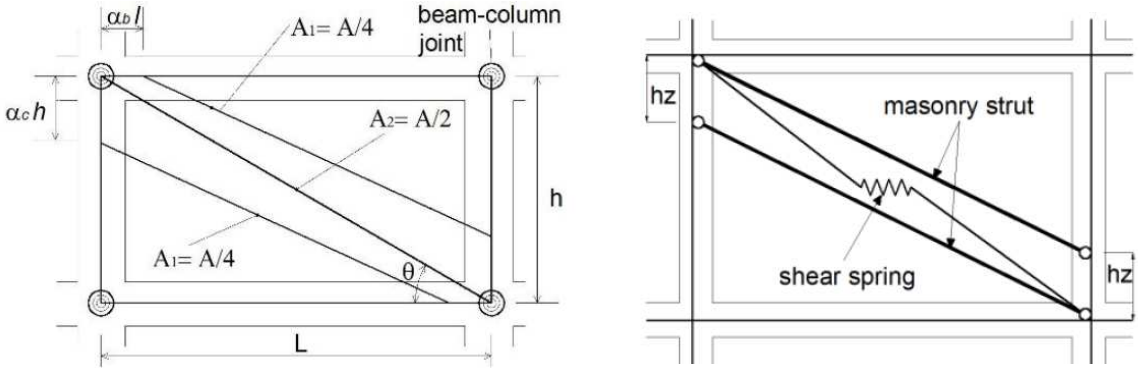

(a) (b)

Figure 2 Multi strut models: (a) El-Dakhakhni et al. 2003; (b) Crisafulli and Carr 2007

Crisafulli and Carr (2007) proposed a modified model presented as a four-node panel element that is connected to the frame at the beam-column joints. This panel element contains internally the model from Crisafulli (1997) (Figure 2b), which has two parallel struts and a shear spring in each direction. The limit of the model is that it is not able to properly predict the bending moment and shear forces in the surrounding frame.

The model proposed by El-Dakhakhni et al. (2003), with the off-diagonal struts not parallel (Figure 2a), was aimed at simulating the experimental results of the tests obtained by them. The total area of the diagonal strut is divided into three parts, where off diagonal struts have one quarter of the area and the middle strut was taken to have one half of the area.

A number of analytical models dealing with the OOP strength of URM infills also exist. They have been derived from past experimental studies carried out by various researchers. McDowell

et al. (1956), for instance, examined an analytical model to predict the maximum uniformly distributed load pattern considering a one-way arch mechanism (see Figure 3).

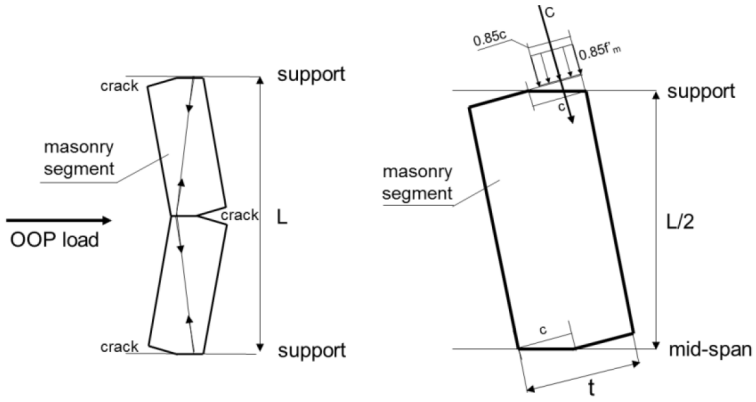

Figure 3 One-way arching action according to McDowell et al. (1956)

Bashandy et al. (1995) (Figure 4a) and Dawe and Seah (1989) (Figure 4b) extended the approach proposed by McDowell et al. (1956) following the principle of virtual works, thus deriving semi-empirical relationships for one-way and two-ways arch mechanisms. Flanagan and Bennett (1999) simplified the formulation derived by Dawe and Seah (1989) based on experimental results. A detailed state-of-the-art on OOP strength models for URM infill walls can be found in Pasca and Liberatore (2015).

So far, only a few experimental studies have been performed to investigate the interaction between IP and OOP behavior of masonry infills.

Based on experimental tests on full-scale infilled steel frames, Henderson et al. (2006) showed that OOP damage reduces the IP initial stiffness, with a limited effect on the initial IP strength of the wall. Similar results were obtained by Angel et al. (1994), Calvi and Bolognini (2001) and Furtado et al. (2016), based on tests on full- and reduced-scale infilled RC frames. In all these experimental tests, clay brick URM infills with slenderness ratio (height/thickness) ranging from 15.3 to 33.9 were tested considering either concentrated or uniformly distributed load patterns. Such studies showed that preliminary IP damage can yield a significant reduction of the OOP strength (even higher than 50%), especially for infill walls with high slenderness ratio. Furtado et al. (2016) proved that OOP infill strength is not significantly influenced by the axial load on columns and/or type of loading path (monotonic or cyclic). Extensive experimental tests, on full-scale infilled steel frames were performed by Flanagan and Bennett (1999) to investigate the IP/OOP interaction in URM infills.

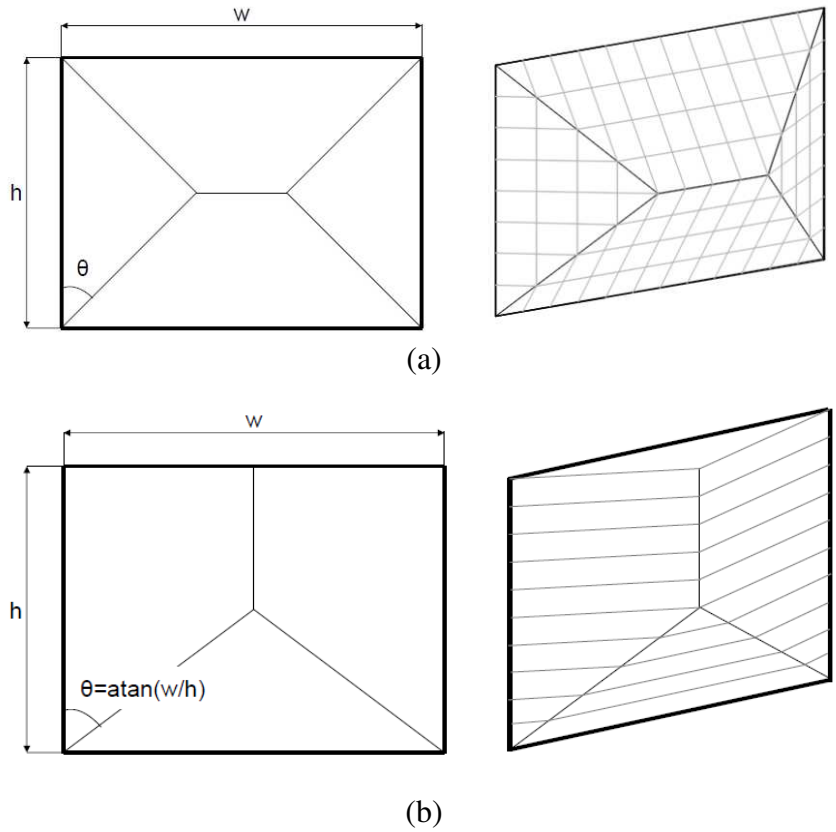

Figure 4 Collapse mechanism considered by Bashandy et al. (1995) (a) and Dawe and Seah (1989) (b)

They showed that the main effect of IP damage is a reduction of the OOP stiffness. As a consequence, out-of-plane displacements are expected to be greater for damaged infills than for undamaged infills, especially under moderate levels of loading and/or high slenderness ratios. Further experimental studies (Pereira et al. (2011); Guidi et al. (2013), Hak et al, (2014)) proved that also the OOP strength of URM infills can be significantly affected by the level of IP damage, especially for infill walls with high slenderness ratio. In addition, when IP/OOP loading is simultaneously applied, high vertical compression forces near the base of the wall can arise due to the combination of the thrust forces around the wall perimeter and the strut forces along the diagonal (Longo et al., (2018)).

Recently, Ricci et al. (2018a, 2018b) and De Risi et al. (2019) performed extensive experimental tests on 2/3-scaled infilled RC frame designed by the seismic Italian seismic Code (NTC2008). The scope of the tests was to investigate in-depth the effects of the IP/OOP interaction and the influence of the slenderness ratio (h/t) on the OOP behavior of URM infills made with clay hollow bricks. URM infills with thickness equal to 80 mm (h/t = 22.9) and 120 mm (h/t=15.2) were tested. Tests were carried out by applying out-of-plane forces after attaining different levels of interstory drifts. A substantial reduction of both lateral stiffness and

strength in the out-of-plane direction was observed, while increasing the drift level reached in the in-plane direction. For instance, as can be seen in the Figure 5 for infills with slenderness ratio h/t=22.9, OOP strength reductions ranging from 25% to 70% were observed while increasing the drift level from 0.28% to 0.58%. For infills with slenderness ratio h/t=15.2, a reduction of the OOP strength of the order of 40% was found for a drift level equal 0.89%.

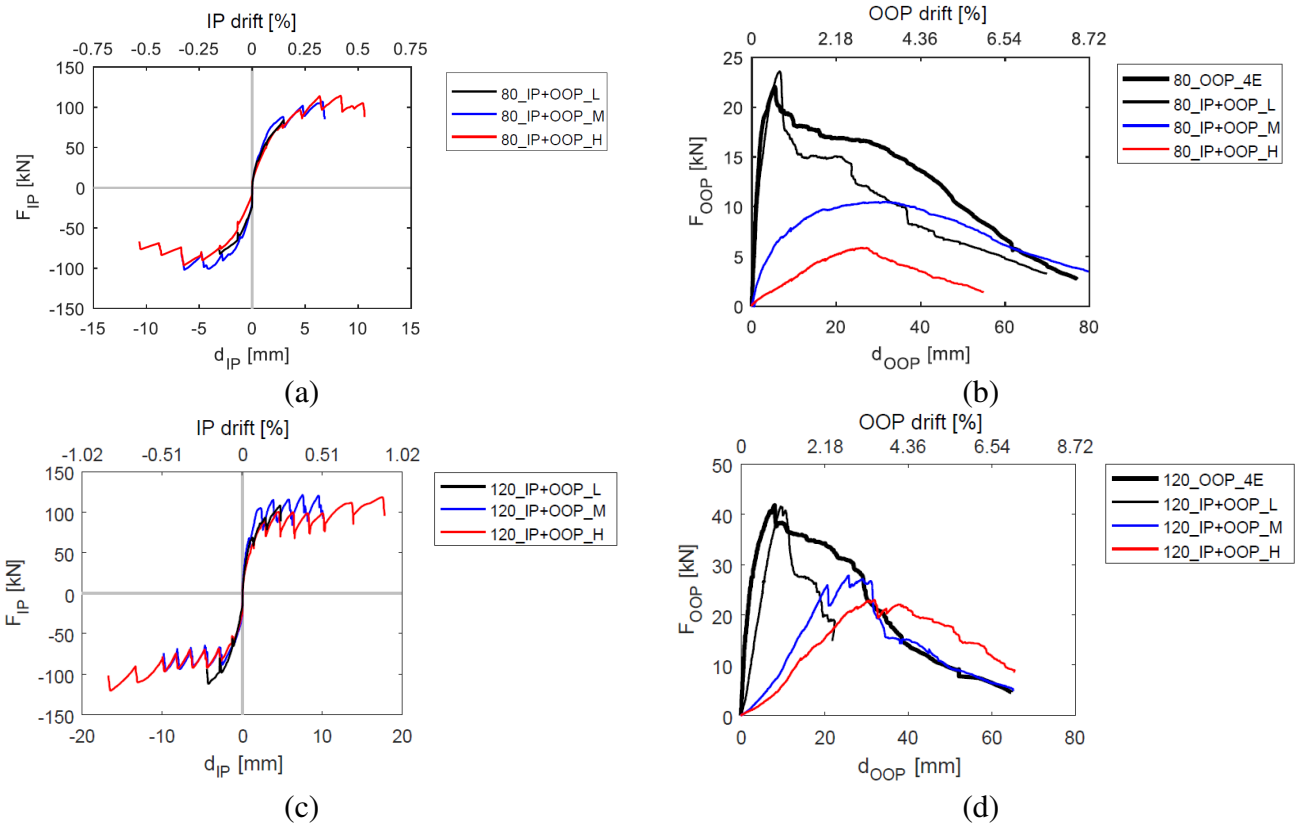

Figure 5 Comparison of the IP/OOP experimental responses of the 80mm (a/b) and 120mm (c/d) thick infills reported in Ricci et al. (2018a, 2018b)

In summary, based on the outcomes of the experimental tests, the most critical variables affecting the OOP behavior of infill walls are the slenderness of the infill and the state of damage (related to maximum IDR) experienced by the wall in the IP direction. Although not directly addressed in the experimental tests, it is clear that also the restraint conditions with the RC frame and the storey of the building where the infill is located play a not negligible role towards the OOP performance of masonry infills.

In the last years, some researchers have started to develop a new generation of numerical macro-models, able to capture the IP/OOP interaction of URM infills subjected to seismic loading. Some authors derived IP/OOP interaction domains expressed in terms of forces or displacements. The IP/OOP interaction curves have been implemented in two different macro-

models featuring compression-only (Hashemi and Mosalam 2007) – Figure 6a) and tension-compression resisting (Kadysiewski and Mosalam 2009 – Figure 6b) diagonal truss elements, respectively. The OOP mass is lumped in the middle of the element.

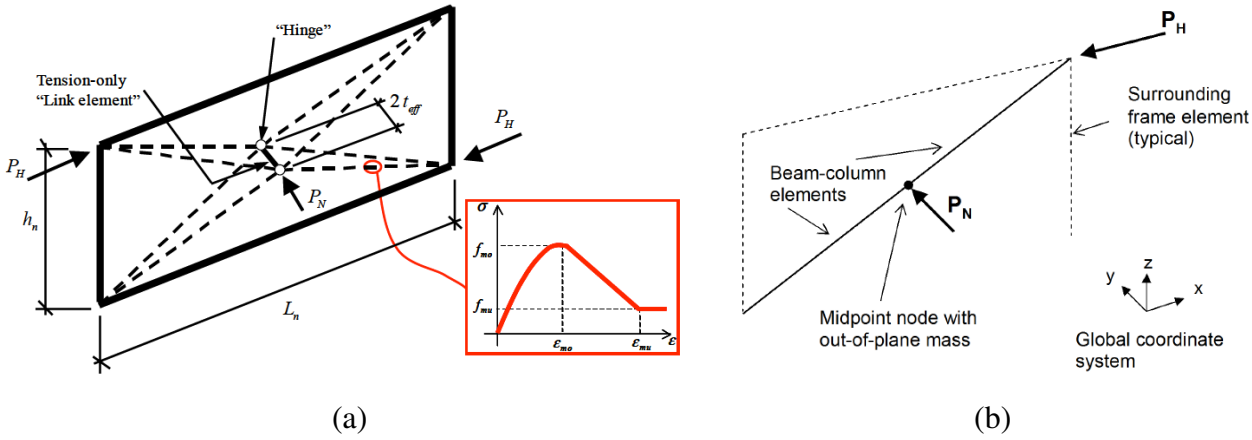

(a) (b)

Figure 6 Macro-models proposed by (a) Hashemi and Mosalam 2007 and (b) Kadysiewski and Mosalam 2009

The model proposed by Kadysiewski and Mosalam (2009) is based on representing the masonry infill with a single diagonal strut, which is sufficient to represent both behaviors of the masonry infill, works in tension and compression, and has a lumped mass at the mid of the diagonal length that works in the out-of-plane direction.

In the model proposed by Hashemi and Mosalam (2007) the infill is represented by eight no-tension truss elements joined in the centre by a tension only truss element.

Mosalam and Gunay (2015) developed a macro-model consisting of two elastic beam-with-hinges elements, placed along one diagonal and pinned to the surrounding RC frame (see Figure 7a). The IP/OOP behavior of the infill is governed by a bi-directional (IP axial load vs. OOP bending moment) domain. The effective mass of the infill is lumped in the midspan node to simulate OOP effects.

Furtado et al. (2015b) proposed an equivalent bi-diagonal strut model where the IP/OOP interaction is defined assuming a linear interaction between IP and OOP ultimate displacement capacity. In this model, the diagonal strut is connected with a nonlinear link element. The out-of-plane masses are assigned to the two extremity nodes of the horizontal element, as illustrated in Figure 7b

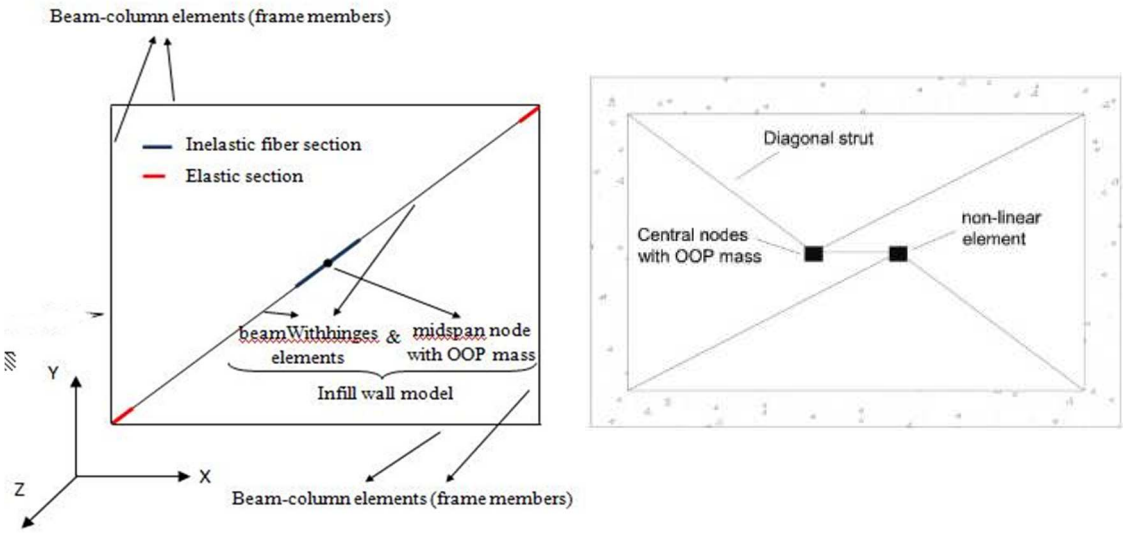

Figure 7 Macro-models proposed by (a) Mosalam and Gunay (2015) and (b) Furtado et al. (2015b)

Di Trapani et al. (2018) calibrated a four-struts macro-element (for pushover analysis) comprising two diagonal fiber beam-column elements (simulating the IP behavior) plus one vertical and one horizontal fiber beam-column element (simulating the arching mechanism in the OOP direction), mutually connected in a node at the midspan (see Figure 8).

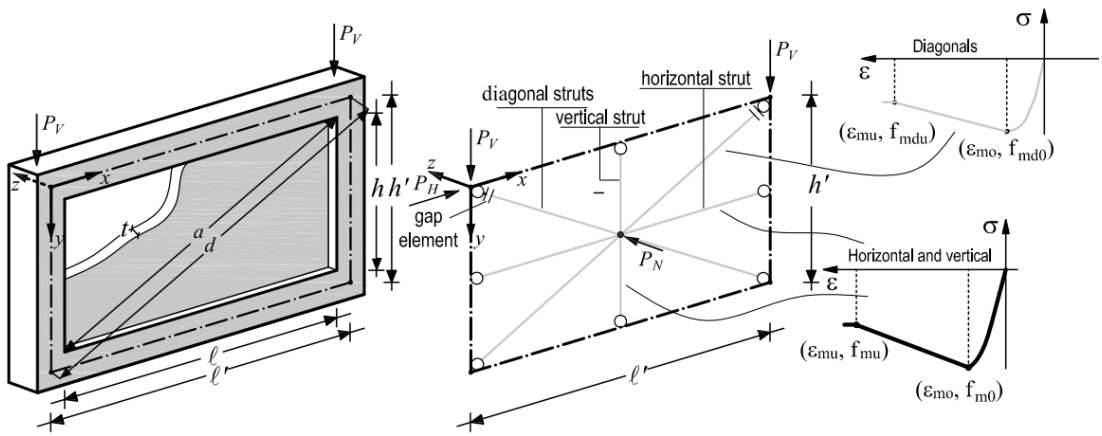

Figure 8 Four-struts macro-element (for pushover analysis) calibrated by Di Trapani et al. (2018)

Recently, Di Domenico et al. (2017) have proposed a new modelling approach for capturing the IP/OOP interaction in masonry infills (see Figure 9). The modelling approach under consideration relies on suitable evolutive degradation relationships derived from experimental results and empirical observations (Ricci et al. 2018a, b), together with a specific algorithm for the removal of infills, as IP/OOP collapse occurs (Mazza, 2019).

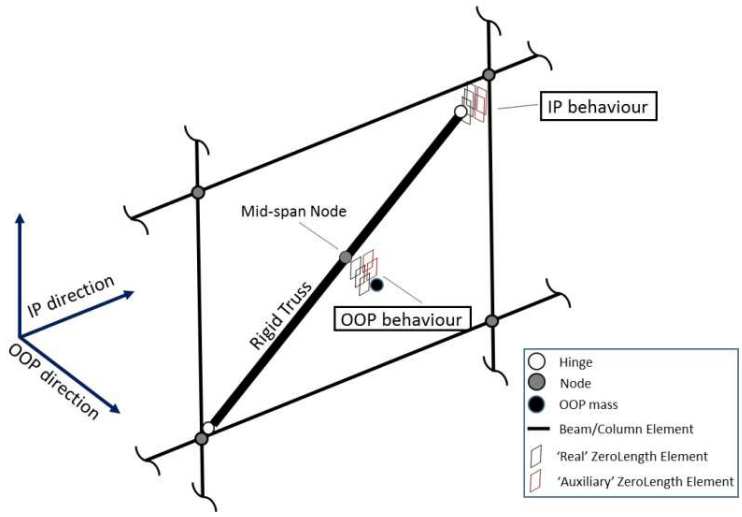

Figure 9 New modelling approach for capturing the IP/OOP interaction in masonry infills proposed by Di Domenico et al. (2017)

The main aim of this section of the thesis work is to investigate the influence of the IP/OOP interaction of URM infills on the seismic performance of typical residential RC buildings realized in Italy (and other European countries) in the second half of the last century. To this end, seven case studies are selected, differing in number of storeys and age of construction (hence structural details and infill characteristics). The modelling approach by Di Domenico et al. (2017), implemented within two sets of nonlinear zero-length link elements incorporated in a V-shaped bi-diagonal struts macro-element, is used to describe the IP/OOP interaction of masonry infills. Extensive Nonlinear response-Time History Analyses (NTHA) are carried out with OpenSees (McKenna et al. (2000)), using ten sets of ground motion pairs, with increasing seismic intensity. For comparison, NTHA are carried out also neglecting the OOP response of the infills. Different building performance levels are then identified to examine the damage scenario experienced by the buildings, considering or neglecting the IP/OOP interaction for masonry infills. Based on results of this study, a set of fragility curves is tentatively proposed to express the probability of exceedance of the selected building performance levels as a function of the earthquake intensity level.

1.2. METHODOLOGY OF THE STUDY

In this section, the influence of the IP/OOP behavior of URM infills in RC frame buildings subjected to seismic loading is investigated following a four steps methodology:

(i) Step 1: Selection of case-study; Modeling assumptions; Ground motion selection.

(ii) Step 2: Definition of seismic Performance Levels (PLs), based on a suitable multi-criterion approach.

(iii) Step 3: Execution of NTHA.

(iv) Step 4: Derivation of fragility curves for different PLs, considering, or alternatively neglecting, the influence of the IP/OOP interaction for masonry infills.

1.2.1. Case-study buildings

Over the last decades, the design criteria and construction practice relevant to RC buildings have considerably changed. Table 1 identifies five classes of RC frame buildings, within the Italian RC buildings stock, as a function of the age of construction, design approach, and main structural/non-structural details. Herein, they are referred to as: (i) GLD: Gravity Load Design buildings, (ii) SSD: Substandard Design buildings, (iii) LSD: Low Seismic Design buildings, (iv) HSD: High Seismic Design buildings, and (v) MD: Modern standard Design buildings. Similar classifications also apply for other countries that feature similar construction practice.

In this study, the attention is focused on three building classes only (namely GLD, SSD and HSD of Table 1), covering a wide spectrum of the current Italian building stock. Seven archetype buildings are considered: three for the SSD class and two for the GLD and HSD class, respectively. All the buildings feature the same plan and elevation configurations (see Figure 10) while differing in the number of storeys (4-, 6- and 8-storeys) and location (the cities of L'Aquila and Napoli, respectively), besides age of construction and structural/non-structural details (see Table 1). The selected buildings can be deemed to be representative of typical low-, medium- and high-rise multi-storeys residential buildings realized in Italy between 50's and 90's, which represent about 80% of the entire Italian RC building stock (ISTAT 2011).

The archetype buildings selected feature a rectangular plan with 27.30 m × 15.30 m dimensions, and 3.00 m interstory height. The GLD buildings feature four frames in the long direction (X-direction in Figure 10a) and two external frames in the short direction (Y-direction in Figure 10a). The SSD and HSD buildings have six additional internal frames in the Y-direction. All the buildings have a central dog-leg stair with cantilever steps sustained by two stiff 'knee'

beams in the Y-dir. Floors are assumed to be realized by one-way concrete slabs with 240mm total thickness.

Table 1. Classification of Italian RC frame buildings

Class*	Age (Design Standard)**	Design approach	Structural details	URM infills
GLD	before 1971 (R.D. 2229/1939)	Gravity loads only	Frames in one direction only Plain rebar. Low strength concrete No ductile seismic details	Double layers
SSD	1971 ÷ 1980 (L. 1086/71; DM 1974)	Equivalent static forces	Frames in one/both directions Plain/deformed rebars. Low strength concrete Internal flat beams No ductile seismic details	Double layers
LSD	1981 ÷ 1995 (DM 1986; DM 1992)	Equivalent static forces	Frames in both directions Deformed rebars Internal flat beams No ductile seismic details	Single Layer
HSD	1995 ÷ 2003 (DM 1996; OPCM 3274)	Response spectrum analysis	Frames in both directions Deformed rebars Not mandatory ductile seismic details	Single Layer
MSD	after 2003 (DM 2008; DM 2018)	Response spectrum analysis +capacity design criteria	Frames in both directions Deformed rebars Mandatory ductile seismic details	Single Layer

(*) GLD: Gravity load design; SSD: Substandard Seismic Design; LSD: Low Seismic Design; HSD: High Seismic Design; MD: Modern Standard Design
(**) for more information see https://www.ingegneriasismicaitaliana.com/it/24/normative/

Structural characteristics (including cross sections of RC columns and beams, reinforcement ratios, etc.) have been derived from a simulated design, in accordance with the technical standards and design rules in force in Italy at that time, adopting the Allowable Stress design method for the GLD and SSD buildings while the Limit State design method for the HSD buildings. For the buildings located in L'Aquila seismic forces have been computed considering a seismic coefficient (C) equal to 0.07g (medium seismic-risk region) and a typical subsoil class and structural behavior ($R=\varepsilon=\beta=1$).

Gravity loads are represented by a dead load of 4.00 KN/m^2 on the top floor and 5.50 KN/m^2 on the other floors, and a live load of 2.0 KN/m^2 for all the floors. An average weight per volume unit of 8.50 KN/m^3 has been considered for masonry infills.

The simulated design of the GLD buildings has been carried out assuming an allowable stress equal to 5.0 N/mm^2 for concrete and 140 N/mm^2 for steel (Aq42 plain steel rebars), in line with

the Italian Royal Decree 2229/1939. For the SSD and HSD buildings, a concrete characteristic compressive strength of 25 MPa and a steel characteristic yield strength of 430MPa (FeB44K deformed steel rebars) have been assumed, corresponding to an allowable stress of 8.5 MPa and 260 MPa, respectively.

Cross section dimensions of beams and columns, derived from simulated design, are reported in Table 2. As can be seen, the cross-section size of RC columns varies in the range of 300×650 – 300×300 mm, depending on the number of floors of the building. For all building types, the cross sections of the RC columns taper by 100 mm every two floors, except the columns at the corners of the building and those around the staircase, which present a constant cross section (300 x 300 mm and 300 x 500 ÷ 300 x 650 mm, respectively) along the entire building height. RC beams located around the perimeter of the building, and around the staircase, have 300×500 mm cross section. The main difference between HSD and SSD buildings is the presence of internal 300 x 400 mm exposed beams (LSD buildings) instead of 600 x 240 mm flat beams (SSD buildings).

For the GLD buildings, the longitudinal reinforcement is realized with 14 mm diameter plain bars with end hooks at the ends; 6mm diameter stirrups are considered as transverse reinforcement. For the SSD and HSD buildings, the longitudinal reinforcement is realized with 16mm (beams) and 18mm (columns) deformed bars; 8mm diameter stirrups are considered as transverse reinforcement. Longitudinal reinforcement ratios and stirrups spacing are reported in Table 2 for each building model.

For GLD and SSD buildings, masonry infills are realized with hollow clay bricks arranged in two layers with 100 mm thickness each, separated by an air cavity of 100 mm, in line with the construction practice of that time. For the HSD buildings, masonry infills are characterized by a single layer of hollow clay bricks with 300 mm thickness. In both cases, the holes of the bricks are arranged in the horizontal direction. For all building configurations, masonry infills located in the long direction (X-dir.) feature large opening while those placed in the short direction (Y dir.) have no openings. In this study, the attention is focused on masonry infills without openings only, the influence of masonry infills with (large) openings being relatively low towards the seismic behavior of the building. Therefore, for simplicity, their contribution has been neglected in the structural model.

The fundamental periods of vibration in the short direction (T_y) of each building model, derived from modal analysis, are listed in Table 2.

The fundamental period of the bare frame structure without the infill stiffness contribution (T_{BF}) is very important to understand their contribution in the global stiffness of the building and are reported in Table 2.

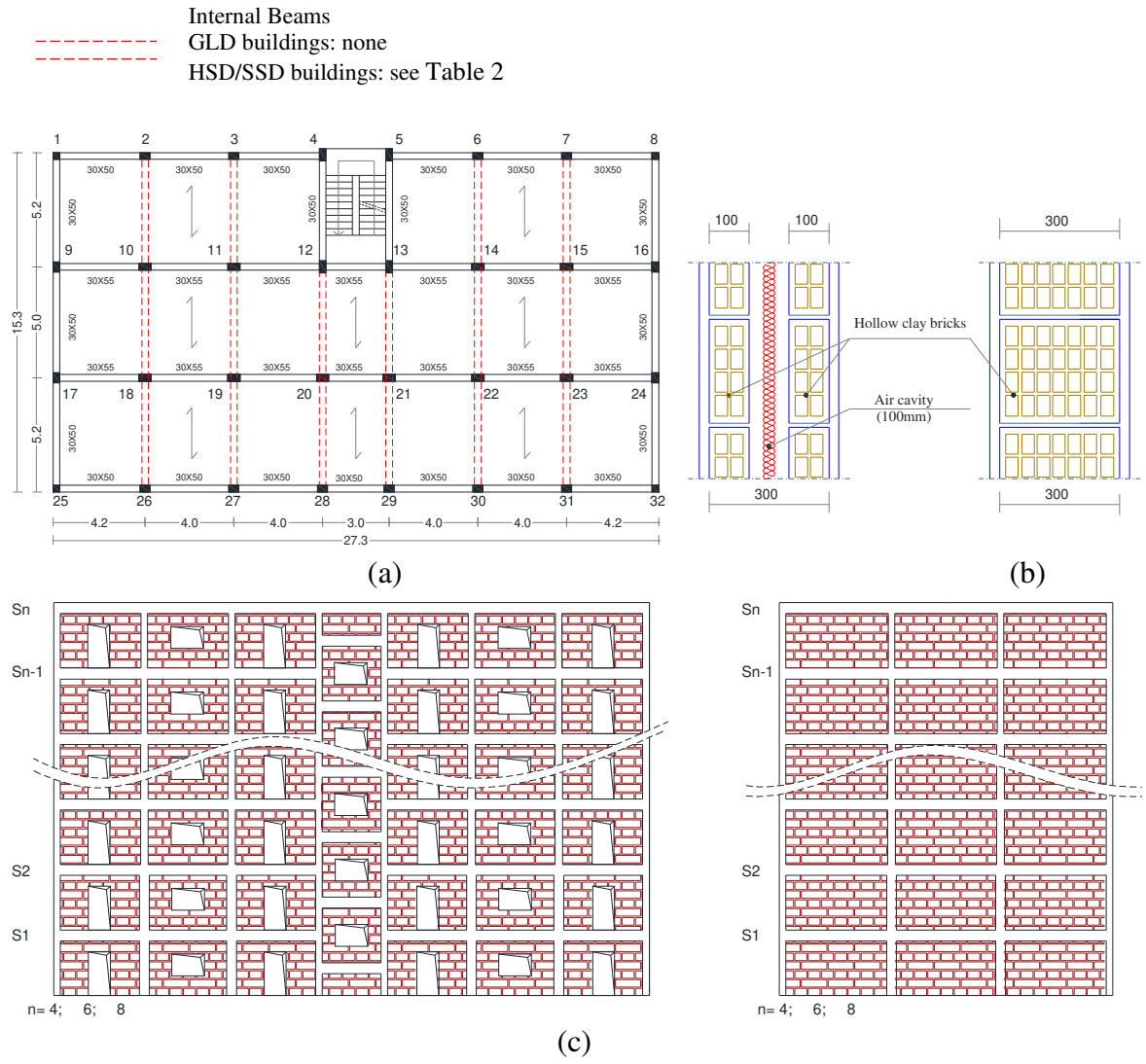

Figure 10 Selected case-study buildings: (a) plan view, (b) masonry infills configuration and (c) lateral view

Table 2.Main geometrical characteristics and steel reinforcement details of the selected building models

Case Study (Type-n. storeys)	Site	Number of frames	Column sections (mm)	Beam sections (mm)	Longitudinal reinforcement ratios (%)	Transverse reinforcement (diameter/spacing)	Type of reinforcement	Masonry infills (hollow clay bricks)
GLD-6st (T_y=0.73 sec) (T_{BF} = 0.98 sec)	Napoli	E (dir. X):2 I (dir. X):2 E (dir. Y):2 I (dir. Y):0	E: 300×300÷300×450 I: 350×300÷550×300 SC: 300×500 C: 300×300	E (dir.X):300×500 I (dir. X):300×550 E (dir.Y):300×500 I (dir. Y): - KB:300×500	B: 0.56÷0.71% C: 0.59÷0.68%	B: Ø6/200 mm C: Ø6/150 mm SC: Ø6/150 mm	smooth (Aq42)	Double layer (100+100 mm)
GLD-8st (T_y= 1.00 sec) (T_{BF} = 1.58 sec)	Napoli	E (dir. X):2 I (dir. X):2 E (dir. Y):2 I (dir. Y):0	E: 300×300÷300×550 I: 350×300÷650×300 SC: 300×550 C: 300×300	E (dir.X):300×500 I (dir. X):300×550 E (dir.Y):300×500 I (dir. Y): - KB:300×500	B: 0.56÷0.71% C: 0.59÷0.79%	B: Ø6/200 mm C: Ø6/150 mm SC: Ø6/150 mm	smooth (Aq42)	Double layer (100+100 mm)
SSD-4st (T_y= 0.48 sec) (T_{BF} = 0.81 sec)	L'Aquila	E (dir. X):2 I (dir. X):2 E (dir. Y):2 I (dir. Y):6	E: 300×300÷300×350 I: 350×300÷450×300 SC: 300×550 C: 300×300	E (dir.X):300×500 I (dir. X):300×550 E (dir.Y):300×500 I (dir. Y): 600×240 KB:300×500	B: 0.62÷0.98% C: 0.87÷1.23%	B: Ø8/100 mm C: Ø8/150 mm SC: Ø8/150 mm	deformed (FeB44k)	Double layer (100+100 mm)
SSD-6st (T_y= 0.71 sec) (T_{BF} = 1.01 sec)	L'Aquila	E (dir. X):2 I (dir. X):2 E (dir. Y):2 I (dir. Y):6	E: 300×300÷300×450 I: 350×300÷550×300 SC: 300×550 C: 300×300	E (dir.X):300×500 I (dir. X):300×550 E (dir.Y):300×500 I (dir. Y): 600×240 KB:300×500	B: 0.62÷1.11% C: 0.95÷1.51%	B: Ø8/100 mm C: Ø8/150 mm SC: Ø8/150 mm	deformed (FeB44k)	Double layer (100+100 mm)
SSD-8st (T_y= 0.97 sec) (T_{BF} = 1.37 sec)	L'Aquila	E (dir. X):2 I (dir. X):2 E (dir. Y):2 I (dir. Y):6	E: 300×300÷300×550 I: 350×300÷650×300 SC: 300×650 C: 300×300	E (dir.X):300×500 I (dir. X):300×550 E (dir.Y):300×500 I (dir. Y): 600×240 KB:300×500	B: 0.68÷1.01% C: 0.95÷1.51%	B: Ø8/100 mm C: Ø8/150 mm SC: Ø8/150 mm	deformed (FeB44k)	Double layer (100+100 mm)
HSD-6st (T_y= 0.67 sec) (T_{BF} = 1.11 sec)	L'Aquila	E (dir. X):2 I (dir. X):2 E (dir. Y):2 I (dir. Y):6	E: 300×300÷300×450 I: 350×300÷550×300 SC: 300×550 C: 300×300	E (dir.X):300×500 I (dir. X):300×550 E (dir.Y):300×500 I (dir. Y): 300×400 KB:300×500	B: 0.72÷0.93% C: 0.95÷1.51%	B: Ø8/80÷Ø8/100 mm C: Ø8/75÷Ø8/100 mm SC: Ø8/150 mm	deformed (FeB44k)	Single layer (300 mm)
HSD-8st (T_y= 0.87 sec) (T_{BF} = 1.48 sec)	L'Aquila	E (dir. X):2 I (dir. X):2 E (dir. Y):2 I (dir. Y):6	E: 300×300÷300×550 I: 350×300÷650×300 SC: 300×650 C: 300×300	E (dir.X):300×500 I (dir. X):300×550 E (dir.Y):300×500 I (dir. Y): 300×400 KB:300×500	B: 0.72÷1.11% C: 0.95÷1.81%	B: Ø8/80÷Ø8/100 mm C: Ø8/75÷Ø8/100 mm SC: Ø8/150 mm	deformed (FeB44k)	Single layer (300 mm)

GLD: Gravity Load Design, SSD: Substandard Seismic Design; HSD: High Seismic Design.
E: External, I: Internal, SC: staircase; KB: knee beams, B: beams; C: columns.
T_y: fundamental periods of vibration in the short direction; T_{BF}= fundamental periods of Bare Frame structure

1.2.2 Ground motion selection

The case-study buildings are supposed to be located in the city of L'Aquila (SSD and HSD buildings) and in the city of Napoli (GLD buildings), respectively, both on soil type C (soft soil), according to the current Italian code classification. It is worth noting that the city of L'Aquila was classified as second seismic category/class (medium level of seismic hazard for Italy) from 1915. The city of Napoli, instead, was classified as seismic area for the first time only in the 1981 (third seismic category/class). According to the current seismic hazard map of Italy, the city of L'Aquila represents one of the city with the highest level of seismicity in Italy with a design earthquake intensity level with 475 years return period of 0.35g for soil type C and 0.47g with 2475 year return period for soil type C. The city of Napoli features a medium level of seismic hazard with a design earthquake intensity level with 475 years return period of 0.25g for soil type C and 0.35g with 2475 years return period for soil type C.

Table 3 compares the earthquake hazard of L'Aquila and Napoli in terms of spectral acceleration for three values of conditioning period, namely: T* = 0.50 s, 0.75 s and 1.0 s, corresponding approximately to the average (in the two orthogonal directions) of the effective fundamental periods of the 4-, 6- and 8-storeys buildings, respectively. Ten earthquake intensity levels, with return periods (Tr) ranging from 30 years to 2475 years, have been derived from the hazard curve provided by the Italian Institute of Geophysics and Vulcanology (INGV). Moreover, for a better understanding of the phenomena, an additional seismic intensity level, with return period equal to 5000 years, has been considered for NTHA. The latter has been extrapolated based on best fit to the hazard curve, using a second-order polynomial law in log space, as proposed by Vamvatsikos (2014).

Table 3. Earthquake intensity levels considered for the building models under scrutiny.

		Spectral acceleration Sa(T*) (g)				
Intensity	Tr	Napoli (GLD models)		L'Aquila (SSD and HSD models)		
Level	(years)	T*=0.75 s	T*=1.0 s	T*=0.5 s	T*=0.75 s	T*=1.0 s
IM1	30	0.096	0.072	0.249	0.166	0.125
IM2	50	0.134	0.101	0.326	0.217	0.163
IM3	72	0.166	0.125	0.389	0.259	0.195
IM4	101	0.200	0.150	0.457	0.305	0.229
IM5	140	0.236	0.177	0.531	0.354	0.266
IM6	201	0.281	0.211	0.616	0.411	0.308
IM7	475	0.396	0.297	0.820	0.564	0.423
IM8	975	0.495	0.371	0.977	0.695	0.521
IM9	2475	0.626	0.469	1.148	0.847	0.635
IM10	5000	0.747	0.560	1.422	1.079	0.809

T*: average fundamental periods (in the two orthogonal directions) of the building model

For each earthquake intensity level, NTHA have been performed using a set of 10 ground motion pairs selected and scaled by Ay et al. (2017), in such a way to be compatible with suitable Conditional Mean Spectra (CMS) (Baker, 2011), derived considering an appropriate M-R-ε (magnitude-distance-epsilon) disaggregation and a suitable attenuation relationship for each building site. The values of T* shown in Table 3 have been used as conditioning periods for the derivation of the CMS. As an example, Figure 11 compares the 5%-damping reference spectrum with the average response spectrum derived from the set of selected ground motions for the city of Napoli (Figure 11a) and L'Aquila (Figure 11b), respectively, for an earthquake intensity level with T_R = 2500 years return period and conditioning period T* = 0.75 s.

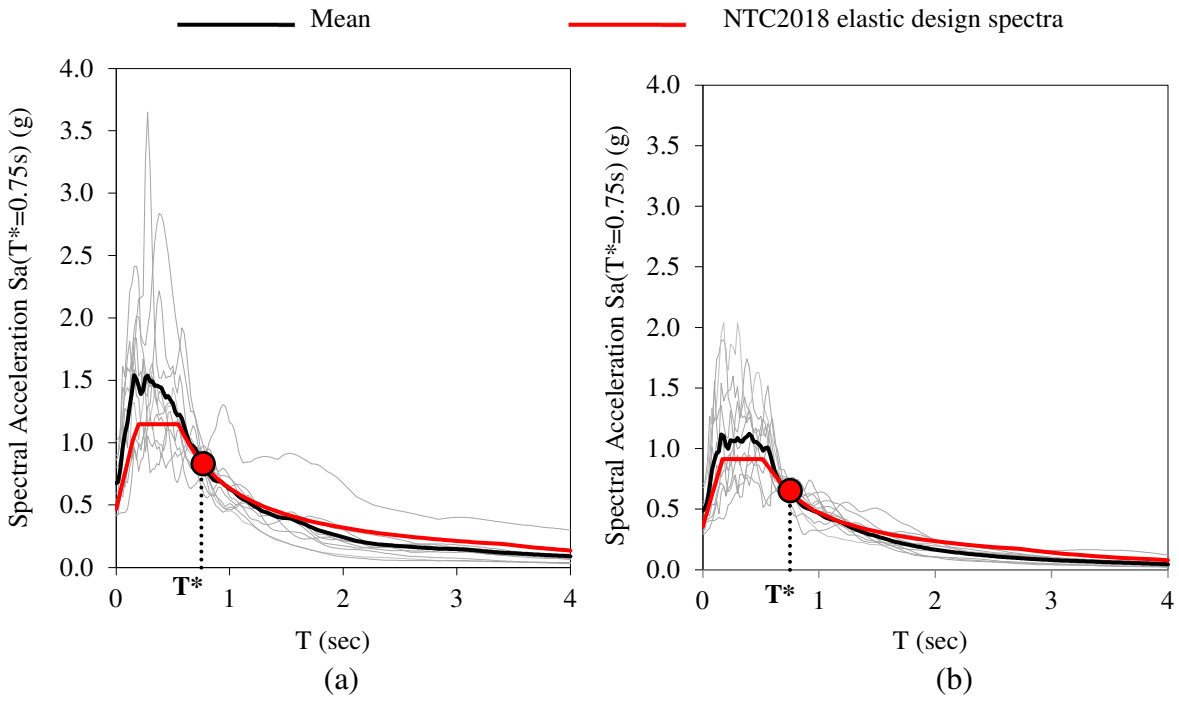

Figure 11 Comparison between code-conforming reference spectrum and average response spectrum of the selected ground motions (T* = 0.75 s, Tr=2475 years, soil C) for (a) L'Aquila and (b) Napoli.

1.2.3. Numerical model

A refined 3D lumped-plasticity model has been implemented in OpenSees (McKenna et al. 2000) for each case-study building. Beam-with-hinges elements have been used to describe the mechanical behavior of RC members, based on given constitutive laws for steel (see Figure 12a) and concrete (see Figure 12b).

For RC members with plain rebars (ref. to GLD models) bar slipping effects have been captured by using a modified constitutive law for steel rebars (see Figure 12a), in accordance with (Braga

et al. 2012), and neglecting the contribution of compression longitudinal rebars, in accordance with evidence from past studies (e.g., Calvi et al., 2002; Fabbrocino et al., 2004). Concrete confinement has been neglected (see Figure 12c), due to the low effectiveness of stirrups in old buildings. In addition, a reduced plastic hinge length (equal to H/3 for beams and H/4 for base columns, see Cardone and Perrone, 2015) has been assumed, to take into account that flexural cracks do not spread along the element during repeated cyclic deformation, while their width increases significantly due to bond slip effect.

Plastic hinges (see Figure 12c) are characterized by a tri-linear cyclic hysteretic behavior, described by the modified Ibarra-Medina-Krawinkler deterioration model (Ibarra et al. 2005). The yielding (M_y) and ultimate bending moment (M_u) (see Figure 12c) have been derived by an accurate moment-curvature analysis on fiber sections characterized by suitable constitutive laws of materials (see Figure 12).

The yielding (θ_y) and ultimate chord rotation (θ_u) have been evaluated using the formula reported in Verderame et al. (2001 a, b) to take into account the poor bond capacity of plain bars. As far as the post capping-rotation capacity (θ_c-θ_u) is concerned, reference to the relationship proposed by Ibarra et al. (2005) has been made. The plastic hinges of the short columns around the stairs have been modified to capture the potential brittle failure of such elements, considering the shear strength formulation proposed by Sezen and Moehle (2004).

As far as the strength of materials is concerned, reference to the experimental results reported in Verderame et al. (2001a, 2001b) has been made, assuming a concrete compression strength of 25 MPa for GLD buildings and 28 MPa for SSD/LSD buildings, respectively, and a steel yield strength of 325 MPa for GLD buildings and 430 MPa for SSD/HSD buildings, respectively.
More details on the modeling assumptions for RC members can be found in Cardone and Perrone (2017).

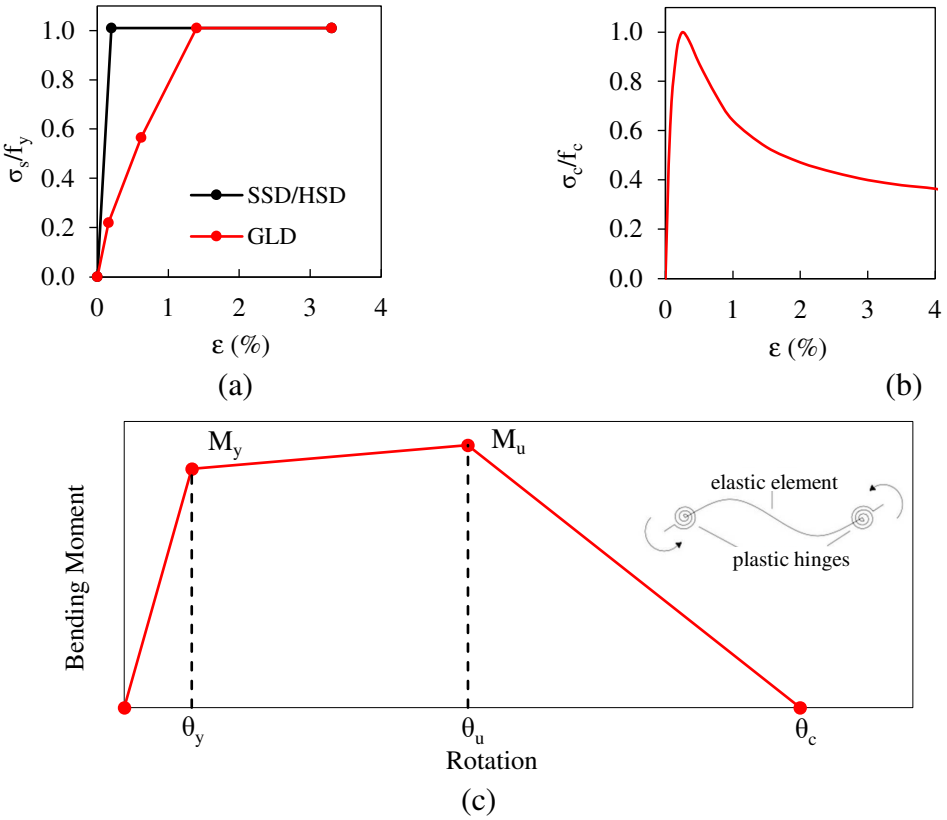

Figure 12 Constitutive law of (a) streel and (b) not-confined concrete and (c) tri-linear moment-rotation curved adopted for plastic hinges.

URM infills have been modelled with a V-shaped bi-diagonal strut macro-element incorporating two sets of nonlinear zero-length link elements lumped in the central node (see Figure 13). The modeling approach proposed by Di Domenico et al. (2017) has been implemented to account for the IP/OOP interaction of masonry infills. The modeling strategy under consideration consists of three main steps:

(i) definition of the skeleton curves representing the IP and OOP undamaged behavior of masonry infills;

(ii) use of semi-empirical relationships to derive a number ("n") of degraded (damaged) backbone curves from the relevant undamaged counterpart, as a function of the Intersorey Drift Ratio (IDR) (OOP degraded curves) and OOP displacements (IP degraded curves), respectively;

(iii) implementation of the "n+1" IP and OOP backbone curves within the selected macro-model using an appropriate routine to remove masonry infill from the building model,

during NTHA, when either IP or OOP collapse occurs (attainment of the ultimate displacement, see Figure 14).

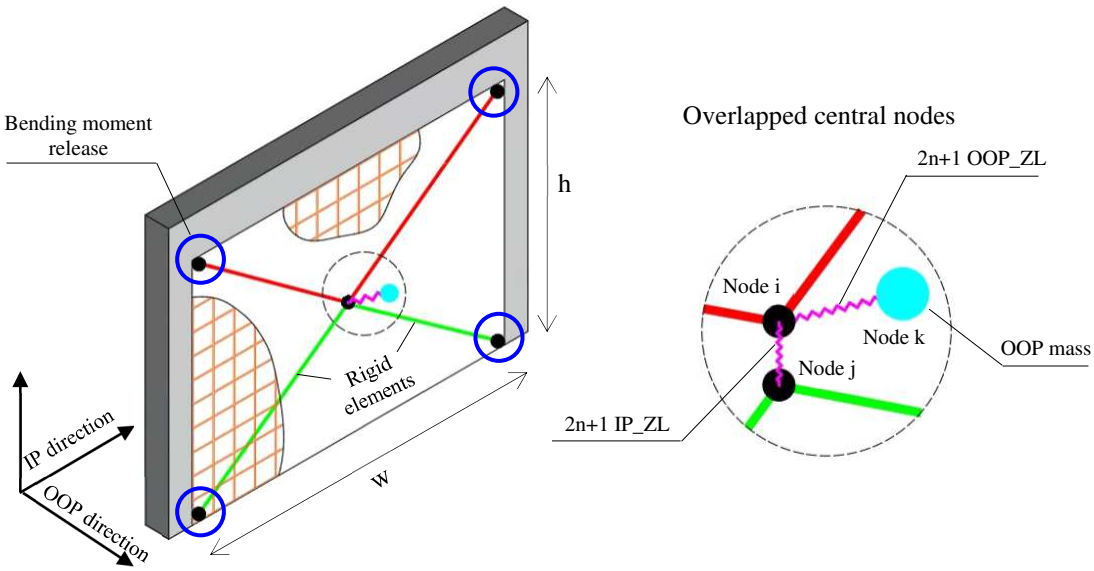

Figure 13 Schematic representation of the macro-model used for URM infills.

Figure 14 shows the two groups of "n+1" tri-linear curves adopted in this study to describe the IP/OOP degrading behavior of double-layer infills (100+100 mm), where "n" has been set equal to 19 in order to get accurate results.

The undamaged IP behavior of the infills has been modeled using the tri-linear skeleton curve proposed in (Sassun et al. 2016), assuming a compressive strength in the vertical direction (f_{mv}) of 1.2 MPa, a shear strength (τ) of 0.3 MPa, and an elastic modulus in the vertical direction (E_{mv}) of 1050 MPa, respectively, in accordance with Decanini et al. (2004).

Moreover, a compression strength in the horizontal direction (f_{mh}) equal to 2.6 MPa and an elastic modulus in the horizontal direction (E_{mh}) of 1960 MPa, corresponding to the average values of the experimental data reported in Table 4, have been assumed.

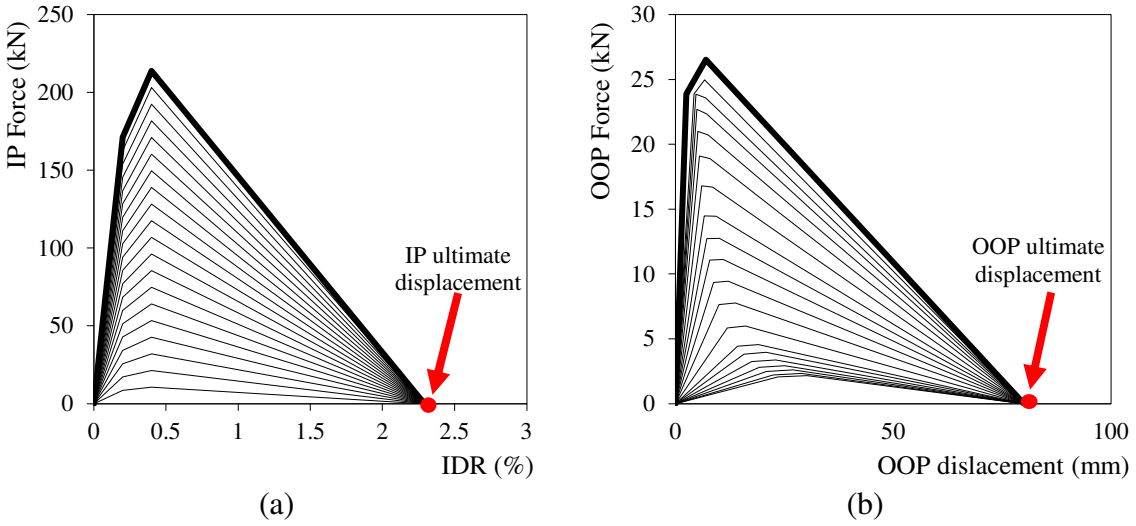

Figure 14 (a) IP and (b) OOP backbone curves adopted for the double-layer infills (100+100 mm thickness)

A set of semi-empirical relationships has been derived to define the undamaged OOP behavior of the infills, as a function of a number of geometric (thickness "t", height "h" and width "w") and mechanical parameters (f_{mv}, f_{mh}, E_{mv}, E_{mh}). To this end, five OOP pseudo-static tests have been considered for the double-layers (100+100mm) infills of GLD/SSD buildings (see Table 4), whose results have been processed following a linear least-squares regression analysis.

Table 4.Experimental tests considered to derive the semi-empirical relationships reported in Eqs. (1)-(4)

Authors	Load Type	Test	t (mm)	h/t	w (mm)	f_{mv} (MPa)	f_{mh} (MPa)	E_{mv} (MPa)	E_{mh} (MPa)	F_{crack} (kN)	K_{crack} (kN/mm)	F_{max} (kN)	K_{max} (kN/mm)
Furtado et al. (2016)	U	Inf-02	150	15.33	1.83	0.53	-	1418	-	50	21.74	52.50*	0.89
Calvi and Bolognini (2001)	C	10	135	23.91	1.53	1.1	1.11	991	1873	29	12.08	33.70	6.48
Ricci et al. (2018a,b)	C	OOP_4E	80	22.88	1.28	1.81	2.45	1090	1255	19.4	5.88	22	4.07
De Risi et al. (2019)	C	OOP	80	22.88	1.28	2.37	4.63	1891	3452	20.12	9.63	29.46	4.93
Ricci et al. (2018b)	C	OOP	120	15.25	1.28	1.65	2.12	1455	1262	27.5	11.00	41.9	5.24

*Corrected by a factor 0.7 to consider different load conditions

U: Uniformly distributed, C: Concentrated; t: infill thickness, h: infill height, w: infill width, f_{mv}: compressive strength of masonry in the vertical direction, f_{mh}: compressive strength in the horizontal direction, E_{mh}: elastic modulus in the horizontal direction, E_{mv}: elastic modulus in the vertical direction; F_{crack} , K_{crack} , F_{max} , K_{max}: see Figure 15.

The relationships thus obtained are reported in Eqs. (1)-(3), which provide: (i) the cracking force F_{crack}, (ii) the secant stiffness K_{crack} and (iii) the peak force F_{max}, respectively. In Table 5, the values of the coefficients a_1, a_2, and a_3 (see Eq. (1)), b_1 and b_2 (see Eq. (2)) and θ_{1v}, θ_{2v}, θ_{3v}, θ_{1h}, θ_{2h}, θ_{3h} (see Eq. (3)) are reported.

$$F_{crack} = \min\left(0.9 \cdot F_{max}; a_1 \cdot f_{mv}^{a_2} \cdot \left(\frac{t}{h}\right)^{a_3} \cdot w \cdot h\right) \quad (1)$$

$$K_{crack} = \frac{1}{12 \cdot \left(\left(\frac{t}{h}\right)^{b_1} \cdot \left(\frac{w}{h}\right)^{b_2}\right) \cdot (1-\nu^2)} \cdot \frac{E_{mv} \cdot w}{\left(\frac{h}{t}\right)^3} \quad (2)$$

$$F_{max} = \left[\theta_{1v} \cdot f_{mv}^{\theta_{2v}} \cdot \left(\frac{t}{h}\right)^{\theta_{3v}} + \theta_{1h} \cdot f_{mh}^{\theta_{2h}} \cdot \left(\frac{t}{w}\right)^{\theta_{3h}}\right] \cdot w \cdot h \quad (3)$$

Table 5.Values of the coefficients of Eqs. (1)-(3)

a_1	a_2	a_3	b_1	b_2	θ_{1v}	θ_{2v}	θ_{3v}	θ_{1h}	θ_{2h}	θ_{3h}
0.75	0.35	1.75	1.82	0.15	5.2	0.15	2.53	0.55	0.84	1.80

It is worth noting that the semi-empirical relationships (1) and (3) are similar to the expressions proposed in the Eurocode 6 (2005) for the evaluation of the lateral strength of masonry walls. Eq. (2), instead, has been derived by the Timoshenko's theory applied to an elastic isotropic plate hinged along the border, replacing the analytical coefficient with the term $[(t/h)^{b1}*(w/h)^{b2}]$. In Figure 15 the experimental values of F_{crack}, K_{crack} and F_{max} listed in Table 4 are compared to those predicted using Eqs. (1), (2) and (3), respectively.

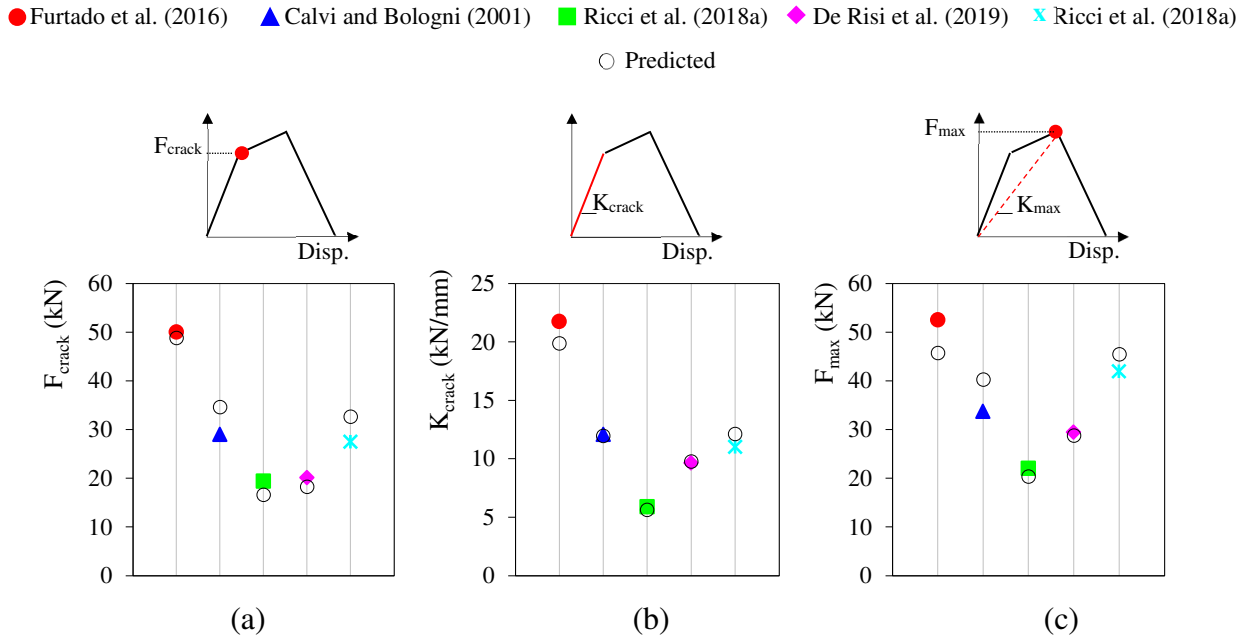

Figure 15 Comparison between experimental data and proposed semi-empirical relationships: (a) cracking force, (b) cracking stiffness, (c) peak force.

The secant stiffness at the peak strength (K_{max}) has been assumed equal to:

$$K_{max} = 0.40 * K_{crack} \tag{4}$$

based on the average values of the stiffness ratio K_{max}/K_{crack} obtained from experimental tests (see Table 4). Finally, the OOP ultimate displacement capacity (d_{OOP}) has been assumed equal to 80% the infill thickness, in accordance with Angel et al. (1994).

In first approximation, the same relationships (ref. to Eqs. (1)-4)) have been used to characterize also the OOP behavior of the 300 mm thickness single-layer infills.

The jump from one skeleton curve to another is governed by the semi-empirical relationships proposed in (Ricci et al. 2018b), which provide the reduction of OOP stiffness and OOP strength as a function of IP damage (and vice-versa).

The IP and OOP skeleton curves thus derived have been implemented in OpenSees (McKenna et al. 2000) within the V-shaped bi-diagonal strut macro-element shown in Figure 13. The equivalent struts feature suitable bending moment releases at the ends close to the RC beam-column joints. The V-shaped bi-diagonal struts are connected by two sets of 2n+1 zero-length nonlinear link elements reproducing the IP degrading cyclic behavior of the infill. To avoid any lability, a type "Equal" constrain is assigned in the OOP direction to the two overlapped nodes of the V-shaped struts (see node "i" and "j" in Figure 13). An additional node with lumped mass equal to the effective mass of the infill (herein taken equal to 80% of the infill total mass, in accordance with (Kadysiewski and Mosalam 2009) is implemented in the middle of the element (see Figure 13). The auxiliary node is linked to the equivalent struts by 2n+1 zero-length nonlinear link elements reproducing the OOP degrading cyclic behavior of the infill. A specific algorithm is used to remove the infill from the structural model when the ultimate IP/OOP displacement is reached.

The hysteretic cyclic behavior of the infills has been captured by the Hysteretic Material rule implemented in OpenSees, in which the stiffness cyclic degradation is described by the so-called β coefficient. In this study, the β coefficient has been set equal to 0.8, in line with experimental results reported by Hak et al. (2014) and Furtado et al. (2016). The pinching factors p_x and p_y, governing the deformation and force behavior during cyclic loading have been taken equal to 0.8 and 0.20, respectively, for the IP cyclic behavior, while equal to 1.0 for the OOP cyclic behavior.

It should be noted that all the relationships used in this study have been defined based on a number of experimental pseudo-static tests on different infill specimens, featuring (i) different units (solid bricks, hollows bricks) and infill materials (clay, concrete), (iii) scale specimens (full- or reduced-scale), (iv) frame-types (steel, RC) and (v) load configuration (uniform, concentrated, linear). Furthermore, a linear least-squares regression analysis has been used to correlate the experimental parameters (IP/OOP force, secant stiffness, cracking, peak strength and ultimate displacements, etc.) with a number of geometric and mechanical characteristics of the infill (thickness, height, elastic modulus, compressive strength, etc.). It is then clear that the

semi-empirical relationships adopted are affected by a number of epistemological uncertainties associated with the difficulty in reproducing the real working conditions of the infills during seismic events and the influence of the statistical process adopted that involves modeling and analyses of several independent variables that are included, all together, in the final proposed relationship. These uncertainties (together with other sources of uncertainties discussed in the next paragraphs) have been taken into account by considering additional dispersion factors (β) in the derivation of fragility curves.

1.3. DEFINITION OF PERFORMANCE LEVELS

Three Performance Levels (PLs), associated with different post-earthquake damage scenarios, have been identified in this study. They are referred to as: (i) Usability Preventing Damage (UPD) performance level, (ii) Life Safety (LS) performance level and (iii) Global Collapse (GC) performance level, respectively. The description of each PL, in terms of expected post-earthquake damage scenario is reported in Table 6. In the same table the multi-criteria approach adopted to define the threshold limits of each PL are summarized.
It's worth noting that the definition of PLs adopted in this study was purposely done to reduce the computational efforts required to process NTHA results at the level of individual elements. However, it is fully reasonable and compatible with the scope of the study.

The UPD performance level has been defined following a multi-criterion approach (Cardone et al. 2017; Perrone et al. 2019) based on the following three conditions (whichever occurs first):

(i) extensive damage of many infills: attainment of the peak lateral strength in more than 50% of the infills, for interstory drifts greater than 0.40 %, in accordance with the definition of DS2 damage state reported in Figure 16 (Cardone and Perrone (2015));

(ii) severe damage of the first infill: strength reduction greater than 50% of the first infill, for interstory drifts greater than 1.4%, in accordance with the definition of DS3 damage state reported in Figure 16 (Cardone and Perrone (2015)), corresponding to a not-repairable condition of the infill;

(iii) onset of structural damage requiring some repair interventions: the top displacement from NTHA exceeds the value corresponding to the attainment of 95% the peak lateral strength (the force level before the peak) from PushOver Analysis (POA).

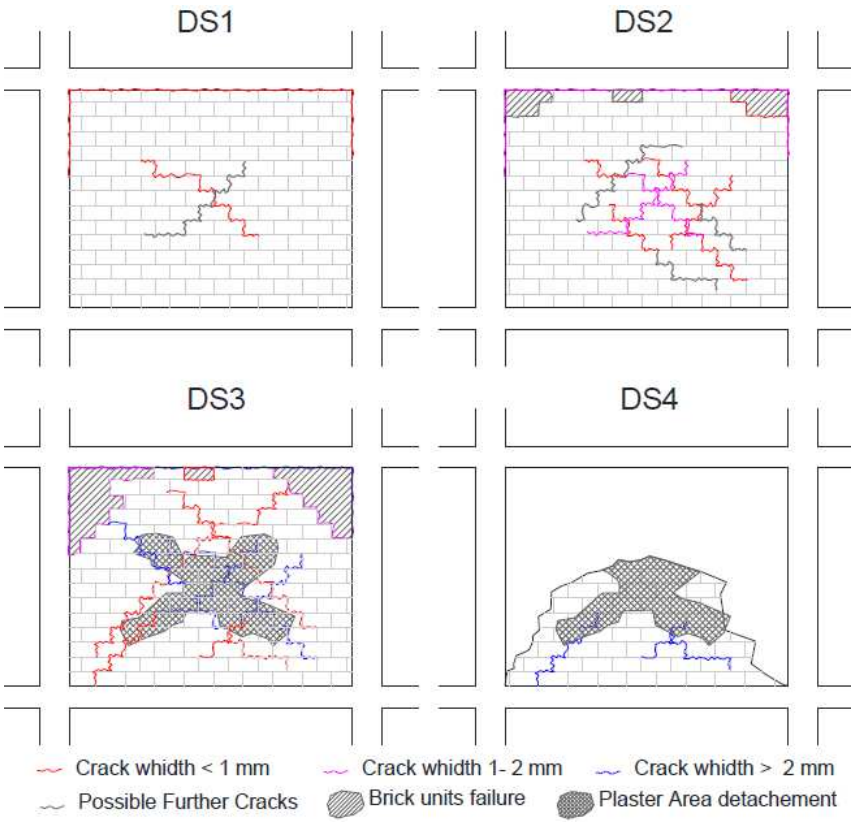

Figure 16 Damage states of masonry infills without openings defined in Cardone and Perrone (2015)

The LS performance level has been defined following a different multi-criterion approach that includes:

(i) out-of-plane collapse of the first infill;

(ii) exceedance of a given interstory drift limit, corresponding to the attainment of a LS performance level in the main structure. The drift limit under consideration has been assumed equal to 1.00% for GLD buildings (in accordance with Masi et al. (2015)), 1.35% for SSD buildings (in accordance with Rossetto and Elnashai, (2003)) and 2.00% for HSD buildings (in accordance with FEMA 356 (2000)).

The IP collapse of the infill does not affect the LS performance level, because it always occurs for drift levels greater the assumed drift limits. Obviously, when the out-of-plane collapse of one infill takes place before extensive/severe in-plane damage of the infills, LS and UPD coincide.

Table 6. Definition of Performance Levels (PLs) and relevant threshold limits.

PL	Definition	Threshold limits
UPD	Buildings that meet this PL level experience negligible damage to their structural elements and easily repairable damage to nonstructural components, which does not jeopardize the normal use of the building after the earthquake.	First condition between: (i) 50% of infills attain their peak lateral strength; (ii) the first infill attains a strength reduction equal to 50%; (iii) the top displacement exceeds the value corresponding to the attainment of 95% of the peak lateral strength from POA.
LS	Buildings that meet this PL level experience significant damage to structural and/or nonstructural components (including the out-of-plane collapse of infill walls) that may pose at risk human life.	First condition between: (i) out-of-plane collapse of the first infill; (ii) maximum interstory drift greater than: 1.00% for GLD (Masi et al., 2015) 1.35% for SSD (Rossetto and Elnashai, 2015) 2.00% for HSD (FEMA 356, 2000)
GC	Buildings that meet this PL level experience an incipient collapse with a high risk for the human life, due to extensive damage to structural and nonstructural components. Damage is not repairable from a technical and/or economical point of view.	First condition between: (i) the top displacement exceeds the value corresponding to a reduction of 50% of the peak lateral strength from POA. (ii) maximum interstory drift greater than: 1.50% for GLD (Masi et al., 2015) 3.00% for SSD (Rossetto and Elnashai, 2015) 4.00% for HSD (FEMA 356, 2000)

Finally, the GC performance level has been defined considering the lowest between the following displacement limits:

(i) the top displacement corresponding to a 50% reduction of the lateral strength of the RC frame (i.e. 50% reduction of the shear forces in the RC columns of the first storey) from POA;

(ii) the interstory drift limit associated with the attainment of a GC performance level for the main structure. The drift limit under consideration has been assumed equal to 1.50% for GLD buildings (in accordance with Masi et al. (2015)), 3.00% for SSD buildings (in accordance with Rossetto and Elnashai, 2003) and 4.00% for HSD buildings (in accordance with FEMA 356 (2000)).

1.4. STRUCTURAL RESPONSE

For each case study, a Push-Over Analysis (POA) in the short direction of the building (see Figure 10a) has been carried out with Opensees, considering, alternatively, a linear (modal proportional) and an uniform (mass proportional) force distribution along the height of the building, concentrated in the center of mass of each floor. Obviously, during POA, the behavior of the infills is governed by the first (undamaged) IP backbone curve only (see Figure 14).

As an example, Figure 17a shows the capacity curves derived from POA for the 8-storey GLD building, plotted in terms of base shear (V_b) vs. top floor displacement (d_{top}). In the same figure, the points corresponding to the attainment of 95% of the peak lateral strength (the force level before the peak) and strength reduction of 50% are also reported. Such values are used in the definition of the UPD and GC performance levels, respectively, as discussed before (see Table 6). Figure 17b compares the capacity curves of the three 8-storey buildings (linear force distributions). As expected, older buildings experience lower values of strength and initial stiffness (K_{in}) with a more pronounced strength reduction after the peak.

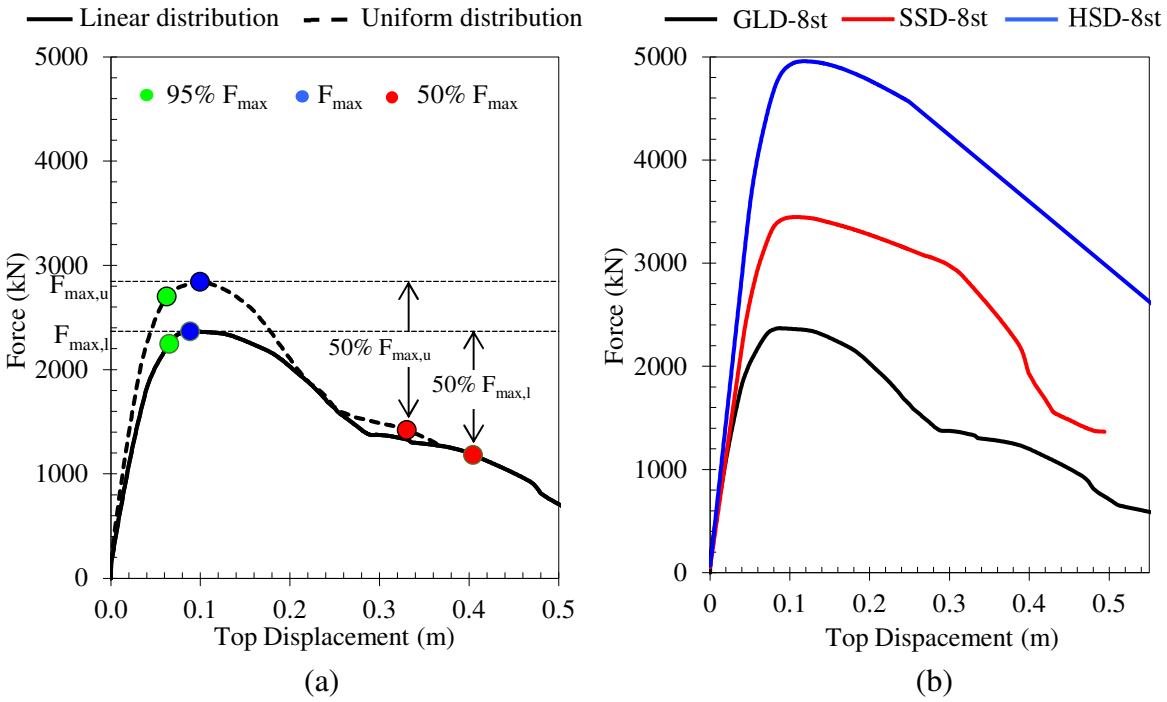

Figure 17 (a) Comparison between capacity curves derived using uniform and linear distribution for the GLD-8st, (b) Capacity curves of the GLD-8st, SSD-8st and HSD-8st building models.

Differences in terms of K_{in} are certainly due to the presence of stronger infills (t=300 mm) for the HSD model (compared to the SSD model) and to the presence of internal frames in the short direction for the SSD model (compared to the GLD model).

Table 7 summarizes the main results derived from POA, expressed in terms of (i) initial stiffness (K_{in}) (ii) maximum strength ($V_{b,max}$) normalized by the weight (W) of the building, (iii) top displacement corresponding to 95% of the peak lateral strength ($d_{top95\uparrow}$) and (iv) top displacement corresponding to 50% reduction of the peak strength ($d_{top50\downarrow}$). The values reported in Table 7 represent the lowest values from POA considering linear and uniform force distributions. As expected (Cardone, 2007), higher values of $V_{b,max}/W$, $d_{top95\uparrow}$ and $d_{top50\downarrow}$ are found for modern buildings (featuring higher seismic standards). The strength ratios ($V_{b,max}/W$) increases while decreasing the number of storeys of the building.

Table 7. Main results derived from pushover analysis for the case study analyzed

Case study	K_{ini} (kN/m)	F_{max}/W	$d_{,top95\uparrow}$ (mm)	$d_{,top50\downarrow}$ (mm)
GLD-6st	66667	0.107	51	217
GLD-8st	52667	0.076	65	398
SSD-4st	100020	0.252	50	189
SSD-6st	70000	0.158	58	357
SSD-8st	55667	0.111	75	426
HSD-6st	91667	0.207	63	378
HSD-8st	76667	0.160	81	518

1.4.1 Interstory drift profiles

Figure 18 shows some typical maximum IDR profiles (average values over 10 ground motion pairs) derived from NTHA for the SSD-6st building model, at three different seismic intensities (i.e. IM6, IM8 and IM10).

As can be seen, the IDR profiles feature a marked bulged shape with higher values at the mid-lower storeys of the building, which increase as seismic intensity increases. As a consequence, also the ductility demands tend to remain concentrated in the mid-lower storeys of the building, in accordance with what observed in (Cardone et al. 2017). Comparing NTHA results for the building models with and without IP/OOP interaction, negligible differences in terms of interstory drift profiles are observed (see Figure 18), regardless the seismic intensities.

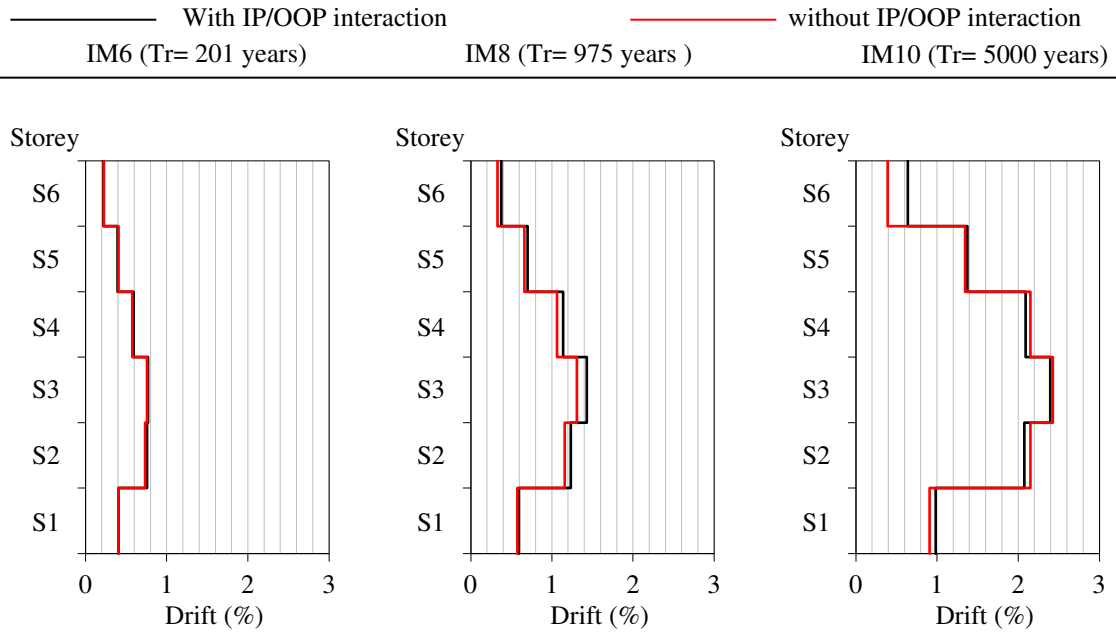

Figure 18 Maximum interstory drift profiles for the SSD-6st building model, considering or neglecting IP/OOP interaction.

This can be explained considering the strong degrading in-plane behavior of the infills, while increasing the interstory drift beyond the peak strength (see Figure 19), regardless the displacement (hence damage) experienced in the out-of-plane direction. In other words, the IP degrading behavior of the infill strongly affects the OOP performance of the infill but not vice versa. That's why, in most cases, the removal of some infills (due to OOP collapse) does not change significantly the maximum drift profile, which is still basically governed by the in-plane mechanical behavior of the infills.

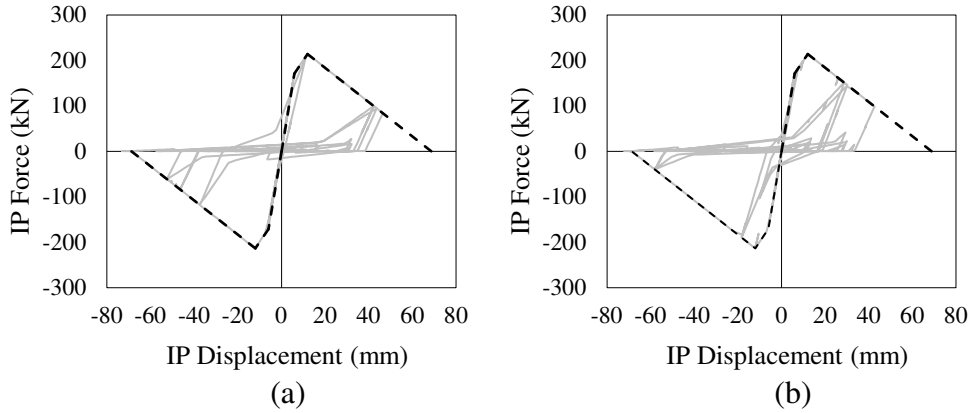

Figure 19 Typical IP force vs displacement cyclic behavior of infills observed during NTHA at the (a) 3rd and (b) 4th storey of the SSD-6st building

1.4.2 Damage scenario of masonry infills

Figure 20-Figure 22 show typical damage scenarios of masonry infills derived from NTHA. Results considering IP/OOP interaction for the infills are compared to results neglecting IP/OOP interaction. Based on the results of this study, which focuses on typical residential RC frame buildings, realized in Italy between '50s and '90, the following observations can be made:

(i) The OOP collapse mechanism is relevant only for the double-layer infills (with 100+100mm thickness, like those used in GLD and SSD buildings) due to the higher slenderness of the walls;

(ii) The extent of damage is overall greater considering IP/OOP interaction. However, when IP/OOP interaction is neglected, the frequency of occurrence of severe IP damage or IP collapse increases;

(iii) Comparing the performance of GLD and SSD building models (both featuring double-layer infills but differing in the structural characteristics of the frame and seismic hazard of the site), one can note that damage to infills is much more widespread and severe for the building located in the site with higher seismicity (L'Aquila), while it is little influenced by the best structural characteristics of the building model (SSD vs. GLD building models). The higher energy content of the L'Aquila records implies more loading cycles and larger displacement amplitudes, hence more pronounced IP/OOP strength and stiffness degradation experienced by masonry infills.

(iv) The progressive strength and stiffness degradation due to IP/OOP interaction plays a fundamental role in the extension, severity and development of infill damage, especially for medium- and high-rise buildings. Considering the 8-storey SSD building located in L'Aquila (higher seismic hazard) (see Figure 20a), for instance, the first OOP collapse of infills occurs at IM2 (Tr=50 years), at the top floor of the building (higher floor accelerations). As seismic intensity increases, passing from IM3 (Tr= 72 years) to IM6 (Tr=201 years), OOP collapse of the infills is registered also at the lower storyes (larger interstory drifts). For further increase of seismic intensity (from IM7 (Tr= 475 years) to IM8 (Tr= 975 years)), infill damage and IP/OOP collapse develop in the mid storeys of the building (mainly 3rd to 5th storey).

Finally, at very high seismic intensities (i.e. IM9 (Tr= 2475 years) and IM10 (Tr= 5000 years)), basically all the storeys of the building register a large number of events with severe IP damage and IP/OOP collapse. Neglecting the IP/OOP interaction (see Figure 20b), severe damage to the infills start to develop at IM6 (Tr=201 years), at the mid storeys of the building (mainly 2nd to 6th storey). While increasing the seismic intensity, severe damage and IP collapse tend to remain concentrated in the mid storeys of the building. First and top storeys are almost not affected by severe damage.

(v) As expected, the seismic intensity at which the first OOP collapse occurs progressively reduces while increasing the number of storeys of the building, being equal to IM6 (Tr=201 years) for the SSD-4st model, IM4 (Tr=101 years) for the SSD-6st model and IM2 (Tr=50 years) for the SSD-8st model.

(vi) The OOP collapse of the first infill tend to precede (first event occurs for lower seismic intensities) the onset of severe IP damage for mid- and high-rise buildings (IM2 vs. IM7 for the SSD-8st building model, IM4 vs. IM5 for the SSD-6st building model), while the contrary holds for low-rise buildings (IM6 vs. IM4 for the SSD-4st building model).

(vii) The first OOP collapse takes place at the upper storeys (higher floor accelerations) for high-rise building (e.g. at the 7th storey of the SSD-8st building), while at mid storeys (larger interstory drifts) for mid-to-low rise buildings (e.g. at the 3rd storey of the SSD-6st building and 2nd storey of the SSD-4st building).The HSD building models, featuring single-layer infills with lower slenderness ratio (h/t=8.33), do not experience any OOP collapse, even at the highest seismic intensities (i.e. IM9-IM10) during which only the IP collapse of the infills located at the mid-lower storeys (higher IDR values) is observed. A critical issue regards the relative importance between slenderness ratio (h/t) and in-plane damage towards the occurrence of OOP collapse. To this end, further NTHA have been run by replacing the single-layer infills (300 mm thickness) with the double-layer infills (100+100 mm thickness) in the HSD-8st building model. Comparing the seismic response and damage scenario of HSD-8st and SSD-8st building models, both with double-layers infills, it turns out that the percentage of infills that undergo OOP collapse is

significantly different, being (on average) equal to 34% for the HSD model and 52% for the SSD model at IM10, due to an increase of the average (over the height of the building) maximum IDR of the order of 20%. This proves that, although the slenderness of the infill is the main parameter governing its OOP behavior, also the in-plane damage plays a fundamental role.

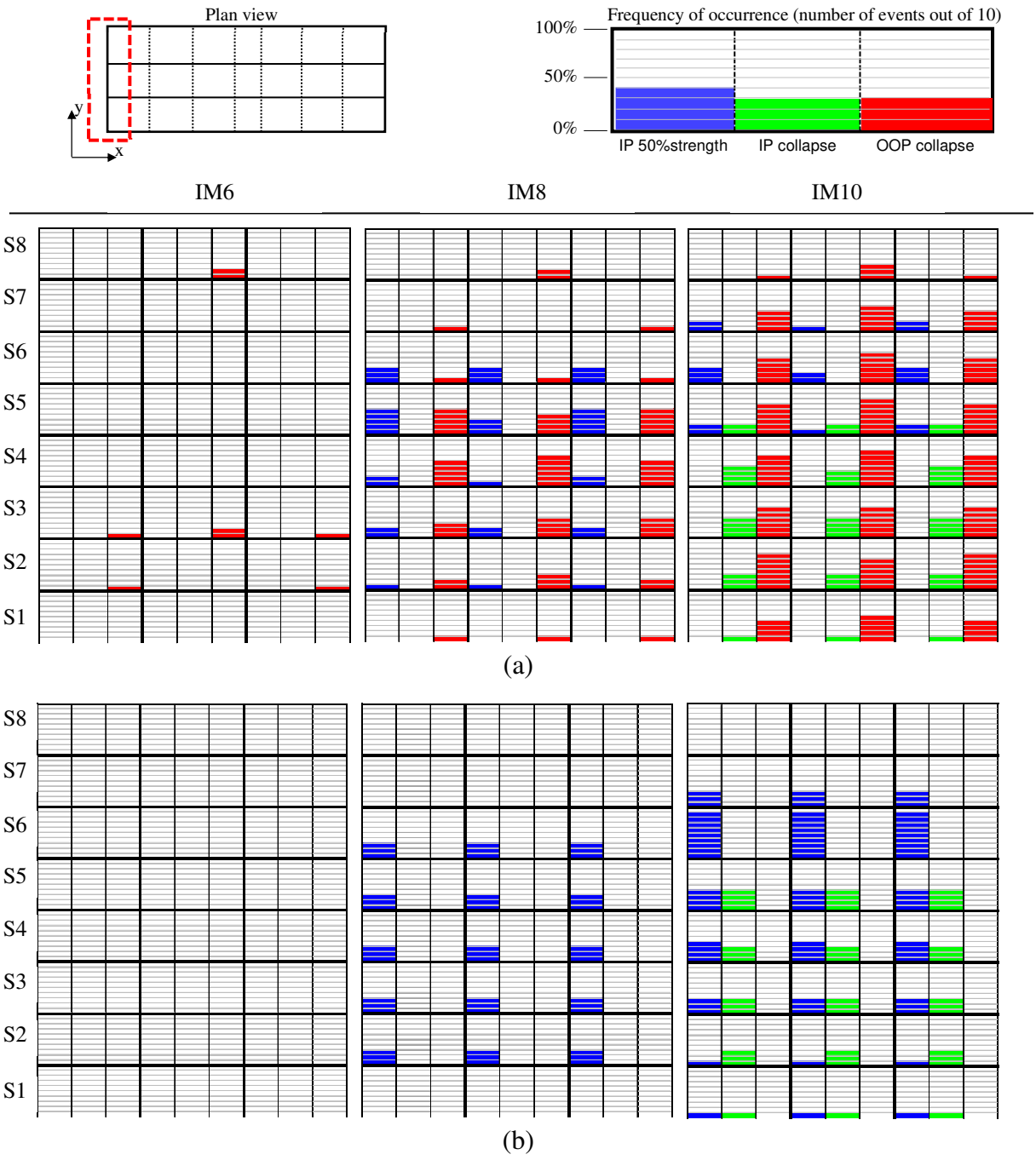

Figure 20 Damage scenarios of masonry infills at different earthquake intensity levels for the SSD-st8 building model located in the city of L'Aquila (high seismic hazard), (a) considering and (b) neglecting IP/OOP interaction

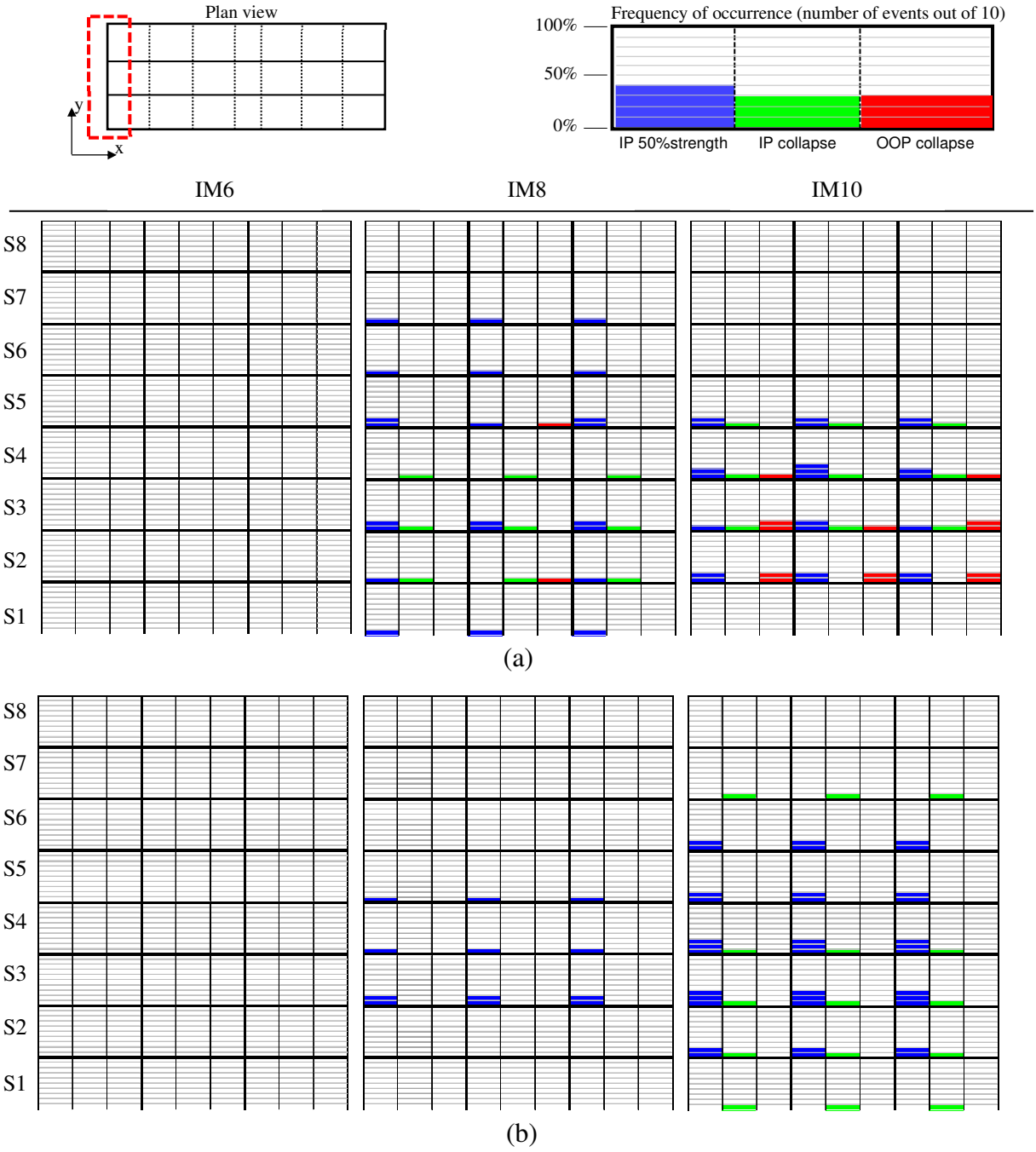

Figure 21 Damage scenarios of masonry infills at different earthquake intensity levels for the GLD-st8 building model located in the city of Napoli (medium seismic hazard), (a) considering and (b) neglecting the IP/OOP interaction

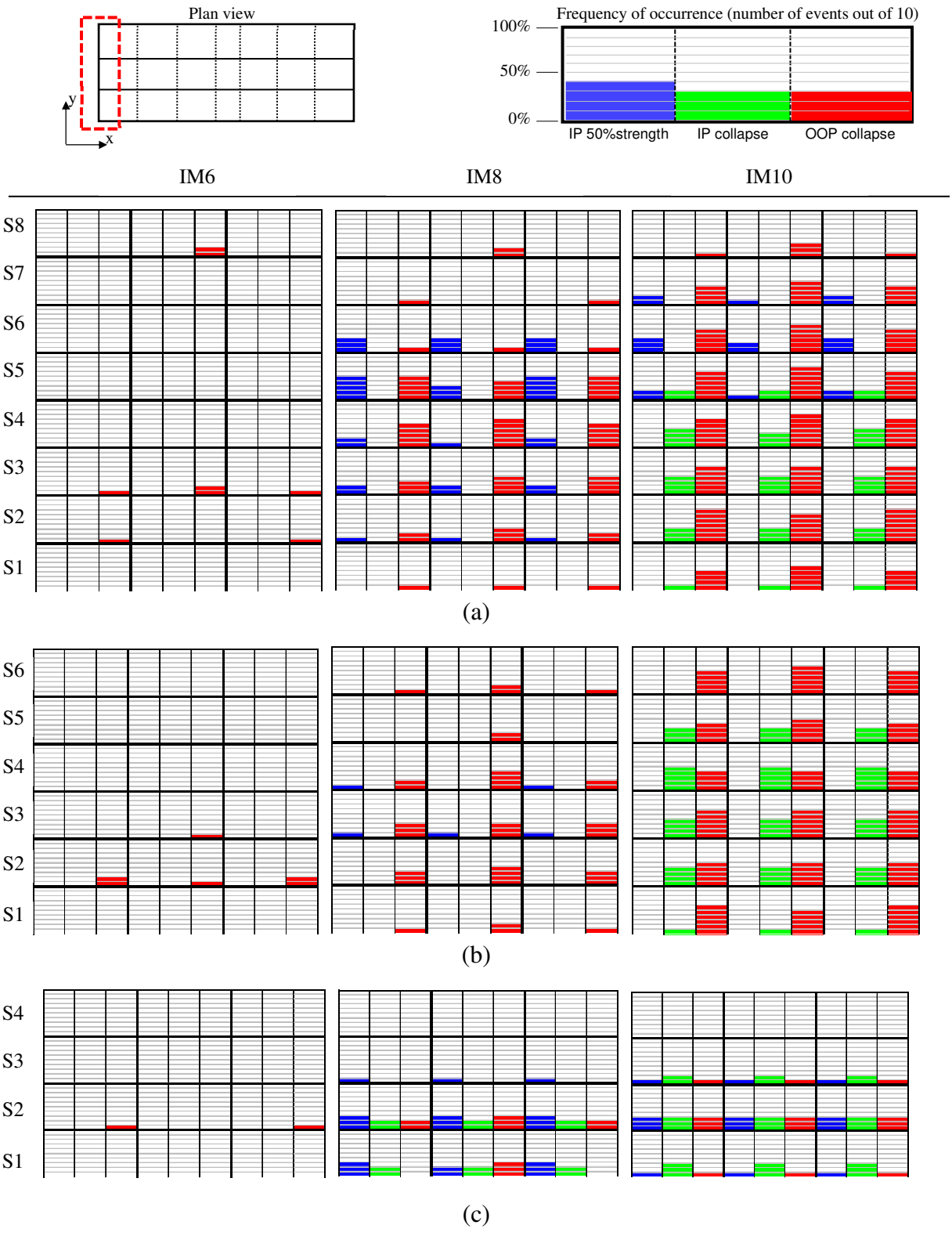

Figure 22 Damage scenarios of masonry infills at different earthquake intensity levels considering IP/OOP interaction: (a) SSD-st8, (b) SSD-st6 and (c) SSD-st4 building models located in the city of L'Aquila (high seismic hazard).

Table 8 shows the Average Percentage of Damage (APD) as a function of IM for the building models with IP/OOP interaction. The values reported in Table 8 represent the percentage of infills (average over 10 ground motion pairs) that experience: (i) Not-Repairable IP damage (NR(IP)) due to exceedance of the drift corresponding to a reduction of 50% of the infill strength; and (ii) Out-Of-Plane (OOP) collapse. Similar results are shown in Table 9 for the building models without IP/OOP interaction (in that case only the NR(IP) index is reported because OOP collapse is neglected).

The APD index is computed with the following equation:

$$APD = \frac{1}{10}\sum_{i=1}^{10}\frac{N_{damage,i}}{N_{infill}} \quad (5)$$

where $N_{damage,i}$ is the total number of the infills experiencing NR(IP) damage and OOP collapse, respectively, recorded during the "i-th" ground motion while N_{infill} is the total number of the infills.

By comparing the results reported in Table 8 and Table 9, one can note that considering the IP/OOP interaction results in a more severe and widespread damage scenario, especially at higher seismic intensity levels. For instance, the values of APD recorded for the models with IP/OOP interaction at IM8-IM10 are (on average) 1.5-1.8 times greater than for the models without IP/OOP interaction. This is mainly due to the significant percentage of infills that experience OOP collapses, especially for the SSD-6st and SSD-8st building models. For the SSD-4st building model, instead, the NR(IP) damage is preponderant (compared to OOP damage) even at the higher seismic intensities for two main reasons: (i) the lower acceleration demand at the upper storeys and (ii) the higher IDR at the lower storeys due to the lower fundamental period of vibration of the building and also to the lower stiffness of the RC frame for 4st building model.

Table 8. Average Percentage of Damage (APD) considering IP/OOP interaction

Building Model	Damage	IM1	IM2	IM3	IM4	IM5	IM6	IM7	IM8	IM9	IM10
SSD-4st	NR(IP)	0.00%	0.00%	0.00%	**1.25%**	**1.25%**	**1.25%**	**13.33%**	**30.83%**	**35.50%**	**44.17%**
	OOP	0.00%	0.00%	0.00%	0.00%	0.00%	**4.58%**	**5.42%**	**8.33%**	**9.17%**	**15.00%**
	NR(IP)+OOP	0.00%	0.00%	0.00%	**1.25%**	**1.25%**	**5.83%**	**18.75%**	**39.16%**	**44.67%**	**59.17%**
SSD-6st	NR(IP)	0.00%	0.00%	0.00%	0.00%	**1.67%**	**1.67%**	**3.61%**	**2.78%**	**16.11%**	**27.78%**
	OOP	0.00%	0.00%	0.00%	**1.39%**	**2.22%**	**3.33%**	**9.17%**	**21.67%**	**41.67%**	**52.50%**
	NR(IP)+OOP	0.00%	0.00%	0.00%	**1.39%**	**3.89%**	**5.00%**	**12.78%**	**24.44%**	**57.78%**	**80.28%**
SSD-8st	NR(IP)	0.00%	0.00%	0.00%	0.00%	0.00%	0.00%	**7.71%**	**15.63%**	**22.92%**	**26.46%**
	OOP	0.00%	**0.21%**	**0.63%**	**1.88%**	**2.50%**	**1.67%**	**17.29%**	**24.58%**	**38.54%**	**52.29%**
	NR(IP)+OOP	0.00%	**0.21%**	**0.63%**	**1.88%**	**2.50%**	**1.67%**	**25.00%**	**40.21%**	**61.46%**	**78.75%**
GLD-6st	NR(IP)	0.00%	0.00%	0.00%	0.00%	0.00%	0.00%	0.00%	**10.00%**	**18.06%**	**30.56%**
	OOP	0.00%	0.00%	0.00%	0.00%	0.00%	0.00%	0.00%	0.00%	**2.22%**	**9.17%**
	NR(IP)+OOP	0.00%	0.00%	0.00%	0.00%	0.00%	0.00%	0.00%	**10.00%**	**20.28%**	**39.72%**
GLD-8st	NR(IP)	0.00%	0.00%	0.00%	0.00%	0.00%	0.00%	**1.25%**	**10.83%**	**13.33%**	**15.79%**
	OOP	0.00%	0.00%	0.00%	0.00%	0.00%	0.00%	0.00%	**1.04%**	**2.92%**	**6.46%**
	NR(IP)+OOP	0.00%	0.00%	0.00%	0.00%	0.00%	0.00%	**1.25%**	**11.87%**	**16.25%**	**22.25%**

NR(IP): Not-Repairable infills due to IP damage/collapse; OOP: Out-Of-Plane collapse

Table 9. Average Percentage of Damage (APD) neglecting IP/OOP interaction

Building Model	Events	IM1	IM2	IM3	IM4	IM5	IM6	IM7	IM8	IM9	IM10
SSD-4st	NR(IP)	0.00%	0.00%	0.00%	0.00%	0.00%	0.00%	**5.00%**	**12.50%**	**41.53%**	**57.50%**
SSD-6st	NR(IP)	0.00%	0.00%	0.00%	0.00%	0.00%	0.00%	**3.33%**	**15.00%**	**40.00%**	**51.67%**
SSD-8st	NR(IP)	0.00%	0.00%	0.00%	0.00%	0.00%	0.00%	**5.00%**	**18.75%**	**36.25%**	**48.75%**
GLD-6st	NR(IP)	0.00%	0.00%	0.00%	0.00%	0.00%	0.00%	0.00%	**3.33%**	**15.00%**	**31.67%**
GLD-8st	NR(IP)	0.00%	0.00%	0.00%	0.00%	0.00%	0.00%	0.00%	**5.00%**	**15.00%**	**21.25%**

NR(IP): Not-Repairable infills due to IP damage/collapse

1.4.3 Code-conforming safety verifications of OOP collapse mechanisms

For the models without IP/OOP interaction, the OOP collapse of the infills can be verified by the simplified approaches provided by modern Codes. Herein, reference to the approach proposed in the Italian seismic Code (NTC2018) has been made, in which the OOP collapse of URM infills is checked a-posteriori comparing the OOP seismic demand to the infill computed with approximate relationships (F_h) with the OOP strength of the infill ($F_{max,OOP}$) derived from reliable formulations from the scientific literature and International Standards. Based on the NTC2018, the OOP seismic demand to the infills can be computed with the following equation:

$$F_h = S_a \cdot \frac{W_a}{g \cdot q} \tag{6}$$

where S_a is the seismic coefficient, corresponding to the maximum acceleration experienced by the infill wall, which can be estimated by a number of semi-empirical relationships as a function of: (i) Peak Ground Acceleration (PGA), (ii) fundamental periods of vibration of the building (T_1) and infill wall (T_a) in the OOP direction, (iii) building height (H), (iv) height of the non-structural element from the ground level (z); W_a is the weight of each single layer of the infill;

g is the acceleration of gravity (9.81 m/sec^2); q is the behavior factor of the infill, taken equal to 1 in accordance with (NTC2018).

As far as the infill strength ($F_{max,OOP}$) is concerned, lacking specific indications in the Italian seismic Code, reference to the formulations reported in three well-known International Standards has been made. They include the Eurocode 6 (2005) (see Eq. 7), the NZSEE-2017 (2017) (see Eq. 8) and FEMA-306 (2000) (see Eq. 9), which provide the OOP strength of the infill as a function of the main geometric characteristics (thickness: t, height: h, and width: w, all expressed in mm) and mechanical properties (compressive strength in the vertical direction: f_{mv}, expressed in MPa or N) of the infill.

$$F_{max,OOP} = \left[f_{mv} \cdot \left(\frac{t}{h}\right)^2 \right] \cdot w \cdot h \tag{7}$$

$$F_{max,OOP} = \left[730\gamma (f_{mv})^{0.75} t^2 \left(\frac{\alpha}{w^{2.5}} + \frac{\beta}{h^{2.5}} \right) \right] \cdot w \cdot h \tag{8}$$

$$F_{max,OOP} = \left[\frac{2 f_{mv}}{(h/t)} \cdot R_1 R_2 \lambda \right] \cdot w \cdot h \tag{9}$$

It is worth noting that, unlike the EC6 (2005), the NZSEE-2017 (2017) and FEMA 306 (2000) code provisions explicitly take into account possible OOP strength reduction due to IP damage through the coefficients γ (see Eq. 8) and R_1 (see Eq. 9), respectively. In particular, the coefficient γ is expressed as a function of the infill vertical slenderness ratio (h/t), while R_1 is expressed as a function of h/t and of the entity of IP damage, assumed as moderate in this study (ref. to Table 8-5 of FEMA 306 (1998)). Moreover, the NZSEE-2017 (2017) and FEMA 306 (1998) take also into account the deformability of the surrounding RC frame, through the coefficients α and β (see Eq. 8) and the coefficient R_2 (see Eq. 9), respectively, which depend on the flexural rigidity of the adjacent RC beams and columns. Assuming the slenderness ratio (l) equal to 0.015 (see Eq. (9)), the OOP strength provided by the FEMA 306 approximately coincides with that predicted by NZSEE.

Figure 23 shows the outcome of the code-conforming OOP collapse safety verifications for the SSD and GLD building models. For comparison, in the same figure there is also a brief

summary of the NTHA results derived from the model with IP/OOP interaction. In the latter case, OOP collapse is deemed to occur when for at least one panel of that storey is attained collapse for at least 50% of seismic events. Looking at Figure 23, one can conclude that the Eurocode 6 (2005) formulation is not conservative overestimating the OOP capacity of masonry infills, especially at the mid-to-lower storeys of the building. On the other hand, the approaches proposed in the NZSEE-2017 (2017) and FEMA-306 (1998) tend to be too conservative, especially for low-rise buildings.

The Code-conforming safety verifications for the HSD building models located in the city of L'Aquila, do not predict any OOP collapse, in good accordance with the NTHA results.

Table 10 compares the percentages of infills that undergo OOP collapse derived considering three alternative approaches, i.e.: (i) NTHA of the model with IP/OOP interaction, (ii) code-conforming OOP safety verifications using either EC6 or FEMA/NZSEE relationships.

Table 10. Percentages of infills that undergo OOP collapse considering alternative analysis and verification approaches

Building Model	Damage State	IM1	IM2	IM3	IM4	IM5	IM6	IM7	IM8	IM9	IM10
SSD-4	$OOP_{\_NTHA}$	0.00%	0.00%	0.00%	0.00%	0.00%	**4.58%**	**5.42%**	**8.33%**	**9.17%**	**15.00%**
	$OOP_{\_EC6}$	0.00%	0.00%	0.00%	0.00%	0.00%	0.00%	0.00%	0.00%	0.00%	0.00%
	$OOP_{\_FEMA/NZSEE}$	0.00%	0.00%	0.00%	0.00%	0.00%	0.00%	0.00%	**25.00%**	**50.00%**	**75.00%**
SSD-6	$OOP_{\_NTHA}$	0.00%	0.00%	0.00%	**1.39%**	**2.22%**	**3.33%**	**9.17%**	**21.67%**	**41.67%**	**52.50%**
	$OOP_{\_EC6}$	0.00%	0.00%	0.00%	0.00%	0.00%	0.00%	0.00%	0.00%	**16.67%**	**50.00%**
	$OOP_{\_FEMA/NZSEE}$	0.00%	0.00%	0.00%	0.00%	0.00%	**16.67%**	**50.00%**	**83.33%**	**83.33%**	**100.00%**
SSD-8	$OOP_{\_NTHA}$	0.00%	**0.21%**	**0.63%**	**1.88%**	**2.50%**	**1.67%**	**17.29%**	**24.58%**	**38.54%**	**52.29%**
	$OOP_{\_EC6}$	0.00%	0.00%	0.00%	0.00%	0.00%	0.00%	0.00%	0.00%	0.00%	**12.50%**
	$OOP_{\_FEMA/NZSEE}$	0.00%	0.00%	0.00%	0.00%	0.00%	0.00%	**12.50%**	**37.50%**	**62.50%**	**87.50%**
GLD-6	$OOP_{\_NTHA}$	0.00%	0.00%	0.00%	0.00%	0.00%	0.00%	0.00%	0.00%	**2.22%**	**9.17%**
	$OOP_{\_EC6}$	0.00%	0.00%	0.00%	0.00%	0.00%	0.00%	0.00%	0.00%	0.00%	0.00%
	$OOP_{\_FEMA/NZSEE}$	0.00%	0.00%	0.00%	0.00%	0.00%	0.00%	0.00%	**33.33%**	**50.00%**	**66.67%**
GLD-8	$OOP_{\_NTHA}$	0.00%	0.00%	0.00%	0.00%	0.00%	0.00%	0.00%	**1.04%**	**2.92%**	**6.46%**
	$OOP_{\_EC6}$	0.00%	0.00%	0.00%	0.00%	0.00%	0.00%	0.00%	0.00%	0.00%	0.00%
	$OOP_{\_FEMA/NZSEE}$	0.00%	0.00%	0.00%	0.00%	0.00%	0.00%	0.00%	0.00%	**12.50%**	**37.50%**

OOP_{NTHA}: Percentage of out-of-plane collapse from NTHA; OOP_{EC6}: Out-of-plane collapse safety verifications by EC6; $OOP_{FEMA/NZSEE}$: Out-of-plane collapse safety verifications by FEMA/NZSEE.

Based on NTHA results (see Table 10), FEMA/NZSEE code provisions seem to overestimate the number of OOP collapses (conservative approach) in a wide range of seismic intensities (Tr ≥ 200 years) for the SSD building models located in L'Aquila (high seismic hazard for Italy) and also at the highest seismic intensities (Tr ≥ 975 years) for the GLD building models located in Naples (medium seismic hazard). Considering the SSD-6st building model, for instance, the FEMA/NZSEE standards predict OOP collapse for the 80% to 100% of infills at IM8-IM10, while the same percentage turns out to be (on average) 4 times less at IM8 and 2 times less at IM9-IM10 based on NTHA results. On the other hand, the approach proposed in the EC6

appears poorly conservative, especially for the SSD building models located in high seismicity region.

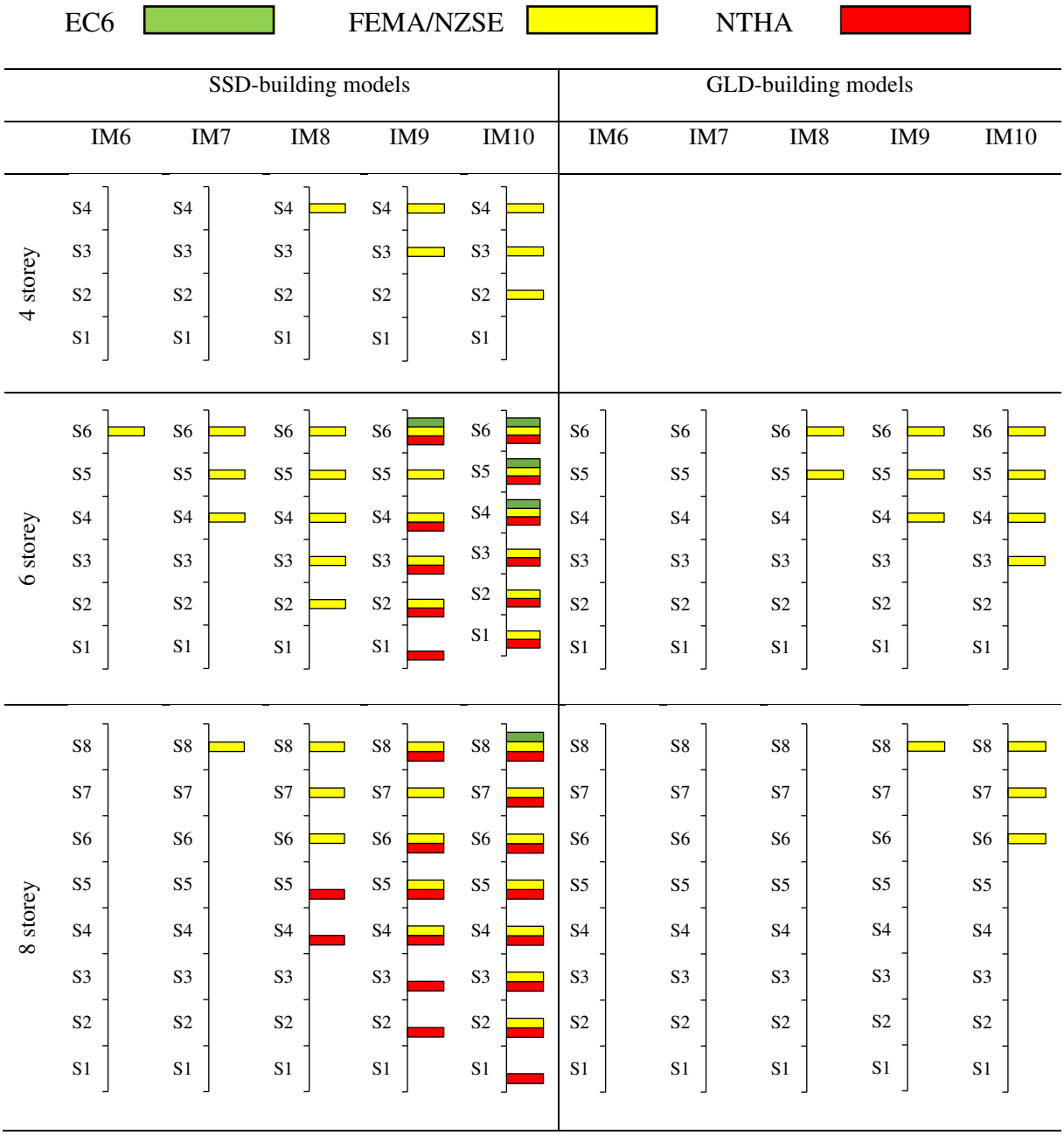

Figure 23 Comparison between NTHA results and Code-conforming safety verification of OOP collapse mechanisms for (left) SSD building models located in the city of L'Aquila (high seismic hazard) and (right) GLD building models located in the city of Napoli (medium seismic hazard).

1.5. DEVELOPING FRAGILITY CURVES

Fragility Curves (FCs) associated with the attainment of UPD and LS performance levels (see Table 6) have been derived for the GLD and SSD building models, based on the NTHA results of the models with and without IP/OOP interaction. The GC performance level has been neglected because the frequency of occurrence of seismic events associated with the attainment of this PL was always less than 50%.

FCs are expressed by a cumulative lognormal distribution with median value ϑ and logarithmic standard deviation (or dispersion) β. FCs provides the conditional probability of the building models to exceed given Performance Levels (PLs), as a function of given seismic intensity measures. Herein, FCs have been developed in terms of spectral acceleration at the effective period of vibration of the buildings (mean value in the two horizontal directions), $S_a(T^*)$, defined for each IM considering the seismic hazard of the site (see Table 3).

A best fit regression analysis of the frequencies of occurrence of seismic records associated with the attainment of each PL has been followed to derive the median ϑ and dispersion β_r due to record-to-record variability. Figure 24 shows the fitted lognormal cumulative distribution functions associated with UPD and LS performance levels, separately for the models with and without IP/OOP interaction.

As expected, for a given probability of exceedance (e.g. 50%), the spectral accelerations corresponding to the attainment of LS performance level are greater than those associated with the UPD performance levels. However, the margin reduces while increasing the number of storeys of the building.

Figure 24 points out that when IP/OOP interaction is considered, the UPD performance level would not be likely to be observed (probability of occurrence less than 10%) for spectral accelerations (on average) smaller than around 0.18g (with a lowest value of 0.13g for the GLD-8st buildings and a maximum value of 0.27g for the SSD-4st building), but it is almost certain to occur (probability of occurrence greater than 90%) for spectral accelerations (on average) greater than around 0.35g (with a lowest value of 0.27g for the GLD-8st building and a maximum value of 0.50g for the SSD-4st building). Neglecting IP/OOP interaction for the infills, the aforesaid average values increase to 0.20g (probability of occurrence less than 10%)

and to 0.45g (probability of occurrence greater than 90%). As a consequence, one can conclude that the UPD performance level is little affected by the IP/OOP interaction of URM infills.

Taking into account IP/OOP interaction of infills in the model, the LS performance level is not likely to be observed (probability of occurrence less than 10%) for spectral accelerations (on average) smaller than around 0.36g (with a minimum value of 0.20g for the SSD-8st building and a maximum value of 0.56g for the SSD-4st building), but it is almost certain to occur (probability of occurrence greater than 90%) for spectral accelerations (on average) greater than around 0.83g (with a minimum value of 0.62g for the SSD-8st building and a maximum value of 1.00g for the SSD-4st building). Neglecting IP/OOP interaction, the aforesaid values increase (on average) to 0.59g (probability of occurrence less than 10%) and to 0.94g (probability of occurrence greater than 90%), respectively.

The same trend is observed for the GLD buildings. Considering the IP/OOP interaction, indeed, the LS performance level is not likely to be observed (probability of occurrence less than 10%) for spectral accelerations (on average) smaller than around 0.27g but it is almost certain to occur (probability of occurrence greater than 90%) for spectral accelerations (on average) greater than around 0.51g. Neglecting IP/OOP interaction, the aforesaid average values increase to 0.30g and 0.64g, respectively. As a consequence, one can conclude that the LS performance level is significantly affected by the IP/OOP interaction of infills, especially in high seismicity regions.

Table 11 summarizes the median values (in terms of spectral acceleration at the fundamental period of vibration of the building) and dispersion of the fragility curves derived. As a matter of fact, neglecting the IP/OOP interaction of infills, the median values (50% probability of exceedance) associated with LS performance level increase on average by about 38% for SSD building models located in L'Aquila (high seismic hazard), and by about 18% for the GLD building models located in Naples (moderate seismic hazard).

Looking at Table 11, one can note that the median values reduce with the number of storeys of the building. For instance, median values associated with the attainment of the UPD (LS) performance levels reduce from approximately 0.37g (0.75g) for the SSD-4st model to 0.27g (0.52g) for the SSD-6st model and 0.21g (0.35g) for the SSD-8st model, due to the premature OOP collapse of some infills. A similar trend is observed also for the GLD building models.

It is interesting to note that, despite the differences in terms of seismic hazard and structural characteristics between GLD and SSD building models, the median values associated with the attainment of UPD and LS performance levels differ no more than 20%, meaning that the most important parameter is represented by the type of infill and its characteristics.

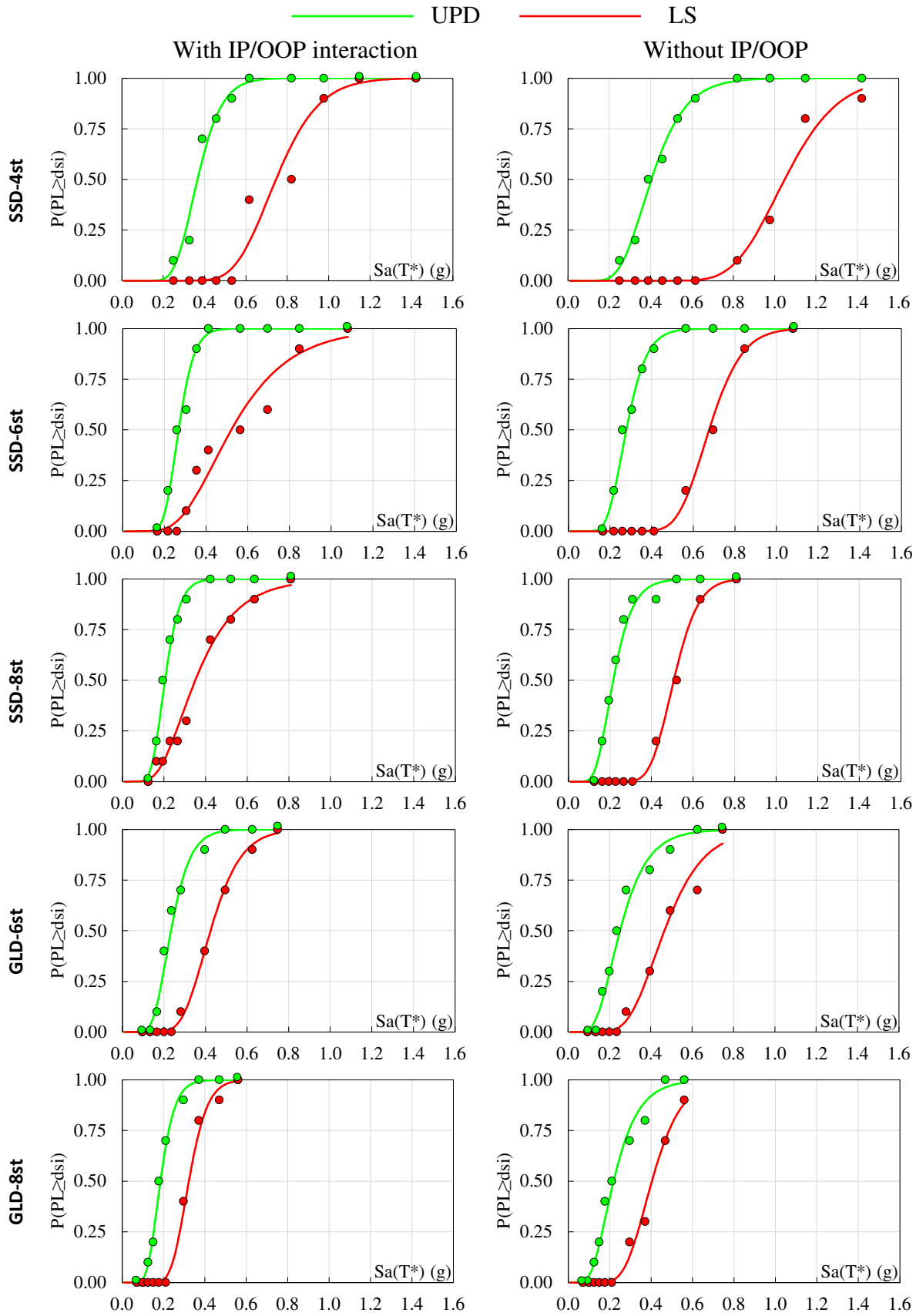

Figure 24 Fragility curves associated with UPD and LS performance levels for SSD and GLD building models.

Table 11. Values of median spectral acceleration Sa(T*) (ϑ) and corresponding dispersion (β_r) of fragility curves associated with UPD and LS performance levels.

Building model	with IP/OOP interaction				without IP/OOP interaction			
	UPD		LS		UPD		LS	
	θ	β_r	θ	β_r	θ	β_r	θ	β_r
SSD-4st	0.37	0.25	0.75	0.22	0.40	0.32	1.05	0.19
SSD-6st	0.27	0.22	0.52	0.42	0.28	0.27	0.68	0.18
SSD-8st	0.21	0.27	0.35	0.45	0.22	0.34	0.51	0.18
GLD-6st	0.23	0.31	0.42	0.27	0.25	0.41	0.47	0.32
GLD-8st	0.19	0.29	0.32	0.22	0.21	0.43	0.40	0.28

Generally speaking, the total dispersion of a FC, β, should take into account also other sources of uncertainty, beyond record-to-record variability (β_r). They include (i) the modeling variability (β_m) and (ii) the uncertainty in the definition of the threshold limits of each PL (β_{th}). In first approximation, in accordance with ATC-58 (2012), β_m can be assumed equal to 0.1 for the model with IP/OOP interaction and equal to 0.4 for the model without IP/OOP interaction considering the quality and completeness of the numerical model used in the analysis (including the relevance of the semi-empirical relationships adopted for the description of the IP/OOP degrading behavior of masonry infills and the representativeness of the experimental data considered to derive those relationships). As far as β_{th} is concerned, values of the order of 0.1-0.3 can be assumed in accordance with Spillatura (2017). The three dispersion values can be then combined using the square root of the sum of squares rule, while keeping the same median value.

1.6. SUMMARY AND RESULTS

In this section, the influence of the interaction between In-Plane (IP) and Out-Of-Plane (OOP) behavior of masonry infills on the seismic performance of typical residential RC buildings, realized in Italy between '50s and '90s, has been examined.

Accurate 3D lumped plasticity models of infilled RC frame buildings have been implemented in OpenSees. A V-shaped bi-diagonal struts macro-element has been used for masonry infills, adopting the modelling approach proposed by Di Domenico et al (2017) and the semi-empirical relationships derived by Ricci et al. (2018a,b) to account for the IP/OOP interaction of infills.

Seven archetype buildings, differing in terms of age of construction ('50s to '90s), number of storeys (from 4 to 8), seismic design approach (gravity loads design, low seismic forces with substandard details, modern seismic design) and type of masonry infills (thin double-layers infills with inner cavity and thick single-layer infills) have been analyzed. The building models have been located in two different sites (Napoli and L'Aquila), featuring moderate and high seismic hazard for Italy, respectively.

Extensive Nonlinear response-Time History Analyses (NTHA) have been carried out for ten earthquake intensity levels, with return periods ranging from 30 years to 5000 years. Seismic performances have been evaluated considering two different Performance Levels (PLs), referred to as: Usability Preventing Damage (UPD), and Life Safety (LS). NTHA have been repeated considering a non-degrading IP-only model for infills, in order to assess the relevance of the IP/OOP interaction and degrading behavior of masonry infills towards the seismic performance of RC frame buildings. Code-conforming simplified approaches, adopted in current practice, have been considered for the models without IP/OOP interaction, in order to check a-posteriori the OOP collapse of infills.

Based on the results of this study, the following main conclusions can be drawn:

(i) Although the slenderness ratio (h/t) is the main parameter governing the OOP behavior of URM infills, also the in-plane damage plays a fundamental role towards the OOP seismic performance of the infills;

(ii) The OOP collapse mechanism results particularly relevant for double-layer infills characterized by relatively high values of slenderness (h/t≈ 25 ÷30); single-layer infills,

characterized by relatively low values of the slenderness (h/t≈ 8 ÷10), are little affected by IP/OOP interaction; however, the interaction could be high (in terms of reduced OOP capacity due to IP damage)

(iii) For mid- and high-rise RC buildings with double-layer infills, the IP/OOP interaction leads to higher damage of infills at high seismic intesities (up to 1.5-2 times collapsed or not repairable infills compared to building models without IP/OOP interaction); IP/OOP interaction, in fact, takes into account a further cyclical deterioration of the infill walls due to both in-plane and out-of-plane displacements that traditional models are unable to capture

(iv) The simplified approaches proposed in the modern codes for the safety verification of the OOP collapse mechanisms of infills can significantly overestimate (ref. to FEMA-306/NZSEE-2017) or underestimate (ref. to EC6) the number of OOP collapses;

(v) Considering the IP/OOP interaction of URM infills in the numerical model does not influence a lot the UPD (Usability-Preventing Damage) performance level of RC buildings (changes in the median values of fragility curves less than 10% in terms of spectral acceleration) but can significantly affect the seismic performance of the RC buildings in terms of LS (Life Safety) performance level (changes in the median values of fragility curves (on average) greater than 30% in terms of spectral acceleration).

SECTION 2:
SEISMIC PERFORMANCE OF MASONRY INFILLS IN BASE ISOLATED BUILDINGS

2.1 INTRODUCTION

Among the different structural types required by the codes, in the recent years, an increasing interest has been showed for the isolated structures, especially after the destructive seismic events occurring in Italy. In fact, base isolation is one of the most common and effective techniques used for seismic protection of buildings and their equipment.

The technique of seismic base isolation of a structure consists in interposing between the ground, on which the foundations are placed, and the structure in elevation a series of elements of low horizontal stiffness, high rigidity vertical stiffness, and high dissipative capacities, which greatly reduce the acceleration perceived by the structure. In this way a dynamic decoupling of the horizontal motion of the structure and of the ground is thus created, which drastically reduces the energy transmitted by the earthquake to the superstructure.

Such a designed isolation system keeps the structure in an elastic range by drastically reducing ground motion accelerations, and allows the structure to withstand strong earthquakes without significant structural damage. These systems need to accommodate large relative displacements in a short space and are thus equipped with particular components properly designed. The isolation system is required to bear the gravity loads of the superstructure and the non-seismic vertical and lateral forces such as wind loads, to avoid engaging the lateral motion when it is not required. Isolation systems are thus provided with a low horizontal stiffness capable of retaining them from moving for low stresses, with a large horizontal capacity, and with a geometry and materials capable of granting the ability to support vertical loads. The increasing of fundamental period reduces, on the one hand, the accelerations on the superstructure, but increases, on the other hand, the spectral displacements. In order to avoid excessive lateral displacements which would affect the design and the safety of building systems, isolation systems feature bearings which are characterized by proper restoring capabilities, or bearings without any restoring capability coupled by supplemental dissipative and recentring devices. Nowadays the base isolation technique is being more and more implemented in the seismic retrofit of existing structures designed with outdated building codes. The social and economic benefits of seismic isolation find their maximum expression in the application onto buildings that are required to remain completely operational even after a strong earthquake, such as hospitals and fire stations and on structures with a content value much higher than that of the structural components, such as museums and banks.

Currently the isolation device (industrial) production is dominated by two main typologies: high damping elastomeric bearings (HDRBs) and friction pendulum sliders (FPSs). Recently, the use of hybrid systems obtained by combining elastomeric devices (HDRBs) and flat surface sliders (FSBs), is increasing. As a matter of fact, the aforesaid configuration is able to guarantee a suitable deformability of the isolation system without compromising the restoring capability and torsional stiffness of the system and prevent uplift phenomena in the sliding bearings.

The present section is part of the RELUIS project (available at http://www.reluis.it) regarding the "implicit risk" assessment of Italian code-conforming and pre-code buildings. The latter is a large research work aimed at assessing the seismic structural reliability, expressed in terms of annual failure rate, of code-conforming and pre-code structures in Italy.

The current Italian code provisions, (NTC 2018) allow engineers to design seismic resistant structures with a certain amount of safety for the attainment of performance levels (e.g., Collapse Limit State – CLS – or Life Safety Limit State – LLS). Although compliance to the code requirements for the capacity design guarantees a certain level of safety, the designer doesn't have any tool to be able to determine probability that the structure, in its life span, under seismic design intensities, will reach (or even exceed) a given performance level. Moreover, the code does not provide an explicit assurance that different structures designed for the same site, or similar structures at different sites, would be characterized by the same safety margin for a given performance level.

The project RINTC (Rischio Implicito delle strutture progettate secondo le NTC, in Italian) conducted the first studies which systematically addressed the issue of estimating such probabilities for several classes of buildings designed according to the current code provisions in Italy (ReLUIS, RINCT Workgroup, 2018), (RINCT Workgroup, 2018a), (RINCT Workgroup, 2018b), (http://www.reluis.it/, ReLUIS). These probabilities of failure knowledge would be a good basis for further considerations regarding the acceptability of the safety margin of current-code-conforming structures. This implies that the performance level failure for these buildings has been assumed to occur when specific, deterministically chosen threshold values for the Engineering Demand Parameters (EDPs) chosen to monitor the structural response, are exceeded. Finally, soil has not been modelled nor its failure accounted for. The defined failure criteria and associated EDP threshold values do not imply that, when exceeded the structure is

expected to experience a total collapse. Thus, reaching or even exceeding such values may result in a structure still standing but completely unserving and unrepairable.

The 2019-2021 RINTC project (RINTC-e project) is the extension of the 2015-2017 RINTC project that assessed, explicitly, the seismic risk of code-conforming Italian structures (i.e., designed according to the seismic code currently enforced). The aim of the RINTC-e project is to extend the methodological framework developed in RINTC to the existing structures (designed and built before 2008), which constitute the vast majority of Italian building stock. In particular, five structural typologies were considered: masonry, reinforced concrete, pre-cast reinforced concrete, steel, and seismically isolated buildings. In the framework of the 2018 project, several archetype structures for each typology have been designed and/or retrofitted according to standard practices consistent with outdated codes, enforced since the eighties, for five sites across Italy spanning a wide range of seismic hazard levels (evaluated according to current standards). The seismic vulnerability of the designed structures was assessed by subjecting three-dimensional nonlinear computer models to multi-stripe non-linear dynamic analysis. Integration of the probabilistic hazard and probabilistic vulnerability (i.e., fragility) yields the annual failure rate for each of the designed and modelled structure.

This section describes the nonlinear analyses carried out on existing RC buildings retrofitted using the seismic isolation technique. Different hazard performance levels ranging from service to design and collapse conditions have been examined. In particular, in this study, the isolation system adopted at the base level of the selected case study buildings is represented by an hybrid isolation system composed by High Damping Rubber Bearings (HDRBs) and Flat Sliding Bearings (FSBs).

In this section, the seismic performance and structural reliability of existing RC frame buildings, seismically retrofitted by base-isolation, are investigated. This is done by performing extensive Multi-Stripe nonlinear dynamic Analyses (*MSAs*) (Jalayer, 2003) of a set of archetype residential RC buildings, differing for construction period (50s-60s, 70s, 80s-90s) design approach (Gravity Load Design and Seismic Load Design based on old technical standards, referred to as GLD and SLD respectively) and building location. In particular, according to the evolution of seismic standards in Italy, GLD buildings are supposed to be located in the city of Naples (characterised by medium seismic hazard for Italy) and SLD buildings are supposed to be located in the city of L'Aquila (characterised by high seismic hazard for Italy). In particular,

in this study, the isolation system adopted at the base level of the selected case study buildings is represented by an hybrid isolation system composed by High Damping Rubber Bearings (HDRBs) in combination with Flat Sliding Bearings (FSBs).

The retrofit interventions were designed in accordance with the NTC18 minimum requirements, following a design approach similar to that proposed in (Matsangar and Jangid, 2008). For all the buildings advanced numerical models have been used for both RC members and seismic isolators.

Two different performance levels are examined, namely: Global Collapse (GC) prevention and Usability Preventing Damage (UPD). The GC performance level is assumed to occur when either the superstructure or the isolation system fails, considering different failure modes for both RC members and isolation devices, as well as suitable collapse conditions for the structure as a whole. Indeed, isolation system and the superstructure represent two elements of the same in-series system. The occurrence of the *UPD* has been assessed based on a multi-criteria approach combining the following main concepts: (*i*) reparability of non-structural elements, (*ii*) full protection of structural elements and (*iii*) no interruption of use of the building after frequent seismic events.

2.2 CASE STUDIES

2.2.1. Archetype Buildings

Figure 25 shows the typical floor plan of the two groups of archetype buildings examined in this study, namely: Gravity Load Design (GLD) buildings (see Figure 25(a)) and Seismic Load Design (SLD) buildings (see Figure 25(b)). The buildings are intended for residential use. They feature 5 x 3 bays and 6 stories above ground. The floor area of the buildings is approximately 240 square meters. The 1st floor height is equal to 3.4 m while that of all the other stories is equal to 3.05 m. The RC frames include knee-joint beams designed to bear the staircases. According to NTC2018, the buildings can be defined as regular, both in plan and in elevation.
Both the GLD and the SLD building groups include three case studies, differing for construction period (50s-60s, 70s, 80s-90s), material and structural characteristics. The building configuration is the same for the all the buildings while they differ for some structural characteristics only, such as the presence (or not) of internal beams in the long direction, the size of beam/column cross sections and the corresponding reinforcement ratios.
The GLD buildings are supposed to be located in the city of Naples (southern Italy), which is characterized by a medium level of seismic hazard for Italy. The SLD buildings are supposed to be located in the city of L'Aquila (central Italy), which is characterized by a high level of seismic hazard for Italy.
The buildings have been defined by means of simulated design (Ricci et al., 2019), in accordance with old technical standards. In particular, the buildings located in Naples (labelled as NA_{GLD} in the following) have been designed for gravity loads only according to (D.M. 30/05/1974). The buildings located in L'Aquila (labelled as AQ_{SLD} in the following) have been defined based on a simulated Seismic Load Design (*SLD*), considering low seismic force levels, in accordance with older seismic classifications standards (D.M. 14/2/1992) and outdated technical standards (D.M. 24/1/1986). Table 12 shows a summary of considered case studies and their relative design code.

Table 12. Summary of case studies considered

Site	Label	Construction age	Design Codes
L'Aquila	S60	1950s-60s	RD 640/1935 – RD 2229/1939
	S70	1970s	L 1684/1962 – DM 30/05 1972 – DM 30/05/1974
	S80	1980s-90s	DM 27/07/1985 – DM 24/07/1986 – DM 14/02/1992
Naples	G60	1950s-60s	RD 2229/1939
	G70	1970s	DM 30/05 1972 – DM 30/05/1974
	G80	1980s-90s	DM 27/07/1985 - DM 14/02/1992

Concerning the structural configuration, the outer beams of all the buildings are deeper than the slab, while internal beams are flat. In the NA_{GLD} buildings, the internal beams are positioned along the short-direction only. All the stories feature the same slab (one way RC slab with hollow clay bricks), whose total thickness is equal to 250mm.

It is worth noting that in the base-isolated configurations, a supplementary floor, realized by a grid of RC beams, has been added at the bottom of the ground storey.

Table 13 summarizes the main structural characteristics of the GLD and SLD buildings, i.e.: (i) ΣA_col/A_floor = total column area /total floor area; (2) $\rho_{c,1,m}$ = average columns' longitudinal reinforcement ratio, (3) $\rho_{b\_deep,1,m}$ = average deep beams' longitudinal reinforcement ratio (top and bottom), (4) $\rho_{b\_flat,1,m}$ = average flat beams' longitudinal reinforcement ratio (top and bottom).

Table 13. Main structural characteristics of the existing RC frame buildings examined in this study.

Type	Construction period	ΣA_col/A_floor (%)	$\rho_{c,1,m}$ (%)		$\rho_{b\_deep,1,m}$ (%)	$\rho_{b\_flat,1,m}$ (%)
GLD 6-story	1950s-60s	1.54	0.68÷0.86	Top	0.15÷1.05	0.36÷0.97
				Bottom	0.15÷0.84	0.28÷1.04
	1970s	1.63	0.50÷0.75	Top	0.15÷0.40	0.30÷1.01
				Bottom	0.15÷0.84	0.24÷0.69
	1980s-90s	1.39	1.03÷2.51	Top	0.15÷0.40	0.36÷0.82
				Bottom	0.15÷0.63	0.31÷0.73
SLD 6-story	1950s-60s	2.19	0.50÷1.57	Top	0.27÷1.05	0.30÷1.44
				Bottom	0.22÷0.87	0.30÷0.72
	1970s	1.74	0.67÷2.44	Top	0.27÷1.05	0.30÷0.69
				Bottom	0.22÷0.87	0.30÷0.46
	1980s-90s	1.71	1.12÷2.90	Top	0.33÷0.57	0.60÷1.07
				Bottom	0.33÷0.46	0.60÷1.07

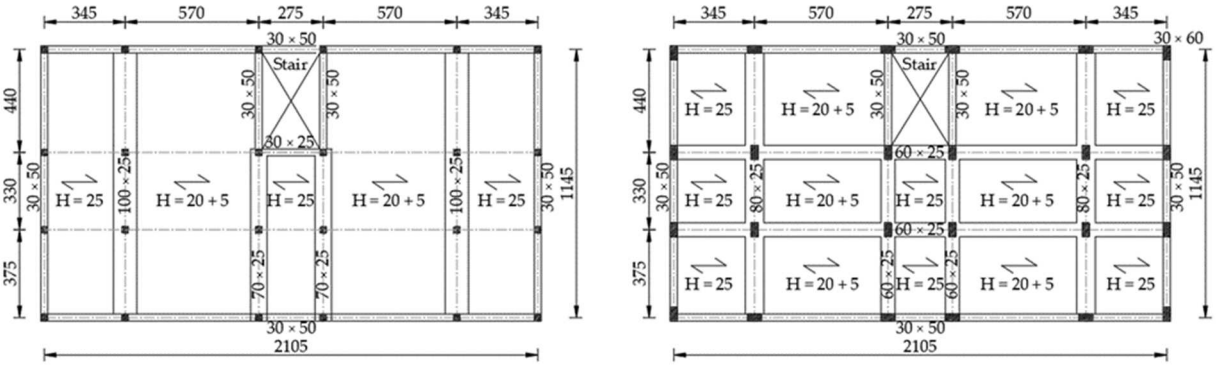

(a) (b)

Figure 25 Typical floor plan of the (a) NA_{GLD} and (b) AQ_{SLD} archetype buildings.

As shown in Figure 26 ,according to the technical practice of the period, masonry infills featuring a double layer of hollow clay bricks (120+80 mm thickness for the 1950s-60s and 70s buildings, 150+80 thickness for the 1980s-90s buildings), with 100 mm (70mm for 1980s-90s buildings) inner cavity, have been considered. Masonry infills are regularly distributed both in plan and in elevation, featuring different percentages of openings in the long direction (in the short direction there are no openings). A good connection of the masonry infill walls with the surrounding RC frame has been assumed for the purpose of the seismic performance assessment of the buildings. More details about the structural details of RC members and masonry infills can be found in (Di Domenico et al., 2022).

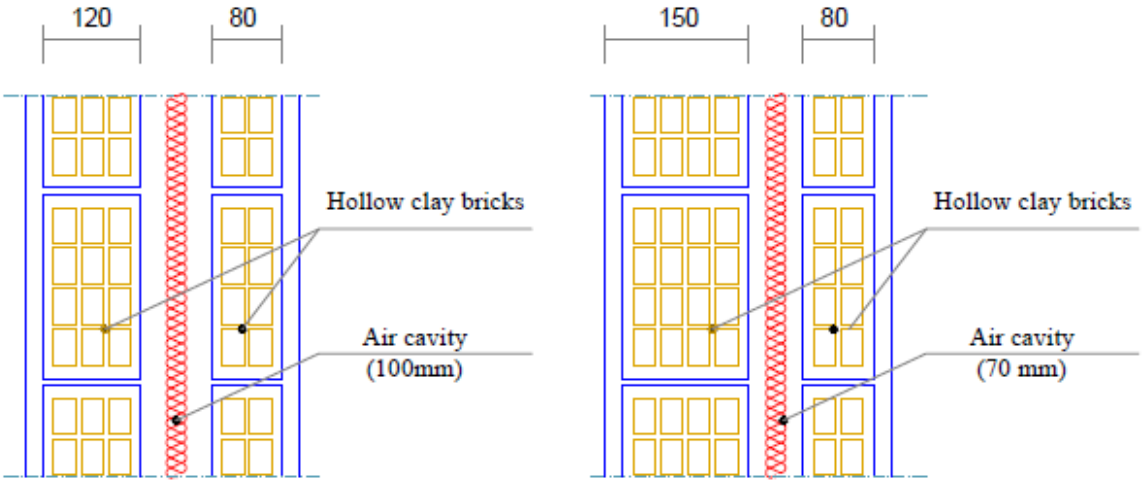

(a) (b)

Figure 26 Masonry infills typology for or the 1950s-60s and 70s buildings (a) and 1980s-90s buildings (b)

2.2.2. Seismic Hazard

According to NTC18, seismic actions (including uniform hazard response spectra and seismic ground motion records) must be derived from probabilistic seismic hazard analysis (PSHA) (Cornell, 1968). In this study, the spectral acceleration, Sa(T*), associated with a suitable conditioning period, T*, has been assumed as Intensity Measure (IM). The conditioning period, T*, has been set equal to 3 s, which is a good estimate of the design value of the effective fundamental period of the base-isolated buildings examined in this study. Hazard curves have been derived from PSHA for ten earthquake intensity levels, associated with the following Return Periods (Tr): 10, 50, 100, 250, 500, 1000, 2500, 5000, 10000 and 100000 years. The first seven earthquake intensity levels correspond to those typically adopted for design/assessment purposes by current technical standards. In order to assess the safety margins against collapse, three additional higher hazard levels have been considered featuring RPs equal to 5000, 10000 and 100000 years, respectively. For each IM, a set of twenty seismic record pairs, consistent with site-specific magnitude-distance disaggregation and compatible (on average) with a suitable Conditional Spectrum (CS) (Lin et al. 2013) with T*=3 s. More details about seismic hazard and record selection can be found in (Iervolino et. al., 2018).

2.2.3. Design of Isolation Systems

Rubber-based isolation systems are based on a proper combination of High Damping Rubber Bearings (HDRBs) and Flat Sliding Bearings (FSBs), to elongate the fundamental period of vibration of the building, thus avoiding or minimizing any strengthening intervention in the superstructure. More in detail, for most of the cases, HDRBs are placed below the columns along the perimeter of the building, while FSBs are placed below the inner columns of the building. However, in some cases FSBs are also placed along the perimeter of the building in order to further increase the isolation period up to values larger than the minimum one resulting from the design approach. All the HDRBs are characterized by a soft compound (shear modulus G equal to 0.4 MPa) and equivalent viscous damping ratio (ξ) of 15% at 100% shear strain.

The design approach followed to define the target value of the isolation period consists in limiting the seismic force transmitted to the superstructure under the “elastic” limit of the superstructure, defined by means of Push Over Analysis (POA) with mass proportional forces (uniform distribution of forces). The elastic limit, in terms of base shear (Vy) of the superstructure (in the fixed-base configuration), has been identified as the force level of the

capacity curve corresponding to the occurrence of the first plastic hinge in the weaker direction of the building (i.e. the minimum base shear at the first yielding). In Figure 27, for each case analysed, the elastic limit is outlined by a circle with the same colour of the corresponding capacity curve. It is worth noting that the identified elastic limits correspond to the first plasticization of all the structural element of the building (beams or columns) excluding those of the staircase, for which a local retrofit is supposed. This assumption was necessary in order to avoid low elastic limits leading, in some cases, to unfeasible isolation systems.

Once the elastic limit has been identified, the minimum fundamental period of the base-isolated building has been derived by estimating the pseudo-acceleration of the equivalent SDOF (Single Degree Of Freedom) system associated to the first plastic hinge ($S_a = V_e/M_{tot}$, where M_{tot} is the total mass of the superstructure) and then by finding the period associated to such value in the pseudo-acceleration spectrum at the Life-safety Limit State (LLS) earthquake intensity level. In this way, isolation periods larger than the target value thus obtained permit to avoid any structural damage up to the earthquake intensity levels equal to that associated with the verification of the Life-safety Limit State (Figure 28a). In order to take into account the structural uncertainties, when possible, the aforesaid spectral acceleration has been divided by a safety factor equal to 1.05. A behaviour factor q=1 for the superstructure and a damping ratio of the isolation system equal to 15% has been assumed. Subsequently, the corresponding value of the maximum displacement (S_{dmax}) has been evaluated using the displacement spectrum associated with the verification of the Collapse prevention Limit State (CLS) (Figure 28b). This value has been opportunely increased using a specific coefficient to account for torsional effects, in order to carry out the safety verifications of the isolation devices.

As a matter of fact, commercial devices have been selected from the manufacturers' catalogues featuring suitable values of effective stiffness and vertical capacity; effective periods have been calculated based on the dimensions of isolators and nominal properties of the isolation bearings at the average design shear strain at the CLS. More details about the design criteria can be found in (Cardone et al., 2019b).

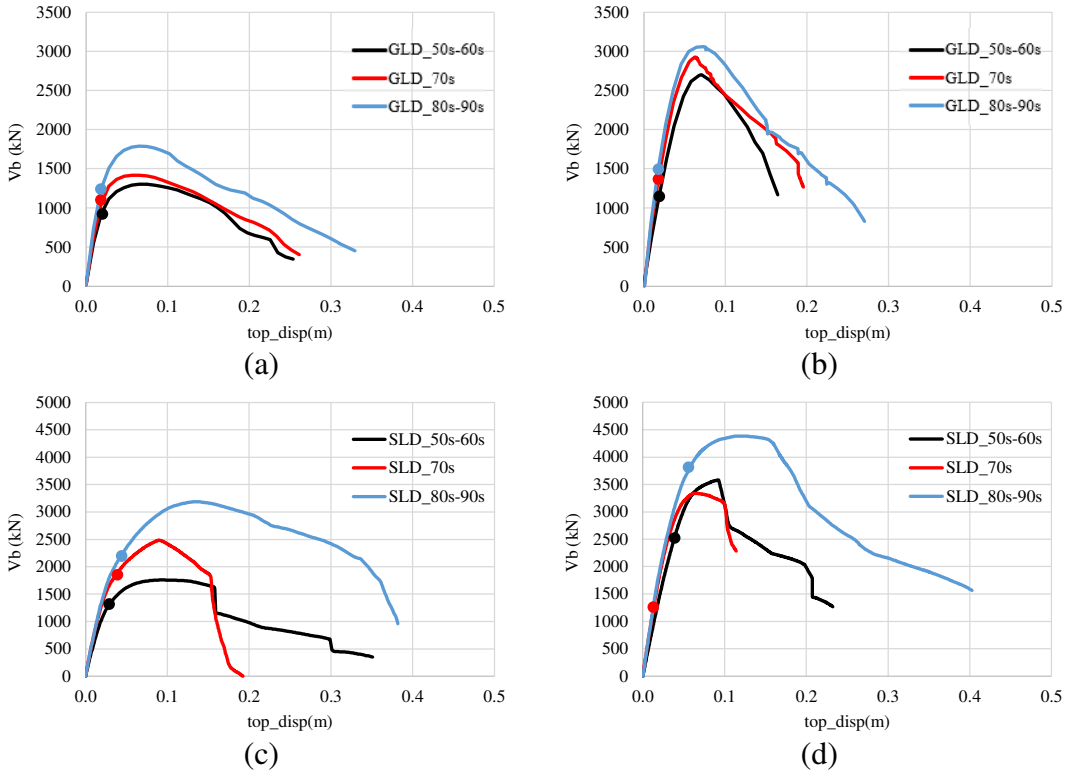

Figure 27 Capacity curve and elastic limit for GLD case studies in X-direction (a) and Y- direction (b) and for SLD case studies in X-direction (c) and Y- direction (d)

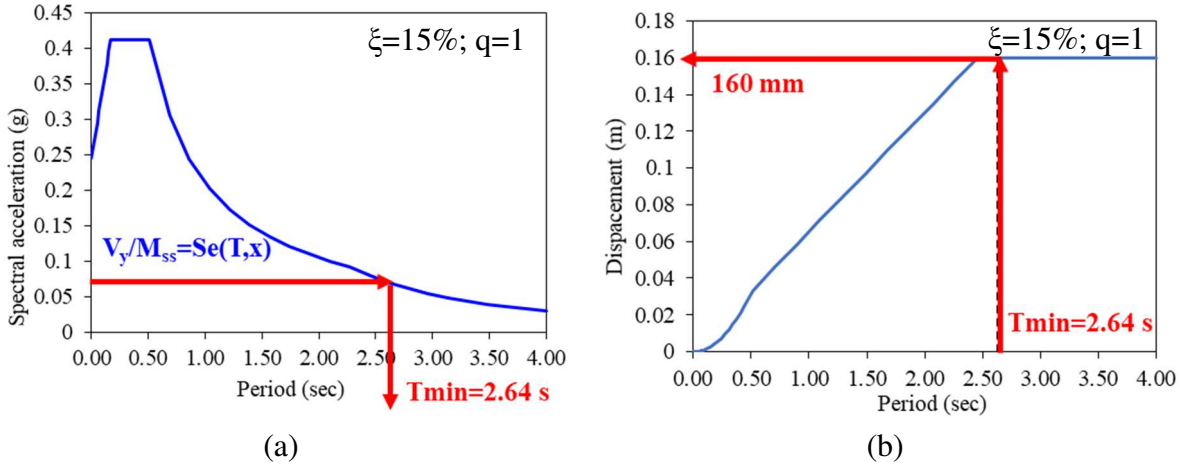

Figure 28 Design procedure for the G80 building at Naples: (a) spectrum at the Life-safety Limit State (LLS); (b) spectrum at the Collapse prevention Limit State (CLS)

The isolation system has been designed following the indications suggested in §7.10.4.2 and C11.9 of the NTC2018. More in details, isolation bearings have been designed so that displacements and forces respect the following limitation:

$$\gamma_s \leq \gamma^*/1{,}5 \leq 2 \qquad (10)$$

where γ_s is the shear deformation of rubber layers due to the total seismic displacement (included torsional effects) and γ^* is maximum shear deformation obtained from qualification tests aimed to assess the effective rubber-steel adhesion. The other limitation considered in the design is:

$$\gamma_t = \gamma_c + \gamma_s + \gamma_\alpha \leq 5 \tag{11}$$

where γ_t is the total deformation, γ_c is the shear deformation of rubber layers due to axial load and γ_α is the shear deformation of rubber layers due to angular rotation. Additionally, for the critical devices it has been checked that the maximum tensile stress is lower than the minimum between $2G_{din}$ and 1 MPa, as stated in §7.10.4.2 of NTC2018, in order to avoid cavitation phenomena. Also the maximum compression acting on the bearings has been checked to be lower than $V_{max,c}/2$, where $V_{max,c}$ is buckling load evaluated as reported in C11.9.7:

$$V_{max,c} = \frac{G_{din} A_r S_1 D}{t_e} \tag{12}$$

where t_e is the total thickness of rubber, A_r is the overlapping area of the isolator, S_1 is the primary shape factor, D is the diameter of the bonded rubber area (steel plate diameter) and G_{din} is the shear modulus of rubber.

Table 14 summarizes the geometric characteristics and design safety verification outcomes for the rubber-based isolation systems adopted in this study. It is worth to notice that as the elastic limit decreases as the minimum isolation period increases. For the cases with the lowest elastic limits (GLD 60, SLD 60 and SLD 70) the obtained minimum values are larger than 3 s. This has required the adoption of a larger number of FSBs with respect to the other cases, where the 16 HDRBs are placed on the building perimeter and the 8 FSBs are placed under the interior columns (see Figure 29). The adopted configurations are reported in Table 14 and those requiring a larger number of sliders are illustrated in Figure 30. In Table 14 the devices are identified by a three-number code composed by the nominal diameter (Ø), the total rubber layer thickness (t_e) and the single rubber layer thickness (t_r). Similarly, the selected *FSBs* are identified by their vertical load capacity (V), the total displacement capacity (d_{tot}=$d_{tot,x}$=$d_{tot,y}$= $2d_{max}$ expressed in mm) and pot diameter ($Ø_p$). The effective fundamental period of the base isolated building (T_{is}) and the nominal (design) maximum displacement capacity of the devices ($d_{max,HDRB}$ and $d_{max,FSB}$) are also shown. For *HDRBs*, $d_{max,HDRB}$ is the value corresponding to the attainment of a maximum design rubber shear strain equal to 2 (i.e. 200%), according to the

explicatory notes of the NTC2018 (CS.LL.PP. 2019, clause C.11.9.7) and the manufacturers' catalogues. For FSBs, $d_{max,FSB}$ is conventionally assumed equal to the design displacement capacity of HDRBs increased by 50 mm. The fundamental period of vibration of the buildings in the as built conditions are also reported in Table 14. Finally, in Table 14 the demand/capacity ratios referred to the design condition, expressed in terms of shear strain (D/C shear), compression load (D/C comp) and tensile stress (D/C tens) are summarized for each case study. As can be observed, all the base-isolation systems have been designed using similar *D/C* ratios, very close to 1, in particular for shear and/or compression.

Table 14. Geometric characteristics and design safety verification outcomes for the rubber-based isolation systems considered in this study.

Case study	$T_{fb,\,x}$ (s)	$T_{fb,\,y}$ (s)	Configuration	HDRB $\phi/t_e/t_r$	FSB $V/d_{tot}/\phi_p$	d_{max} (mm) HDRB	d_{max} (mm) FSB	$T_{is,min}$ (s)	T_{is} (s)	T_{is}/T_{fb}	D/C shear	D/C comp	D/C tens
$NA_{GLD\_50s\text{-}60s}$	0.73	0.70	14 HDRB + 10 FSB	450/102/6	3100/500/250	200	250	3.06	3.20	4.38	0.93	0.91	0.00
NA_{GLD_70s}	0.78	0.76	16 HDRB + 8 FSB	450/102/6	3500/500/250	200	250	2.80	3.00	3.85	0.89	0.98	0.00
NA_{GLD_80s}	0.74	0.73	16 HDRB + 8 FSB	500/102/6	3500/500/250	200	250	2.64	2.80	3.78	0.89	0.58	0.00
$AQ_{SLD\_50s\text{-}60s}$	0.74	0.64	12 HDRB + 12 FSB	600/176/8	3500/800/250	350	400	3.07	3.20	4.32	0.87	0.75	0.12
AQ_{SLD_70s}	0.77	0.69	12 HDRB + 12 FSB	600/176/8	3500/800/250	350	400	3.15	3.22	4.18	0.89	0.86	0.00
AQ_{SLD_80s}	0.76	0.68	16 HDRB + 8 FSB	600/152/8	3500/700/250	300	350	2.50	2.70	3.55	0.82	0.93	0.14

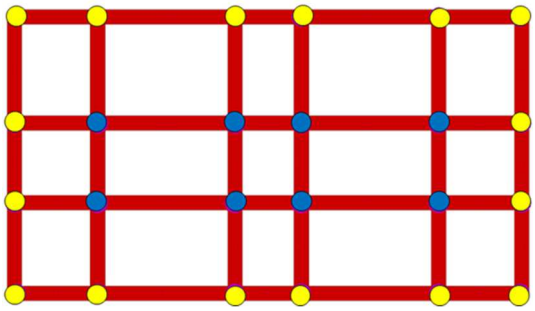

16 HDRB + 8 FSB

Figure 29 Base-isolation system configurations including HDRBs (yellow dots) and FSBs (blue dots) for case studies without large isolation periods

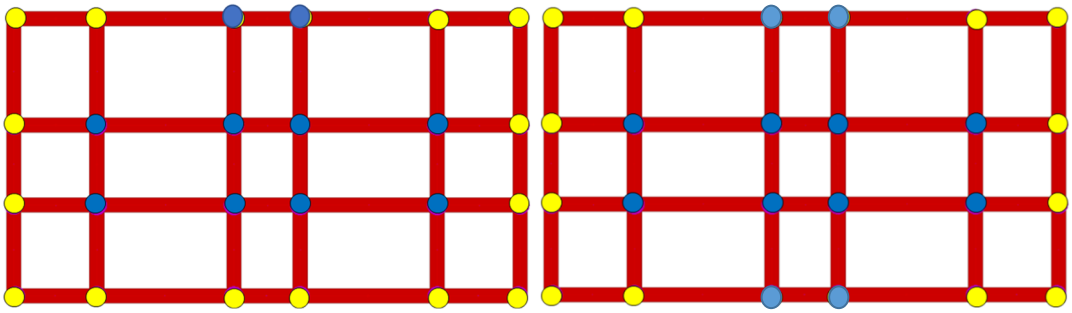

Figure 30 Base-isolation system configurations including HDRBs (yellow dots) and FSBs (blue dots) for case studies with large isolation periods

2.2.4. Definition of Performance Levels

The seismic performances of the examined case studies have been evaluated considering two specific performance levels, referred to as: *Usability-Preventing Damage* (*UPD*) and *Global Collapse* (*GC*) performance level, respectively.

The occurrence of both performance levels has been assessed following a heuristic approach based on a multi-criterium method, considering differing failure modes and conditions for both superstructure and isolation system.

Generally speaking, the *UPD* performance level is associated with interruption of use of the building due to either (i) light-extensive or serious-limited damage to non-structural elements or (ii) onset of damage in structural elements.

In RC buildings the main non-structural elements coincide with masonry infills and partitions, whose repair costs after a seismic event always represent the largest part of the repair cost for the entire building. According to the construction practice of the time, masonry infills and partitions were (and actually still are in most of the cases) realized completely in contact with the surrounding RC frame without any gap or connection able to accommodate relative displacement between masonry panels and RC members. Masonry infills are on-site built just after the surrounding RC frame is hardened; as a consequence, they are assumed as non-load bearing elements and commonly treated as non-structural elements. It is worth noting that damage to masonry infills can represent a threat to life (due to falling mass or hampering safe evacuation of a building). Repairing infills and partitions (and those elements affected by damage to infills, such as electrical wiring, hydraulic pipes, doors and windows, etc.) may require significant efforts and high costs.

All that considered, in this study both the in-plane and out-of-plane behavior of hollow clay bricks masonry infills was considered in the numerical model and in the definition of the UPD performance level. As anticipated, the attention was focused on double layers infills with inner cavity, as they represent the infill type most widely used in the past for RC frame buildings in Italy (and other European countries).

According to Cardone and Perrone (2015), the in-plane damage states of masonry infills, can be described as follows (see Figure 31) (1) DS1 (Light Cracking). At DS1, damage results in detachment of the masonry panel from the RC frame, at the intrados of the top beam and along the upper half-height of the columns. Light diagonal cracking of the infill (one or two cracks with width <1 mm) in both directions may also occur; (2) DS2 (Extensive cracking). At DS2, the cracks developed at DS1 widen (1 mm<width<2 mm). In addition, new diagonal cracks are expected to form in both directions (25-35% of the panel area is assumed to be affected by cracks at DS2). Possible failure of some brick units, located on the upper corners and top edge of the infill (corresponding to 10% of the panel area), is expected; (3) DS3 (Corner crushing). At DS3, detachment of large plaster area and significant sliding in the mortar joints are expected to occur. In addition, crushing and spalling of brick units are more widespread on the panel (30% of the panel area is assumed to be affected by crushing/spalling of bricks).

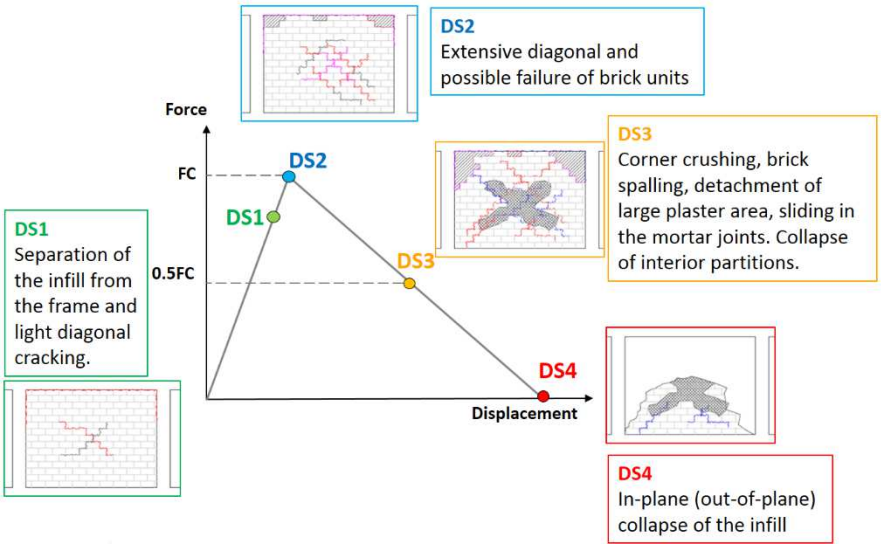

Figure 31 In-plane damage states for masonry infills.

The wall is not repairable at reasonable costs (it is more convenient to demolish and reconstruct the entire wall). Frames (if any) are not damaged and can be retrieved and re-installed; (4) DS4 (Collapse). DS4 corresponds to the in-plane or out-of-plane (whichever occurs first) global collapse of the wall. Frames (if any) are damaged and cannot be retrieved and used again.

All that considered, in this study, the UPD performance level is deemed to occur when the relative global displacement limit is attained. The relative global displacement of the building is computed subtracting the isolation system displacement from the building roof in each main direction and the threshold value has been derived from pushover analysis (uniform-acceleration distribution of forces) on the superstructure in the fixed-base configuration (see Table 15). In particular, different threshold values are estimated, corresponding to different limit conditions for non-structural elements, and the lowest value has been considered in the nonlinear analyses. The three main limit conditions, verified by pushover analysis, for the definition of the UPD performance level, are : (i) Attainment of a light widespread damage condition, corresponding to the attainment of a maximum lateral force around the peak strength in the relevant skeleton curve (DS2 according to Cardone and Perrone (2015)), for no more than 50% of masonry infills in each main direction; (ii) Attainment of a severe damage state, corresponding to the attainment of 50% strength drop from the peak strength in the relevant skeleton curve (DS3 according to Cardone and Perrone (2015)) for the first masonry infill; (iii) Attainment of a limit value of base shear (corresponding to 95% of the peak strength of the capacity curve from pushover analysis, corresponding to a condition where the structure still keeps its original strength and most of its original stiffness (no need for structural repair)). In addition, the out-of-plane response of masonry infills was monitored during nonlinear dynamic analyses. The UPD performance level was deemed to occur if any infill wall attained an out-of-plane collapse condition on any floor of the building.

Table 15. UPD superstructure limit displacements (mm)

Direction	$NA_{GLD\_50s\text{-}60s}$	NA_{GLD_70s}	$NA_{GLD\_80s\text{-}90s}$	$AQ_{SLD\_50s\text{-}60s}$	AQ_{SLD_70s}	$AQ_{SLD\_80s\text{-}90s}$
X	39.8	34.1	41.3	57	73	96
Y	50.5	47.6	46.0	66	61	74

Regarding the *GC* performance level, the isolation system and the superstructure represent two elements of the same in series system that can attain their own collapse condition. As a consequence, the *GC* performance level is deemed to occur if either the superstructure or the isolation system fails. For what concerns the superstructure, the collapse is associated with the occurrence of the first of the following conditions (Ricci et al. 2018): (i) attainment (in any main horizontal directions) of a relative global displacement equal to that associated with a 50% decrease of the lateral strength on the capacity curve from pushover analysis of the building in the fixed-base configuration; (ii) loss of axial load carrying capacity for the first RC column

liable to shear failure (in first approximation this is assumed to occur when a chord rotation of 0.10 is reached (Ricci et al. 2019), see Table 16).

Table 16. GC superstructure limit displacements (mm)

Direction	$NA_{GLD\_50s\text{-}60s}$	NA_{GLD_70s}	$NA_{GLD\_80s\text{-}90s}$	$AQ_{SLD\_50s\text{-}60s}$	AQ_{SLD_70s}	$AQ_{SLD\_80s\text{-}90s}$
X	232	241	264	300	160	370
Y	146	132	192	230	129	360

The failure modes considered for the isolation system depend on the isolation system type. For rubber-based isolation systems, four different failure modes have been considered, namely: cavitation, shear failure, buckling and attainment of ultimate displacement capacity by flat sliding bearings (if any). The cavitation failure of a single isolator is assumed to occur for an axial tensile strain of 50% in the post-cavitation branch of the axial load vs. axial strain curve of the device. For shear failure, an ultimate shear strain of 350% is assumed, considering the deformation capacity of currently available isolation devices (Nishi et al. 2019; Nakazawa et al. 2011). Finally, for the compression behavior it is worth to note that the numerical model adopted for HDR bearings is able to predict their post-elastic behaviour, i.e. the reduction of the vertical and horizontal stiffness of the bearings as the displacement increases (without losing their bearing capacity). Thus, there is not the attainment of a "buckling load" and compression failure of a single isolator is assumed to occur for an axial compression strain of 50% in the post-buckling branch of the axial load vs. axial strain curve of the device. This is a realistic value, since experimental results show that rubber bearings can sustain even higher axial deformations after buckling (Monzon et al, 2016). Furthermore, since the collapse of one device does not lead to the collapse of the isolation system, the global collapse of the isolation system is conventionally deemed to occur when the axial/shear strain in (at least) 50% of the devices simultaneously exceed the aforesaid limit values. For the shear deformation this approach permits to account for also torsional effects due, for example, to impacts (gap closures).

All isolation systems examined in this study are based on the combination between rubber isolators (typically placed below the outer columns of the bearings) and flat sliding bearings (usually placed below the inner columns of the building). The failure criterium for flat sliding bearings is related to the attainment of an ultimate horizontal displacement capacity. In this study, the ultimate displacement capacity of sliding bearings was set considering a limit value of compression stress in the sliding interfaces equal to 60 MPa in line with (CEN-EN 1337-2 2000, clause 6.8.3). As a matter of fact, indeed, as the horizontal displacement increases, the

effective resisting area of the sliding interfaces reduces after the attainment of the limit of the sliding surface and, as a consequence, the contact pressure increases. Numerical simulations (Cardone et al. 2019c) showed that the aforesaid compression limit is generally reached for a value of the horizontal displacement approximately equal to the nominal displacement capacity of the device ($d_{max,FSB}$) increased by an extra-stroke displacement of the order of magnitude of half diameter (½ Ø) of the PTFE (or any other low-friction plastic material used in currently available sliding bearings) pads.

The global collapse of a hybrid isolation system due to flat sliding bearings is deemed to occur when the horizontal displacement of the centre of gravity of the isolation floor is equal to the aforesaid limit value.

Failure modes and collapse conditions considered in this study for rubber-based isolated buildings are summarized in Table 17.

Table 17. Failure modes and collapse conditions for rubber-based isolated buildings

	Failure modes	Collapse conditions
Superstructure	Superstructure collapse	The first between: (*i*) attainment of a relative (top floor minus isolation level) global lateral displacement equal to that corresponding to a peak strength reduction of 50% on the negative slope of the capacity curve (from POA) of the building in any main direction and (*ii*) attainment of a chord rotation of 0.01 in RC columns liable to brittle shear failure.
Rubber Isolation Systems	Compression	50% of elastomeric devices reaches an axial compression strain (ε_c) equal to or greater than 50%
	Tension	50% of elastomeric devices reaches an axial tensile strain (ε_t) equal to or greater than 50%
	Shear	50% of elastomeric devices reaches a shear strain (γ_r) equal to or greater than 350%
	Overstroke	The horizontal displacement of the center of gravity of the isolation system exceeds a limit value related to the maximum contact pressure between sliding interfaces (*60 MPa*)

2.3 MODELLING ASSUMPTIONS

2.3.1 Superstructure

A lumped plasticity model has been adopted for RC beams and columns, whereas elastic beams have been used to model the base floor grid above the isolation system. The choice of modelling the superstructure of base-isolated buildings with nonlinear elements is justified by the results of recent studies on this topic (Cardone et al., 2013; Cardone and Flora, 2016), which pointed out the relevant effects of the inelastic behaviour of the superstructure on the seismic response of base isolated buildings. The structural model also includes the staircase structure featuring inclined beams and cantilever steps.

As reported in De Risi et al. (2022) for the flexure-controlled response, two distinct phenomenological macro-models for members with deformed or plain bars are used to account for the different flexibility due to the different steel-concrete bond behavior. The Pinching 4 material model and the ModIMKPeakOriented material (Ibarra and Krawinkler, 2005; Ibarra et al., 2005) implemented in OpenSees are used in for the elements with plain and deformed bars respesctively. Di Domenico et al. (2021) calibrated the hysteretic parameters needed for the cyclic response of plain bars hinges, while Haselton's et al. (2008) empirical predictive equations for deformed bars hinges were used.

Possible shear failures (before or after flexural yielding) have been taken into account in the model. To this end, all the hinges have been pre-qualified either as (i) ductile (shear failure does not occur: the moment-rotation skeleton curve is not modified), or (ii) shear critical (shear failure is expected for a given level of displacement (hence rotation): the moment-rotation skeleton curve is modified beyond the critical rotation by a softening branch whose slope is derived from the empirical formulation reported in (Aslani and Miranda, 2005). More details about this collapse criterion can be found in (Ricci et al. 2019).

Concerning beam-column joints, the joint panel model referred to as "scissors model" has been adopted. In scissor model, joint shear deformation is simulated by a rotational spring model with degrading hysteresis. The element is implemented in OpenSees (McKenna, 2011) through defining duplicate nodes, node "i" (master) and node "j" (slave), with the same coordinates at the centre of the joint (intersection of beam and column centrelines); the element connectivity is set such that node "i" is connected to the column rigid link and node "j" is connected to the beam rigid link. Next, a Zerolength rotational spring is used to connect the two nodes so that

the column rigid link is connected to one end of the spring while the beam rigid link is connected to the other. It is a very simple and computationally efficient joint model, but also sufficiently accurate in predicting the experimental beam-column joint panel behaviour of non-ductile RC frames (De Risi et al., 2017).

2.3.2 Masonry infills

Particular care has been taken in the description of the mechanical behaviour of masonry infills, as they can strongly affect the seismic response of older RC frame buildings (featuring double-layers masonry walls with high slenderness ratio and weak beam-column joints without adequate shear reinforcement), triggering local failure mechanisms and threatening human life in case of out-of-plane collapse.

The In-Plane (IP) behaviour of masonry infills has been modelled following an equivalent compression-only strut approach. The skeleton curve of the diagonal struts has been defined according to a modified version of the Decanini model (Sassun et al., 2016), where the effect of openings is taken into account by suitable strength/stiffness reduction factors.

Figure 32a shows the modelling strategy used for the infills; each infill is described by means of two parallel no-tension struts in each direction; therefore, the nonlinear IP behaviour of each strut is assumed equal to 50% of the total one.

This modelling choice is adopted to better capture the transfer of shear stresses from the infill to the adjacent column (the model used in section 1 did not take it into account).

The modelling strategy proposed by (Ricci et al. 2018) has been adopted to account for both the pure Out-Of-Plane (OOP) response and the IP/OOP interaction effects (i.e., the degradation of the OOP strength/stiffness due to IP damage and vice versa) of masonry infills. Basically, the OOP behaviour of the infills is incorporated in the equivalent diagonal struts. More precisely, each strut has a central node connected to a geometrically coincident node provided with a mass in the OOP direction. Nonlinear OOP force-displacement springs are introduced between these two nodes. Since four struts (two parallel struts for each inclined direction) are adopted for each infill leaf, four OOP masses are implemented in the model for each infill leaf, each one corresponding to one-fourth the total tributary mass of the infill (around 65% of the mass wall). Zerolength nonlinear springs are inserted between two overlapped central nodes to

reproduce the OOP force-displacement behaviour (see Figure 32(b)). The undamaged OOP behaviour of the infills is described by means of a ZeroLength element with a trilinear force-displacement curve. The IP/OOP interaction is modelled by means of a number of auxiliary springs (hence force-displacement curves) that mutually-neutralize (or activate) themselves based on the displacement demands recorded during the nonlinear time-history analysis (see Figure 32(c) and Figure 32(d)). In particular, the OOP force degradation is governed by the corresponding interstorey drift level in the frame; similarly, the IP degradation depends on the OOP displacements recorded. When either the IP or the OOP ultimate displacement of a generic leaf is reached, that leaf is removed.

The equations used for modeling the out-of-plane response are those proposed in Ricci, Di Domenico, and Verderame (2020) for infills in which the out-of-plane response is governed by a two-way arching effect resisting mechanism. As reported in (Di Domenico et al., 2022), in this study, the out-of-plane collapse displacement is set equal to 0.80 times the leaf thickness; IP/OOP interaction is modelled based on the equations proposed by Ricci, Di Domenico, and Verderame (2018b, c).

Local shear interaction (between masonry infills and adjacent RC column) is captured through suitable shear springs (featuring a typical brittle behavior with a quite steep softening branch after the peak strength) implemented at the ends of the columns to reproduce the column nonlinear shear response triggered by the additional shear demand imposed by the equivalent compression-only diagonal strut. The cyclic response of the shear spring was characterized by no strength or stiffness degradation nor by any pinching effect, solely for the sake of simplicity. More information about superstructure and infills modelling can be found in (Di Domenico et al, 2022).

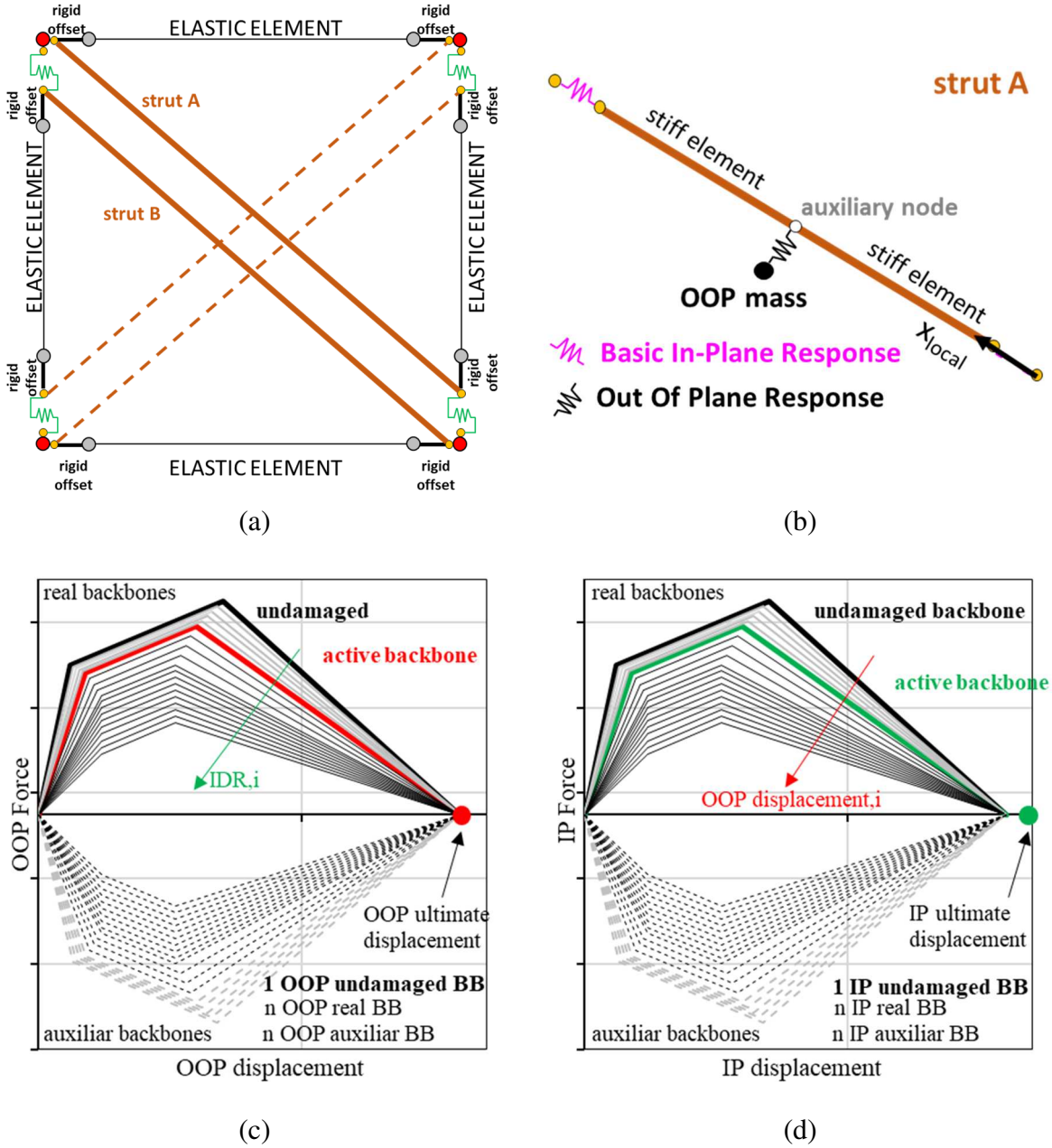

Figure 32 (a) Lumped plasticity macro model adopted for infills (from Di Domenico et al, 2022); (b) close up view of each strut; (c) real and auxiliary OOP curves to simulate the IP-OOP interaction; (d) real and auxiliary IP curves to simulate the IP-OOP interaction

2.3.3 Rubber isolators

To simulate the behaviour of HDRBs, the Kikuchi Bearing Element, recently implemented in OpenSees, has been used. It is a fully 3D model whose main characteristics is to take into account the coupled behaviour in the vertical and horizontal direction through its large displacement formulation. In other terms, it is able to capture the reduction of the horizontal stiffness related to the increase of vertical load and horizontal displacement (i.e. the so called "P-Δ" effect). More in detail, the three-dimensional analytical model features triaxial

interaction between the two horizontal components, and the vertical component. The shear bidirectional behaviour is based on the use of Multi Shear Spring model (MSS) (Wada and Hirose, 1987) while the vertical Euler column buckling behaviour is based on the Multi Normal Spring model (MNS). The arrangement of MSS and MNS is shown in Figure 33.

Such feature is essential for the reliability of the analyses because for severe earthquake shaking external bearings may show a strongly asymmetric hysteretic cycle with a substantial pure shear behaviour for one side of the cycle (lowest compression) and a possible post-buckled behaviour in the other side (higher compression) (Kikuchi et al., 2010; Takaoka et al. 2011).

For the Multi Shear Spring (MSS) model, the KikuchiAikenHDR material has been used. The original version implemented in Opensees features only a limited set of pre-calibrated rubber compounds all showing a limited hardening behaviour for high shear deformation and a negligible first cycle effect (also called as Mullins effect or scragging (Mullins, 1969)), in line with the Japanese production. Such material can be slightly adjusted using three correction coefficients controlling respectively: the equivalent shear modulus (c_g), the equivalent viscous damping ratio (c_h) and the ratio of shear force at zero displacement (cu). However, the base behaviour cannot be changed.

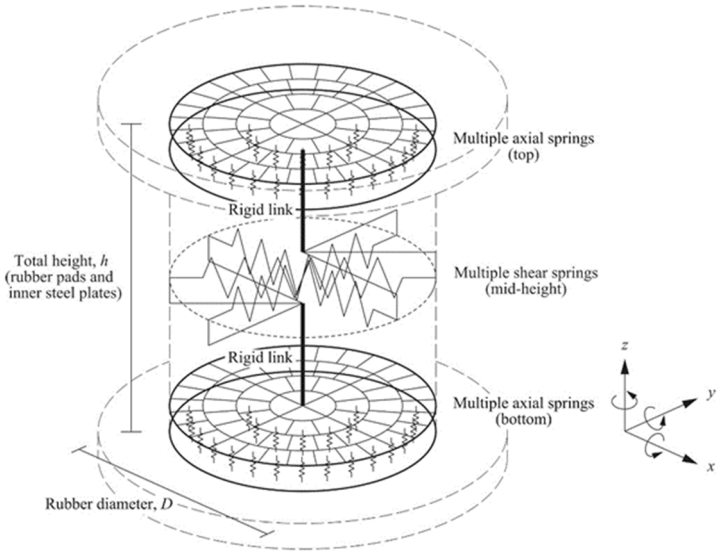

Figure 33 Multi spring mechanical model for circular elastomeric bearing (from Ishii and Kikuchi 2019).

Thus, in this work, the shear behaviour of HDRBs has been calibrated with reference to the third cycle (according to (EN15129, 2009)) of a typical rubber compound used in the Italian context for HDRBs, under the hypothesis that the behaviour in the virgin state (Tubaldi et al 2017; Ragni et al 2018b) is not significant towards the final performance assessment. In

particular, the results of an experimental campaign (Brandonisio et al 2017) performed at the SisLab (Materials and Structures Test Laboratory) of the University of Basilicata on three circular HDRBs, have been used for the model calibration of the rubber bearings. Details of the model calibration can be found in (Micozzi et al 2021).

Figure 34 shows the numerical (dashed red line) vs experimental (solid black line) comparison of the shear behaviour of the bearing tested to calibrate the model. The tests are performed up to the maximum shear displacement and increasing vertical compression: (6, 10, 14, 20 MPa). The bearing shown in c has the following characteristic:

(i) Outer diameter Ø equal to 700 mm
(ii) Innner steel shim diameter Ø' equal to 690 mm
(iii) Single layer rubber thickness tr equal to 9 mm
(iv) Total rubber layer thickness te equal to 207 mm
(v) Primary shape factor S1=Ø'/4tr equal to 19.5
(vi) Secondary shape factor S2=Ø'/te equal to 3.4
(vii) Shear stiffness G equal to 0.4 MPa
(viii) Damping factor ξ equal to 15%.

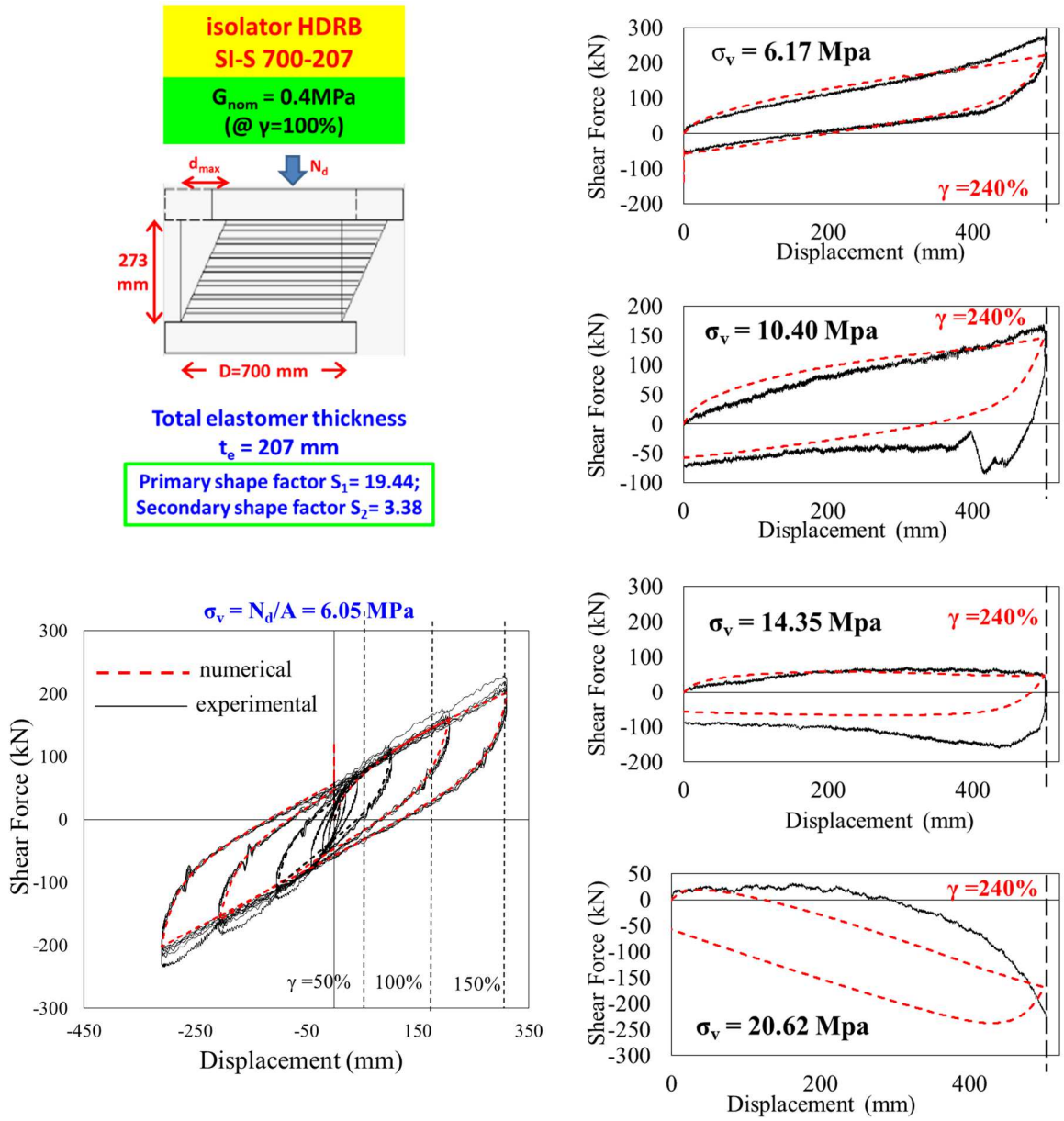

Figure 34 Comparison experimental results and calibrated model for SI-S 700-207

For the Multi Normal Spring (MNS) model, the AxialSP material, already implemented in the OpenSees material library, has been used. Such material is fully defined by the following parameters: (i) initial elastic vertical stiffness E_{init}, (ii) post elastic stiffness in tension ($1/100E_{init}$) and compression ($1/2E_{init}$), (iii) cavitation stress and (iv) compression yielding stress. The parameters have been set according to (Ishii and Kikuchi, 2019). However, as described in detail (Micozzi et al 2021), bearings tested within that work feature shape factors that are higher than 30. For slender bearings, with primary shape factor around 20, generally used in the Italian context, such parameters lead to a significant overestimation of the "P-Δ" effects, due to the local cavitation of the bearing before the buckling. In order to avoid this, the

material used for the MNSs has been replaced by a simple elastic material with stiffness equal to E_{init} and the model is used in-series with a rigid plastic spring describing the global cavitation of rubber as shown in Figure 35. The external spring is characterized by a rigid behaviour under compression and in the range of tension forces lower than the cavitation threshold while it is properly calibrated to describe the inelastic post-cavitation behaviour above the mentioned threshold (see Figure 36). In particular, as the AxialSP material does not feature any cyclic degradation of the post-cavitation behaviour, median values of the post-cavitation stiffness and force threshold have been adopted in the model (similar to the third-cycle concept used for the shear behaviour), leading to a cavitation force of 2GA and a post-cavitation stiffness equal to 0.43% E_{init}, based on experimental result of (Warn 2006). In this way, the global building model is able to capture the influence of cavitation on the rocking motion during an earthquake.

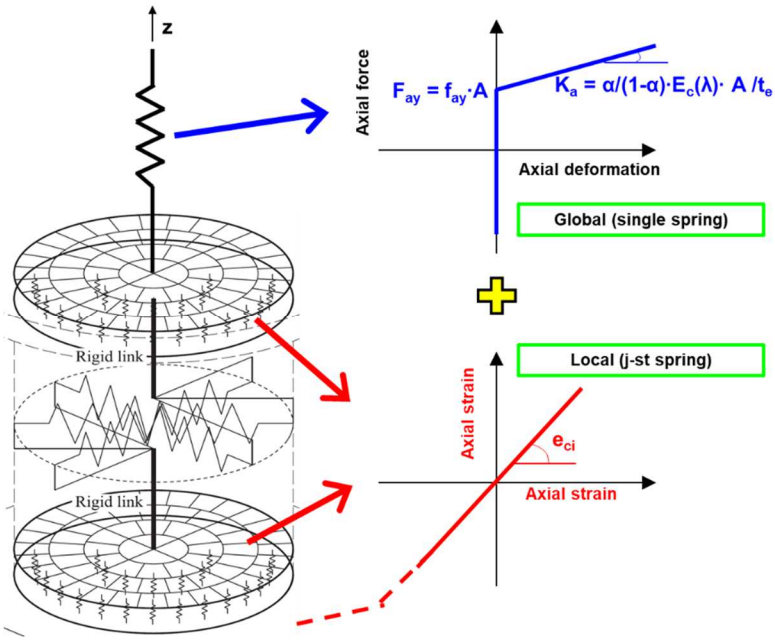

Figure 35 Choice of axial modelling bearing adopted

As far as the modeling of flat sliding bearings is concerned, the element flatSliderBearing has been used adopting a velocity-dependent and axial-load-dependent friction model (Constantinou et al., 1990), and assuming a friction coefficient at the maximum load capacity equal to 1% for fast velocities and 0.5% for low velocities, based on the results of manufacturer's type tests (see Figure 37). More details about slider modelling can be found in (Cardone et al., 2019a). It is worth noting that such low damping coefficients implies a negligible effect of the sliders on the isolation system behaviour (i.e. extra-damping). This must be assessed by suitable acceptance tests on materials or devices.

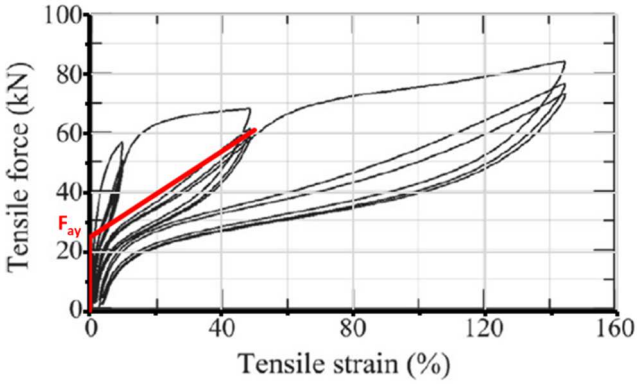

Figure 36 Uniaxial constitutive model of the vertical in-series rigid-plastic spring for cavitation behaviour (superimposed on test from Warn 2006).

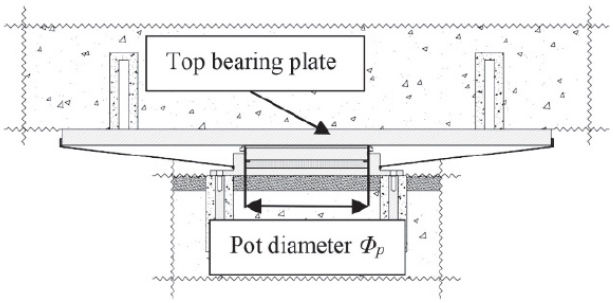

a_{Slow}	constant for coefficient of friction at low velocity	0.02073
n_{Slow}	exponent for coefficient of friction at low velocity	0.9
a_{Fast}	constant for coefficient of friction at high velocity	0.04146
n_{Fast}	exponent for coefficient of friction at high velocity	0.9
α_0	constant rate parameter coefficient	0.00458
α_1	linear rate parameter coefficient	0
α_2	quadratic rate parameter coefficient	0

Figure 37 Flat Slider Bearing device and model parameter

2.4 NON-LINEAR TIME HISTORY ANALYSIS (NTHA)

2.4.1 Seismic Imput

Multi-Stripe non-linear dynamic Analyses (MSA) have been performed to evaluate the seismic performances of the examined case-studies towards GC and UPD performance levels. As mentioned before, 10 earthquake intensity (IM) levels have been investigated. Considering that the fundamental periods of the examined case-studies range from 2.5 to 3.3 s, a unique conditioning period (T*) equal to 3.0 s has been assumed for the seismic performance assessment. The values of Sa(T*) for each IM level and for the two considered sites (expressed in terms of geometric mean) are summarized in Table 18. Each "stripe" of seismic response has been then analysed running a set of 20 ground motion pairs featuring the mentioned conditioning period. It is worth noting that, according to Italian Seismic Code (NTC2018), the IM associated with level 2 and 6 (labelled as IM2 and IM6 in what follows) correspond to the earthquake intensity levels for the verification of the Damage and Collapse Limit States, respectively.

Ground-motion prediction equation (GMPE), defining probability distribution of ground motion intensity, of (Akkar and Bommer, 2010) was employed for T*=3.0s.

Table 18. Spectral accelerations Sa(T^*=3s), expressed in unit of g, for each earthquake intensity level

IM	**1**	**2**	**3**	**4**	**5**	**6**	**7**	**8**	**9**	**10**
RP (years)	10	50	100	250	500	1000	2500	5000	10000	100000
L'Aquila	0.0002	0.011	0.031	0.062	0.11	0.177	0.271	0.384	0.576	1.053
Naples	0.001	0.009	0.026	0.044	0.067	0.093	0.126	0.162	0.216	0.348

2.4.2 NTHA results for rubber-based isolation systems

In this section, NTHA results are reported for both the GC and the UPD performance levels. Regarding the GC, results are given in Figure 38 in terms of number of failures and collapse modalities (i.e. the collapse condition that first occurs) for both the SLD cases (S60, S70 and S80 reported in the left column) and GLD cases (G60, G70 and G80 reported in the right column). The first remark is about the collapse modalities that involve sliders and superstructure for the SLD cases whereas HDRBs (shear failure) and superstructure for the GLD cases. The reason can be find looking at the design choices and the performance levels definition, as illustrated in the relevant sections. More in details, for the GLD cases (located at

Naples) the isolation system design displacement is lower than the one for SLD cases (located at L'Aquila) (200 mm vs. 300-350 mm, respectively, see Table 14), due to the lower seismic hazard level. Consequently, the rubber thickness of HDRBs and their displacement capacity (corresponding to the ultimate shear deformation assumed equal to 350%) are different for the various cases. In particular, the displacement capacity is 357 mm for the GLD cases at Naples (total rubber thickness of HDRBs equal to te=102mm), 616 mm for the cases S60 and S70 (total rubber thickness of HDRBs equal to te=176mm) and 532 mm for the S80case (total rubber thickness of HDRBs equal to te=152mm). For the sliders the displacement capacity is assumed equal the nominal displacement capacity of the device increased by an extra-stroke displacement equal to half diameter of the internal pad. The nominal displacement capacity is assumed 50 mm larger than that of HDRBs, thus the final capacity values are: 250+250/2=375 mm for the GLD cases, 350+250/2=475 for the cases S60 and S70 and 300+250/2=425 for the S80 case. Ultimately, for the GLD cases, the sliders displacement capacity is larger than the HDRBs one, while the contrary holds for the SLD cases. This is the reason behind the difference between the two groups of buildings (GLD and SLD) in terms of both collapse number and failure mode of the isolation system.

More in details, for all the case studies no failure of the isolation system is observed up to IM6 (corresponding to the earthquake intensity level assumed in the design for the verification of the CLS (Collapse prevention Limit State) of the isolation system), with the only exception of the case S60, for which two failure events are registered at IM6, although they involve the superstructure only. After IM6, the number of failures rapidly increases for the SLD cases, due to the exceedance of the capacity limit of the sliders. On the contrary, for the GLD cases, the number of collapses slowly increases up to IM9, and collapse mainly involves the shear failure of HDRBs. This last situation is more suitable due to the lower number of collapses but also because the shear failure of HDRBs does not lead to a sudden loss of bearing capacity like for the failure of sliders. Such outcome suggests that sliders should be always designed in such a way to have a displacement capacity larger than the ultimate displacement capacity of the HDRBs. This can be obtained by amplifying the maximum design displacement at least by the ratio between the ultimate shear capacity and the design shear deformation of HDRBs (in this case 350/200=1.75). Regarding the superstructure, the number of collapses is directly related to the superstructure over-strength, i.e. the ratio between the design shear (i.e. the elastic limit defined by means of POA with mass proportional forces in the fixed-base configuration of the

superstructure) and the maximum base shear. As can be seen from the capacity curves depicted in Figure 27, with reference to the X-direction (i.e. the weakest direction), for the GLD cases the overstrength ratio increases passing from the older to the more recent buildings, leading to a progressive reduction of the number of superstructure collapse. For the SLD cases, the trend would be the same looking at the X-direction of the capacity curves of Figure 27. However, it should be kept in mind that the S70 case has been designed by considering a lower elastic limit, due to a premature yielding of the superstructure in the Y-direction. Consequently, in the X-direction, it is characterized by the highest over-strength ratio, that leads to a very low number of superstructure collapses. Also, in this case a general conclusion can be drawn, i.e. the over-strength ratio of the superstructure play a fundamental role in controlling the superstructure collapses, thus only an adequate over-strength ratio of the superstructure ensures suitable extra margins towards the collapse of the superstructure for earthquake intensity levels higher than the CLS design level. In addition to the considerations above, it should be remembered that the difference between the two hazards levels characterizing the two sites considered in this study (i.e. Naples and L'Aquila) influences significantly the number of collapses, as already highlighted in previous studies (Ragni et al. 2018; Micozzi et al. 2021).

The results in terms of UPD performance level are reported in Figure 39 for the SLD buildings and in Figure 40 for the GLD buildings, where, for each IM, the D/C values registered during the analysis are provided. Moreover, the total number of failure cases (i.e. analysis cases in which D/C≥1) is reported on the top of the diagrams. It is worth noting that, if the collapse of the isolation system is registered (GC), the UPD limit state is considered attained too, regard-less of the D/C ratio value (spot highlighted with black X). As can be seen, for the SLD cases (located at L'Aquila) the first failure event is registered between IM4 and IM5, always along the weaker direction (i.e. the X direction). Very low D/C values are observed at IM2, which represents the earthquake intensity level associated with the verification of the Damage Limit State, according to the Italian seismic Code (NTC2008). Therefore, safety margins larger than expected are observed towards the attainment of the UPD performance level, as already found for new base-isolated buildings (Ragni et al., 2018; Micozzi et al, 2021).

Moreover, it is found that the first collapse is always due to the in-plane behaviour of the infills. In other words, the out-of-plane collapse of the infills does not influence the attainment of UPD conditions for base-isolated buildings. This low OOP failure rate is related to the low

acceleration experienced by the isolated structure and consequently the only failure of the infill is related to the IP failure due to the deformability of the superstructure.

It is also worth noting that all cases show seismic performance rather different in the two horizontal directions, this is probably due to the absence of internal beams in one direction, which strongly affects the horizontal stiffness of the superstructure in that direction and because the X direction is the one with the lower peak shear resistance. Consequently, the higher displacement demand is always attained in X direction.

For GLD cases (located in Naples), the intensity level at which the first failure (D/C≥1) occurs is even higher, being equal to IM5 for the G60 and G70 cases and to IM7 for the G80 case, once again along the X direction. Obviously, also in this case, the D/C values registered at IM2 are largely lower. The number of failures decreases passing from L'Aquila to Naples, even though the buildings are not seismically designed in the latter case. Moreover, for both sites, the older buildings show a little higher number of failures.

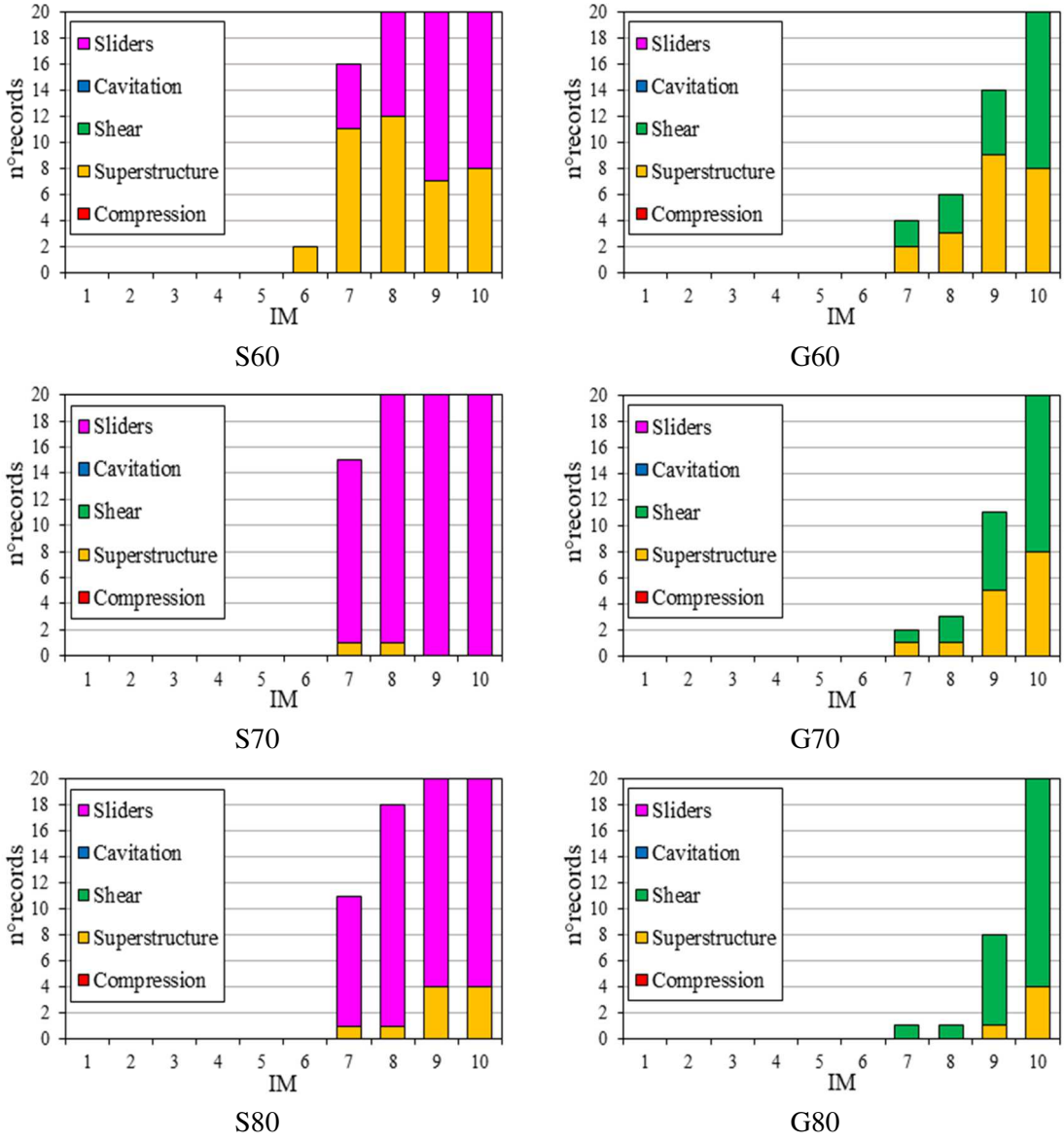

Figure 38 GC results for six case study buildings with rubber-based isolators.

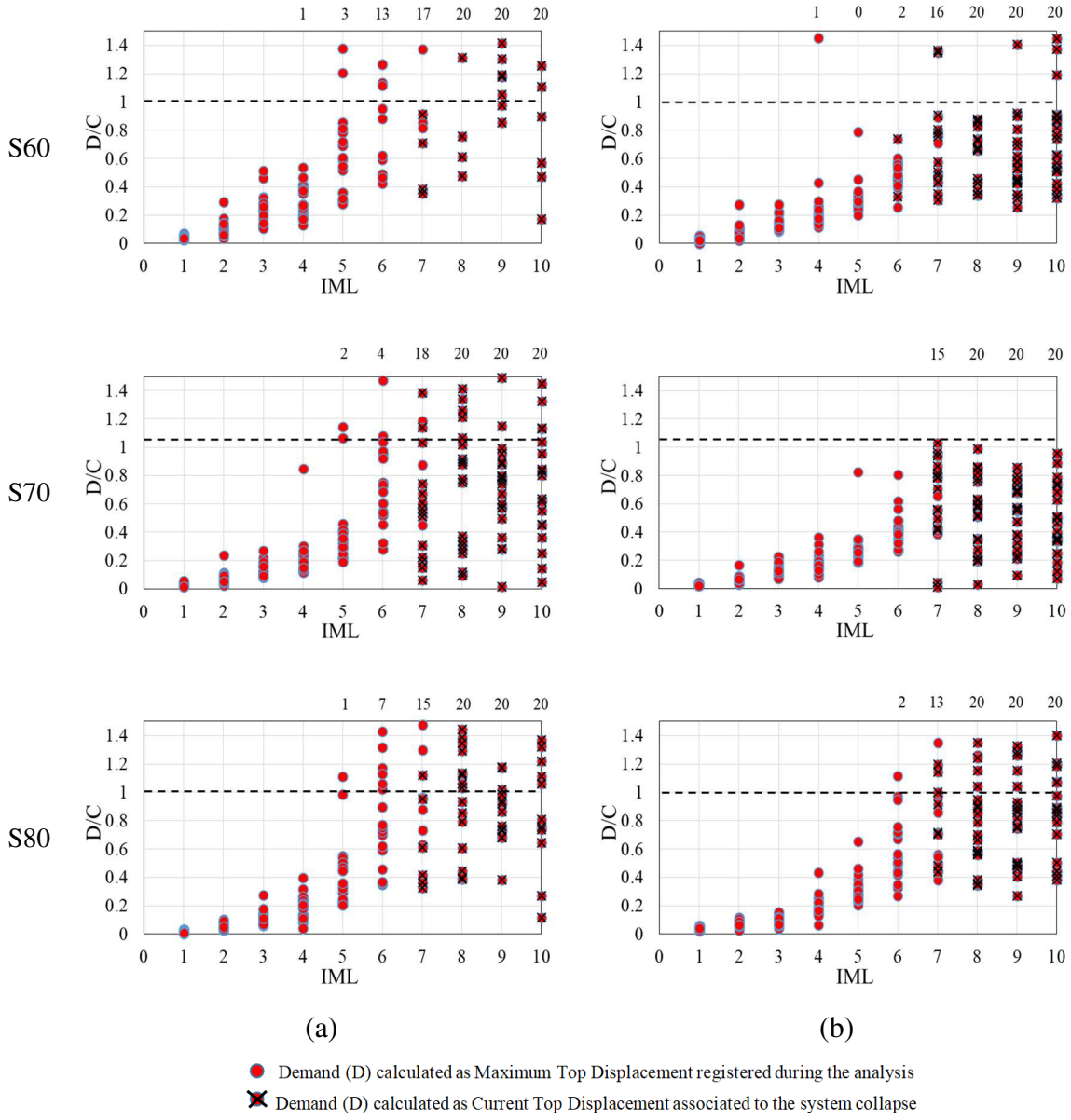

Figure 39 D/C displacement ratios associated with the attainment of the UPD performance level for the SLD buildings located at L'Aquila: X-directions (a) and Y-direction (b).

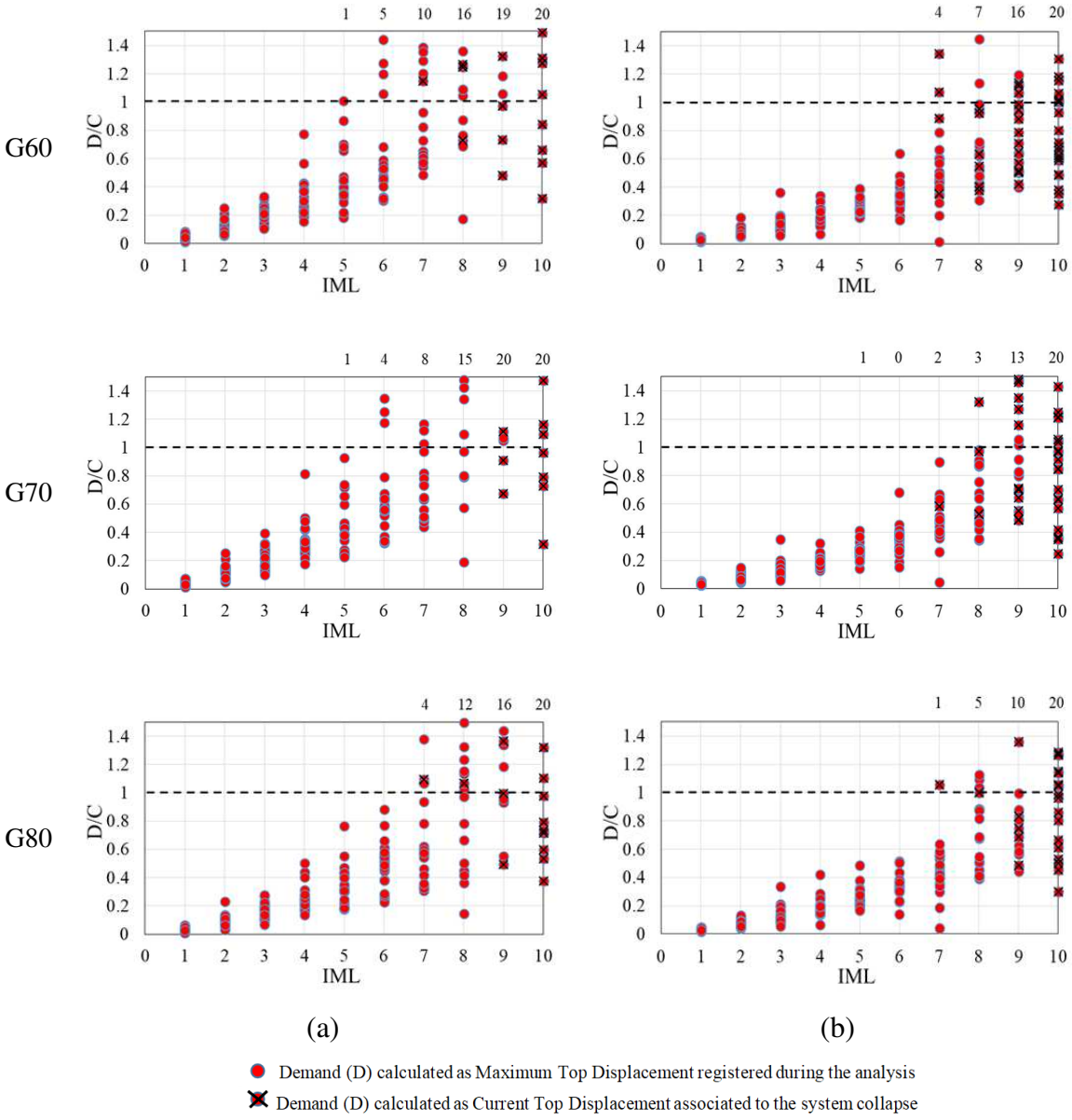

Figure 40 D/C displacement ratios associated with the attainment of the UPD performance level for the GLD buildings located at Naples: X-directions (a) and Y-direction (b).

2.4.3 Comparison with fixed base buildings

Figure 41 and Figure 42 respectively show the results related to the UPD performance level for GLD and SLD buildings both in the fixed-base and in the base isolated configuration. Obviously, the analyses on the fixed-base buildings were conducted using pairs of accelerograms with a period conditionally equal to 1 second (T*=1s); this value is very close to the mean of the vibration periods.

It is very important to recall that a different GMPE was used in the hazard definition; the GMPE selected for computing the hazard for spectral accelerations at periods shorter than 2.0s is the one of (Ambraseys et al., 1996), which use as IM the maximum spectral acceleration between the horizontal components. For longer periods, needed for predicting the response of base isolated structure, the GMPE of Ambraseys et al. (1996) was not applicable because its maximum period is 2.0s. For this reason, GMPE of (Akkar and Bommer, 2010) was employed for T*=3.0s.

White dots drawn in the diagrams concerning fixed-base buildings (column (b)) represent the number of UPD achievements due to at least one early out-of-plane collapse of at least one infill (regardless of the direction in which it occurs). While, stars drawn in the diagrams related to isolated base configuration (column(c)) represent the number of failures of the isolation system that occurred before the UPD performance level reachment. Finally, column (a) represents the trend of the D/C ratio (demand (D) on capacity (C)) referred to the performance level UPD as the seismic intensity increases; in particular, the marked lines refer to the fixed-base configuration, while the thin ones refer to the base isolated configuration in x (red lines) and y (blue lines) directions respectively.

The building code adopts the capacity design method, based on the definition of performance levels (or limit states). Four are the reference performance levels that needs to be accounted for, and verified in the design process:

- Operability Limit State (OLS): it is one of the serviceability limit states (SLE), and requires all the structural and non-structural components to be fully operational and undamaged after the seismic event;
- Damage Limit State (DLS): this a SLE too and requires all structural and non-structural elements to only suffer light damages. Furthermore, the structural elements stiffness and ductility shall not be invalidated. Overall damages should be easily repaired;

- Life Safety Limit State (LLS): is one of the ultimate limit states (SLU) and refers to the condition in which non-structural elements suffer significant damages but structural elements stiffness and strength are reduced but not impaired. The structural integrity may be restored through local and global reinforcement actions;
- Collapse prevention Limit State (CLS): is a SLU too and refers to the condition in which both structural and non-structural elements suffer severe damages. The structure is not operational but, thanks to the structural elements' residual stiffness and strength against vertical loads it is not collapsed.

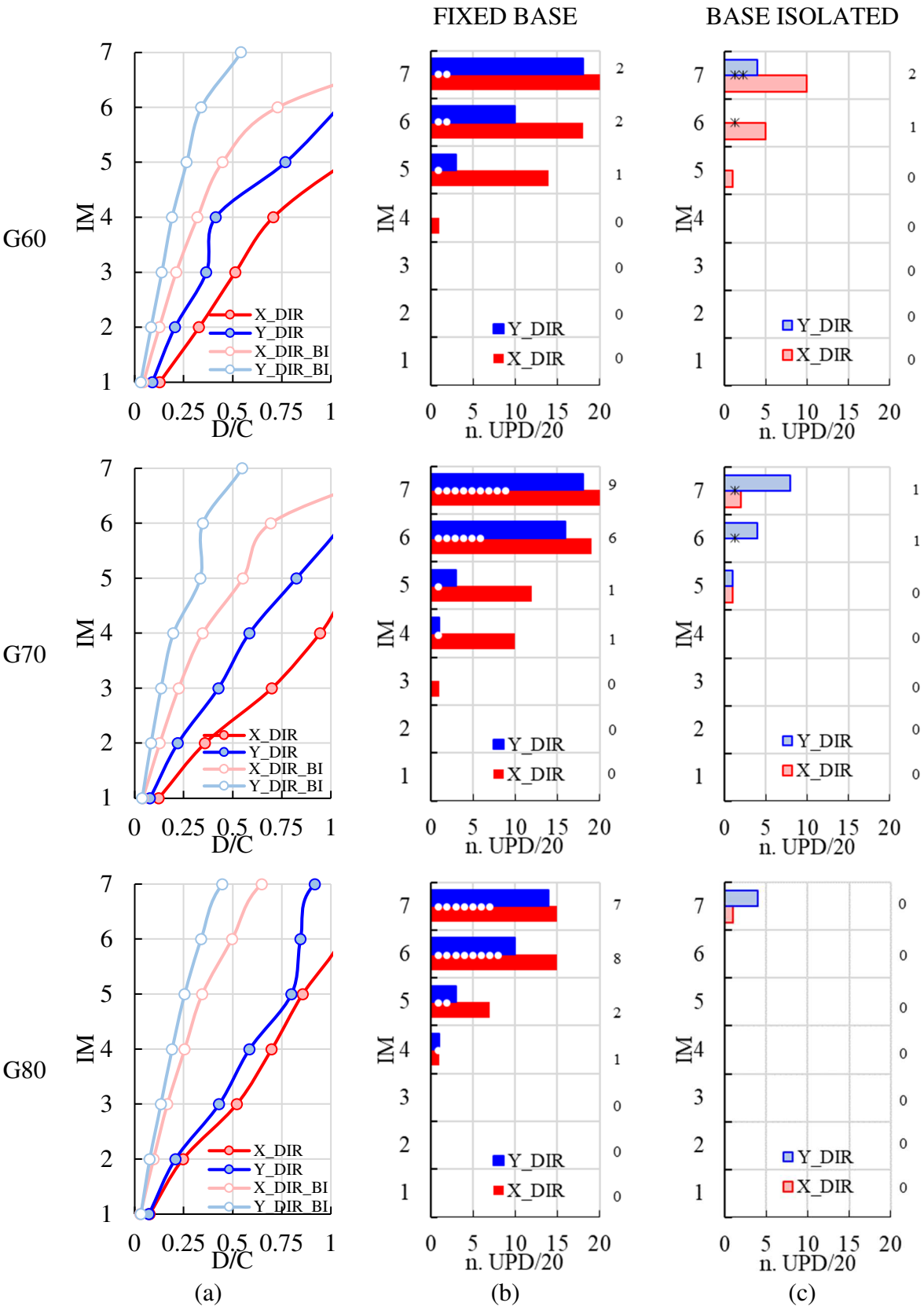

Figure 41 Comparison UPD results GLD models

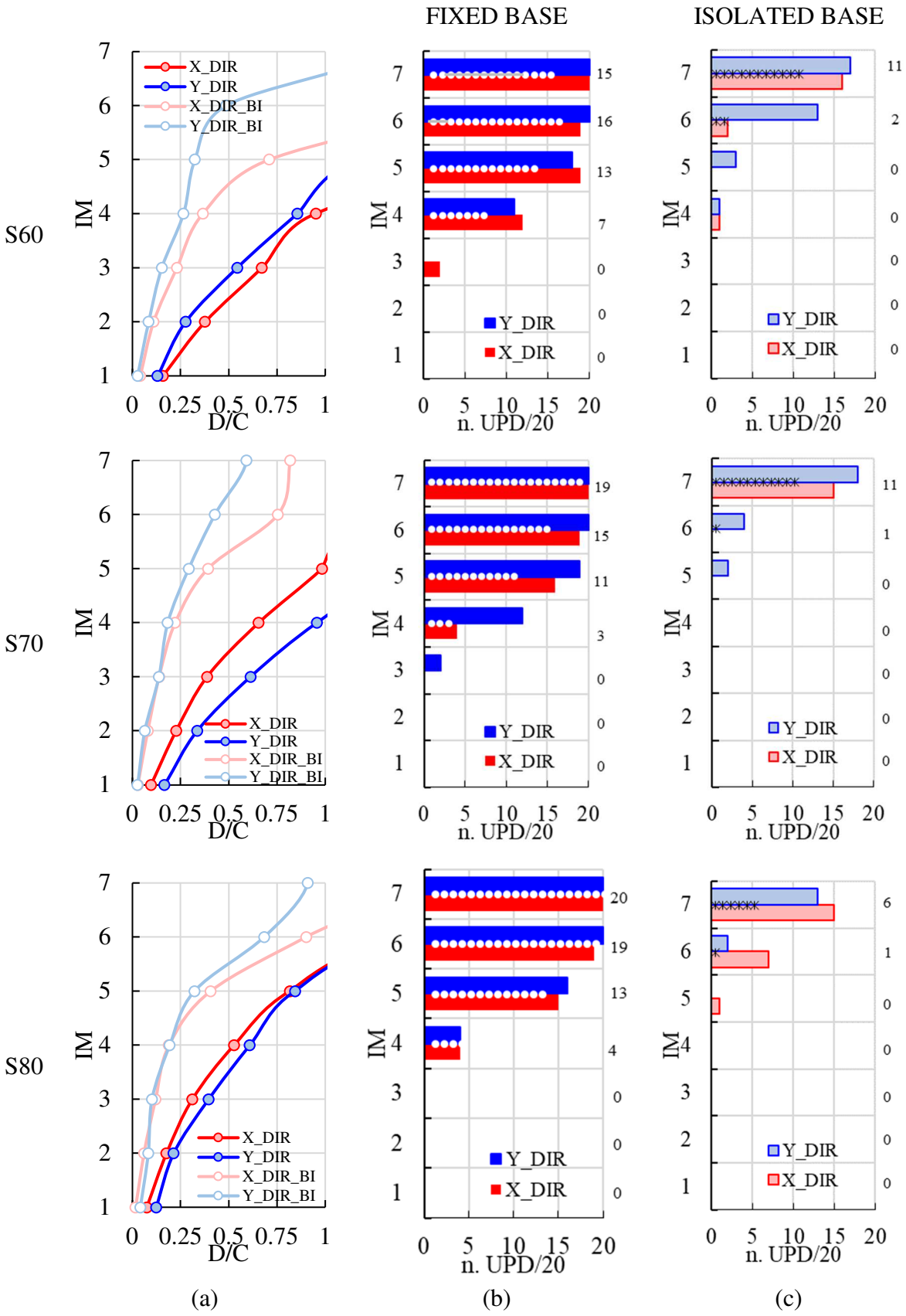

Figure 42 Comparison UPD results SLD models

The Italian building code adopts the Poisson model to predict the temporal uncertainty of an earthquake with a return period equal to: $TR = -VR/ln(1 - \rho VR)$, where ρVR is the exceedance probability within the reference period VR of the considered limit state (see Table 19).

Table 19 Limit States exceeding probability and return periods for a reference period of 50 years

Limit State		Exceeding probability ρVR	Return Period TR (y) Vr= 50y
Serviceability Limit States (SLE)	OLS	81%	30
	DLS	63%	50
Ultimate Limit States (SLU)	LLS	10%	475
	CLS	5%	975

For this reason, the graphs in Figure 41 and Figure 42 extend to the maximum intensity with a return period of 2500 years.

The diagrams in column (a) show how the isolation system significantly reduces the slope of of the straight lines representing the D/C ratios; moreover, these ratios almost never reach saturation (D/C=1).

Generally speaking, all the results concerning the usability-preventing performance level point out that all isolation systems work effectively in limiting the building damage for seismic intensities much higher than the intensity level considered in the design (corresponding to IML2, i.e. return period equal to 50 years). In fact, a significant damage rate of non-structural components occurs only at IML 6 and many of these damages are linked to the collapse mechanism of the isolation system.

All the results and especially the ones corresponding to the high seismicity site (L'Aquila) show that all the isolation systems are characterized by a little margin beyond the intensity level considered in the seismic design (corresponding to IML6, i.e. return period equal to 1000 years).

This limited margin associated to the collapse failure of base-isolated structures seems to be related to the more controlled behavior during design and the lower margin of safety with respect to collapse beyond the maximum design displacement. For the same reason, they show lower risk with respect to the usability-preventing damage.

Figure 43 shows the fragility curves of anticipated out-of-plane collapses recorded before IP damage of infills in fixed-base buildings. As can be seen, the slope of the curves is inversely proportional to the construction period: this behaviour is more related to the acceleration

experienced by the superstructure: G80 has higher shear capacity; consequently, the acceleration experienced by the infills is higher because the "softening " branch of the superstructure is reached later.

On the other hand, with seismic isolation the out-of-plane collapses of the panels are not decisive in the definition of the UPD; in other words, seismic isolation, in addition to limiting the extent of damage on non-structural elements (number of UPD achievements) but also improves the mode of occurrence (only in plane damage).

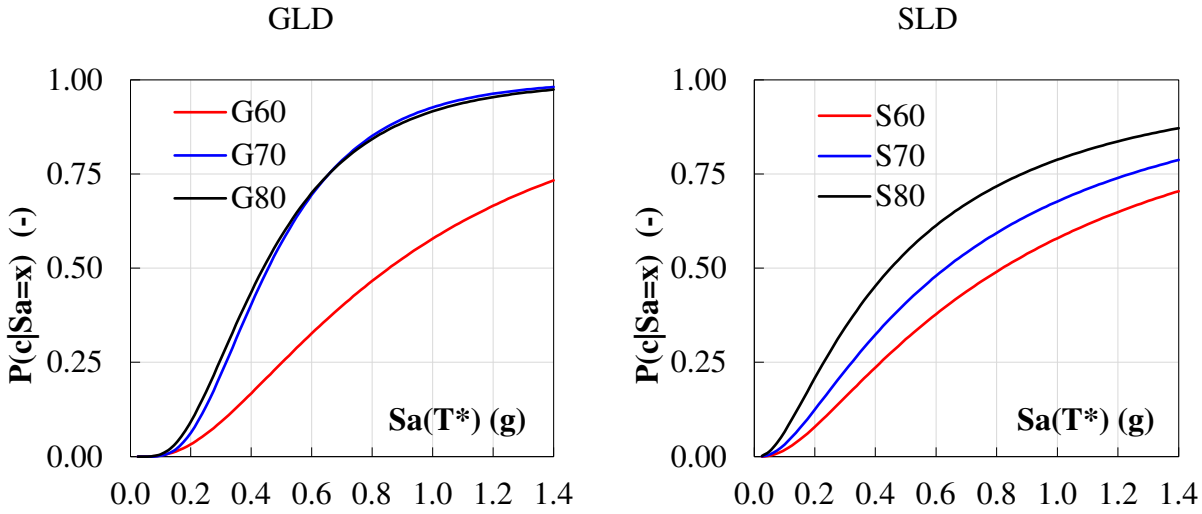

Figure 43 Fragility curves of anticipated out-of-plane collapses recorded before IP damage of infills in fixed-base buildings GLD (left) and SLD (right)

2.5 SUMMARY AND RESULTS

The study presented in this section was developed within the activities of the ReLUIS-DPC 2019-2021 research program, funded by the Italian Dept. of Civil Protection.

The analyses performed within the *RINTC* research project on existing RC buildings retrofitted with seismic isolation according to the Italian minimum code requirements have been presented in this section.

In particular, a wide set of archetype residential RC buildings, differing for construction period (50s-60s, 70s, 80s-90s) and design approach (Gravity Load Design, GLD, and Seismic Load Design, SLD, based on old technical standards) have been considered. GLD buildings are supposed to be located in the city of Naples (characterized by medium seismic hazard for Italy) and SLD buildings are supposed to be located in the city of L'Aquila (characterized by high seismic hazard for Italy). Moreover, rubber-based isolation systems using standard high damping rubber bearings (HDRBs), in combination with flat sliding bearings are considered. All the isolation systems have been designed to avoid any damage of the superstructure up to the Life Safety limit State (i.e. return period equal to around 500 years), in accordance with the current Italian Seismic Code.

All the case studies have been assessed by means of multi-stripe nonlinear time history analysis, computing the probability of occurrence for two performance levels, namely *Global Collapse* (*GC*) and *Usability Preventing Damage* (*UPD*). As base-isolated buildings are in-series systems (being composed by the isolation system and the superstructure) and isolation devices can undergo different failure modes, a multi-criteria approach has been followed for the definition of the aforesaid performance levels. The most advanced numerical models have been used to simulate the behaviour of the isolation devices. To describe the nonlinear cyclic behaviour of *HDRBs* the *Kikuchi Bearing Element* (available in Opensees) has been used in the analyses, due to its capability of simulating the behaviour of HDRBs under large displacements and high axial loads.

The results relevant to GC show that existing RC buildings retrofitted by seismic isolation work effectively in limiting damage to the superstructure, but they may exhibit a low margin with respect to the global collapse of structure, especially for high seismicity regions. The collapse arises on the superstructure or on the isolation system (either sliders or HDRBs depending on the safety margin assumed in the design), mainly depending on the hardening behavior of HDRBs at large displacements. For this reason, the over-strength ratio of the superstructure plays a fundamental role in controlling the number of collapses on the superstructure side. On

the isolation side, since a larger shear capacity characterizes the HDRBs, sliders should be designed to have a comparable displacement capacity.
The results of the buildings located in moderate seismicity regions show larger safety margins than those located in high seismicity regions. This confirms the significant influence of the site hazard on the seismic performance of retrofitted base-isolated structures.

Moreover, it is found that the the first collapse is always linked to the in-plane infills behaviour suggesting a negligible contribution provided by the OOP behaviour in the attainment of UPD failure conditions; on the other hand, with seismic isolation the out-of-plane collapses of the panels are not decisive in the definition of the UPD; in other words, seismic isolation, in addition to limiting the extent of damage on non-structural elements (number of UPD achievements) but also improves the mode of occurrence (only in plane damage).

SECTION 3:
SEISMIC PERFORMANCE OF MASONRY INFILLS WITH DECOUPLING SYSTEM

3.1. INTRODUCTION

The results of the study carried out by Gesualdi et al. (2020) presented in the first section, confirmed the importance of correct modelling of non-structural element, showing that the IP/OOP interaction of masonry infills can significantly affect both the usability and life-safety seismic performance of RC buildings. It is also important to note that the OOP collapse of URM walls is a very dangerous failure mechanism because it might seriously threaten human life either inside or outside the building.

For these reasons, in the last years, different solutions for the improvement of the seismic behaviour of masonry infills and partitions are proposed. A number of solutions are based on the idea of increasing load-bearing capacity of masonry infills rigidly connected to RC frames. For instance (see Figure 44), this can be achieved by providing additional horizontal and vertical reinforcement bars in infill walls (da Porto et al. 2013, Silva et al. 2016), placing steel reinforcement in bed joints and mesh reinforcement on the panel surfaces (Calvi and Bolognini 2001) or by using plaster reinforcements made of textile meshes (see Figure 45) (Valluzzi et al. 2014; Akhoundi et al. 2018).

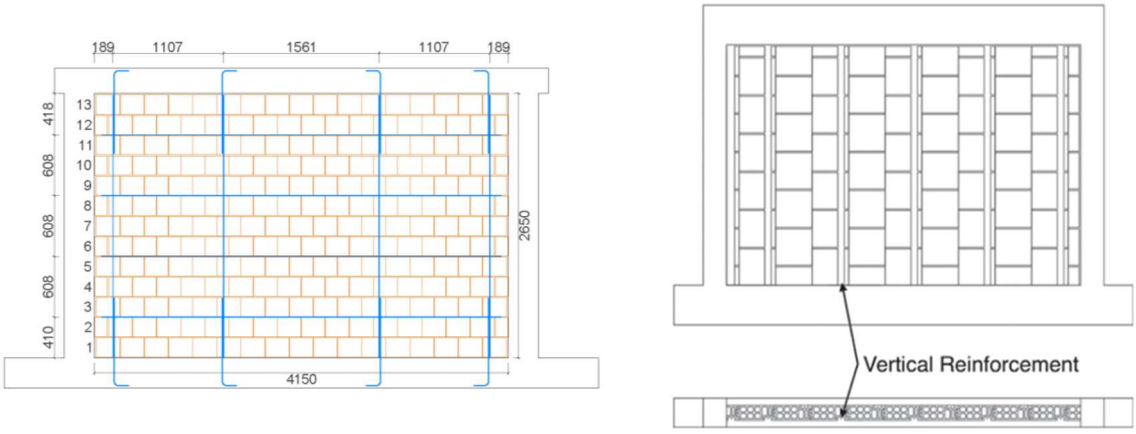

(a) (b)

Figure 44 Masonry reinforcement: (a) Porto et al. 2013, (b) Silva et al. 2016

The solution proposed by da Porto et al. 2013 (Figure 44a) uses brick masonry with vertical holes and special recesses for vertical reinforcing bars; in these units two webs can be removed forming an open "C" pocket that can be used to easily cast the vertical reinforcement bars anchored both on RC base and on the upper beam. The construction system proposed at University of Minho in Silva et al. 2016 (Figure 44b) also uses masonry units made of clay with vertical holes and a tongue and groove interlocking in vertical direction; these masonry units have grooves at the surface that make possible the addition of vertical reinforcement bars. In

both cases, the construction process is slightly different from a traditional infill and the addition of vertical reinforcement implies that previous works need to be done.

The strengthening technique based proposed by Calvi and Bolognini, 2001 is realized by applying a light wire mesh adequately anchored in the concrete frames using special steel connectors.

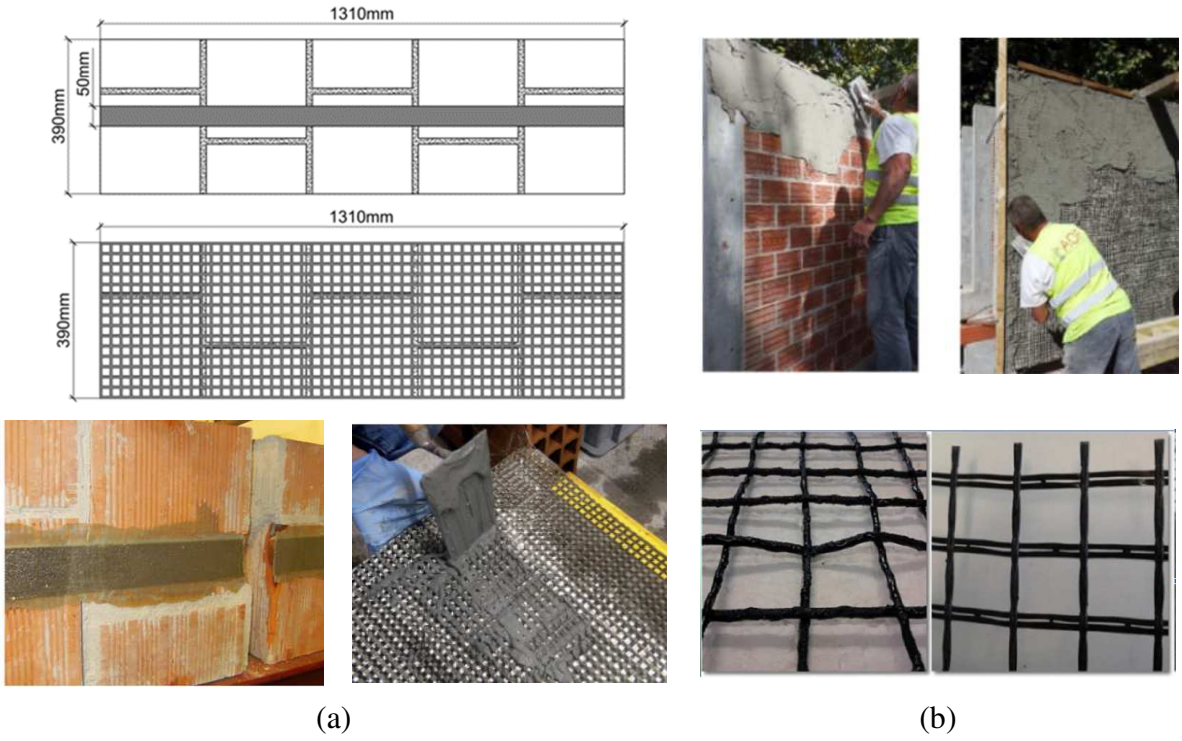

(a) (b)

Figure 45 Masonry reinforcement: (a) Valluzzi et al. 2014; (b) Akhoundi et al. 2018

However, the high costs of complicated execution could easily limit the use of these solutions in everyday practice. Additionally, strengthened masonry infills become load-bearing elements which require appropriate design. It has to be pointed out, that stiffening of infill walls changes the fundamental period of vibration of the structure and leads to an increased seismic demand.

Furthermore, another group of solutions aims to increase the deformation capacity of masonry infill walls by adding different types of sliding surfaces in the wall (see Figure 46a) (Verlato et al. 2016; Morandi et al. 2018; Preti and Bolis 2017). This approach is based on keeping the infill walls rigidly attached to the frame, or slightly disconnected, but at the same time increasing the deformability of the infill wall using special construction measures in the wall. The basic intention is to provide ductile behaviour to the infill walls with the reduction of interaction stresses and at the same time increase of damping level, thanks to the dissipative action of deformable or sliding elements.

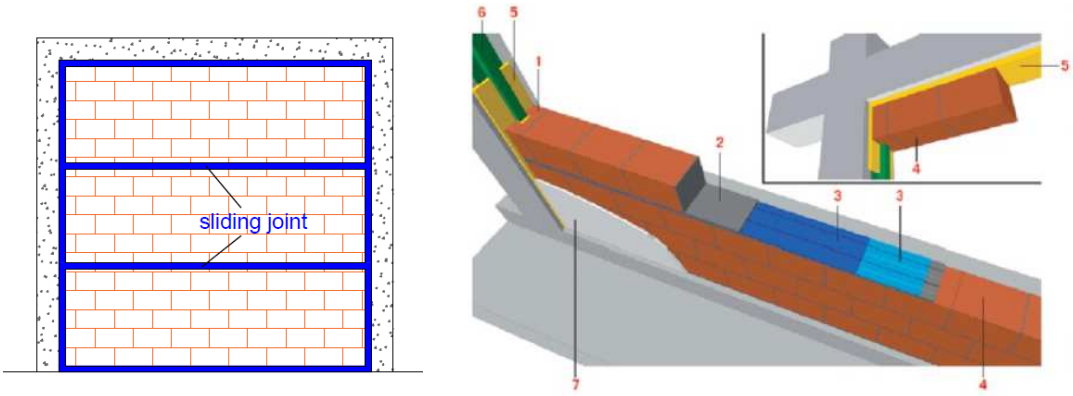

(a) (b)

Figure 46 Partitioned masonry infill wall (a); details of the innovative masonry infill with sliding joints (b) 1. C-shape units; 2. mortar bed-joints; 3. sliding joints; 4. clay units; 5. interface joints; 6. shear keys; 7. Plaster (Morandi et al. 2018).

The technique proposed by Morandi et al. 2018 (see Figure 46b) is realized introducing a predetermined number of horizontal sliding surfaces in the wall in combination with a deformable layer between masonry infill and RC frame at the top of the panel. The out-of-the-plane stability of masonry infills with this system is ensured by special steel shear keys connected to the columns and brick blocks with specially shaped ends. The out-of-the-plane flexural strength is also improved through the application of a thin layer of fiber-reinforced plaster.

Preti and Bolis 2017 (see Figure 47), on the other hand, pursued an approach in which the wall is subdivided by vertical sliding surfaces allowing the individual wall sections to rotate independently. In this proposed solution, the out-of-plane (see Figure 47b) loads are transferred in vertical direction through shear connectors to the frame transom. For thermal and acoustic performance, the gaps are meant to be sealed with a soft material. The planks stay in the thickness of the infill, so they can be covered by plaster to obtain a homogeneous facing. Additional internal or external insulating layers can be added, provided that they are sufficiently flexible in their plane.

In case of window and door openings, this type of systems must be supplemented by further edge profiles to provide reliable boundary conditions.

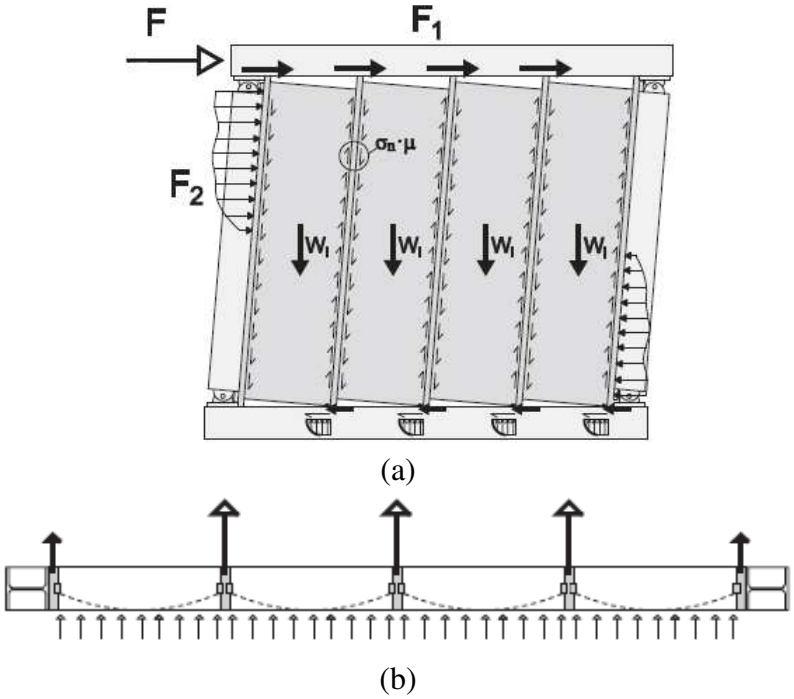

Figure 47 In Plane (a) and Out-Of-Plane (b) mechanism in the infill with vertical sliding surfaces proposed by Preti and Bolis (2017)

The main disadvantage of these approaches is practical application, as the quality of production and installation of sliding surfaces might significantly affect effectiveness of the system. Furthermore, issues related to the shear failure of the surrounding frame as well as out-of-plane loads are present.

Therefore, the third approach is to separate the frame and infill so that deformations in the frame do not generate any force in the infill (see Figure 48), thus allowing relative displacements between the wall and the frame to occur without interactions. These systems are providing decoupling of the infill wall and the frame.

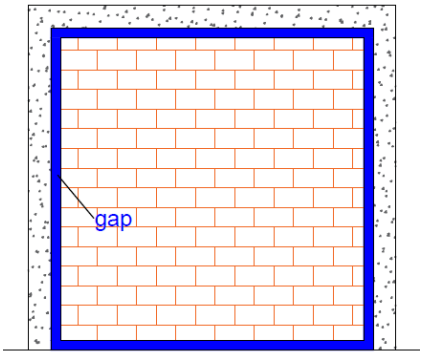

Figure 48 Masonry infill with decoupling system

One of the most promising solutions is the system INODIS based on the idea of decoupling of masonry infill from the surrounding frame. The INODIS system increases the IP and OOP

resistance of URM infills by means of dissipative and sliding connections placed along the contact areas between the infill (partition) and the surrounding RC frame. The efficiency of the described INODIS system is already shown on the full-scale experimental test (Marinković and Butenweg 2019) and a comprehensive numerical study (Marinković and Butenweg 2022). However, the execution of case studies of the seismic performance on a building level are still missing.

In this study, the advanced non-linear numerical model previously implemented in Opensees by (Di Domenico et al. 2022) presented in second section of this work is further developed and calibrated to capture the specific IP/OOP behaviour of decoupled infills. The model is then used to examine, for the first time, the seismic response of a building model with decoupled infills. By means of this model, seismic performance and expected losses of real buildings under different earthquake intensity levels will be evaluated, comparing traditional and innovative (INODIS) solutions for masonry infills/partitions. For needs of this study, the seismic performance of a case-study building, representative of typical residential buildings realized in Italy in the ‘90s, is examined, at different earthquake intensity levels, with return period equal to 50, 500 and 2500 years, respectively.

3.2 INODIS SYSTEM

Motivation for the development of the INODIS system is a lack of the available cost-effective solutions that can successfully reduce the seismic damage in masonry infill walls. The proposed INODIS system is based on the concept of decoupling of masonry infill from the surrounding RC frame. Figure 49 shows masonry infill installed with INODIS system. At the top of the infill wall and along the vertical edges U-shaped elastomers are placed around plastic bars which are previously attached to the surrounding RC frame. First layer of U-shaped bearings is made of soft elastomeric material which allows later activation of masonry infills under in-plane deformation of RC frame. Moreover, sliding surfaces are glued on the plastic profiles, concrete and U-shaped elastomer in order to reduce the friction effects and provide sliding between masonry infill and RC frame. The second layer of U-shaped profile is made of stiffer elastomer. In combination with plastic bar attached to the surrounding frame U-shape elastomers represent the shear key for the wall in the OOP direction and thus prevent the OOP movement of the wall. At the bottom of the infill wall decoupling is achieved by three stiffer elastomer strips. The middle strip is glued to the bottom beam, while outer strips are glued to the infill wall. In this way shear key effect is provided at the bottom too.

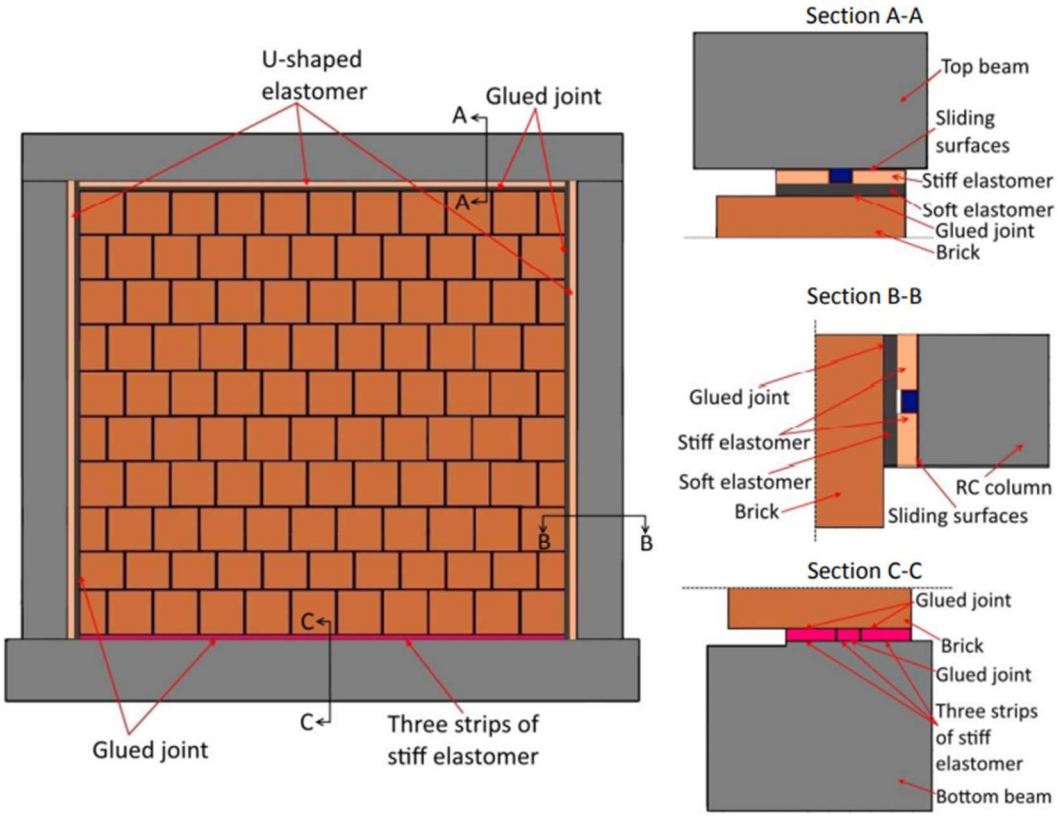

Figure 49 INODIS decoupling system (Marinković and Butenweg 2019)

The steps required to install the system are shown in Figure 50. In the first step, the plastic profile is attached to the frame with screws or nails using a screwdriver or a nail gun. In the next two steps, the sliding surfaces are glued on the plastic profiles and concrete frame and the preassembled U-Profile is pushed on the plastic profile. In the fourth step, a strip made of elastomeric cellular material is installed at the bottom. First the middle strip is glued to the bottom beam. Thereafter the outer strips are inserted and glued to the bottom row of bricks when bricking up of the infill starts.

In the fifth step the infill wall is bricked up as usual, whereby the bricks at the end of each row are glued to the U-Profile. In the final step, the last row of bricks can be installed and glued to the U-Profile at the top beam. After performing the steps described, the system is installed and fully functional. The installation steps of the INODIS system clarifies that the traditional building technique for constructing the infill wall remain almost unchanged in addition, the system is simple, can be installed quickly and appears sufficiently robust for use on construction sites.

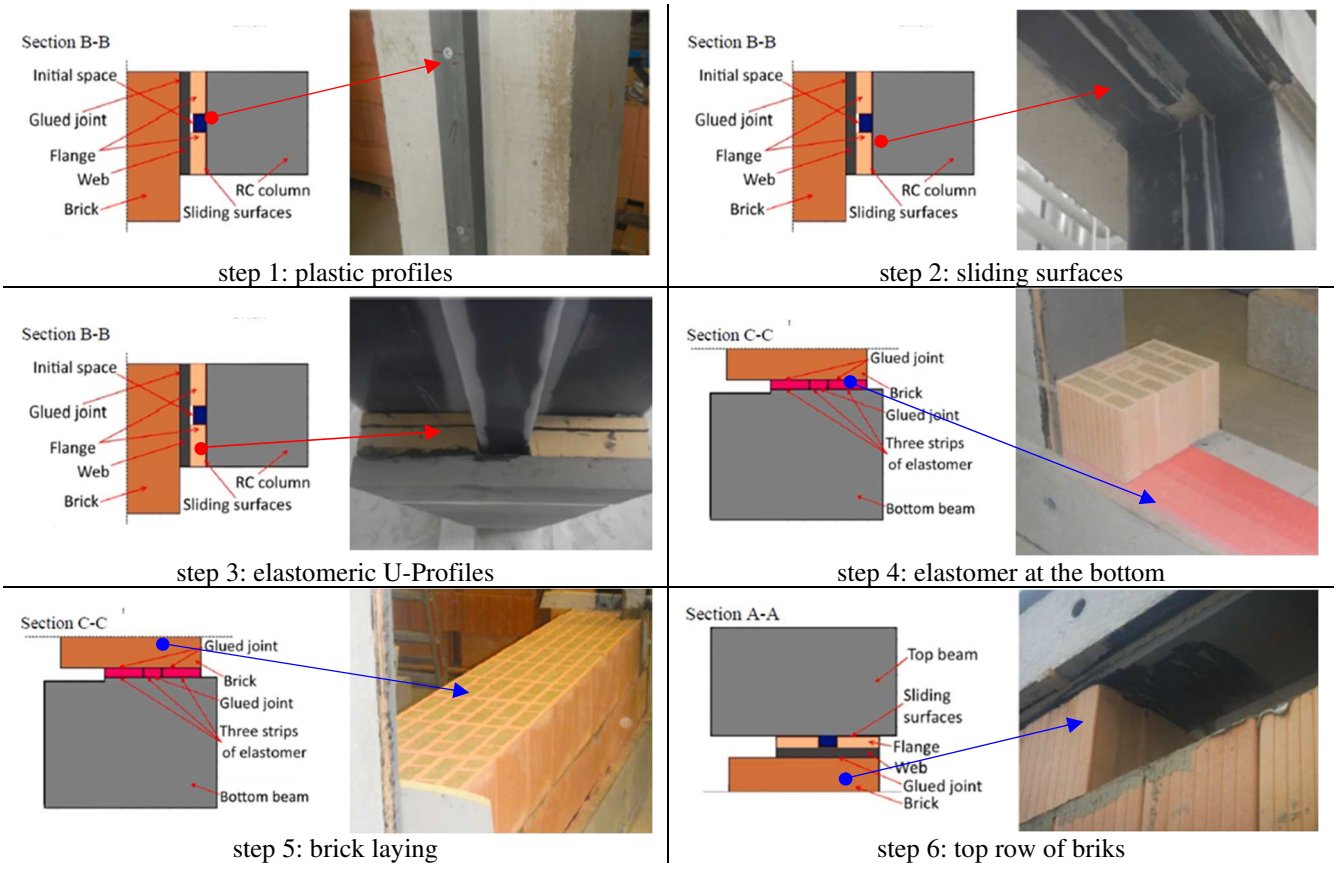

Figure 50 Working steps for installation of the INODIS system.

The additional advantage of INODIS system is that it can be easily modified for different levels of seismic events by varying thickness and stiffness of elastomers. Therefore, INODIS system

can successfully provide high levels of seismic safety to various configurations of masonry infills subjected to different separate or combined in-plane and out-of-plane actions.

3.3 METODOLOGY OF THE STUDY

The influence of the IP / OOP interaction of URM walls on the seismic response of RC frame buildings is investigated following a four steps methodology: (i) Step 1: Selection of case-study, Modeling assumptions, Ground motion selection; (ii) Step 2: Definition of seismic Performance Levels (PLs); (iii) Step 3: Non-linear Time History Analyses (NTHA); (iii) Step 4: Assessment of non-structural damage.

The basic idea of this study is to compare the behaviour of the framed building infilled with traditional infills and the same building with decoupled infills installed with the INODIS system. This can help to investigate the motivation of replacing the original infills (e.g. because extensively damaged by a previous earthquake), with new infills equipped with the innovative decoupling system (INODIS).

3.3.1 Case-study building and ground motion selection

A 6-storeys RC frame building, designed for seismic loads (implicitly for high ductility class but with sub-standard seismic details), representative of typical multi-storey residential buildings realized in Italy in the ’90s (see Figure 51) is selected.

Specifically, the building under review is referred to as S80 in the previous section.

The building features an in-plane rectangular shape with 21.40 m × 11.80 m dimensions, 3.40 m interstorey height for the first level and 3.05 m for the upper ones. It features five frames in the long direction (X-dir. In Figure 51) and three external frames in the short direction (Y-dir. Figure 51). In the Y-dir., a dog-leg stair with cantilever steps is sustained by two stiff ‘knee’ beams. Structural characteristics (geometric dimensions, reinforcement ratios, structural details, etc.) are derived from a simulated design, according to the Standards and state of practice enforced in Italy before ’90s (Ministerial Decree DM 03/03/1975 and the decrees that followed DM 19/06/1984 and DM 24/1/1986). URM infill walls realized with hollow clay bricks arranged in two single layers (150 + 80 mm thickness), separated by an air-cavity, are considered (see Figure 52(a)). The URM infills feature large openings in the X-direction (equal, on average, to 40%), while there are no openings in the Y-direction. The presence of the openings is taken into account when characterizing the in-plane and the out-of-plane infills’ responses.

The retrofit intervention aims at replacing the original double-layers infills with modern single-layer (365mm thickness) infills equipped with the decoupling INODIS system (see Figure 52(b)).

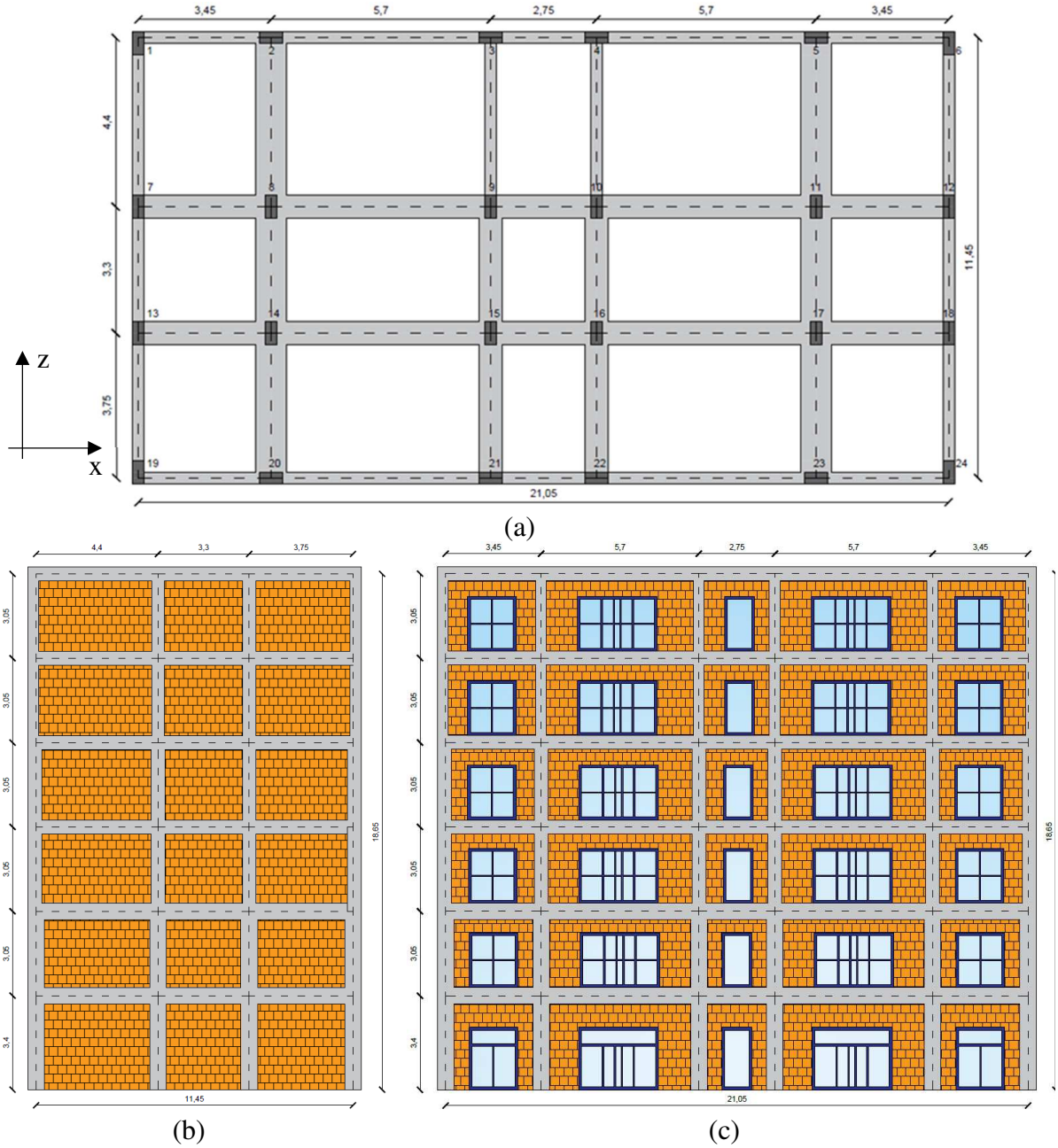

Figure 51 Case Study: (a) typological floor plan; (b) short side elevation; (c) long side elevation

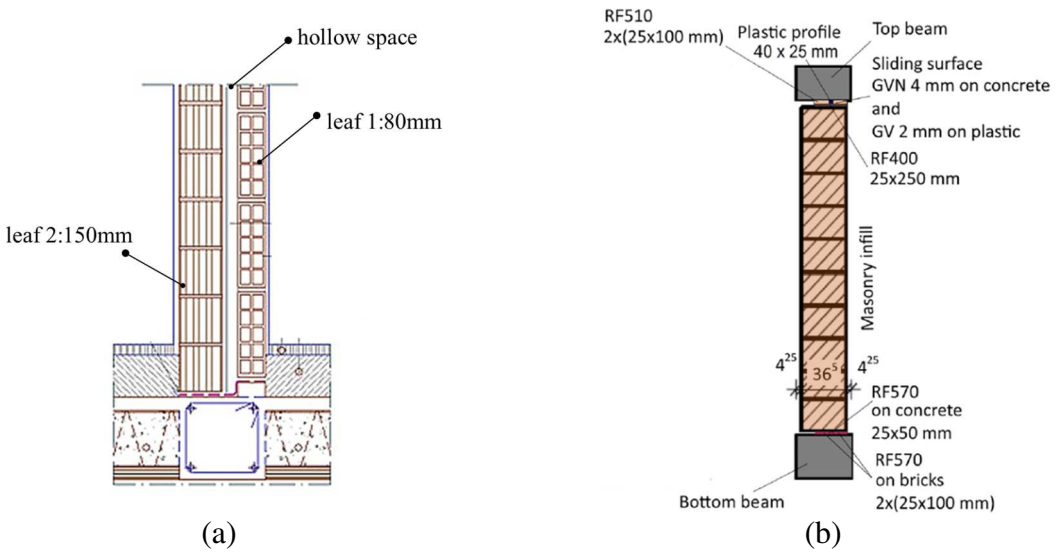

Figure 52 Types of infill considered: (a) older double layer infill and (b) modern single layer infill with INODIS system (Marinković and Butenweg 2019)

The case-study building is supposed to be located in the city of L'Aquila (central Italy) on soil type C (soft soil). The aforesaid site and soil conditions are purposely selected to investigate the seismic performance of this class of buildings for the highest levels of seismic hazard expected in Italy. Three different earthquake intensity levels, with return periods equal to 50 years (0.156 g PGA on soil type C), 500 (≈0.347 g PGA on soil type C) and 2500 (≈0.467 g PGA on soil type C), is selected for NTHA. The conditioning Intensity Measure Level (IML) for the record selection is the 5%-damping spectral pseudo-acceleration Sa(T*) at the site, at the fundamental period of vibration T*. T* was assumed equal to 1.0 s. For each seismic intensity, a set of twenty ground motion pairs, compatible with suitable Conditional Mean Spectra, derived considering the M-R-ε (Magnitude-Distance-Deviation) disaggregation and a proper attenuation relationship for the city of L'Aquila, is used. As an example, Figure 53 shows the spectra of 20 pairs of records for L'Aquila, soil type C, conditioned to Sa(T*) = 0.365g, which corresponds to the spectral acceleration with 500 years return period; the spectral acceleration values Sa at the conditioning period T* = 1s for the three seismic IMLs are shown in Table 20. Ground-motion prediction equation (GMPE) selected for computing the hazard for spectral accelerations is the one of (Ambraseys et al., 1996) which use as IM the maximum spectral acceleration between the horizontal components.

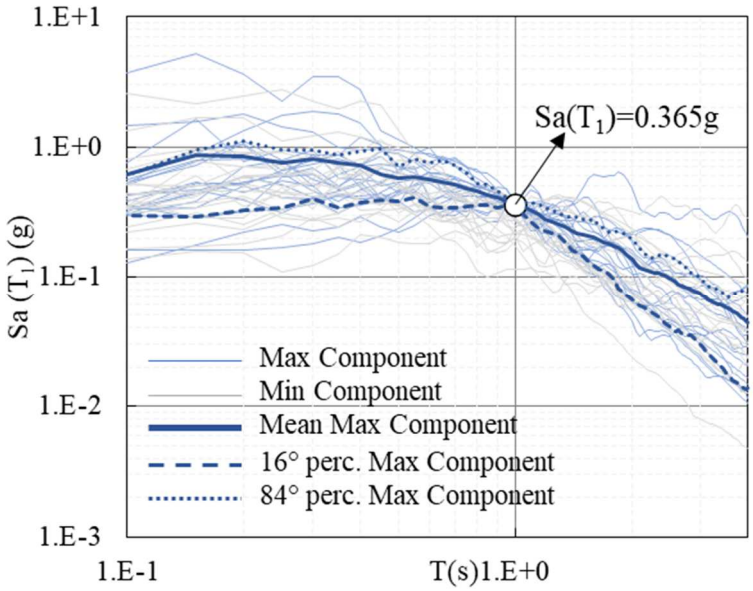

Figure 53 Response spectra of both horizontal components of the selected records for the case of L'Aquila, Soil Type C, with return period 500 years

Table 20. Seismic hazard and selected intensity measure levels

Intensity Measure Level	Return period (years)	PGA (g)	Sa(T_*=1s) (g)
IM 2	50	0.156	0.073
IM 5	500	0.347	0.365
IM 7	2500	0.467	0.855

3.3.2 Numerical model

The seismic behaviour of the selected case-study building is described through a refined 3D lumped-plasticity model implemented in OpenSees (McKenna, 2011). As explained in the previous section, a lumped plasticity model is adopted for RC beams and columns. The structural model also includes the staircase structure featuring inclined beams and cantilever steps. The model by Ibarra-Medina-Krawinkler (Ibarra and Krawinkler, 2005; Ibarra et al., 2005), implemented in OpenSees (McKenna, 2011) as modIMKmodel, is selected to describe the cyclic degrading behaviour of plastic hinges. Possible shear failure (before or after flexural yielding) is taken into account in the model. More details about this collapse criterion can be found in (Ricci et al. 2019). Concerning beam-column joints, the joint panel model referred to as "scissors model" is adopted.

It is a very simple and computationally efficient joint model, but also sufficiently accurate in predicting the experimental beam-column joint panel behaviour of non-ductile RC frames, according to Di Domenico et al. (2022).

Particular care is taken in the description of the mechanical behaviour of masonry infills, as they can strongly affect the seismic response of older RC frame buildings (featuring double-layers masonry walls with high slenderness ratio and weak beam-column joints without adequate shear reinforcement), triggering local failure mechanisms and threatening human life in case of the out-of-plane collapse. As mentioned above, in this study traditional double-layer infills are replaced by innovative panels with INODIS technology.

The modelling strategy used for the infills is the same used in the previous section, according to Di Domenico et al. 2022.

The IP behaviour of masonry infills is modelled following an equivalent compression-only strut approach.

The effect of the openings on the IP force-displacement curves is taken into account by suitable strength/stiffness reduction factors according to (Decanini et al., 2014).

The local shear interaction (between masonry infills and adjacent RC column) is captured through suitable shear springs (featuring a typical brittle behaviour with a quite steep softening branch after the peak strength), implemented at the ends of the columns to reproduce the column nonlinear shear response triggered by the additional shear demand imposed by the equivalent compression-only diagonal strut.

The IP skeleton curves of the traditional infills are implemented using the Concrete01 uniaxial material in OpenSees (McKenna, 2011). This material model successfully simulates the brittle failure of traditional infills (Figure 54), and is in accordance with the model proposed by Decanini and Fantin (Decanini and Fantin 1986).

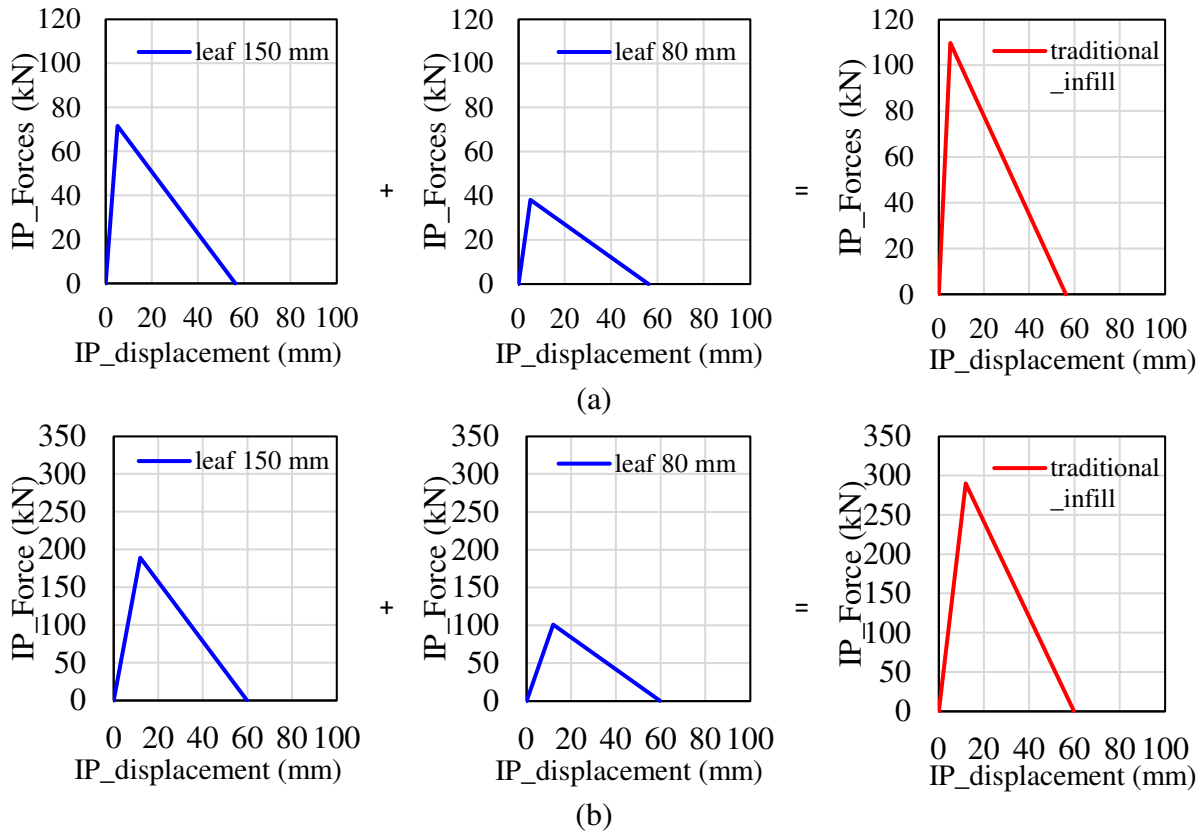

Figure 54 IP behaviour of a typical double-layer traditional infill with (a) and without openings (b)

The IP behaviour of the decoupled infills with INODIS is modelled by fitting available numerical and experimental results of the test DIO carried out on RC frame with decoupled infill (Marinković and Butenweg, 2019).

In the DIO test, loading protocol presented in Table 21 and Figure 55 was applied. Table 22 shows the amplitude steps for in-plane loading in different phases. The experimental test contained 5 phases in which the decoupled infill was tested under different loading combinations.

In Phase 1 pure in-plane load was applied up to a maximum interstorey drift of 1.25 %. Afterwards, in Phase 2 constant pure out-of-plane load equal to 35 kN was applied to the wall by means of four air bags.

Phase 3 was the first phase in which the specimen was subjected to simultaneous loading. In-plane sinusoidal load was increased up to a maximum interstorey drift of 1 % and a constant out-of-plane load of 10.5 kN was applied to the wall.

In Phase 4 in-plane sinusoidal load was imposed to the specimen up to a maximum interstorey drift of 1.8 %. Simultaneously with in-plane load out-of-plane load was applied. The level of out-of-plane load varied during the Phase 4. First the out-of-plane load of 34.5 kN was applied and then the in-plane load from 0 % to 0.5 % of drift. In the next cycles in-plane load was applied from 0.6 % to 1.8 % drift, but level of out-of-plane load was modified each two cycles. Basically, each two amplitudes of in-plane displacements were first applied together with 17.5 kN of out-of-plane load and then the same two in-plane amplitudes were repeated, but with the increased level of out-of-plane load (34.5 kN). Phase 4 was stopped due to limitations of measuring equipment and the test was continued in Phase 5.

In Phase 5 first the higher level of out-of-plane load was applied to the wall (43.63 kN) in combination with in-plane drift of 1.0 % which was applied in two cycles. After these first two cycles in Phase 5, out-of-plane load was decreased to 10.5 kN. This level of out-of-plane load was then applied simultaneously with in-plane drifts increasing from 1.0% until 3.25 %. The detailed description of loading protocol is also available in Marinković (2018) and Marinković and Butenweg (2019).

Table 21. Load phases in the loading protocol of the DIO test (Marinković 2018)

Phase 1	Increasing In-Plane sinusoidal load up to a maximum interstorey drift of 1.25% (34.375mm)
Phase 2	Constant Out-Of-Plane load of 5kN/m^2 (35kN)
Phase 3	Simultaneous load: Increasing In-Plane sinusoidal load up to a maximum interstorey drift of 1.0% (27.5mm) and a costant OuT-Of-Plane load of 1.5 kN/m^2 (10.5kN)
Phase 4	Simultaneous load: Increasing In-Plane sinusoidal load up to a maximum interstorey drift of 1.8% (49.5mm) and avariable OuT-Of-Plane load varying from 2.5 to 5 kN/m^2 (10.5kN)
Phase 5	Simultaneous: Increasing In-Plane sinusoidal load starting with a interstorey drift of 1.0% (27.5mm) up to a maximum interstorey drift of 3.25% (89.375mm). The OuT-Of-Plane load starts at an initial of 6.25 kN/m^2 (43.63kN) and is then reduced to 1.5 kN/m^2 (10.5kN)

As reported in Marinković (2018), in the first three phases of the DIO test, infill wall remained completely undamaged.

In Phase 1 infilled frame reached the drift of 1.25 % under pure in plane loading. The out-of-plane displacements in this loading phase were negligible.

In the next loading phase (Phase 2), the wall was loaded purely out-of-plane and reached the out-of-plane force of 35 kN. It should be pointed out that this value does not represent the out-of-plane capacity of this infill wall. Phase 2 was stopped at this load level because reaching this force level confirmed that the decoupled infill wall is able to resist the limit levels of

perpendicular forces induced by seismic actions defined in the codes. The infill wall experienced the rigid body movement in this loading phase. The out-of-plane displacements were larger at the top of the wall due to the smaller stiffness of the elastomers applied at the top in comparison to those applied at the bottom. However, there were no residual displacements after the load was removed. There were also no cracks in the wall as it remained inactive in this phase and the arching action was still not activated.

Table 22. In-Plane drifts of the test DIO (Marinković 2018)

Stage	Phase 1 Drift (%)	Phase 3 Drift (%)	Phase 4 Drift (%)	Phase 5 Drift (%)
1	0.018	0.018	0.018	1.00
2	0.036	0.036	0.036	1.00
3	0.055	0.055	0.055	1.25
4	0.073	0.073	0.073	1.50
5	0.10	0.10	0.10	1.80
6	0.20	0.20	0.20	2.10
7	0.30	0.30	0.30	2.40
8	0.40	0.40	0.40	2.70
9	0.50	0.50	0.50	3.00
10	0.60	0.60	0.60	3.25
11	0.80	0.80	0.80	-
12	1.00	1.00	0.60	-
13	1.25	-	0.80	-
14	-	-	1.00	-
15	-	-	1.25	-
16	-	-	1.00	-
17	-	-	1.25	-
18	-	-	1.50	-
19	-	-	1.80	-
20	-	-	1.50	-
21	-	-	1.80	-
22	-	-	-	-

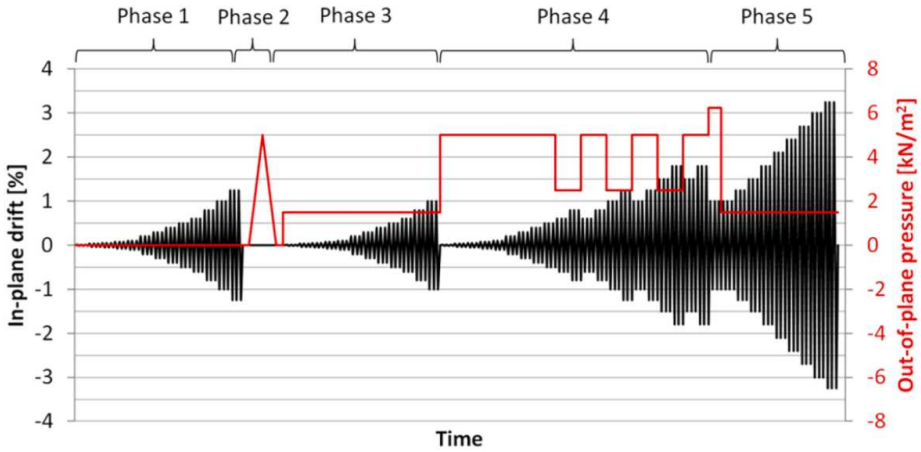

Figure 55 Load protocol of the test DIO (Marinković 2018)

Results of Phase 3 show that this decoupled infill wall was able to withstand out-of-plane load of 10.5 kN and in-plane load up to 1.0 % of drift without any damage.

In Phase 4 the specimen behaved linearly up to 1.8 % of drift due to the elastic deformations of U-shaped elastomer connection. First horizontal crack was noticed in the third bed joint from the bottom of the infill together with the first sound of cracking during the first cycle of in-plane drift of 1.8 % combined with out-of-plane load of 35 kN (Figure 56a). During the third cycle of 1.8 % drift, the vertical crack appeared on the right side of the wall, through the units (Figure 56b). After this point the out-of-plane deformation started to increase. Both cracks arose when the frame deformed from left to the right. Both horizontal and vertical crack occurred due to increase in bending stresses from out-of-plane load and exceedence of the flexural strength of masonry infill. The reason for this is reduction of clamping effect in the unloaded corners of masonry infill that occur due to the frame deformation. Reduced clamping effect in the bottom left corner led to the occurrence of horizontal crack, while vertical crack formed as a result of reduced clamping effect in the top right corner. However, although the deformation increased and some of the deformations caused by the formation of cracks remained in the wall, after removal of the load, the deformations in the hyperelastic elastomers reversed for most of the wall. Despite the crack formation, the wall stayed stable in the frame at the end of Phase 4 due to circumferential support provided by elastomers.

(a) (b)

Figure 56 (a) Appearance of the first crack in the wall (Marinković 2018); (b) Cracks in the wall at the end of Phase 4 (Marinković 2018)

Phase 4 was stopped as the testing equipment needed to be replaced.

The test was continued in Phase 5. As a first step in Phase 5 out-of-plane surface load equal to total force of 43.63 kN was applied to the specimen. It was kept constant and simultaneously two cycles of in-plane displacement up to 1.0 % of drift were applied. Despite the cracks that occurred in bed joints and some brick units at the end of the Phase 4, specimen behaved linearly and showed that it still had high strength and deformation capacity. Out-of-plane displacements increased in this loading phase due to the cracks developed at the end of Phase 4, but reversible displacements were still evident due to the elastomer connection. Further in Phase 5, out-of-plane load of 10.5 kN was applied simultaneously with in-plane drift increasing from 1.0 % to 3.25 %. Maximum in-plane resistance of 150 kN was reached at an interstory drift of 2.2 %. The strength fell slowly and at the ultimate drift of 3.25 % it was 135 kN.

The hysteresis was also stable and wide even in this high range of in-plane drifts. Figure 57 shows the damage pattern after the completion of the fifth load phase. It could be seen that the propagation of cracks matches the one recorded in the fourth phase, but at the end of the fifth phase these cracks were much more evident. Similar damage pattern could be seen on the backside of the wall too. The most damaged bricks were those placed above and below the bed joint that was sliding and also in the right part of the wall, next to the vertical crack. Even at the end of the Phase 5, when the wall was highly damaged, it did not lose the out-of-plane stability what is very important from safety aspects.

(a) (b)

Figure 57 (a) Damage at the front side at the end of DIO test (Marinković 2018); (b) Damage at the back side at the end of DIO test (Marinković 2018)

Experimental curves in Figure 58a represent envelopes obtained from in-plane loading phases of the experimental test DIO carried out on RC frame with decoupled infill (Marinković and

Butenweg, 2019), while numerical curve is taken from pure in-plane loading simulation on a simplified micro-model of a corresponding RC frame with decoupled infill (Marinković and Butenweg 2022) (see Figure 58(a)). Since experimental test DIO is carried out in several loading phases with different combinations of in- and out-of-plane loads, results of numerical simulation are used too, as RC frame with decoupled infill is loaded in simulation only in-plane up to its collapse. A bilinear horizontal force-displacement relationship is adopted both for the traditional and decoupled infills, using the Uniaxial Material Hysteretic model of OpenSees (McKenna 2011), whose cyclic behaviour (for a typical decoupled infill with INODIS) is shown in Figure 58(b).

According to (Rossetto and Elnashai, 2003), older RC frame buildings with substandard seismic details experience extensive damage, for maximum interstorey drifts larger than 3%. Moreover, damage of structural and non-structural components for higher drift levels can also represent a risk for human lives. Therefore, in this study, the onset of the damage in the IP direction is assumed, for decoupled infills with INODIS, for drifts greater than 3%, as a result of the significant damage experienced by the RC members (after 3% of drift, actions are needed to restore the panel in its original position and replace some connections).

Experimental results (Marinković et al., 2019) show that for infills equipped with INODIS, the OOP loads do not affect the IP behaviour under combined seismic actions. Hence, damaged IP curves coincide with the undamaged IP curve (see Figure 58(b)).

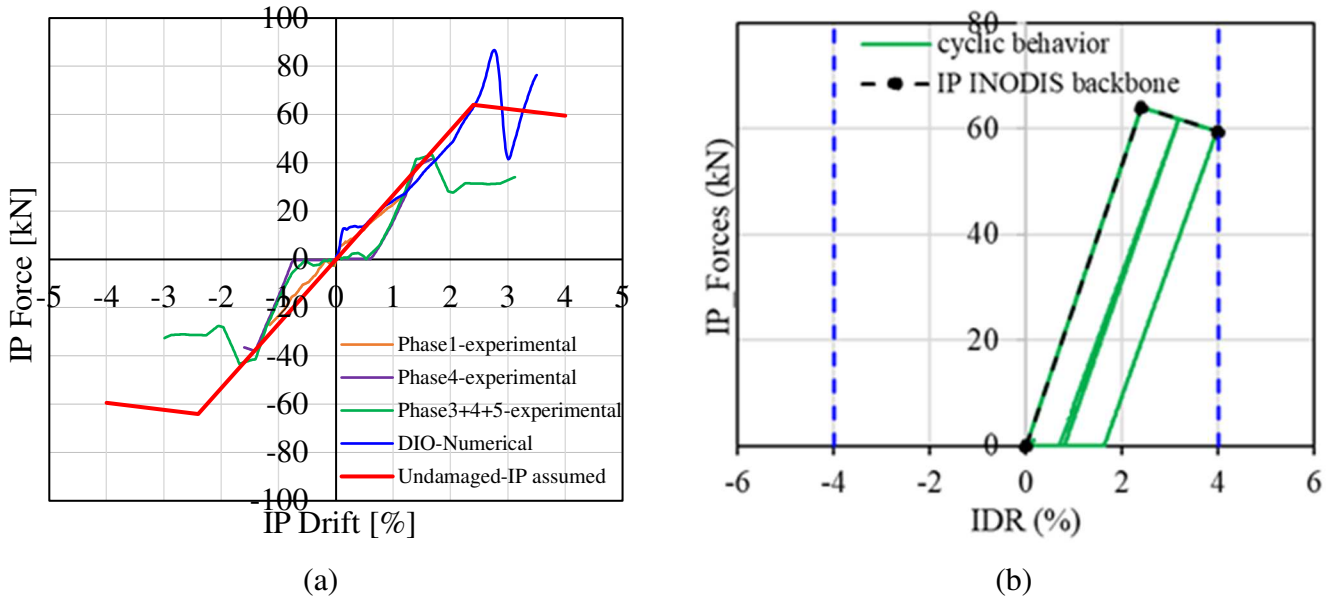

(a) (b)

Figure 58 (a) In-Plane (IP) skeleton curve and (b) cyclic behavior of a typical decoupled infill with INODIS

Figure 59 compares the IP backbone curves of a traditional infill (with and without openings), located at the first storey of the building in the (a) long and (b) short direction, with those of the same infill with decoupling system (INODIS). Decoupled infills show significantly lower lateral stiffness than the traditional infills and an apparent ductile behaviour, with a slight post-peak degrading behaviour. Therefore, decoupling of the infills from the surrounding frame achieved by elastomeric profiles strongly limits the interaction between the masonry infills and RC frame.

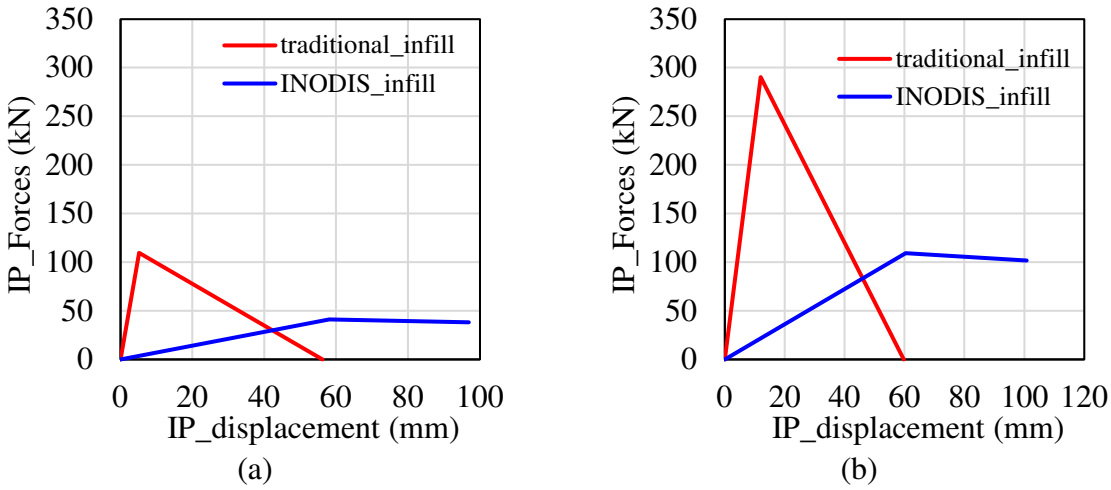

Figure 59 IP behaviour of traditional infill vs decoupled infills (with INODIS system) with (a) and without (b) openings

As already explained in the previous section, the out-of-plane behaviour of traditional infill walls is described by means of the relationships proposed by (Ricci et al., 2018) and subsequently updated by (Di Domenico et al. 2021). The trilinear force-displacement skeleton curves are implemented in OpenSees (McKenna, 2011) through the Unixial Hysteretic Material. The ultimate out-of-plane displacement of the panel is heuristically assumed to be 0.8 times the thickness of the panel. Therefore, the two leaves exhibit different ultimate displacement. For traditional infills, the IP/OOP interaction is defined based on the semi-empirical relationships derived by (Ricci et al 2018 (b)-(c)).

The OOP skeleton curves for decoupled infills with INODIS system are tentatively derived in this study based on the results of the experimental tests reported in (Marinković et al., 2019), together with some additional assumptions concerning the OOP degradation due to very large drifts (larger than 3%, see before). A set of trilinear curves is then obtained (see Figure 60) and implemented in the model using the Uniaxial Material Hysteretic rule available in OpenSees (McKenna, 2011). In total, one undamaged (continuous line in Figure 60) plus 19 damaged

skeleton curves (dashed lines in Figure 60) are defined, covering a range of drift values ranging from 0 to 4%.

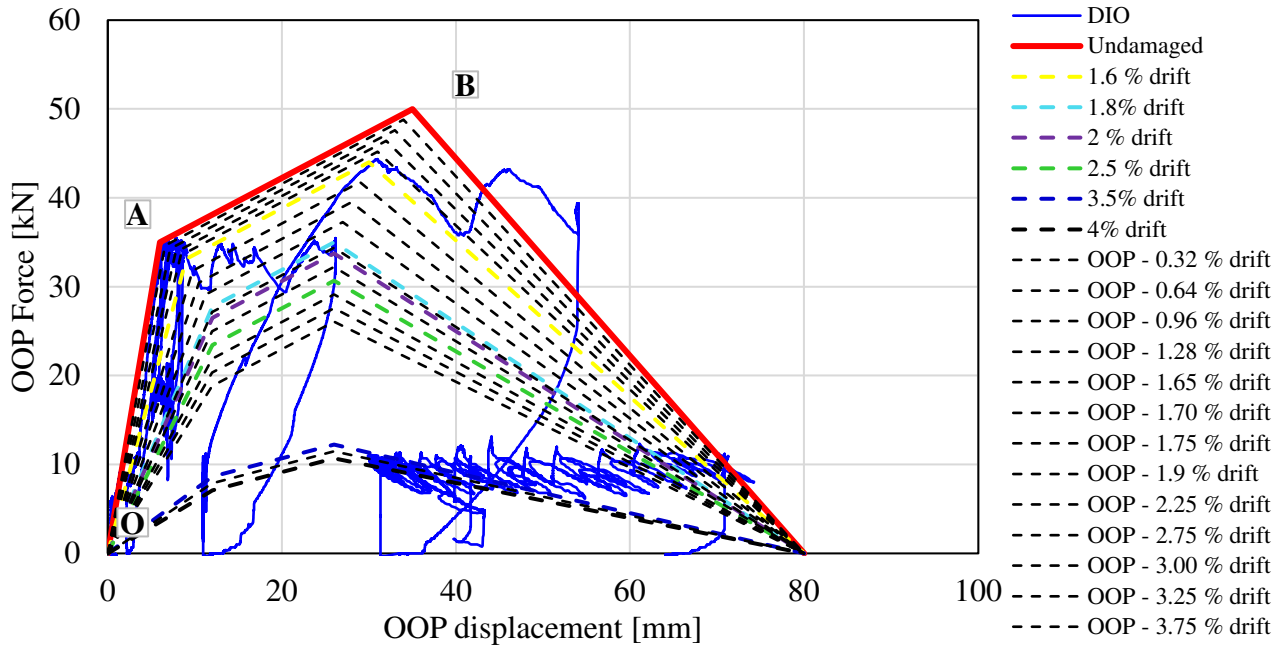

Figure 60 Updated OOP backbone curves

Part of the undamaged curve between points O and A is defined to have the same slope as in the Phase 2 of the DIO test where the undamaged infill wall was loaded purely out-of-plane up to total out-of-plane force of 35 kN. Furthermore, at the end of this pure out-of-plane phase (Phase 2), the measured out-of-plane displacement was about 6 mm. Therefore, for point A the out-of-displacement of 6 mm and out-of-plane force of 35 kN were adopted. Even though the wall did not experience any cracking, not activation of arching effect, it was decided to define that at the force of 35 kN first cracking could be expected which could cause the change of the stiffness. One of the reasons for that is that in the Phase 4 of the DIO test arching action was activated at the force of 35 kN, but it needs to be taken into account that in-plane drift of 1.8 % was applied to the specimen in combination with this out-of-plane force. Therefore, this force level could still be considered as an assumption.

Furthermore, the out-of-plane capacity is estimated to be 50 kN. One of the reasons for that is that in the Phase 5 of the DIO test the specimen was able to withstand the force of almost 45 kN applied in combination with 1.0 % of in-plane drift and after the initiation of first cracking that occurred at the in-plane drift of 1.8 % and out-of-plane force of 35 kN at the end of Phase 4. For this reason, the estimation of out-of-plane capacity of 50 kN can be considered as a

realistic and conservative value. The corresponding displacement for point B of undamaged curve is estimated to be equal to 35 mm.
Since the maximum out-of-plane displacements measured in the DIO test are about 75 mm (which was measured when the wall was already highly damaged at the high in-plane drifts (Δ = 2-3.5 %), it was decided to fix the ultimate out-of-plane displacement value to 80 mm.

Out-of-plane curve taking into account simultaneously applied 1.8 % of in-plane drift was defined based on the DIO test results and a few assumptions.

The out-of-plane strength was adopted to be equal to 35 kN as at that level of out-of-plane force and 1.8 % drift, the cracking occurred in Phase 4. However, this was not the out-of-plane capacity, but the assumption of this value is also on the safe side and the force of 35 kN represents the out-of-plane force value that was actually reached in the DIO test. As previously mentioned, and reported in Marinković 2018, at the out-of-plane force of 35 kN and in-plane drift of 1.8 % in Phase 4, the out-of-plane displacements increased too. Therefore, the value of out-of-plane displacement measured at the end of Phase 4 was adopted for point B (26 mm). In this way, point B was completely defined according to the real values obtained from the DIO test with a rather conservative assumption for out-of-plane capacity.

The slope of the O-A line was calculated to be the same as the initial slope of the out-of-plane force-displacement curve obtained from the Phase 5 of the DIO test. Since in Phase 5 the specimen was first loaded in out-of-plane direction, after 1.8 % of drift reached at the end of Phase 4, this slope can quite well depict the initial stiffness of decoupled infill previously subjected to in-plane drift of 1.8 %. Point A is determined as intersection of the line O-A which is defined by its slope and line A-B whose slope is adopted to be equal to the one of the undamaged curve.
The other damaged OOP skeleton curves for decoupled infills with INODIS system curves were obtained in the same way; some additional assumptions concerning the OOP degradation due to very large drifts (larger than 3%, see before) have been carried out.

The cyclic degrading parameter of the OOP model is defined based on the previous studies. In particular, the parameters governing the shape of the cycles for the Uniaxial Hysteretic Material are: (i) β, which controls the stiffness degradation during unloading, (ii) PinchX and PinchY, which control the pinching effect. These parameters are calibrated by Noh et al. (2017) by comparing numerical and experimental results for infilled RC frames. The values thus obtained

are: 0.1, 0.9 and 0.1 for β, PinchX and PinchY, respectively. Damage parameters are not considered. The same choice is made in this study. The cyclic behaviour thus obtained is shown in Figure 61(a). Figure 61(b) and Figure 61(c) show a single loading / unloading cycle and a single loading / unloading / reloading cycle, respectively, for different loading and unloading phases.

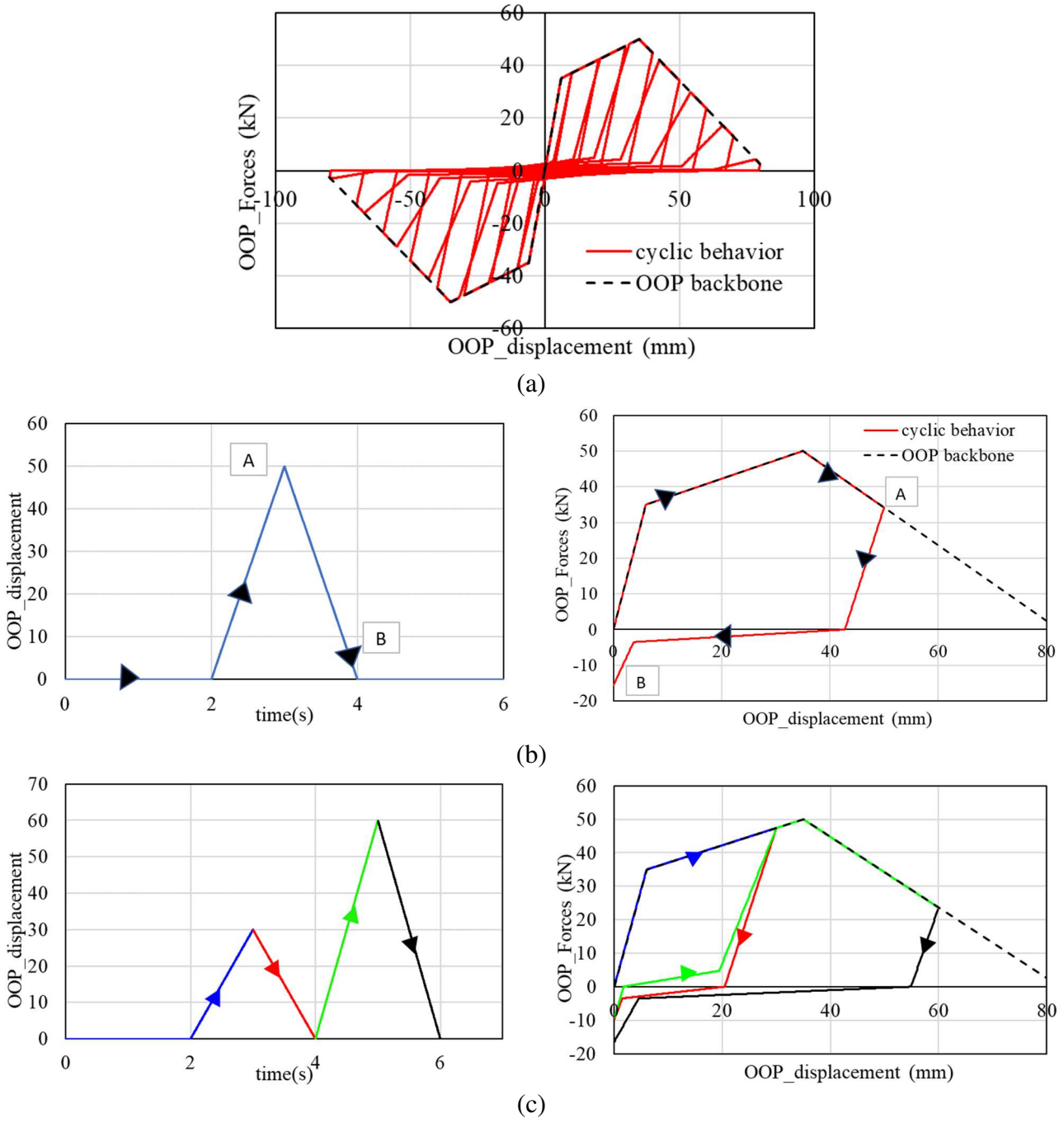

Figure 61 Cyclic behavior of the uniaxial hysteretic material used to describe the OOP behaviour of infills: (a) full cyclic behavior; (b) single loading / unloading cycle; (c) loading / unloading / reloading cycle.

The OOP strength of the infills is reduced to account for the presence of the openings, according to the formulation proposed by Mays et al. (1999). Experimental IP/OOP curves are converted into building specific IP/OOP curves based on the infill's cross-section area (for the IP behaviour) and infill's length (for the OOP behaviour). Figure 62 shows the OOP backbone curves of typical traditional infill (thick and thin leaf) and decoupled infill with INODIS, used for the numerical simulations.

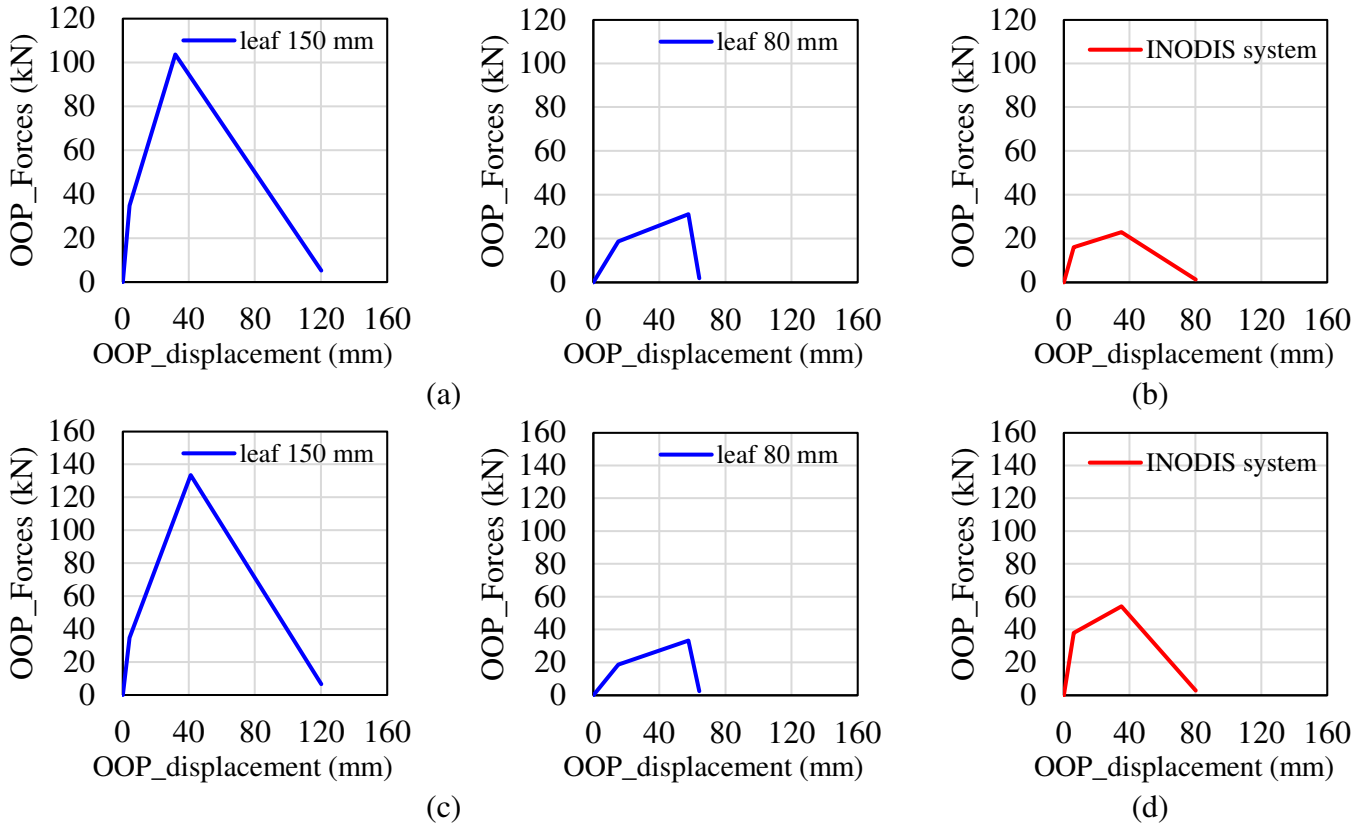

Figure 62 OOP behavior of traditional double-layer infill (blue line) and decoupled infill with INODIS system, with openings (a,b) and without openings (c,d)

3.4. ANALYSES RESULTS

3.4.1 Modal analysis

Modal analysis is performed after the application of gravity loads on the beams. The fundamental periods of vibration of the building model in the two orthogonal directions are reported in Table 23. Table 23 clearly points out that the presence of decoupled infills does not significantly affect the period of vibration of the RC frame. Traditional infills, instead, significantly increase the lateral stiffness of the building, thus strongly reducing its fundamental periods of vibration. Smaller periods of vibration imply greater seismic accelerations, hence higher seismic forces have to be withstood by the structure.

Table 23. Fundamental periods of vibration

	T_x(s)	T_y(s)
Bare frame (BF)	1.295	0.967
Infilled frame with traditional infills (IF)	0.76	0.68
Infilled frame with decoupled infills (IF-I)	1.203	0.912

Common infills always increase the stiffness and consequently the seismic input.

3.4.2 Pushover analyses

Pushover analysis (POA) is performed to derive the displacement capacity of the case-study building associated with some noticeable performance points, such as: (i) first yielding, (ii) attainment of peak strength and (iii) 15% reduction of the peak lateral strength. Both modal (M) and uniform (U) load patterns are used in the two orthogonal directions (X and Z). Figure 63 shows the capacity curves derived from POA. The thick lines correspond to the capacity curves of the infilled frame while the thin lines represent the contribution of the RC frame only. It is interesting to note that (see Figure 64), for the building with decoupled infills, the maximum drift associated with the first yielding is lower than 0.5%, while the maximum drift at the peak force is around 2%. At 15% drop of the lateral strength of the RC frame, the maximum drift exceeds 3% in the X-direction (long direction, with wide openings in the infills), and it is around 2.5% in the Z-direction (short direction, full infilled without openings). This is in excellent agreement with the indications of (Rossetto and Elnashai, 2003). No shear failure due to the RC column/masonry infill interaction is observed.

Figure 63 clearly shows the stiffening contribution of traditional infills, especially in the short direction (no openings). The capacity curves of the model with decoupled infills look similar

to those of the bare frame for the whole range of displacement. As expected, the capacity curves of the model with traditional infills tend to overlap the capacity curves of the bare frame for large displacements, due to the extensive damage of the masonry infills.

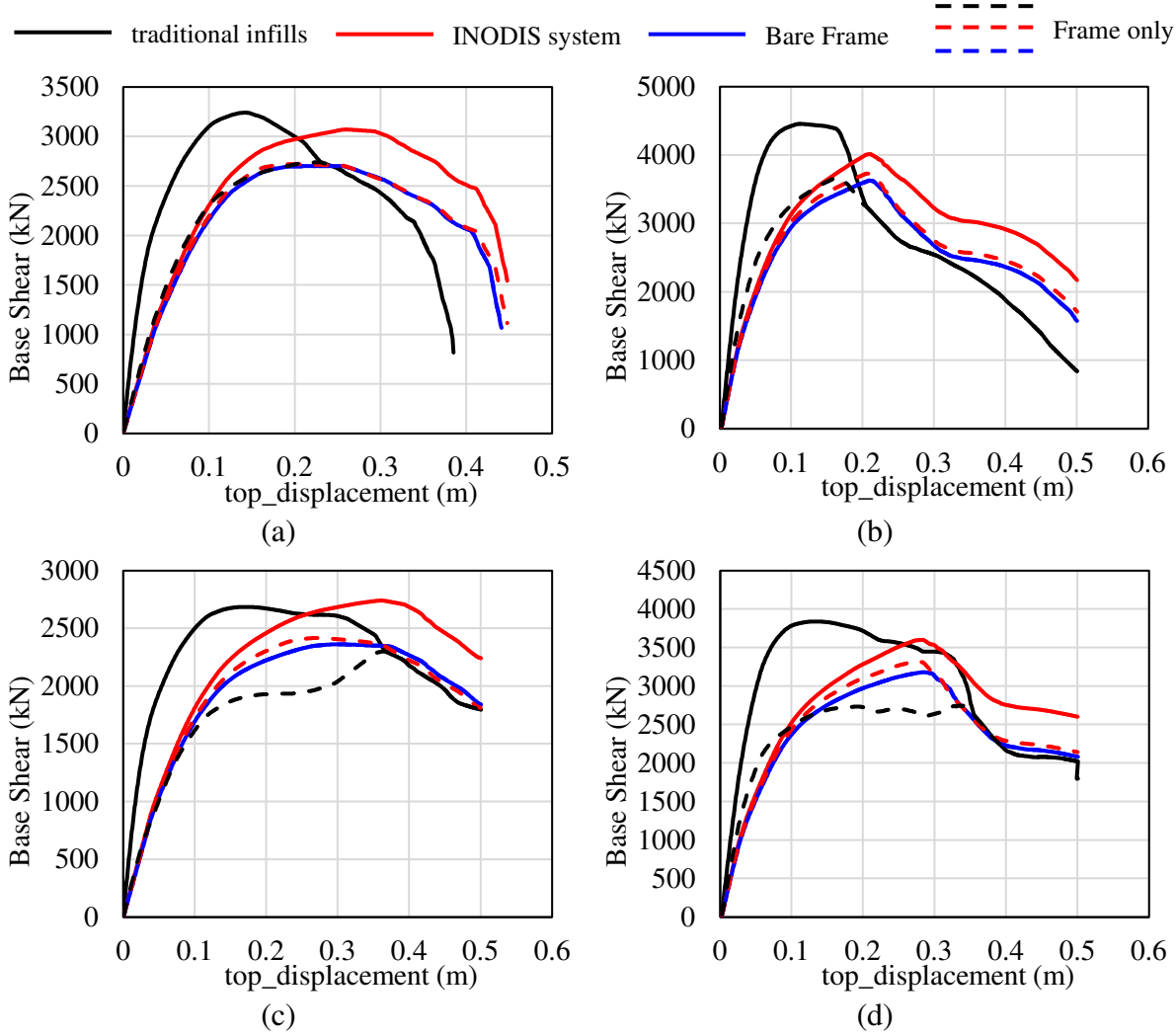

Figure 63 Pushover curves of the building under consideration: uniform force distribution in X (a) and Z (b) direction; modal force distribution in X (c) and Z (d) direction.

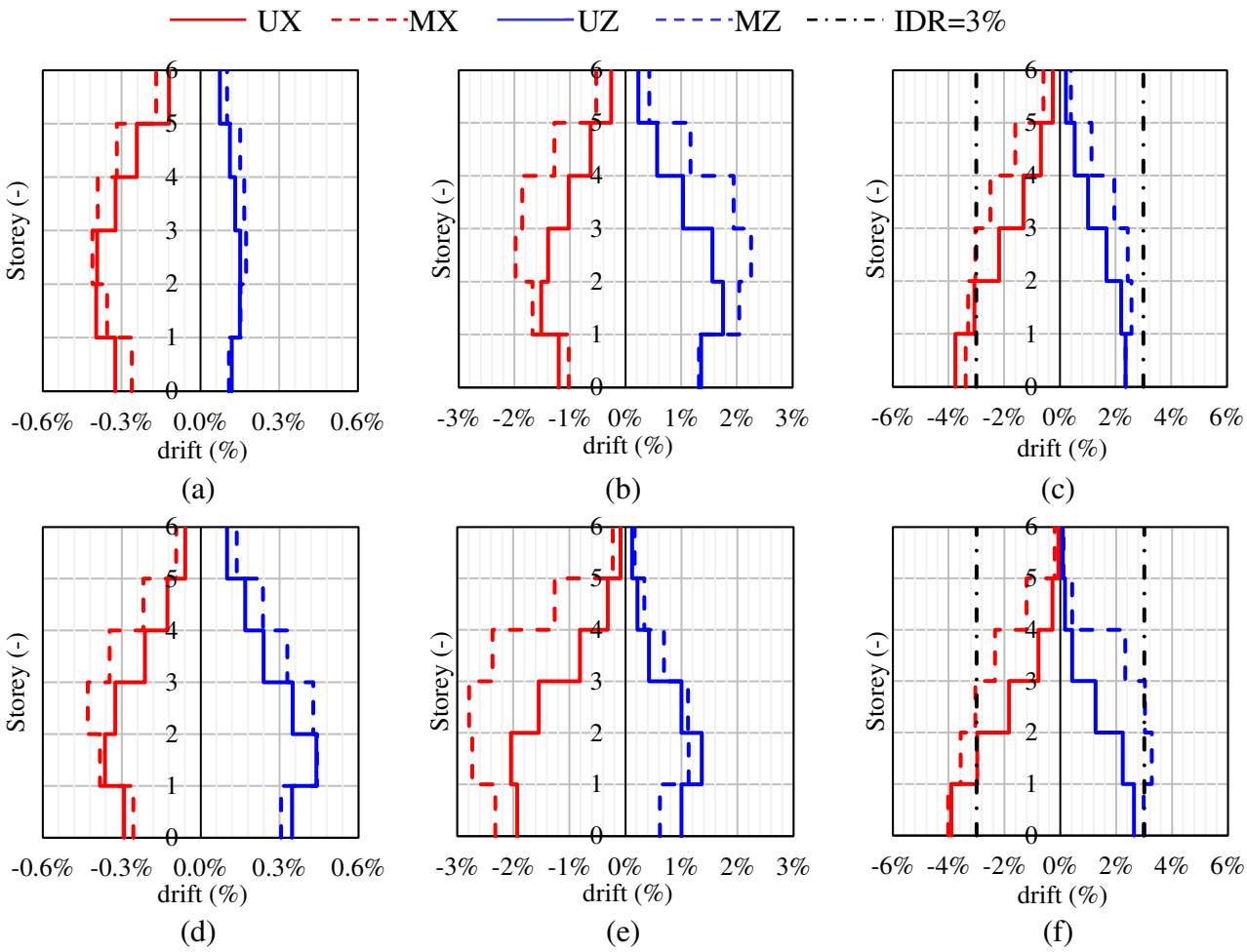

Figure 64 Drift profiles associated with (a) first yielding, (b) peak strength and (c) 15% drop of lateral strength for INODIS system and traditional infills (d,e,f)

3.4.3 Non-Linear Time-History Analyses

Non-linear time-history analyses (NTHA) is performed to evaluate the seismic performance of the case study building at three different earthquake intensity levels (EQ-IL), with return periods equal to 50 years, 500 years and 2500 years. For each seismic intensity 20 pairs of bidirectional records are selected; overall, 60 NTHA are performed for each model.

Figure 65 shows the cyclic behaviour of some structural elements for model with INODIS system during the 16th run at 50 yrs EQ-IL, 12th run at 500 yrs EQ-IL and 15th run at 2500 yrs EQ-IL, respectively. More precisely, Figure 65 shows the cyclic behaviour of a beam, a column, and a beam-column joint located at the 3rd storey of the building. As it can be seen, plastic deformations start to develop at 500 yrs EQ-IL. All RC elements experience extensive plastic deformations and degradation effects at the highest seismic intensity (2500 yrs EQ-IL).

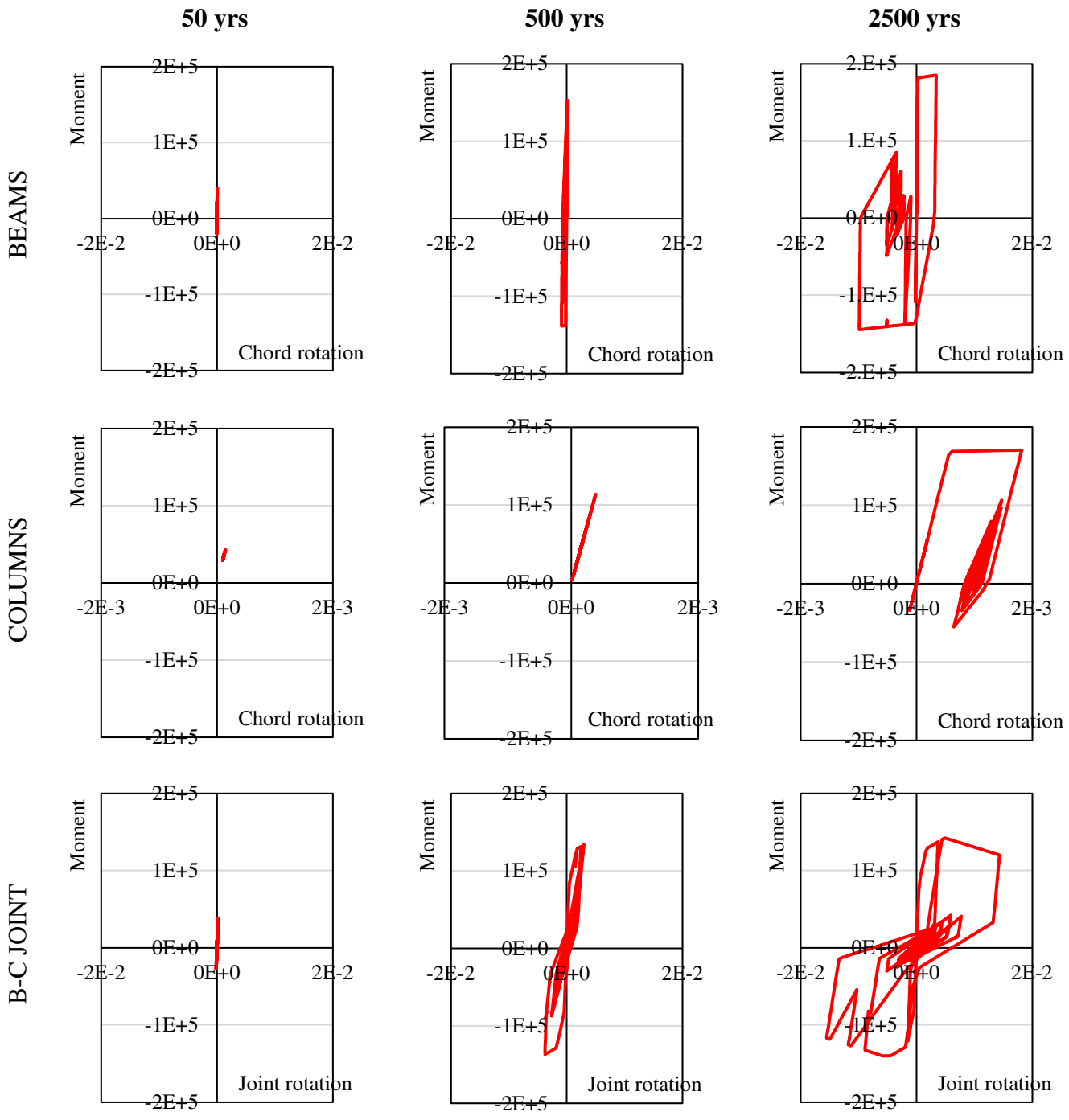

Figure 65 Cyclic behaviour of a 3rd storey beam, column and beam-column joint during run 16 at 50 yrs EQ-IL, run 12 at 500 yrs EQ-IL and run 15 at 2500 yrs EQ-IL.

Figure 66 and Figure 67 show the interstorey drift profiles (IDR) derived from NTHA at the three EQ-Ils for the model with traditional infills and with decoupled infills, respectively. Grey lines represent the maximum values recorded for i-th run, while the black thick line indicates the average value over 20 ground motion pairs. On average, maximum drift values of the order of 0.2%, 1% and 2% are recorded at 50 yrs EQ-IL, 500 yrs EQ-IL and 2500 yrs EQ-IL,

respectively, for both models. It's interesting to note that at 2500 yrs EQ-IL, 6 out of 20 ground motions determine maximum drift values greater than 3% in the X-direction; as explained before, this drift value is identified as a threshold for achieving severe structural damage. As it can be seen, the IDR profiles feature a marked bulged shape with higher values at the mid-lower storeys of the building, which increase as seismic intensity increases. As a consequence, also the ductility demand tends to remain concentrated in the mid-lower storeys of the building, in accordance with what observed in Cardone et al. (2017).

Figure 68 compares the average maximum drift profiles obtained at each seismic intensity in the two directions. At low intensities the model with traditional infills shows lower drift profiles due to the higher lateral stiffness of the infills. With the occurrence of damage in traditional infills, the drift profiles tend to be similar to each other. This is because the contribution of traditional infills to the frame lateral stiffness is significantly decreased or even completely lost, depending on the damage level on traditional infills. Due to this, traditionally infilled RC frames tend to behave like bare frames for higher intensities. On the other side, decoupled masonry infills with INODIS system do not affect the lateral stiffness of frame structures and their behaviour is almost the same as the one of bare RC frames. Therefore, especially for stronger earthquakes (high intensities), drift profiles of frames infilled with traditional and decoupled system are similar. However, traditional infills are severely damaged or destroyed, while decoupled infills remain mostly inactive.

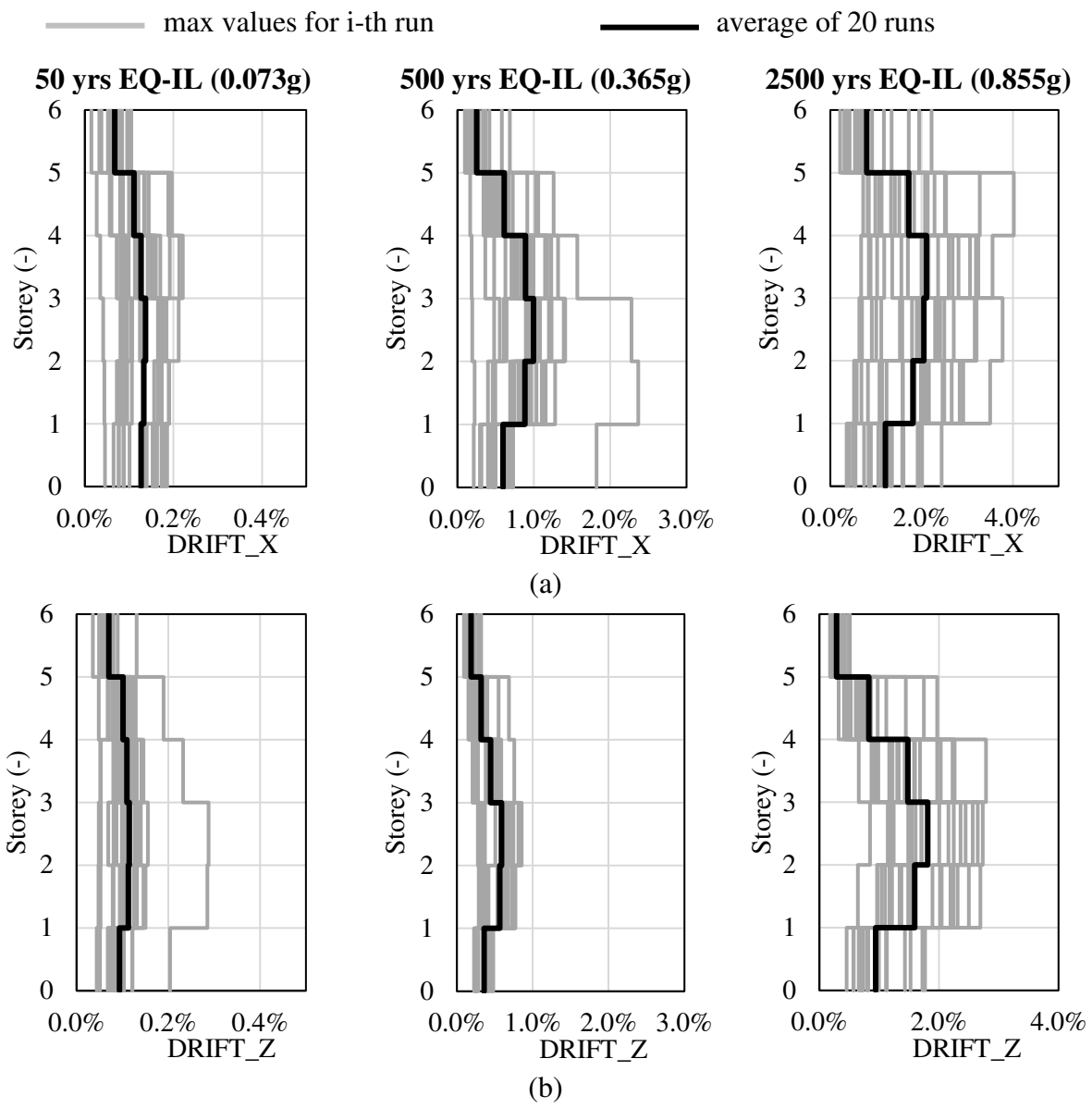

Figure 66 Drift profiles obtained from the analysis: (a) X-direction (long side); (b) Z-direction (short side) of the model with traditional infills

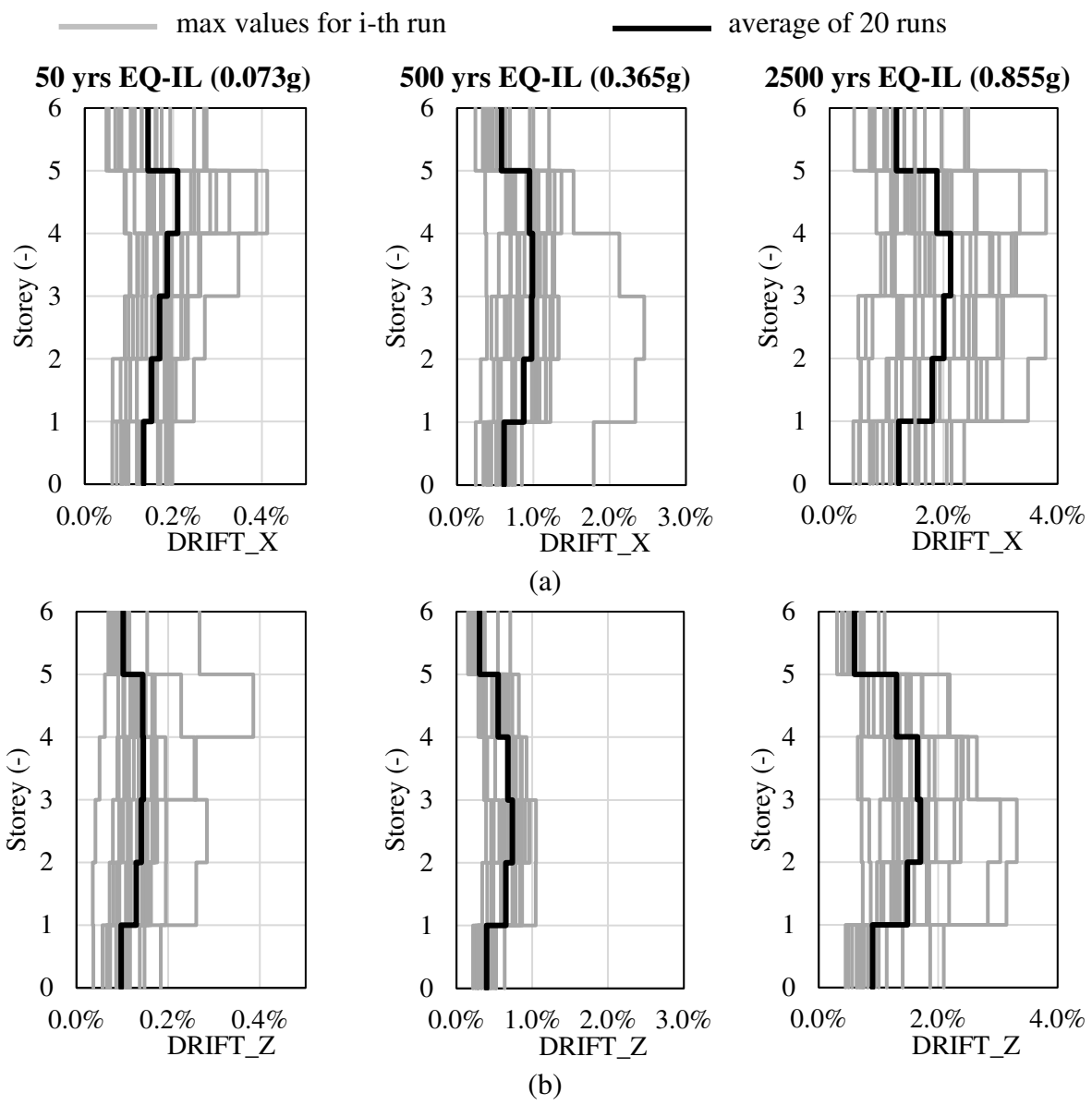

Figure 67 Drift profiles obtained from the analysis: (a) X-direction (long side); (b) Z-direction (short side) of the model with decoupled infills

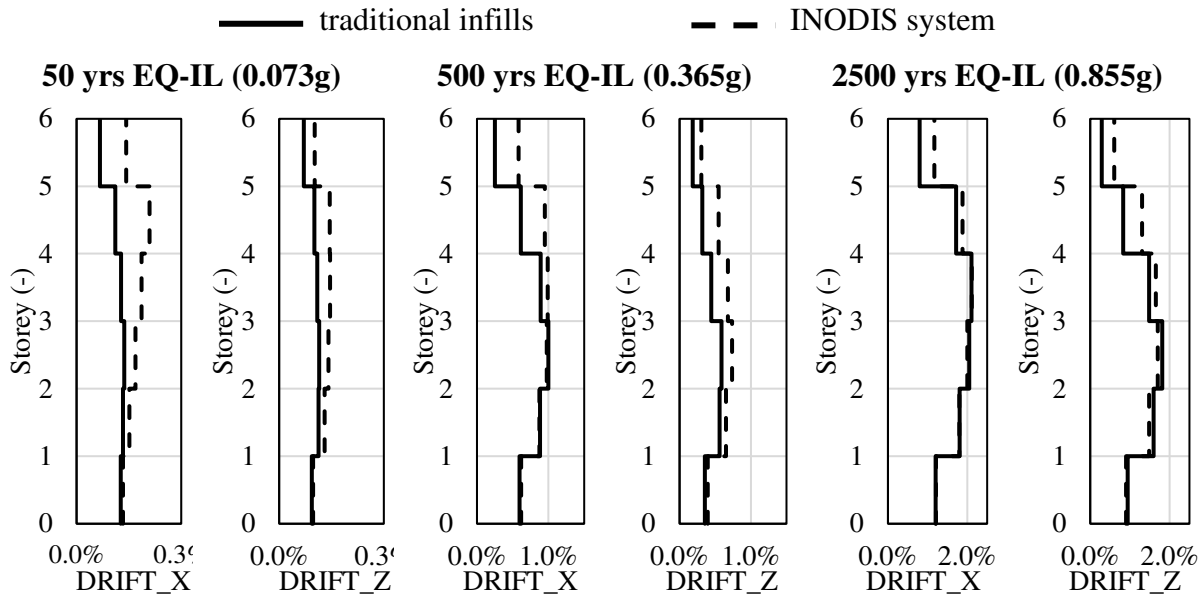

Figure 68 Comparison of average drift profiles at different seismic intensities in the two directions

Figure 69 and Figure 70 compare the average values of the maximum floor accelerations, maximum mid-floor accelerations (mean between i^{th} and $i+1^{th}$ storey) and the maximum accelerations recorded in the center of the infills, evaluated along two verticals of the building, located in the long (V1) and short (V2) direction, respectively. Generally speaking, greater accelerations (compared to floor accelerations) are observed for the infills with openings (V1), especially in the middle storeys of the building, probably due to the closer frequencies of the walls with openings to the building frequencies. On the other hand, no particular differences are observed between maximum floor accelerations and maximum infill accelerations on the short side of the building (V2), where there are no openings.

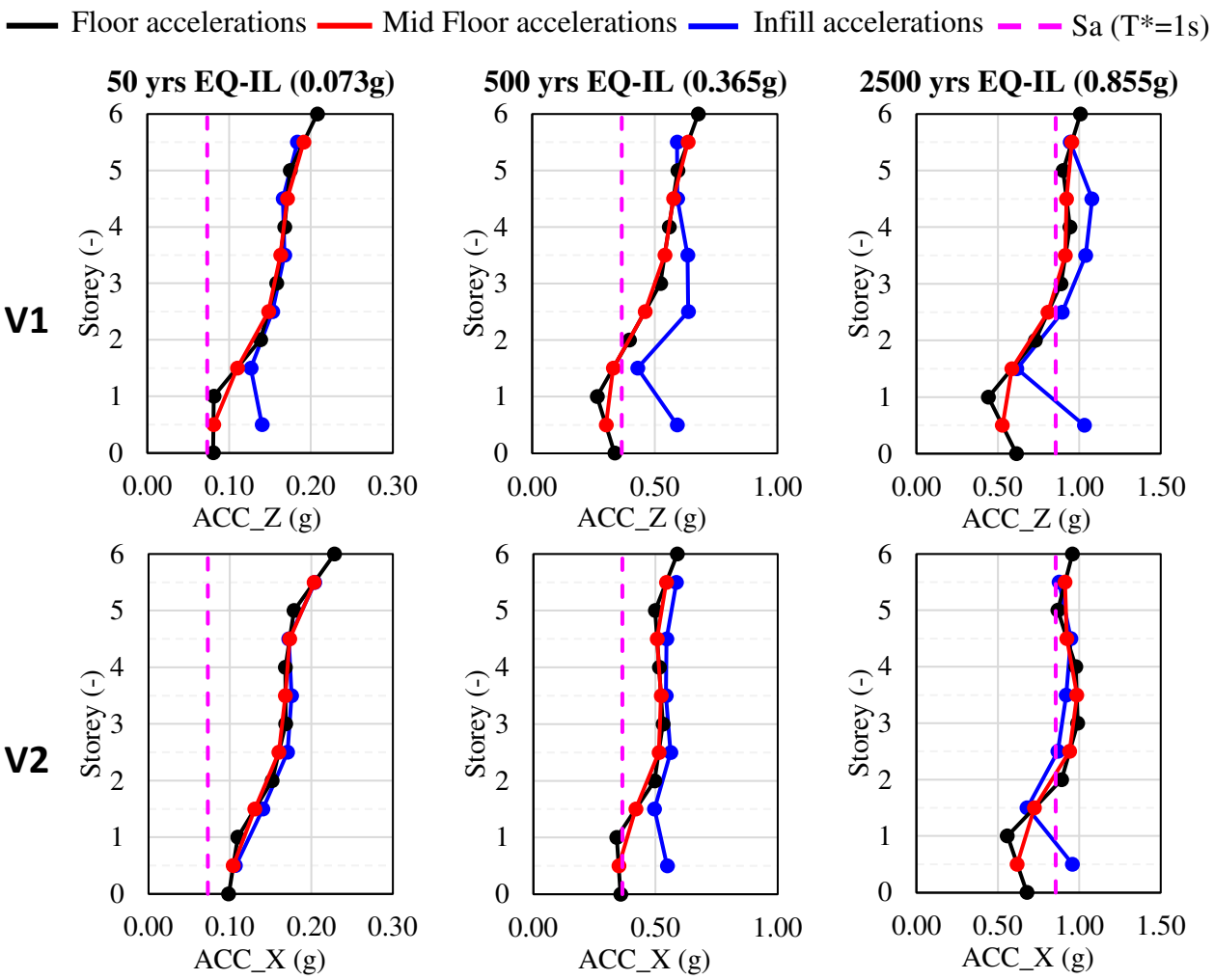

Figure 69 Comparison between maximum floor accelerations and maximum infill accelerations for the model with traditional infills. The pink dashed lines correspond to the Sa(T*=1s).

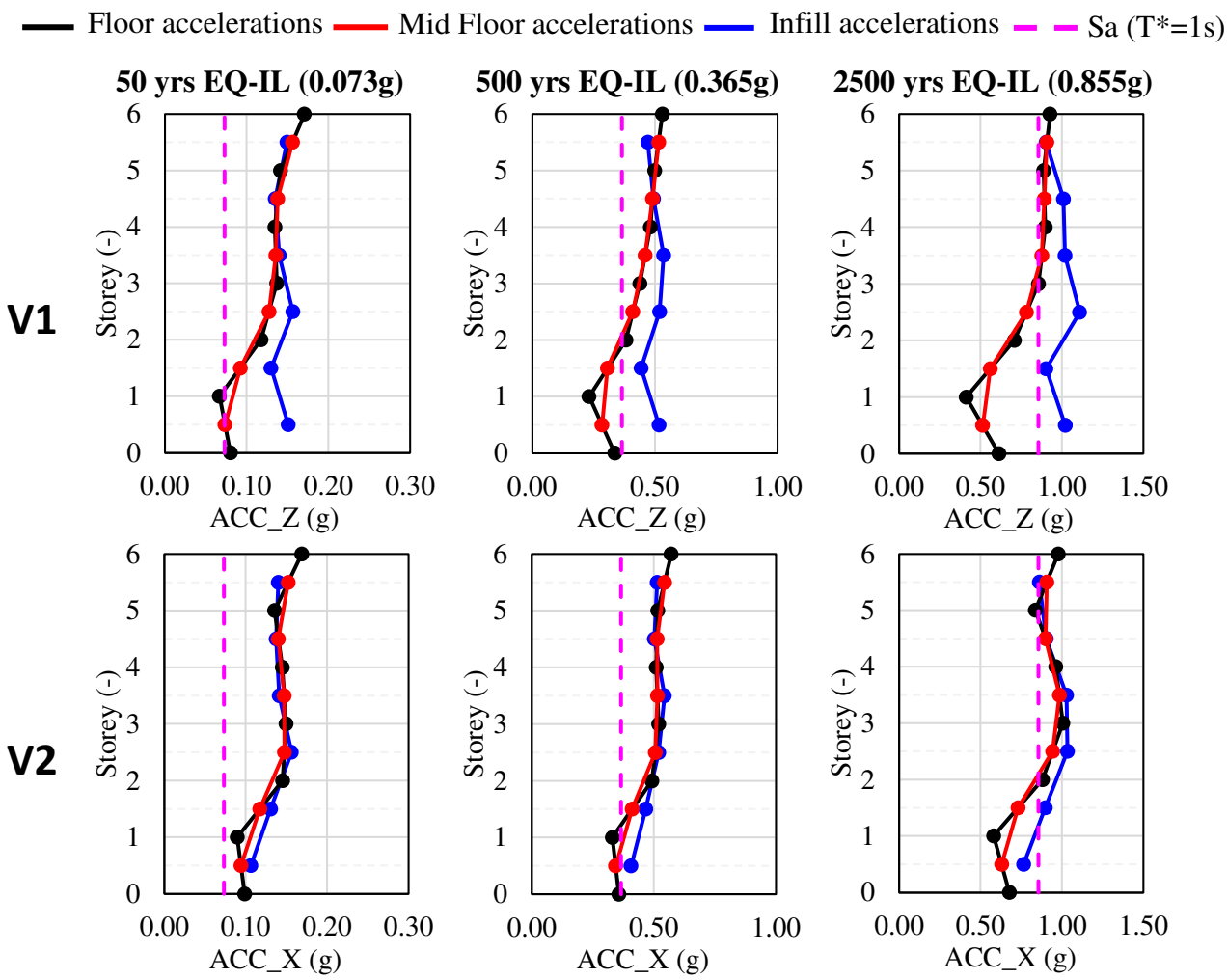

Figure 70 Comparison between maximum floor accelerations and maximum infill accelerations for the model with decoupled infills. The pink dashed lines correspond to the Sa(T*=1s)

Figure 71 compares the average maximum storey accelerations (out of 20 accelerograms) recorded for each seismic intensity for the two models examined: being more rigid, the models with traditional infills exhibit greater accelerations at low seismic intensities; the trend then changes passing to higher intensities, where the profiles become almost comparable, due to the damage of traditional infills.

Figure 72 shows the typical cyclic behaviour of one traditional infill experiencing the out-of-plane collapse. The infill is located at the first storey of the building. The OOP collapse is mainly due to the severe damage suffered in the IP direction. The infill undergoes a maximum interstorey drift of 2% and then collapses in the out-of-plane due to a maximum acceleration of 1.95g. The OOP stiffness/strength degradation due to the high values of interstorey drifts reached is the main reason for the OOP collapse. This example clearly proves the effectiveness

and importance of the algorithm implemented in Opensees (McKenna, 2011) in capturing the IP/OOP interaction of masonry infills during seismic events.

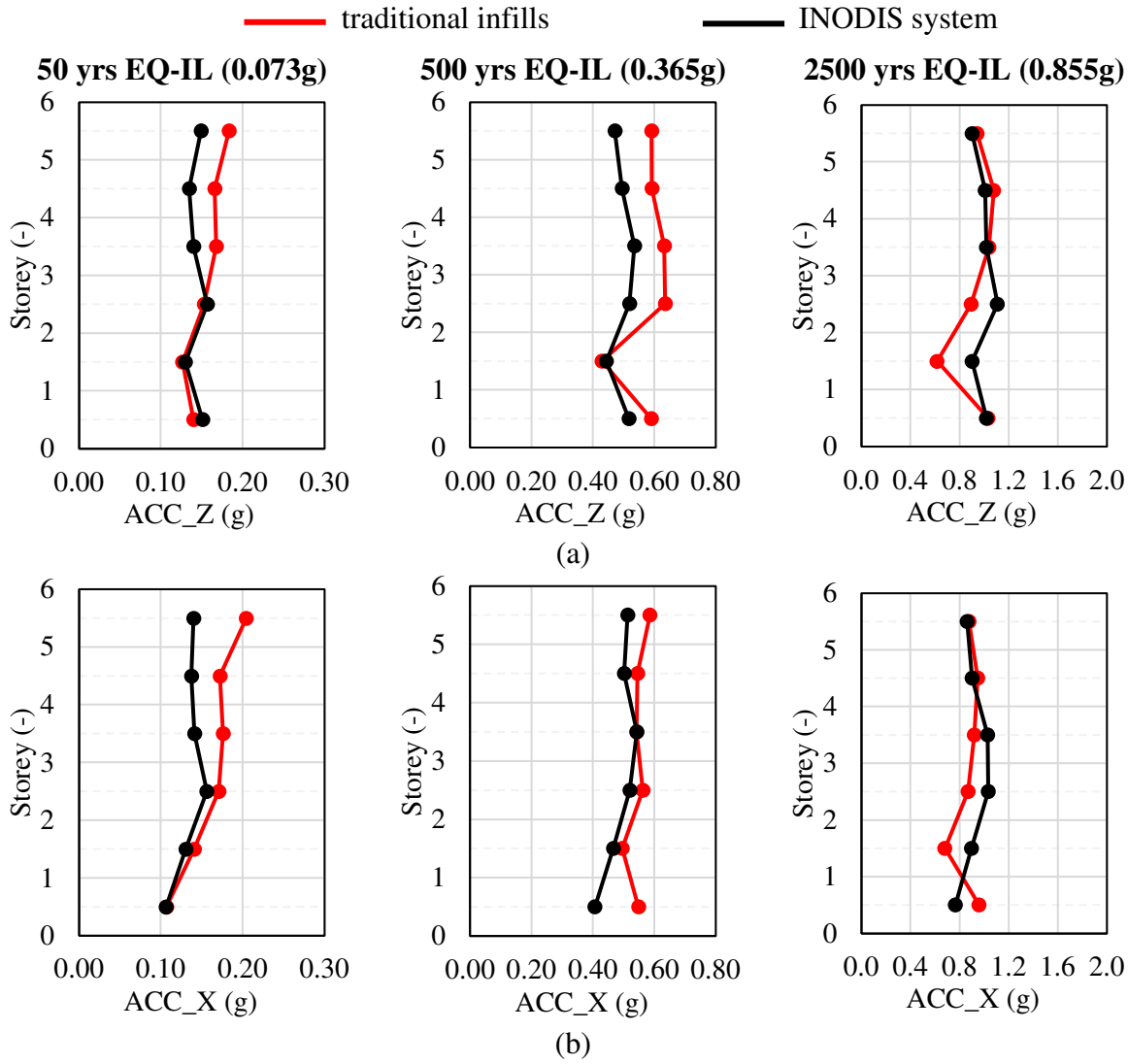

Figure 71 Comparison in terms of average (out of 20 accelerograms) maximum storey accelerations, at different seismic intensities

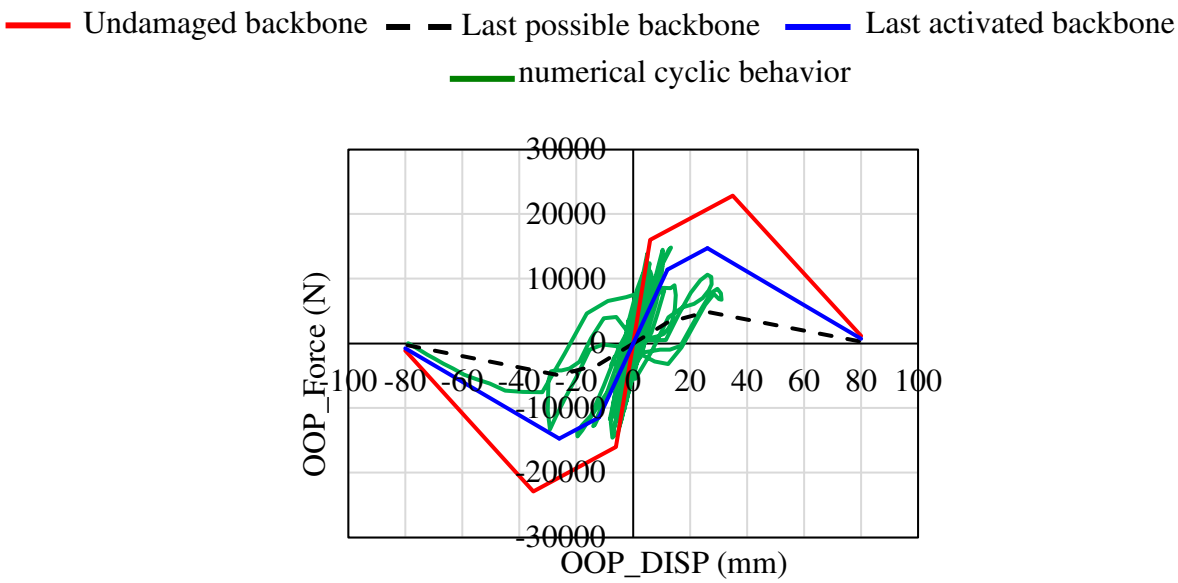

Figure 72 Typical cyclic behavior of infills experiencing OOP collapse (1st storey infill; run11 at 2500 yrs EQ-IL).

Figure 73 identifies some remarkable performance points, related to different damage levels of the infills: (i) IP / OOP first cracking (yellow), (ii) attainment of IP / OOP peak force (orange), (iii) IP / OOP severe damage (light blue), conventionally assumed to occur when a drop of 20% in the peak force of the current (degraded) backbone curve is reached, (iv) OOP collapse (red) and (v) IP collapse (dark green). Performance points are used to describe the damage scenario of the two building models (Table 24-Table 25).

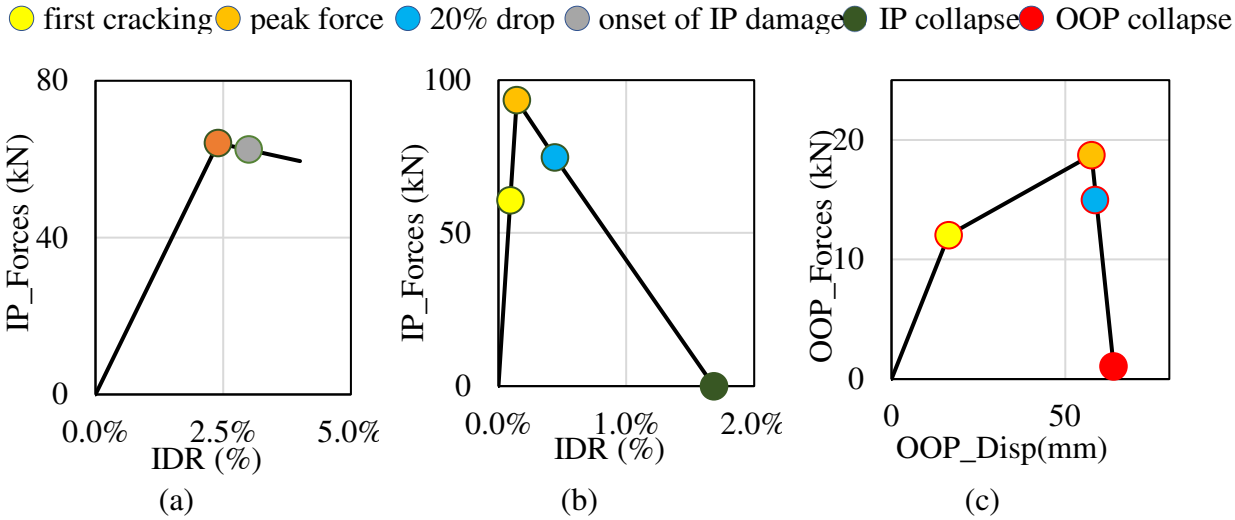

Figure 73 Remarkable performance points: IP behaviour for (a) INODIS system and (b) traditional infills; OOP behaviour of both (c)

The only performance point for INODIS system in the IP direction is represented by the onset of the IP damage due to severe damage in the adjacent RC frame (grey in Figure 73); as anticipated, at this point, actions are needed to restore the decoupling panel in its original position and replace some connections.

The aforesaid performance points are monitored taking into account the maximum IP / OOP displacements attained in the last step of NTHA, i.e. with reference to the last available degraded backbone curve.

Figure 74 and Figure 75 give an overview of infill collapses recorded at 500 yrs EQ-IL (a) and 2500 yrs EQ-IL, respectively, for the model with decoupled infills (with INODIS system) (left) and the model with traditional infills (right). Figure 74 and Figure 75 confirm the great effectiveness of the INODIS system in protection of the infills from the IP / OOP damage. The OOP collapse is recorded only for 3 ground motions out of 20 at 2500 yrs EQ-IL and only in the long direction (with openings), involving infills located on the lower storeys of the buildings. The number of the OOP collapses is very small compared to the number of the events (20) thus highlighting a low probability of occurrence of the phenomenon.

At 500 yrs EQ-IL there is no collapse for the model with decoupled infills, neither in-plane nor out-of-plane. At 500 yrs EQ-IL, only a few infills undergo out-of-service conditions due to the severe damage to the adjacent structural elements. For the model with traditional infills, the OOP collapses already occur at 500 yrs EQ-IL, at the mid-storeys of the building, especially in the long direction; at 2500 yrs EQ-IL, the percentage of collapses (IP and OOP) is very high (> 50%) and comparable in both directions.

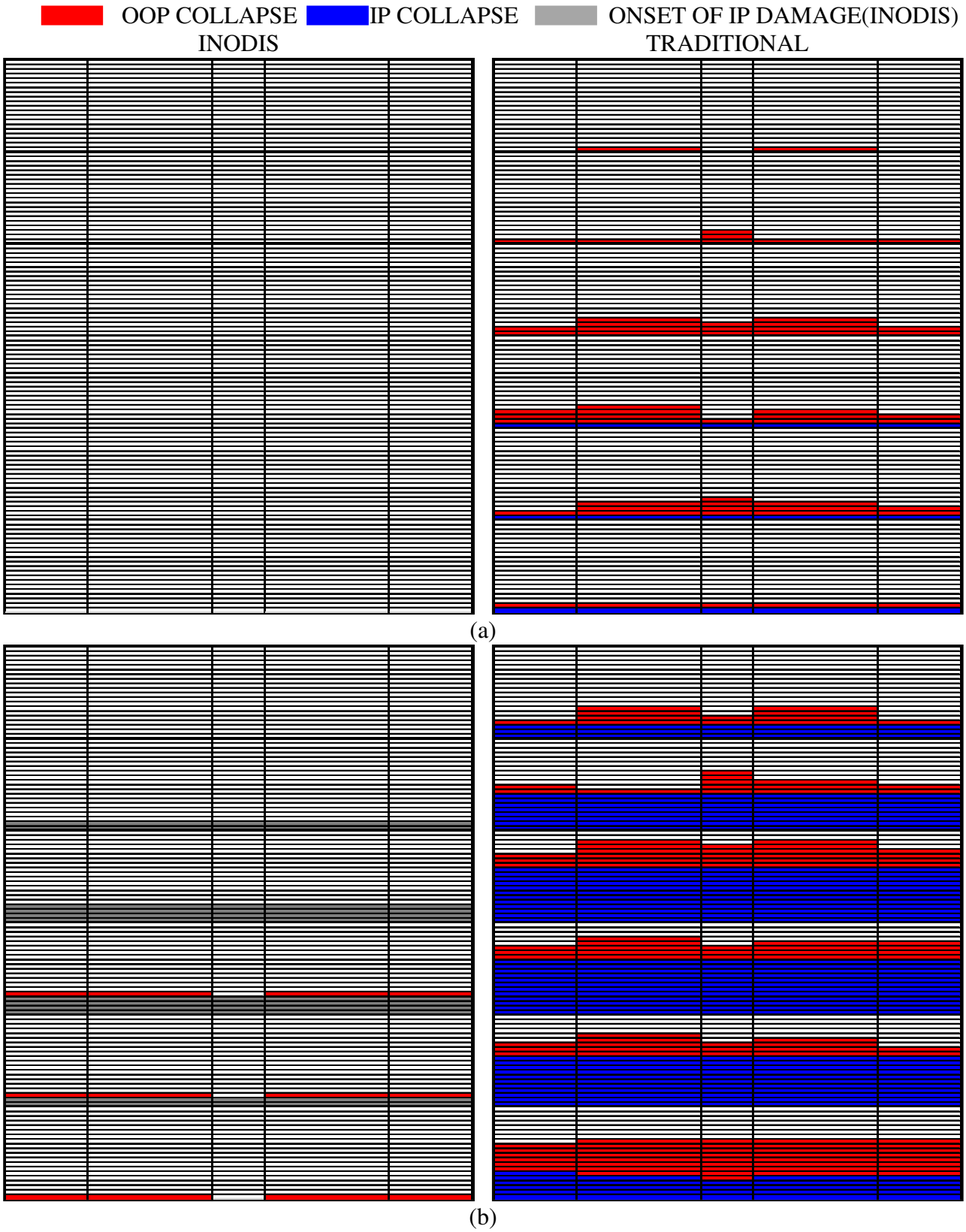

Figure 74 IP and OOP collapses of infills recorded at 500 yrs EQ-IL (a) and 2500 yrs EQ-IL (b) (infills with openings located on the long side of the building)

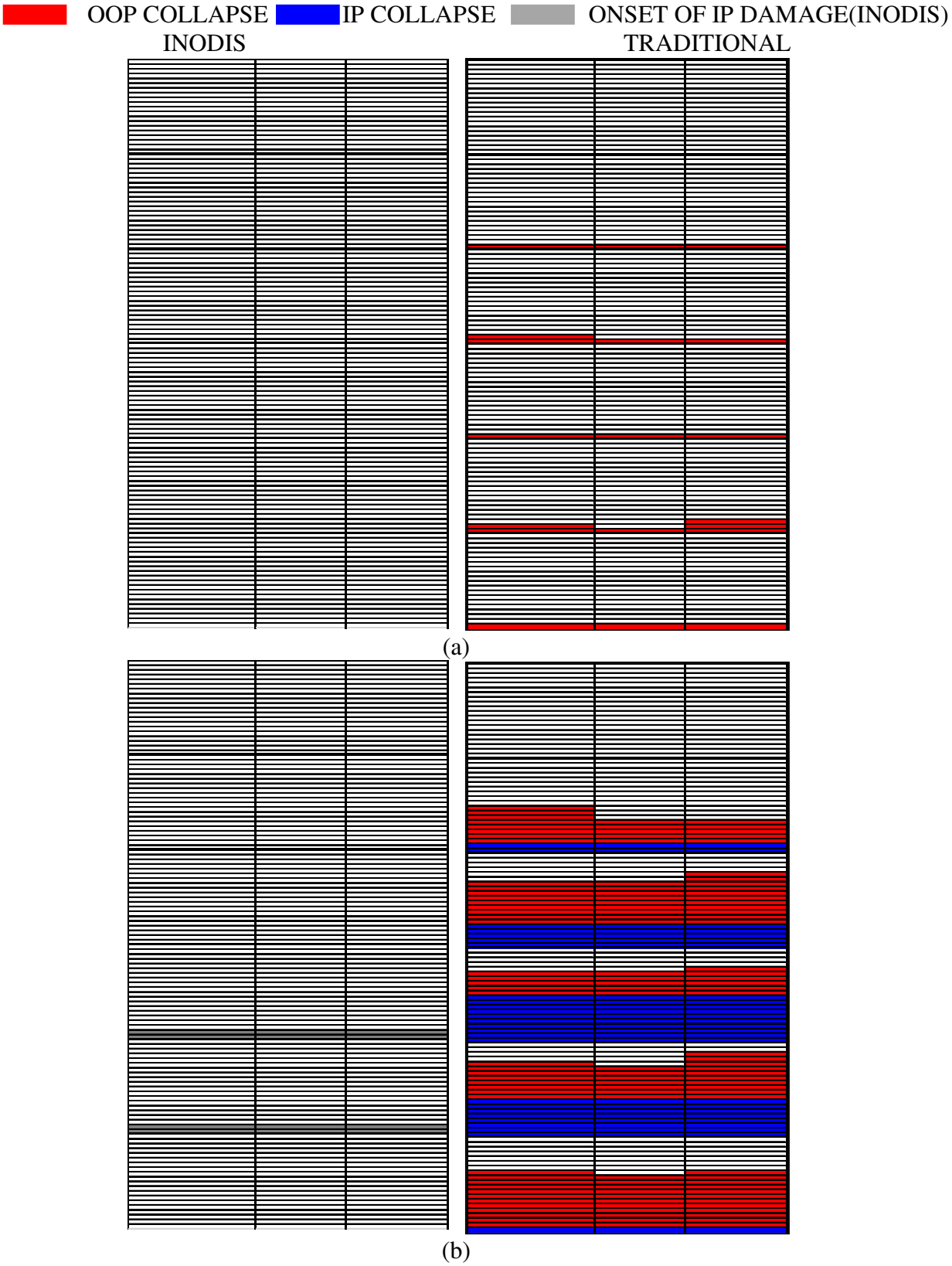

Figure 75 IP and OOP collapses of infills recorded at 500 yrs EQ-IL (a) and 2500 yrs EQ-IL (b) (infills without openings located on the short side of the building)

Table 24. Percentage of infills exceeding different levels of IP damage (from first cracking to collapse) for the model with traditional infills and with decoupled infills, respectively.

	TRADITIONAL INFILL								***INODIS SYSTEM***					
	X-direction (long side)				Z-direction (short side)				X-direction (long side)			Z-direction (short side)		
	repairable damage		*not repairable damage*		*repairable damage*		*not repairable damage*		*repairable damage*	*not repairable damage*		*repairable damage*	*not repairable damage*	
	IP first crack	IP peak force	IP 20% drop	IP coll.	IP first crack	IP peak force	IP 20% drop	IP coll.	IP first crack	Onset of significant IP damage	IP coll.	IP first crack	Onset of significant IP damage	IP coll.
500 yrs EQ-IL	100.0%	97.5%	72.5%	2.5%	84.2%	58.3%	19.2%	**-**	0.8%	-	**-**	**-**	-	**-**
2500 yrs EQ-IL	100.0%	100.0%	91.7%	43.8%	96.7%	86.7%	75.0%	23.3%	22.5%	9.2%	**-**	5.8%	3.3%	**-**

Table 25. Percentage of infills exceeding different levels of OOP damage (from first cracking to collapse) for the model with traditional infills and with decoupled infills, respectively.

	TRADITIONAL INFILL								**INODIS SYSTEM**							
	X-direction (long side)				Z-direction (short side)				X-direction (long side)				Z-direction (short side)			
	repairable damage		*not repairable damage*		*repairable damage*		*not repairable damage*		*repairable damage*		*not repairable damage*		*repairable damage*		*not repairable damage*	
	OOP first crack	OOP peak force	OOP 20% drop	OOP coll.	OOP first crack	OOP peak force	OOP 20% drop	OOP coll.	OOP first crack	OOP peak force	OOP 20% drop	OOP coll.	OOP first crack	OOP peak force	OOP 20% drop	OOP coll.
500 yrs EQ-IL	10.6%	9.8%	9.8%	9.8%	5.0%	4.7%	4.7%	4.7%	2.2%	-	-	-	-	-	-	-
2500 yrs EQ-IL	40.6%	32.3%	32.0%	20.4%	46.8%	38.3%	38.1%	33.5%	14.0%	2.6%	2.6%	2.2%	-	-	-	-

Table 24 and Table 25 point out the global damage scenario of the building (related to the infills only). The percentages reported in Table 24 and Table 25, indeed, refer to the totality of masonry infills. At medium-high seismic intensities (500 yrs EQ-IL), more than 70% of traditional infills in the long direction experience a 20% drop in strength; at very high seismic intensities (2500 yrs EQ-IL), the IP collapse involves almost 50% of traditional infills in the long direction of the building. On the other side, less than 5 % (10 %) of decoupled infills experience significant IP damage in long (short) direction of the building, respectively, because of severe damage in the adjacent RC members. It is noted that, while the IP damage evolves quite gradually, the OOP collapse in traditional infills follows the first cracking quite abruptly.

3.5. SUMMARY AND RESULTS

This section presents the results of the investigation of seismic performance of RC frame building, where the infills are decoupled using INODIS system. In the previous studies, the benefits of the INODIS system were shown on a full-scale experimental test on one infilled frame (Marinković and Butenweg 2019) and corresponding numerical simulations (Marinković and Butenweg 2022). However, in this article the first investigation conducted to confirm the benefits of the INODIS system on a building level is carried out. In order to compare the behaviour of the traditional double-layer infills and behaviour of modern single-layer infills with the INODIS system, numerical simulations are performed in the software Opensees (McKenna, 2011). A typical 6-storey residential building realized in Italy in the '90s is used as a case-study building. Location of case-study building is in the city of L'Aquila. The building model is subjected to modal, pushover and NTHA analyses.

Results of modal analysis clearly show that the periods of vibration of the RC frame building remain virtually unchanged when decoupled infills with INODIS system are installed. On the other side, due to the rigid connections of traditional infills to the surrounding RC frame, significantly higher lateral stiffness of the building is achieved in comparison to the bare RC frame structure. For RC frame building with traditional infills this results in strongly reduced fundamental period of vibration and completely different dynamic characteristics in comparison to those estimated for bare RC frame in the building design. As decoupled infills affect fundamental periods only slightly, such misestimating of dynamic characteristics is not possible for RC buildings with INODIS system.

Furthermore, in pushover analysis, capacity curves for bare frame, frame with traditional and decoupled infill configuration are obtained. These results show further advantages of the INODIS system. While the capacity curves of the model with decoupled infills look similar to those of the bare frame for the whole range of displacement, traditional infills contribute significantly to the frame stiffness. However, for large displacements, the capacity curves of the model with traditional infills tend to overlap the capacity curves of the bare frame, due to the extensive damage of the masonry infills.

For the NTHA, three different earthquake intensity levels, with return periods equal to 50, 500 and 2500 years, are chosen. A total of 20 pairs of bidirectional records are selected for each

seismic intensity. Results of NTHA show that the INODIS system can successfully prevent dangerous OOP failure modes caused by the IP-OOP interaction. Traditional infills already experience the OOP collapse at 500 yrs EQ-IL. At 2500 yrs EQ-IL the percentage of traditional infills that collapse in the OOP direction is 20.4 % and 33.5 % in the long and short building direction, respectively. On contrary, no OOP collapse occurs for infills with the INODIS system at 500 yrs EQ-IL, while only 2.2 % of the wall collapses at the long side, for the 2500 yrs EQ-IL. The collapse of the traditional infills in the OOP direction takes place in the mid- and lower storeys of building due to the pronounced interaction of IP and OOP loading. At these storeys, the OOP capacity is significantly decreased due to the high IP loads. On the other side, OOP capacity of decoupled infills is reduced only at very high IP drifts, due to the delayed activation of masonry infills. Moreover, due to the infill-frame interaction, traditional infills suffer IP collapse already for the rare earthquakes (500 yrs EQ-IL), while the IP collapse is quite prominent for the 2500 yrs EQ-IL. On contrary, no IP collapse occurs for the INODIS system, for all the recorded earthquakes.

This study clearly points that the application of the INODIS system significantly improves the seismic performance of masonry infilled RC frame buildings, but only in terms of damage to the infills and not in general to the whole frame performance. The reduced damage to non-structural elements leads to the smaller need for the wall repairment after the earthquakes, which shows the high economic benefits when using cost-efficient INODIS system.

SECTION 4:
COMPARISON OF RESULTS

4.1 SEISMIC PERFORMANCE

As already mentioned, the building presented in section 3 has been studied in three different configurations. The first is the as built configuration (fixed-base with double layer traditional infills in Figure 76a); two different seismic improving techniques have been proposed: (i) hybrid base isolation system (Figure 76b) and (ii) replacement of traditional infills with innovative ones with decoupling system (Figure 76c).

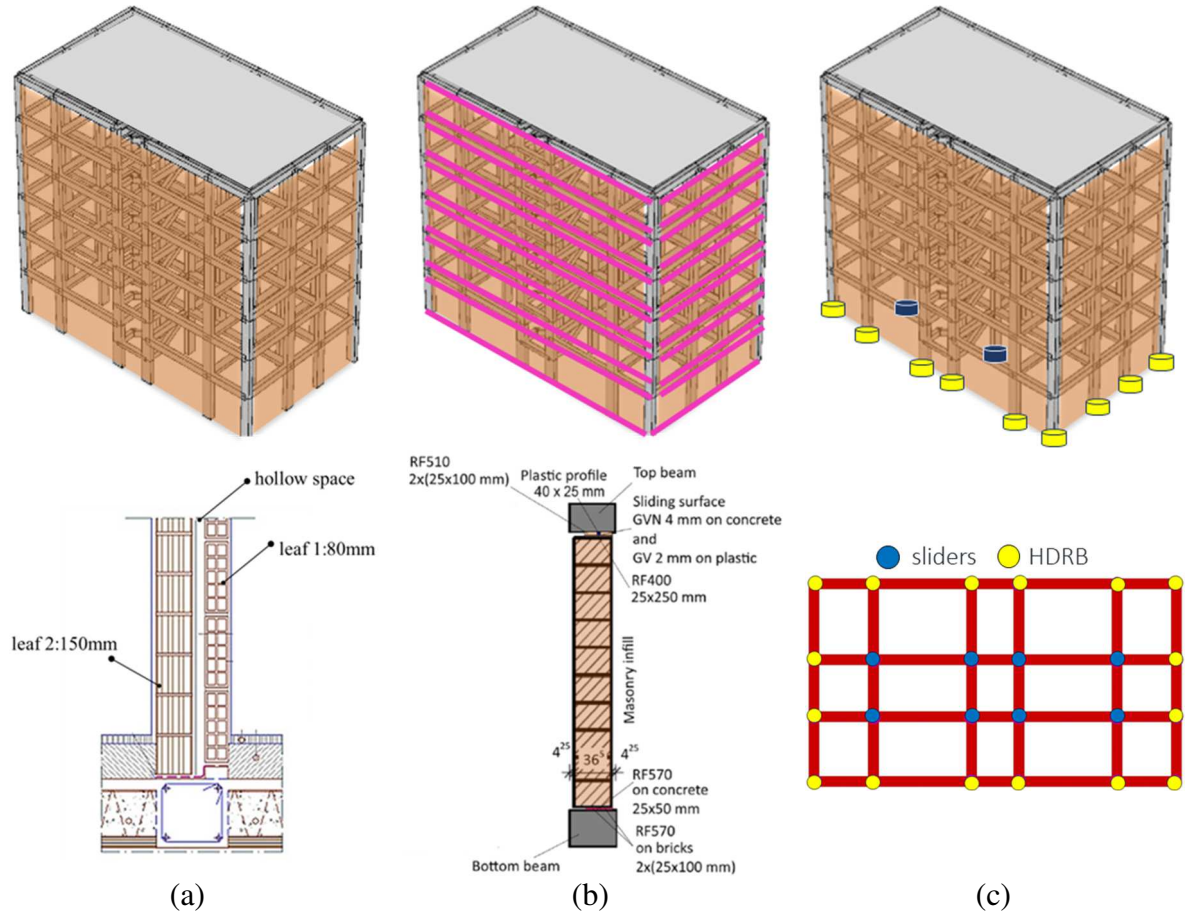

Figure 76 Three different building configurations examined: (a) fixed-base with double layer traditional infills; (b) fixed-base with decoupling infill; (c) base isolated configuration

Starting to the performance points in Figure 73, a damage level (related to the infills only) comparison between the three configurations is shown in the Table 26 and Table 27.

The percentages reported in Table 26 and Table 27 refer to the totality of masonry infills and represent the percentage of infills (average over 20 ground motion pairs) that experience one of the performance points by Figure 73 .

At low seismic intensities (50 yrs EQ-IL) both systems are fully efficient; in fact, as expected, not a single layer infill exceeds even the first crack both in plane and out of plane direction; at medium-high seismic intensities (500 yrs EQ-IL), less than 10% (5%) of traditional infills in

the long (short) direction reaches the peak force but a significant percentage (above 30%) exceeds the first cracking. At very high seismic intensities (2500 yrs EQ-IL), the IP collapse involves less than 10% of traditional infills in the long direction of the base isolated building. Compared to the solution with the decoupling system, at 2500 yrs EQ-IL the isolation system protects infill walls less from in-plane damage but it is highly performing at all seismic intensities for protection to out of plane damage.

Figure 77 and Figure 78 show the damage levels achieved on a typical traditional infill subjected to experimental tests in the literature (reported in Hak et al, 2013 and Di Domenico, 2018) in plane and out of plane respectively. In both cases it can be assumed that:

(i) before reaching point A (first cracking, approximately equal to 65% of the peak force) the panels are not damaged;
(ii) between point A and point A* (approximately equal to 85% of the peak strength) the range of light repairable damage is defined: it is an aesthetic, marginal damage whose repair is usually postponed during ordinary maintenance interventions;
(iii) between point A* and point C (approximately equal to 20% drop of the peak force) the range of repairable damage is defined;
(iv) beyond point C the range of not repairable damage is defined, including the out-of-service of decoupled infills due to severe damage in the adjacent structural elements.

Table 26. Percentage of infills exceeding different levels of IP damage (from first cracking to collapse) for the three models examined

	TRADITIONAL INFILL								***INODIS SYSTEM***						***ISOLATION SYSTEM***							
	X-direction (long side)				Z-direction (short side)				X-direction (long side)			Z-direction (short side)			X-direction (long side)				Z-direction (short side)			
	IP first crack	IP peak force	IP 20% drop	IP coll.	IP first crack	IP peak force	IP 20% drop	IP coll.	IP first crack	Onset of IP damage	IP coll.	IP first crack	Onset of IP damage	IP coll.	IP first crack	IP peak force	IP 20% drop	IP coll.	IP first crack	IP peak force	IP 20% drop	IP coll.
50 yrs EQ-IL	**61.7%**	35.0%	**-**	**-**	7.5%	**-**	**-**	**-**	**-**	-	**-**	**-**	-	**-**	**-**	**-**	**-**	**-**	**-**	**-**	**-**	**-**
500 yrs EQ-IL	**100.0%**	**97.5%**	**72.5%**	2.5%	**84.2%**	**58.3%**	19.2%	**-**	0.8%	-	**-**	**-**	-	**-**	42.5%	7.5%	4.2%	**-**	9.2%	2.5%	2.5%	**-**
2500 yrs EQ-IL	**100.0%**	**100.0%**	**91.7%**	43.8%	**96.7%**	**86.7%**	**75.0%**	23.3%	22.5%	9.2%	**-**	5.8%	3.3%	**-**	**92.5%**	**64.2%**	47.1%	6.7%	**43.3%**	36.7%	15.8%	**-**

Table 27. Percentage of infills exceeding different levels of OOP damage (from first cracking to collapse) for the three models examined

	TRADITIONAL INFILL								***INODIS SYSTEM***								***ISOLATION SYSTEM***							
	X-direction (long side)				Z-direction (short side)				X-direction (long side)				Z-direction (short side)				X-direction (long side)				Z-direction (short side)			
	OOP first crack	OOP peak force	OOP 20% drop	OOP coll.	OOP first crack	OOP peak force	OOP 20% drop	OOP coll.	OOP first crack	OOP peak force	OOP 20% drop	OOP coll.	OOP first crack	OOP peak force	OOP 20% drop	OOP coll.	OOP first crack	OOP peak force	OOP 20% drop	OOP coll.	OOP first crack	OOP peak force	OOP 20% drop	OOP coll.
50 yrs EQ-IL	-	-	-	-	-	-	-	**-**	-	-	-	-	-	-	-	-	-	-	-	-	-	-	-	-
500 yrs EQ-IL	10.6%	9.8%	9.8%	9.8%	5.0%	4.7%	4.7%	4.7%	2.2%	-	-	-	-	-	-	-	1.0%	0.8%	0.7%	-	-	-	-	-
2500 yrs EQ-IL	40.6%	32.3%	32.0%	20.4%	46.8%	38.3%	38.1%	33.5%	14.0%	2.6%	2.6%	2.2%	-	-	-	-	1.1%	0.9%	0.9%	-	3.1%	1.7%	1.4%	

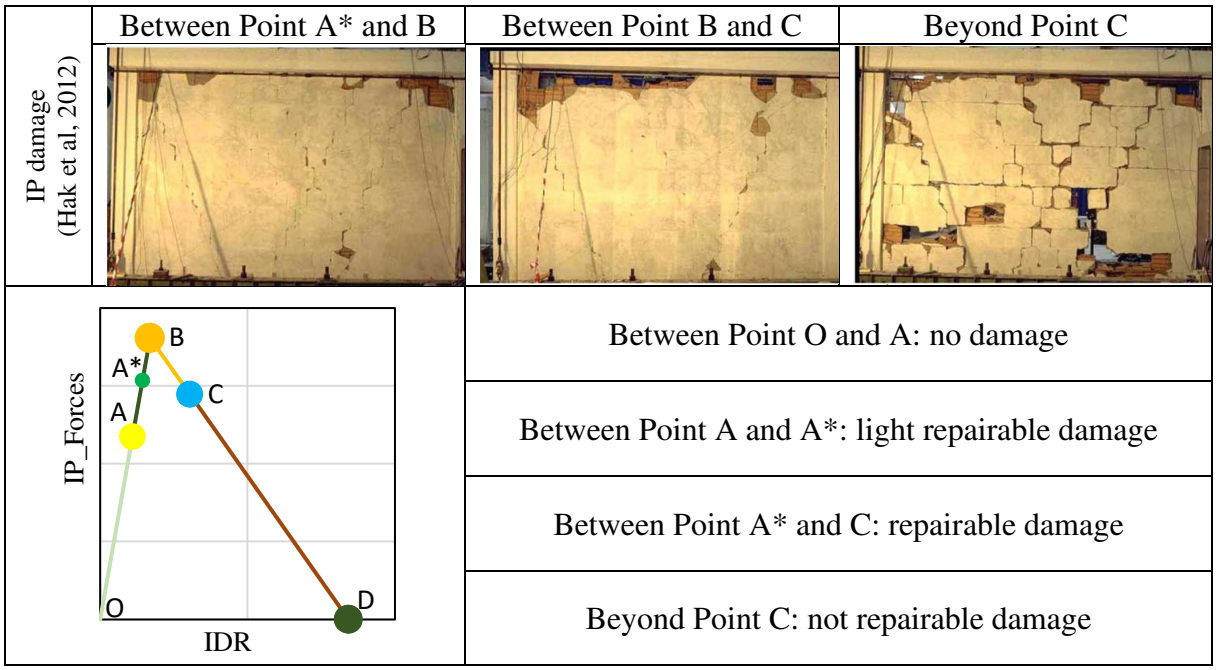

Figure 77 Definition of In Plane Damage Levels for traditional infills

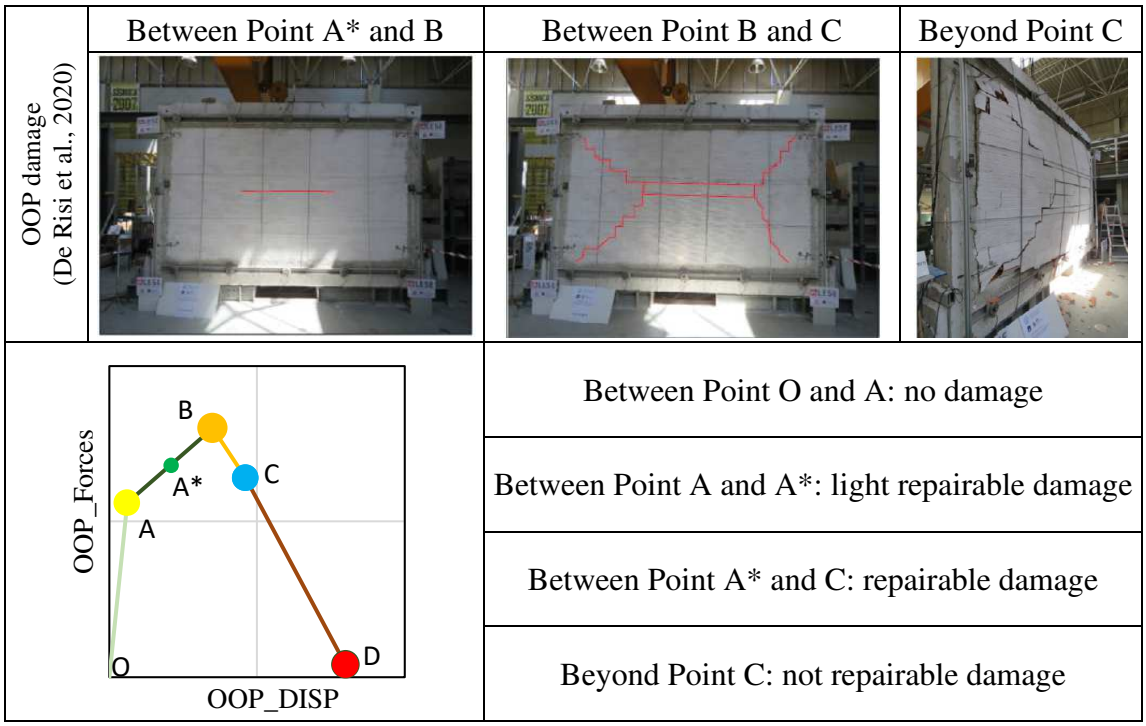

Figure 78 Definition of Out of Plane Damage Levels for traditional infills

Concerning modern decoupling infills, however, as explained in section 3, the damage to the non-structural element can essentially always be considered repairable up to a limit drift assumed to be equal to 3%. Beyond this threshold, it is considered not-reparable damage because the frame begins to be significantly damaged; moreover, at this point, actions are needed to restore the decoupling panel in its original position and replace some connections.

Figure 79(a) shows total percentages of infills experiencing light repairable, repairable and not-repairable damage in the three configurations of the analyzed building; the percentages shown exclude any overlaps between the two directions of analysis. A detail is also proposed for each single seismic intensity: low Figure 79(b) , medium Figure 79(c) , high Figure 79(d) respectively.

Aggregating the IP and OOP damage and referring to the entire building (long and short direction), it can be observed that (see Figure 79) decoupled infills guarantees the absence of any significant damage for rare earthquakes (500 years of return period) and the reduction of not-repairable damage from around 85% to around 15% of the infills for very rare earthquakes (2500 years return period). On the other hand, for very frequent earthquakes (50 years of return period) over 40% of the traditional infills show damage, mor then half of which is not-light. In the base isolated building, the light damage of the (traditional) infills is the greatest for earthquakes with a return period of 500 years. At the maximum intensity analysed (2500 years of return period) the seismic isolation system provides a significant reduction (≈50%) in not repairable damage compared to the fixed base configuration but it's less performing than the INODIS system. In fact, starting from this seismic intensity, the isolation system (which is designed for earthquakes with a return period of 1000 years) shows the first failures which therefore make it inefficient. This confirms what has already been partially stated in section 2; in fact, the Italian seismic code provides for base isolated buildings the satisfaction of the following checks:

(i) verification of non-structural elements for earthquakes with a return period of 50 years;
(ii) verification of the life safety for earthquakes with a return period of 500 years;
(iii) verification of the isolation system for earthquakes with a return period of 1000 years
(iv) different GMPEs have been used

It is easy to see that the condition (i) is guaranteed with a much wider margin than the minimum standard requirement; in fact, the first significant non-structural damage occurs at a return period ten times higher than that required by the seismic code. On the other hand, the margin with respect to the collapse is much less marked.

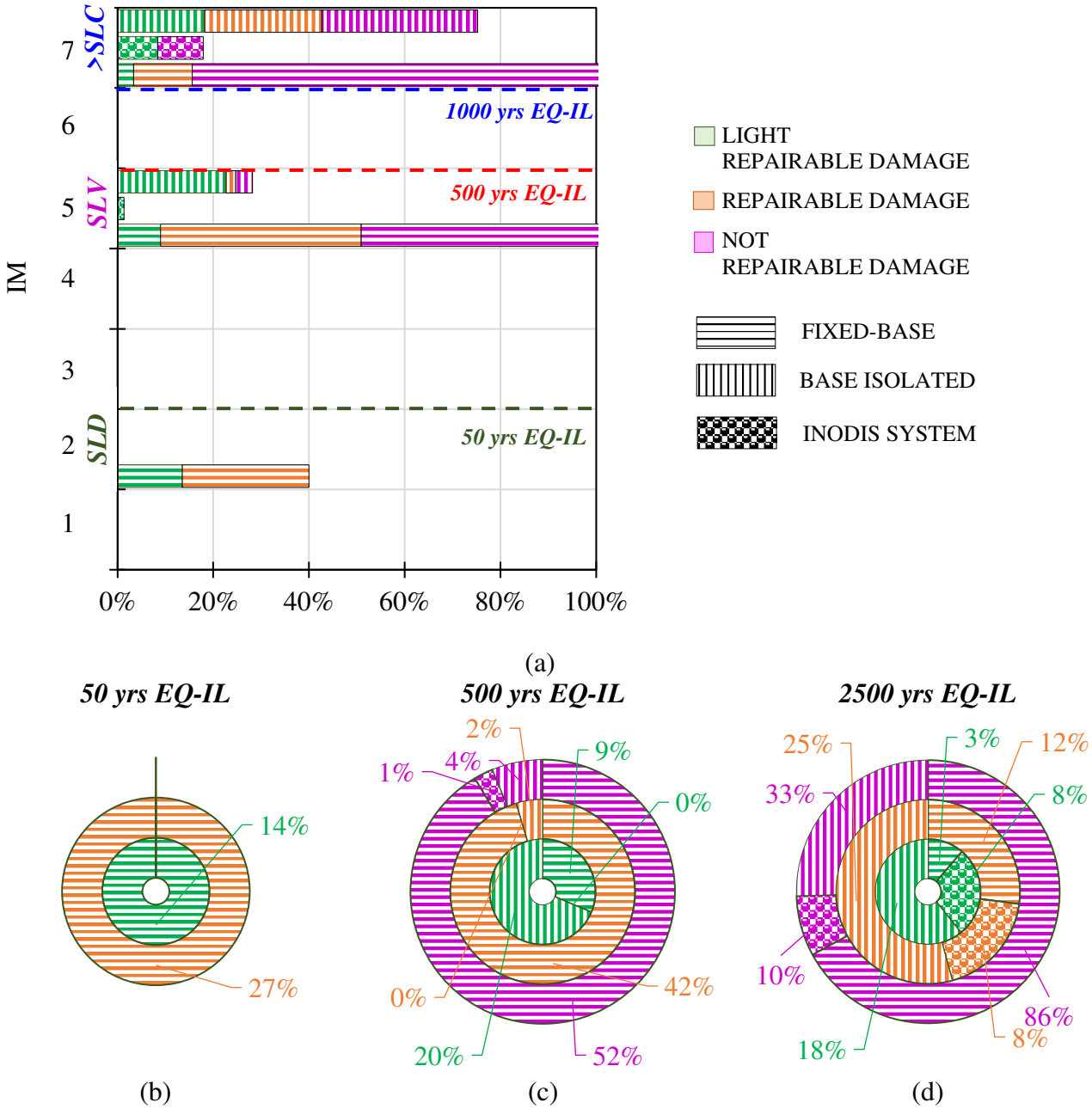

Figure 79 Total percentages of infills experiencing light repairable, repairable and not-repairable damage (figures obtained by aggregating IP and OOP damage without overlaps, over the entire building): (a) global view; (b) low seismic intensity; (c) medium seismic intensity and (c) high seismic intensity

4.2 ECONOMIC ISSUES

A preliminary cost analysis is presented below, to make an economic comparison between the three configurations (fixed-base, base isolated and with decoupling infills) of the examined building.

In particular, it is essential to note that the proposed evaluation concerns only the non-structural elements and does not include the Reinforced Concrete (RC) frame in the calculation.

From the study of the behaviour under monotonic load of the traditional masonry infill walls shown in Figure 77 it is possible to identify the typical cracking/damage models, to be considered for repair intervention in the cost evaluation.

Consequentially, a number of damage states (DSs) have been defined to characterize damage development in masonry infill walls. Damage states are defined by observations on extent and severity of cracking, failure of brick units, damage on frames (windows, French windows and doors), etc., supported and/or complemented by other macroscopic damage indicators, such as the attainment of the peak force or given strength reduction ratios.

According to European Macroseismic Scale (EMS-98), as reported in De Risi et al. 2019, the selected damage states can generally be described as follow Table 28:

Table 28 Damage description according to European Macroseismic Scale (EMS-98)

DS	Damage Description
DS0	***No Damage***
DS1	***Negligible to Slight damage***: Fine cracks in partitions and infills.
DS2	***Moderate damage***: Cracks in partition and infill walls
DS3	***Substantial to Heavy damage***: Large cracks in partition and infill walls, failure of individual infill panels

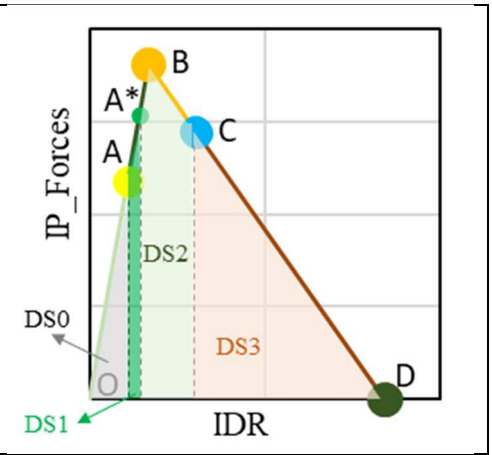

Table 28 also locates the defined Damage States on a generic in-plane backbone of a traditional masonry infill wall.

De Risi et al. 2019 gives a detailed cost analysis related to the main operations in repairing a single infill panel damaged during a seismic event has to be defined.

The unit cost of each elementary operation to restore the infill panel to its undamaged state has been evaluated from the Price List of Public Works in Abruzzi Region.

According to the definition of EMS-98, the total failure of the infill is included in DS3.

Table 29 shows the repair costs for double leaf hollow clay briks reported in De Risi et al, 2019 for three panel typologies (with and without openings, whit windows opening or with door opening).

Table 29 Repair costs for double leaf hollow clay briks (De Risi et. Al 2019)

Hollow+Hollow Clay briks (€/m^2)	C_{DS0}	C_{DS1}	C_{DS2}	C_{DS3}
Solid Panel	**0**	**77.0**	**105.3**	**285.8**
Panel with window	**0**	**73.0**	**101.3**	**331.4**
Panel with door	**0**	**69.2**	**97.4**	**374.9**

However, these costs mainly refer to in plane damage of the infill neglecting the increase due to overlapping out-of-plane damage. About that, Figure 80 shows the results of experimental tests carried out by Abrams et al., 1996 in order to evaluate the effect of in-plane damage on out-of-plane strength of the infill.

Masonry infills cracked in the in -plane and in the out-of-plane directions following the path of least resistance including reopening of previously formed cracks as well as forming new cracks as shown in Figure 80 (compare figures in column "a", and "b"). In-plane and out-of-plane cracks far each specimen compared favorably.

The formation of the final crack pattern observed less resistance by the previously cracked specimens. Tue resistance by the masonry decreased because of the presence of existing cracks that just re-open during the test; new cracks were created as the out-of-plane loadings increased. Therefore, an increase in damage of about 15% is assumed.

As a result, the repair costs shown in Table 29 will be considered increased by approximately 15% below.

Finally, for simplicity, the cost of repositioning the INODIS system was assumed to be equal to the cost of installing a PVC window frame.

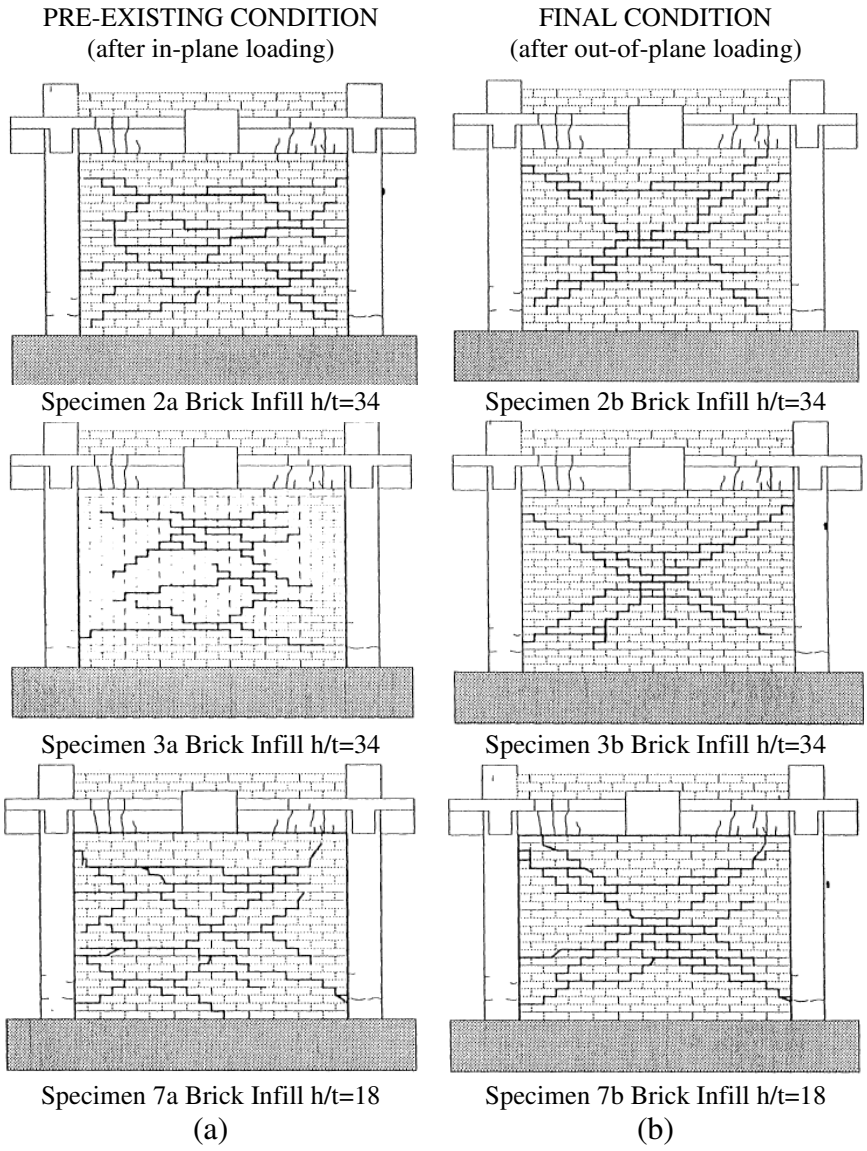

Figure 80 Crack pattern after In-Plane and after Out-Of-Plane Loading (Abrams et al., 1996)

Figure 81(b) shows the retrofit costs relating to the two systems proposed in this study.

In particular, it should be remembered that the two strategies are applied to the same existing structure, initially assumed to be undamaged.

The two proposed interventions include:

(i) installation of the isolation system preserving the double-layer infills on the as-built building;

(ii) complete replacement of the as-built double-layer infills with the innovative decoupled ones (INODIS system).

Obviously, solution (i) is a purely structural intervention (and therefore the cost also relates to a structural intervention). However, the performance is always evaluated considering the response of the non-structural elements only.

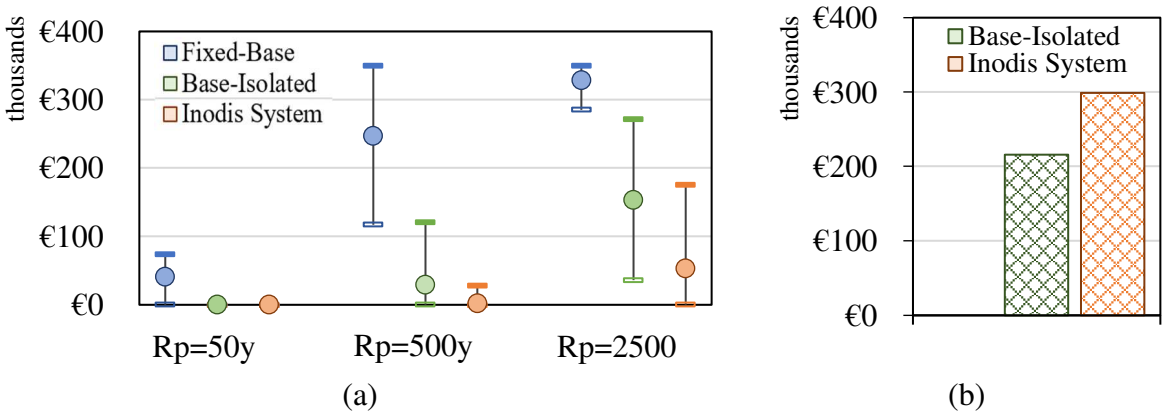

Figure 81 Repair (a) and Retrofit (b) Costs

In particular, according to Cardone et al., 2017 a retrofit cost with seismic isolation ranging from approximately 600 to 700 €/m^2 (corresponding to approximately 8,000-9,000 €/column), as a function of the height of the building and isolation type, has been thus obtained.

It should be noted that the retrofit costs herein considered do not include the costs related to design activities, permitting processes, administration, management, and financing, which may increase considerably the costs of the intervention. Therefore, the aforesaid estimates provide a lower bound on the actual cost of intervention.

For the decoupled infills, instead, an extra cost of around 20% was considered, compared to the construction cost of a traditional infill.

This is very interesting and, where the seismic isolation is not suitable, INODIS system is one of the most effective ways to take action. However, isolation system guarantees not only the infill protection, but also all the acceleration susceptible components and the structure protection, while INODIS improve only infill performance.

This assessment is in agreement with what is stated in Cardone et al., 2017. The retrofit cost of the INODIS system, for the assumptions made in this study, includes the previous demolition of the pre-existing traditional infill walls and the construction of new decoupling infills, on the entire building. It should be noted that this is a purely theoretical assumption, which is badly placed in a realistic context, in which the intervention to be proposed would have been specifically requested for the most vulnerable floors of the building. For this reason, it can still be said that the two systems substantially show a comparable retrofit cost, but neglecting indirect costs due to downtime and ancillary work.

However, in this case, a vertical irregularity could cause the system to activate soft floor mechanisms if the intervention is limited to a single storey of the building.

Generally speaking, however, non-linear dynamic analyses presented in section 1 show that the greatest damage to the infill walls is concentrated in the medium-low floors of the buildings (where, among other things, the greatest inter-floor drifts are recorded) and almost never on a single floor. In these terms, therefore, the intervention could potentially exclude the highest storeys of the building, where the drift requests are probabilistically smaller; on the other hand, however, the higher accelerations are usually recorded on the upper storeys, which could in any case favour the out of plane collapse of the infills.

Consequently, limiting the intervention to a single portion of the building could both cause a drastic modification of the structural behaviour (which should be studied for each specific case, based on the geometry and stiffness of the structure) and not fully protect the non-structural elements of the buildings.

Therefore, to avoid changes in the structural response of the building, seismic isolation should be preferred as a retrofit intervention, unless the replacement of the panels extends to the whole building.

Furthermore, installation of isolation system is certainly non-invasive compared to infills replacement; in fact, this second intervention strategy provides for the preventive demolition of existing ones and the obligation of the occupants to leave their homes during the works.

Probably, the innovative decoupled infills would be more functional for new buildings, compared to a retrofit intervention. The advantage of seismic isolation as a retrofit intervention is its non-invasiveness; on the contrary, the great invasiveness of the infills replacing and the

possible consequences linked to an application not extended to all storeys, suggest probably that it is a more suitable solution for new rather than existing buildings.

Figure 81(a) shows the repair costs related to the three seismic intensities considered, in the three different configurations of the building. In the same figure, the dots represent the average value calculated on 20 ground motion pairs, while the lines represent the minimum and the maximum values for each seismic intensity. For Fixed-Base building, it is necessary to spend on average of around 50000 € to repair the damage caused by an earthquake with a high probability of occurrence (return period equal to 50 years), around 250000 € (over 300000 €) for an earthquake of medium (high) intensity.

With the isolation system, the repair costs are completely zero for very frequent earthquakes (Rp=50 yrs) and are reduced by about 90% and 50% compared to the building with the fixed base configuration for rare (Rp=500 yrs) and very rare (Rp=2500 yrs) earthquakes respectively.

By the INODIS system, up to return periods of 500 years, repair costs are practically zero and do not exceed the threshold of about 50000€ for earthquakes with return period equal to 2500 years.

Figure 81(a) also shows the variability of the result obtained, essentially linked to the ground motion pairs using during the non-linear dynamic analysis.

Base Isolated technique halves the repair costs at the maximum intensity investigated.

Under 500 years return period, repair costs are almost zero for both innovative technique; seismic isolation appears slightly less performing than decoupling infills, but: (i) isolation system was designed for 1000 years return period seismic intensity; (ii) decoupled infills were designed for new buildings and are oversized for the existing building under consideration.

Moreover, generally speaking, compared to the local strengthening measures, seismic isolation is a less invasive technique that allows limiting the intervention at the level of the isolation system only, preserving the integrity of the other parts of the structure. Another great advantage of seismic isolation is that it guarantees the full serviceability of the building immediately after the seismic event, thanks to a high level of protection of the structure and its content.

CONCLUSIONS AND FURTHER DEVELOPMENTS

The main focus of the present doctoral dissertation was the study of the seismic response of masonry infill walls, considering alternative techniques and approaches to improve their performance.

The numerical investigations performed herein allowed to identify many parameters which influence the seismic response of these non-structural elements, considering different superstructure characteristics, isolation system types and infill technologies. The research covered a large number of case study structures analyzed by employing complex non-linear models.

More than 3,000 analyses (between Modal Analyses, Pushover Analyses (POA) and Nonlinear Time History Analyses (NTHA) have been performed within this research work considering a wide range of seismic intensities. Results from all the analyses pointed out the fundamental role of the infills in determining the seismic performance of the structures.

The main findings and conclusions drawn from this work are here summarized.

In the first section, seven archetype buildings, differing in terms of age of construction (‘50s to ‘90s), number of storeys (from 4 to 8), seismic design approach (gravity loads design, low seismic forces with substandard details, modern seismic design) and type of masonry infills (thin double-layers infills with inner cavity and thick single-layer infills) have been analyzed. The building models have been located in two different sites (Napoli and L’Aquila), featuring moderate and high seismic hazard for Italy, respectively.

Extensive Nonlinear response-Time History Analysis (NTHA) have been carried out for ten earthquake intensity levels, with return periods ranging from 30 years to 5000 years. Seismic performances have been evaluated considering two different Performance Levels (PLs), referred to as: Usability Preventing Damage (UPD), and Life Safety (LS). NTHA have been repeated considering a non-degrading IP-only model for infills, in order to assess the relevance of the IP/OOP interaction and degrading behavior of masonry infills towards the seismic performance of RC frame buildings. Code-conforming simplified approaches, adopted in

current practice, have been considered for the models without IP/OOP interaction, in order to check a-posteriori the OOP collapse of infills.

Based on the results of this study, the following main conclusions can be drawn.

Although the slenderness ratio (h/t) is the main parameter governing the OOP behavior of URM infills, also the in-plane damage plays a fundamental role towards the OOP seismic performance of the infills; the OOP collapse mechanism results particularly relevant for double-layer infills characterized by relatively high values of slenderness (t/h≈ 25 ÷30); single-layer infills, characterized by relatively low values of the slenderness (t/h≈ 8 ÷10), are little affected by IP/OOP interaction.

Considering the IP/OOP interaction of URM infills in the numerical model can significantly affect the seismic performance of the RC buildings in terms of LS (Life Safety) performance level.

The simplified approaches proposed in the modern codes for the safety verification of the OOP collapse mechanisms of infills can significantly overestimate (ref. to FEMA-306/NZSEE-2017) or underestimate (ref. to EC6) the number of OOP collapses.

The analyzed case studies in the second section, comprise six archetype residential RC buildings differing for construction periods (1950s-60s, 1970s, 1980s-90s) and design approach (Gravity Load Design, GLD, and Seismic Load Design, SLD, based on old technical standards). The analyses have been performed within the RINTC research project on existing RC buildings retrofitted with seismic isolators according to the Italian minimum code requirements.
GLD buildings are supposed to be located in the city of Naples (characterized by medium seismic hazard for Italy), SLD buildings are supposed to be located in the city of L'Aquila (characterized by high seismic hazard for Italy). Isolation systems have been designed to avoid any superstructural damage up to the Life safety Limit State (LLS), in accordance with the current Italian Seismic Code. All case studies have been assessed by means of Multi Stripe nonlinear time history Analysis (MSA), computing the annual failure rates for two performance levels, namely Global Collapse (GC) and Usability Preventing Damage (UPD). As base-isolated buildings are in-series systems (being composed by the isolation system and the superstructure) and isolation devices can undergo different failure modes, a multi-criteria approach has been followed for the definition of the aforesaid performance levels. One of the

most advanced numerical model currently available for the description of the nonlinear cyclic behaviour of HDRBs (namely the Kikuchi Bearing element implemented in OpenSees) has been used in the analyses, due to its capability of simulating the behaviour of HDRBs under large displacements and high axial loads. The model parameters have been calibrated against experimental results of an extensive experimental investigation.

All the results concerning the usability-preventing performance level point out that all isolation systems work effectively in limiting the building damage for seismic intensities much higher than the intensity level considered in the design (corresponding to return period (Rp) equal to 50 years), but they are characterized by a little margin beyond the intensity level considered in their seismic design (corresponding to 1000 years return period).

This limited margin associated with the collapse failure of base-isolated structures seems to be related to the optimized design of the isolation system and the lower margin of safety with respect to collapse beyond the maximum design displacement.

Moreover, the seismic performances of retrofitted base-isolated structures are significantly affected of the site hazard (the buildings located in moderate seismicity regions show larger safety margins than those located in high seismicity regions).

Therefore, more detailed and specific indications about the safety margins to be assumed in the retrofit of existing buildings with seismic isolation should be given by current design Codes in order to avoid poor performance for earth-quake intensity levels greater than design. The indications should be tailored for different base-isolation systems and should be different for low, medium and high seismic zones in order to get homogeneous reliability levels.

In the section three the first investigation conducted to confirm the benefits of the INODIS system on a building level is carried out. In order to compare the behaviour of the traditional double-layer infills and behaviour of modern single-layer infills with the INODIS system, numerical simulations are performed in the software Opensees. A typical 6-storey residential building realized in Italy in the ‘90s is used as a case-study building. Location of case-study building is in the city of L’Aquila. The building model is subjected to modal, pushover and NTHA analyses.

Results of NTHA show that the INODIS system can successfully prevent dangerous OOP failure modes caused by the IP-OOP interaction. Traditional infills already experience the OOP collapse at 500 years earthquake intensity level (yrs EQ-IL). On contrary, no OOP collapse occurs for infills with the INODIS system at 500 yrs EQ-IL. OOP capacity of decoupled infills is reduced only at very high IP drifts, due to the delayed activation of masonry infills. Moreover, due to the infill-frame interaction, traditional infills suffer IP collapse already for the rare earthquakes (500 yrs EQ-IL), while the IP collapse is quite prominent for the 2500 yrs EQ-IL. On contrary, no IP collapse occurs for the INODIS system, for all earthquakes considered.

The use of decoupled infills guarantees the absence of any significant damage for rare earthquakes (500 years of return period) and the reduction of not-repairable damage of around 80% for very rare earthquakes (2500 years return period). At the maximum intensity analysed (2500 years of return period) the seismic isolation system provides a significant reduction (≈50%) of not repairable damage compared to the fixed base configuration but it's less effective than the INODIS system. Indeed, starting from this seismic intensity, the isolation system (which is designed for earthquakes with a return period of 1000 years) shows the first failures which therefore make it inefficient to protect the superstructure from seismic damage.

With the isolation system, the repair costs are completely zero for very frequent earthquakes (Rp=50 yrs) and are reduced by about 90% and 50% compared to the building with the fixed base configuration for rare (Rp=500 yrs) and very rare (Rp=2500 yrs) earthquakes respectively. With the INODIS system, up to return periods of 500 years, repair costs are practically zero; they do not exceed the threshold of about 50000€ for earthquakes with return period equal to 2500 years.

The design assumptions regarding the two innovative protecting techniques (seismic isolation and decoupled infills) considered in this study play a fundamental role in the obtained results and, as a consequence, in the conclusions reported herein. The retrofit cost of the INODIS system, for instance, includes the demolition of the existing traditional infill walls and the construction of new decoupled infills, on the entire building. It should be noted that this is a purely theoretical assumption, which is difficult to achieve in a realistic context, in which the intervention would be limited to previously damaged infills or at least to the most vulnerable floors of the building. For this reason, it can still be said that the two systems substantially show a comparable retrofit cost.

However, in this case, a vertical irregularity could cause the system to activate soft floor mechanisms if the intervention is limited to a single storey of the building.

Therefore, to avoid changes in the structural response of the building, seismic isolation should be preferred as a retrofit intervention, unless the replacement of the panels extends to the whole building.

Furthermore, installation of isolation system is certainly non-invasive compared to infills replacement; in fact, this second intervention strategy provides for the preventive demolition of existing ones and the obligation of the occupants to leave their homes during the works.

Probably, innovative decoupled infills would be more functional for new buildings, compared to a retrofit intervention. The advantage of seismic isolation as a retrofit intervention is its non-invasiveness; on the contrary, the great invasiveness of the infills replacing and the possible consequences linked to an application not extended to all storeys, suggest probably that it is a more suitable solution for new rather than existing buildings.

Seismic isolation appears slightly less performing than decoupling infills, but: (i) isolation system was designed for 1000 years return period seismic intensity; (ii) decoupled infills were designed for new buildings and are oversized for the existing building under consideration. Compared to the local strengthening measures, seismic isolation is a less invasive technique that allows limiting the intervention at the level of the isolation system only, preserving the integrity of the other parts of the structure. Another great advantage of seismic isolation is that it guarantees the full serviceability of the building immediately after the seismic event, thanks to a high level of protection of the structure and its content; INODIS system also guarantees the functionality of the building, but cannot fail to protect its contents

The work carried out in this thesis is a preliminary study regarding the alternative techniques for improving the seismic performance of masonry infills. Many problems have been highlighted but further investigations are required to provide more general and robust conclusions. One limitation of the study presented is related to the restricted set of models investigated, especially with regard to the INODIS system. Further experimental tests are needed to verify this technique in order to probe the generality of the conclusions herein proposed. Additionally, a more refined cost analysis (also including the cost for repairing damage to the main structure) should be performed to accurately compare expected losses and

better highlight the advantages of the two innovative techniques. Another possible improvement of the work is the use of newly developed GMPE for the hazard assessment (Lanzano et al. 2019)

REFERENCES

Akhoundi, F., Vasconcelos, G., Lourenço, P., Silva, L. M., Cunha, F., & Fangueiro, R. (2018). In-plane behavior of cavity masonry infills and strengthening with textile reinforced mortar. *Engineering Structures*, *156*, 145-160.

Akkar, S., Bommer, J.J., 2010. Empirical Equations for the Prediction of PGA, PGV, and Spectral Accelerations in Europe, the Mediterranean Region, and the Middle East. Seismological Research Letters 81, 195–206. https://doi.org/10.1785/gssrl.81.2.195

Ambraseys, N.N., Simpson', K.A., Bommer', J.J., 1996. PREDICTION OF HORIZONTAL RESPONSE SPECTRA IN EUROPE. Earthquake Engineering & Structural Dynamics 25, 371–400. doi:10.1002/(SICI)1096-9845(199604)25:4<371::AID-EQE550>3.0.CO;2-A.

Angel R, Abrams DP, Shapiro D, Uzarski J, Webster M (1994) Behavior of Reinforced Concrete Frames with Masonry Infills. Department of Civil Engineering, University of Illinois, Urbana-Champaign, IL, USA

Aslani, H, Miranda, E 2005. Probabilistic earthquake loss estimation and loss disaggregation in buildings. Report No. 157. The John A. Blume Earthquake Engineering Center, De-partment of Civil and Environmental Engineering, Stanford University, Stanford, CA, USA.

Asteris P, Cotsovos DM, Chrysostomou CZ et al (2013) Mathematical micromodeling of infilled frames: state of the art. Eng Struct 56:1905–1921

Asteris, P. G., Repapis, C. C., Tsaris, A. K., Di Trapani, F. and Cavaleri, L. (2015). Parameters affecting the fundamental period of infilled RC frame structures. Earthquakes and Structures, 9(5), 999-1028.

ATC – Applied Technology Council, FEMA P-58 (2012) Next-generation Seismic Performance Assessment for Buildings, Volume 1 – Methodology, Federal Emergency Management Agency, Washington, D.C.

Ay BÖ, Fox MJ, Sullivan TJ (2017) Technical Note: Practical Challenges Facing the Selection of Conditional Spectrum Compatible Accelerograms. Journal of Earthquake Engineering 21(1), 169-180

B.U.R.A. Price List of Public Works in Abruzzi Region; Regione Abbruzzo: L'Aquila, Italy, 2017. (In Italian)

Baker JW, (2011) Conditional Mean Spectrum: Tool for ground motion selection, Journal of Structural Engineering, 137(3), 322-331

Bashandy T, Rubiano NR, Klingner RE (1995) Evaluation and analytical verification of infilled frame test data. Phil M. Ferguson Structural Engineering Laboratory, University of Texas at Austin.

Braga F, Gigliotti R, Laterza M, D'Amato M, Kunnath SF (2012) Modified Steel Bar Model Incorporating Bond-Slip for Seismic Assessment of Concrete Structures, J. Struct. Eng, ASCE, 138:1342-1350

Braga, F., Manfredi, V., Masi, A., Salvatori, A., & Vona, M. (2011). Performance of non-structural elements in RC buildings during the L'Aquila, 2009 earthquake. *Bulletin of Earthquake Engineering*, *9*(1), 307-324.

Brandonisio, G., Ponzo, F., Mele, E., Luca, A.D. 2017. Experimental tests of elastomeric isolators: influence of vertical load V and of secondary shape factor, Proc. of 17th ANIDIS Conference, Pistoia, Italy

Calvi GM, Magenes G, Pampanin S (2002) Relevance Of Beam-Column Joint Damage And Collapse In Rc Frame Assessment, Journal of Earthquake Engineering, 6:Special Issue 1, 75-100

Calvi, G. M., & Bolognini, D. (2001). Seismic response of reinforced concrete frames infilled with weakly reinforced masonry panels. *Journal of Earthquake Engineering*, *5*(02), 153-185.

Camata, G., Celano, F., Risi, M.T.D., Franchin, P., Magliulo, G., Manfredi, V., Masi, A., Mollaioli, F., Noto, F., Ricci, P., Spacone, E., Terrenzi, M., Verderame, G.M. 2017. RINTC project: nonlinear dynamic analyses of italian code-conforming reinforced concrete buildings for risk of collapse assessment, (COMPDYN 2017), Rhodes Island, Greece. https://doi.org/10.7712/120117.5507.17050

Cardone D (2007) Nonlinear static methods vs. experimental shaking table test results, Journal of Earthquake Engineering, Vol. 11 (6), pp. 847-875., DOI: 10.1080/13632460601173938

Cardone D, Perrone G (2015) Developing fragility curves and loss functions for masonry infill walls. Earthquakes and Structures 9 (1): 257–79

Cardone D, Perrone G (2017) Damage and loss assessment of pre-70 RC frame buildings with FEMA P-58. J Earthq Eng 21(1):23–61

Cardone D, Perrone, G (2017) Damage and loss assessment of pre-70 RC frame buildings with FEMA P-58. Journal of Earthquake Engineering, 21 (1), 23-61

Cardone D, Sullivan TJ, Gesualdi G, Perrone G (2017) Simplified estimation of the expected annual loss of reinforced concrete buildings, Earthquake Engineering & Structural Dynamics 46(12): 2009-2032

Cardone, D., Conte, N., Dall'Asta, A., Di Cesare, A., Flora, A., Lamarucciola, N., Micozzi, F., Ponzo, F., Ragni, L. 2019b. RINTC-e project: the seismic risk of existing italian rc buildings retrofitted with seismic isolation, in: Proceedings of the 7th International Conference on Computational Methods in Structural Dynamics and Earthquake Engineering (COMPDYN 2019), Crete, Greece, pp. 3403–3421. https://doi.org/10.7712/120119.7156.19921

Cardone, D., Flora, A., 2016. An alternative approach for the seismic rehabilitation of existing RC buildings using seismic isolation. Earthquake Engineering & Structural Dynamics 45, 91–111. https://doi.org/10.1002/eqe.2618

Cardone, D., Flora, A., Gesualdi, G., 2013. Inelastic response of RC frame buildings with seismic isolation. Earthquake Engineering & Structural Dynamics 42, 871–889. https://doi.org/10.1002/eqe.2250

Cardone, D., Gesualdi, G., Perrone, G. 2019c. Cost-Benefit Analysis of Alternative Retrofit Strategies for RC Frame Buildings, Journal of Earthquake Engineering, 23:2, 208-241, DOI: 10.1080/13632469.2017.1323041.

Cardone, D., Perrone, G., Piesco, V. 2019a. Developing collapse fragility curves for base-isolated buildings. Earthquake Engng Struct Dyn; 48: 78– 102. https://doi.org/10.1002/eqe.3126

CEN (2005) Eurocode 6: design of masonry structures–Part 1-1: General Rules for Reinforced and unreinforced masonry structures. European Committee for Standardization, Brussels (EC6 2005)

CEN. 2000. EN 1337-2. Structural bearings - Part 2: Sliding elements, Brussels, Belgium.

CEN-EN 2005. Design of structures for earthquake resistance, part 1, Eurocode 8, Brussels.

Circolare Esplicativa 21 gennaio 2019, n. 7 C.S.LL.PP. Istruzioni per l'applicazione dell'«Aggiornamento delle "Norme tecniche per le costruzioni"» di cui al decreto ministeriale 17 gennaio 2018, Rome (in italian)

Constantinou, M.C., Mokha, A., Reinhorn, A. 1990. Teflon bearings in base isolation. II: Modeling.Journal of Structural Engineering (ASCE) 1990; 116(2): 455-474)

Cornell, C.A., 1968. Engineering seismic risk analysis. Bulletin of the Seismological Society of America; 58 (5): 1583–1606. doi: https://doi.org/10.1785/BSSA0580051583

Crisafulli FJ, Carr AJ (2007) Proposed macro-model for the analysis of infilled frame structures. Bull N Z Soc Earthq Eng 40(2):69–77

Crisafulli, F. J., (1997). Seismic behaviour of reinforced concrete structures with masonry infills. Department of Civil Engineering, University of Canterbury, Christchurch, New Zealand.

CS.LL.PP. 2018. Aggiornamento delle norme tecniche per le costruzioni, Gazzetta Ufficiale della Repubblica Italiana 42. (In Italian.)

CS.LL.PP. 2019 Circolare n. 7 - Istruzioni per l'applicazione dell'Aggiornamento delle Norme tecniche per le costruzioni di cui al decreto ministeriale 17 gennaio 2018, Gazzetta Ufficiale della Repubblica Italiana 35. (In Italian.)

D.M. 14/2/1992. Decreto Ministeriale 14 febbraio 1992. Norme tecniche per le opere in c.a. normale e precompresso e per le strutture metalliche. Gazzetta Ufficiale n. 65 del 18 marzo 1992. (in Italian).

D.M. 24/1/1986. Decreto Ministeriale 24 gennaio 1986. Norme tecniche relative alle costruzioni antisismiche. Gazzetta Ufficiale n. 108 del 12 maggio 1986. (in Italian).

D.M. 30/5/1974. Decreto Ministeriale 30 maggio 1974. Norme tecniche per la esecuzione delle opere in cemento armato normale e precompresso e per le strutture metalliche. Gazzetta Ufficiale n. 198 del 29 luglio 1974. (in Italian).

Da Porto, F., Guidi, G., Dalla Benetta, M., & Verlato, N. (2013, June). Combined in-plane/out-of-plane experimental behaviour of reinforced and strengthened infill masonry walls. In *12th Canadian masonry symposium* (pp. 2-5).

Daniel P. Abrams, MEERI, Richard Angel, and Joseph Uzarski, MEERI Out-of-Plane Strength of Unreinforced Masonry Infill Panels, Earthquake Spectra, Volume 12, No. 4, November 1996

Dawe JL, Seah CK. (1989) Out-of-plane resistance of concrete masonry infilled panels. Can J Civ Eng16(6):854–64

De Luca F, Verderame GM, Gómez-Martínez F, Pérez-García A (2014) The structural role played by masonry infills on RC building performances after the 2011 Lorca, Spain, earthquake, Bulletin of Earthquake Engineering 12(5). 1999–2026

De Risi MT, Di Domenico M, Ricci P, Verderame GM, Manfredi F (2019) Experimental investigation on the influence of the aspect ratio on the inplane/out-of-plane interaction for masonry infills in RC frames, Engineering Structures 189, 523–540

De Risi, M.T., Ricci, P., Verderame, G.M. 2017. Modelling exterior unreinforced beam-column joints in seismic analysis of non-ductile RC frames. Earthquake Engineering & Structural Dynamics 46, 899–923. https://doi.org/10.1002/eqe.2835

Decanini L-, G.E. Fantin [1986]. Modelos simplificados de la mampostería incluidas en porticos. Características de rigidez y resistencia lateral en estado límite. Actas de las VI Jornadas Argentinas de Ingenieria Estructural, Buenos Aires, Argentina, October 1–3, 1986. (in Spanish)

Decanini L, Mollaioli F, Mura A, Saragoni R (2004) Seismic performance of masonry infilled R/C frames, Proc.13th WCEE, Paper 165, Vancouver, B.C., Canada, August 1-6

Decanini L., Liberatore L., Mollaioli F. [2014] "Strength and stiffness reduction factors for infilled frames with openings", Earthquake Engineering and Engineering Vibration, 13(3): 437-454, September, 2014.

Di Domenico M, Ricci P, Verderame GM (2017) Empirical unreinforced masonry infill macro-model accounting for in-plane/out-of-plane interaction. In: COMPDYN 2017 -6th international thematic conference, pp 1606–1624

Di Domenico M, Ricci P, Verderame GM [2021]. Floor spectra for bare and infilled reinforced concrete frames designed according to Eurocodes. Earthquake Engineering and Structural Dynamics 50(13), 3577-3601.

Di Domenico M., Ricci P., Verderame G.M. (2021). Empirical calibration of hysteretic parameters for modeling the seismic response of RC columns with plain bars, Engineering Structures, 237.

Di Trapani F, Shing PB, Cavaleri L (2018) Macroelement Model for In-Plane and Out-of-Plane Responses of Masonry Infills in Frame Structures, Journal of Structural Engineering, vol. 144, no. 2, p. 04017198, 2018

DM 03/03/1975. Approvazione delle norme tecniche per le costruzioni in zone sismiche. Gazzetta Ufficiale n. 93 del 8 aprile 1975. (In Italian).

DM 19/06/1984. Norme tecniche relative alle costruzioni sismiche. Gazzetta Ufficiale n. 208 del 30 luglio 1984. (in Italian).

DM 24/01/1986. Norme tecniche relative alle costruzioni antisismiche. Gazzetta Ufficiale n. 108 del 12 maggio 1986. (in Italian).

Dolšek M, Fajfar P (2008) The effect of masonry infills on the seismic response of a four-storey reinforced concrete frame—a deterministic assessment. Eng Struct 30:1991–2001

Donatello Cardone, Giuseppe Gesualdi & Giuseppe Perrone (2017): Cost-Benefit Analysis of Alternative Retrofit Strategies for RC Frame Buildings, Journal of Earthquake Engineering, DOI: 10.1080/13632469.2017.1323041

El-Dakhakhni, Wael W, Mohamed Elgaaly, Ahmad A Hamid (2003) Three-strut model for concrete masonry infilled steel frames. Journal of Structural Engineering 129.2 (2003): 177-185

EN15129 2009. Antiseismic Devices, European Committee for Standardization, Brussels, Belgium.

Fabbrocino G, Verderame GM, Manfredi G, Cosenza E (2004) Structural models of critical regions in old-type r.c. frames with smooth rebars, Engineering Structures 26, 2137–2148.

Fardis MN, Panagiotakos TB (1997) Seismic design and response of bare and masonry-infilled reinforced concrete buildings. Part II: infilled structures. J Earthq Eng 1:475–503

Federal Emergency Management Agency (1997) NEHRP commentary on the guidelines for the seismic rehabilitation of buildings. FEMA-274, Applied Technology Council, Washington, D.C.

Federal Emergency Management Agency (1998) Evaluation of Earthquake Damaged Concrete and Masonry Wall Buildings, Basic Procedures Manual. FEMA-306, Washington, D.C.

Federal Emergency Management Agency (2000) Prestandard and commentary for the seismic rehabilitation of buildings. FEMA-356, Applied Technology Council, Washington, D.C.

Flanagan RD, Bennett RM, (1999) Bidirectional Behavior of Structural Clay Tile Infilled Frames. Journal of structural engineering, 125(3), 236-244

Flora, A., Perrone, G., Cardone, D. 2020. Developing risk-target based design approaches for base isolated Buildings. Proceedings of the 17th World Conference on Earthquake Engineering, 17WCEE Sendai, Japan - September 13th to 18th 2020

Furtado A, Rodrigues H, Arêde A, Varum H (2015b) Simplified macro-model for infill masonry walls considering the out-of-plane behaviour. Earthq Eng Struct Dyn 45:507–524

Furtado A, Rodrigues H, Arêde A, Varum H (2016) Simplified macro-model for infill masonry walls considering the out-of-plane behaviour, Earthquake Engineering & Structural Dynamics 45, 507-524

Furtado A, Rodrigues H, Arêde H, Varum H (2015a) Influence of the in Plane and Out-of-Plane Masonry Infill Walls' Interaction in the Structural Response of RC Buildings, Procedia Engineering, vol. 114, pp. 722-729

Gesualdi, G., L. R. S. Viggiani, and D. Cardone. 2020. Seismic performance of RC frame buildings accounting for the out-of-plane behavior of masonry infills. Bulletin of Earthquake Engineering 18 (11): 5343–81. doi: 10.1007/s10518- 020-00904-1.

Grunthal, G. Cahiers du Centre Europeen de Geodynamique et de Seismologie: Volume 15—European Macroseismic Scale; European Center for Geodynamics and Seismology: Luxembourg, 1998.

Guidi G, da Porto F, Dalla Benetta M, Verlato N, Modena C (2013) Comportamento sperimentale nel piano e fuori piano di tamponamenti in muratura armata e rinforzata. Proceedings of the XV ANIDIS, L'Ingegneria Sismica in Italia, Padua, Italy, 2013, 30. (in Italian)

Hak S, Morandi P, Magenes G (2014) Out-of-plane experimental response of strong masonry infills. 2nd European Conference on Earthquake Engineering and Seismology

Hak, S., Morandi, P., and Magenes, G. (2017). Prediction of inter--storey drifts for regular RC structures with masonry infills based on bare frame modelling. Bulletin of Earthquake Engineering, 1--29.

Haselton C.B., Liel A.B., Taylor-Lange S., Deierlein G.G. (2008). Beam-column element model calibrated for predicting flexural response leading to global collapse of RC frame buildings, PEER Report No. 2007/03. Pacific Earthquake Engineering Research Center, University of California, Berkeley, CA, USA.

Hashemi A, Mosalam KM (2007) Seismic evaluation of reinforced concrete buildings including effects of masonry infill walls. Pacific Earthquake Engineering Research Center, University of California, Berkeley

Henderson RC, Porter ML, Jones WD, Burdette EG (2006) Influence of prior out-of-plane damage on the in-plane behavior of masonry infilled frames, TMS J., 24 (1), 71-82.

Hermanns, L., Fraile, A., Alarcón, E., & Álvarez, R. (2014). Performance of buildings with masonry infill walls during the 2011 Lorca earthquake. *Bulletin of Earthquake Engineering*, *12*(5), 1977-1997.

Holmes M (1961) Steel frames with brickwork and concrete infilling, Proceedings of the Institution of Civil Engineers 19, 473–478 (eISSN 1753-7789)

Holmes, M. Combined loading on infilled frames. Proc. Inst. Civ. Eng. 1963, 25, 31–38.

Ibarra LF, Medina RA, Krawinkler H (2005) Hysteretic models that incorporate strength and stiffness deterioration. Earthquake Engineering and Structural Dynamics 34: 1489–511

Ibarra, L.F., Krawinkler, H., 2005. Global Collapse of Frame Structures under Seismic Excitations. Rep. No. TB 152, The John A. Blume Earthquake Engineering Center.

Iervolino, I., Dolce, M. 2018. Foreword to the Special Issue for the RINTC (The Implicit Seismic Risk of Code-Conforming Structures) Project. Journal of Earthquake Engineering 1–4. https://doi.org/10.1080/13632469.2018.1543697

Iervolino, I., Spillatura, A., Bazzurro, P. 2018. Seismic Reliability of Code-Conforming Italian Buildings. Journal of Earthquake Engineering 22, 5–27. https://doi.org/10.1080/13632469.2018.1540372

INSYSME (2016). Innovative systems for earthquake resistant masonry in reinforced concrete buildings, http://www.insysme.eu.

Ishii, K., Kikuchi, M. 2019. Improved numerical analysis for ultimate behavior of elastomeric seismic isolation bearings. Earthquake Engng Struct Dyn 48, 65–77. https://doi.org/10.1002/eqe.3123

ISTAT (2011) Censimento delle Popolazione e delle Abitazioni, 2011. http://dati-censimento popolazione, istat.it/#. Accessed 2 Dec 2015

Jalayer, F. 2003. Direct Probabilistic seismic analysis: implementing nonlinear dynamic assessment, Ph.D. thesis, Department of Civil and Environmental Engineering, Stanford University, Stanford,CA, USA.

Jangid, R.S., 2005. Computational numerical models for seismic response of structures isolated by sliding systems, Structural Control and Health Monitoring, Vol. 12(1), pp. 117-137, 2005

Kadysiewski S, Mosalam KM (2009) Modeling of unreinforced masonry infill walls considering in-plane and out-of-plane interaction. Pacific Earthquake Engineering Research Center, University of California, Berkeley

Kikuchi, M., Nakamura, T., Aiken, I.D. 2010. Three-dimensional analysis for square seismic isolation bearings under large shear deformations and high axial loads. Earthquake Engng. Struct. Dyn. 39, 1513–1531. https://doi.org/10.1002/eqe.1042

Lam NTK, Griffith M, Wilson J, Doherty K (2003) Time–history analysis of URM walls in out-of-plane flexure. Eng Struct 25:743–754

Lanzano, G., Luzi, L., Pacor, F., Felicetta, C., Puglia, R., Sgobba, S., D'Amico, M., 2019. A Revised Ground-Motion Prediction Model for Shallow Crustal Earthquakes in Italy. Bulletin of the Seismological Society of America 109, 525–540. https://doi.org/10.1785/0120180210

Lin, T., Haselton, C.B., Baker, J.W. 2013. Conditional spectrum-based ground motion selection. Part I: Hazard consistency for risk-based assessments. Earthquake Engineering & Structural Dynamics 42, 1847–1865. https://doi.org/10.1002/eqe.2301.

Longo F, Wiebe L, da Porto F, Modena C (2018) Application of an in-plane/out-of-plane interaction model for URM infill walls to dynamic seismic analysis of RC frame buildings. Bulletin of Earthquake Engineering (2018) 16:6163–619.

M. Di Domenico, M.T. De Risi, V. Manfredi, M. Terrenzi, G. Camata, F. Mollaioli, F. Noto, P. Ricci, P. Franchin, A. Masi, E. Spacone & G.M. Verderame (2022) Modelling and Seismic Response Analysis of Italian Pre-Code and Low-Code Reinforced Concrete Buildings. Part II: Infilled Frames, Journal of Earthquake Engineering, DOI: 10.1080/13632469.2022.2086189

Mainstone RJ (1971) On the stiffness and strength of infilled frames, Proc. Instn. Civ. Engrs., supplement IV, 57–90 (paper 7360S).

Maria Teresa De Risi, André Furtado, Hugo Rodrigues, José Melo, Gerardo Mario Verderame, Arêde António, Humberto Varum, Gaetano Manfredi,Experimental analysis of strengthening solutions for the out-of-plane collapse of masonry infills in RC structures through textile reinforced mortars, Engineering Structures, Volume 207,2020,110203,ISSN 0141-0296,https://doi.org/10.1016/j.engstruct.2020.110203.

Maria Teresa De Risi, André Furtado, Hugo Rodrigues, José Melo, Gerardo Mario Verderame, Arêde António, Humberto Varum, Gaetano Manfredi, Experimental analysis of strengthening solutions for the out-of-plane collapse of masonry infills in RC structures through textile reinforced mortars, Engineering Structures, Volume 207, 2020, 110203, ISSN 0141-0296, https://doi.org/10.1016/j.engstruct.2020.110203.

Maria Teresa De Risi, Carlo Del Gaudio, Gerardo Mario Verderame (2019) Evaluation of Repair Costs for Masonry Infills in RC Buildings from Observed Damage Data: the Case-Study of the 2009 L'Aquila Earthquake, Buildings 2019, *9*(5), 122; https://doi.org/10.3390/buildings9050122

Maria Teresa De Risi, Mariano Di Domenico, Vincenzo Manfredi, Marco Terrenzi, Guido Camata, Fabrizio Mollaioli, Fabrizio Noto, Paolo Ricci, Paolo Franchin, Angelo Masi, Enrico Spacone & Gerardo M. Verderame (2022) Modelling and Seismic Response Analysis of Italian pre-code and low-code Reinforced Concrete Buildings. Part I: Bare Frames, Journal of Earthquake Engineering, DOI: 10.1080/13632469.2022.2074919

Marinković, M. (2018). Innovative system for seismic resistant masonry infills in reinforced concrete frame structures. PhD Doctoral Dissertation. University of Belgrade.

Marinković, M., & Butenweg, C. (2019). Innovative decoupling system for the seismic protection of masonry infill walls in reinforced concrete frames. *Engineering Structures*, *197*, 109435.

Marinković, M., & Butenweg, C. (2022). Numerical analysis of the in-plane behaviour of decoupled masonry infilled RC frames. *Engineering Structures*, *272*, 114959.Mays, G.C., Hetherington, J.G., and Rose, T.A. [1998]. Resistance-deflection functions for concrete wall panels with openings. Journal of Structural Engineering, 124(5): 579-587.

Marinković, Marko, Markel Baballëku, Brisid Isufi, Nikola Blagojević, Ivan Milićević, and Svetla"a Brzev. "Performance of RC cast-in-place buildings during the November 26, 2019 Albania e"rthquake." *Bulletin of Earthquake Engineering* (2022): 1-54.

Masi A, Chiauzzi L, Santarsiero G, Manfredi V, Biondi S, Spacone E, Del Gaudio C, Ricci P, Manfredi G, Verderame GM (2019) Seismic response of RC buildings during the Mw 6.0

August 24, 2016 Central Italy earthquake: the Amatrice case study, Bulletin of Earthquake Engineering, journal article vol. 17, no. 10, pp. 5631-5654, October 01 2019

Masi A, Digrisolo A, Manfredi V (2015) Fragility curves of gravity-load designed RC buildings with regularity in plan, Earthquakes and Structures, Vol. 9, No. 1, 1-27

Matsangar, V.A., Jangid R.S., 2008. Base Isolation for Seismic Retrofitting of Structures. Practice Periodical on Structural Design and Construction, Vol. 13, Issue 4 (November 2008). https://doi.org/ 10.1061/(ASCE)1084-0680(2008)13:4(175).

Mazza, F. In-plane–out-of-plane non-linear model of masonry infills in the seismic analysis of r.c.-framed buildings. Earthquake Engng Struct Dyn. 2019; 48: 432– 453. https://doi.org/10.1002/eqe.3143

McDowell EL, McKee KE, Sevin E (1956) Arching action theory of masonry walls. J. Struct. Div 82.2:915

McKenna F, Fenves GL, Scott MH (2000) Open system for earthquake engineering simulation. University of California, Berkeley, CA

McKenna, F. 2011. OpenSees: A Framework for Earthquake Engineering Simulation. Computing in Science Engineering 13, 58–66. https://doi.org/10.1109/MCSE.2011.66

Mehrabi AB, Shing PB (1997) Finite element modeling of masonry-infilled RC frames, J. Struct. Engrg., 123, 604-613.

Micozzi F., Flora A., Viggiani L.R.S., Cardone D., Ragni L., Dall'Asta A. 2021 Risk Assessment of Reinforced Concrete Buildings with Rubber Isolation Systems Designed by the Italian Seismic Code, Journal of Earthquake Engineering, DOI: 10.1080/13632469.2021.1961937

Micozzi, F. 2020. Seismic reliability of buildings isolated with rubber bearings. Ph.D. Dissertation,University of Camerino, Italy. http://hdl.handle.net/11581/446064

Milanesi, R. R., Morandi, P. and Magenes, G. (2018). Local effects on RC frames in-duced by AAC masonry infills through FEM simulation of in-plane tests. Bulletin of Earthquake Engineering, 1-28.

Monzon, E.V., Buckle, I.G., Itani, A.M. 2016. Seismic Performance and Response of Seismically Isolated Curved Steel I-Girder Bridge. J. Struct. Eng. 142, 04016121. https://doi.org/10.1061/(ASCE)ST.1943-541X.0001594

Morandi P, Magenes G, Hak S (2013) Simplified Out-of-plane Resistance Verification for Slender Clay Masonry Infills in RC Frames, XV Convegno ANIDIS - L'ingegneria Sismica in Italia

Morandi P, Milanesi RR, Magenes G. (2018) Innovative solution for seismic-resistant masonry infills with sliding joints: in-plane experimental performance. Eng Struct 2018;176:719–33

Mosalam KM, Günay S, (2015) Progressive collapse analysis of RC frames with URM infill walls considering in-plane/out-of-plane interaction. Earthquake Spectra 31(2): 921-943

Mullins L. 1969. Softening of rubber by deformation, Rubber Chemistry and Technology, 42(1): 339-362.

Nakazawa, T., Kishiki, S., Qu, Z., Miyoshi, A., Wada, A., 2011. Fundamental study on probabilistic evaluation of the ultimate state of base isolated structures. Nihon Kenchiku Gakkai Kozokei Ronbunshu 76, 745–754. https://doi.org/10.3130/aijs.76.745

Nishi, T., Suzuki, S., Aoki, M., Sawada, T., Fukuda, S. 2019. International investigation of shear displacement capacity of various elastomeric seismic-protection isolators for buildings. J Rubber Res 22, 33–41. https://doi.org/10.1007/s42464-019-00006-x

Noh N.M, Liberatore L., Mollaioli F, Solomon Tesfamariam S. (2017); "Modelling of masonry infilled RC frames subjected to cyclic loads: State of the art review and modelling with OpenSees"

NTC2018 (2008) D.M. 17.01.2018. Aggiornamento delle Norme Tecniche per le Costruzioni, Rome (in italian)

NZSEE (2006) Assessment and improvement of the structural performance of buildings in earthquake. Recommendations of a NZSEE Study Group, New Zealand Society for Earthquake Engineering, Wellington, New Zealand.

NZSEE (2017), Structural Engineering Society New Zealand Inc. (SESOC), New Zealand Geotechnical Society Inc., Ministry of Business, Innovation and Employment, Earthquake Commission. The Seismic Assessment of Existing Buildings (the Guidelines), Part C – Detailed Seismic Assessment, (NZSEE-2017). http://www.eq-assess.org.nz/

Ozkaynak H, Yuksel E, Yalcin C et al (2013) Masonry infill walls in reinforced concrete frames as a source of structural damping. Earthq Eng Struct Dyn 43:949–968

Panagiotakos TB, Fardis MN (1996) Seismic response of infilled RC frames structures Proc.XXI World Conf. of Earthquake Engineering, Acapulco, Mexico

Pasca M, Liberatore L (2015) Predicting models for the evaluation of out-of-plane ultimate load carrying capacity of masonry infill walls, WIT Transactions on the Built Environment, 152, 83-94

Pavese, A.; Furinghetti, M.; Casarotti, C. 2018. Experimental assessment of the cycle response of friction-based isolators under bidirectional motions. Soil Dyn. Earthq. Eng. 114, 1–11.

Pereira MFP, Pereira MFN, Ferreira JED, Lourenço PB (2011) Behavior of masonry infill panels in RC frames subjected to in plane and out of plane loads. In: 7th international conference on AMCM2011, Kraków, Poland

Perrone G, Cardone D, O'Reilly GJ, Sullivan TJ (2019) Developing a Direct Approach for Estimating Expected Annual Losses of Italian Buildings, Journal of Earthquake Engineering DOI: 10.1080/13632469.2019.1657988

Perrone, D., Calvi, P. M., Nascimbene, R., Fischer, E. C., & Magliulo, G. (2019). Seismic performance of non-structural elements during the 2016 Central Italy earthquake. *Bulletin of Earthquake Engineering*, *17*(10), 5655-5677.

Polyakov SV (1960) On the interaction between masonry filler walls and enclosing frame when loaded in the plane of the wall, Translations in Earthquake Engineering. EERI, San Francisco, 36–42

Ponzo, F.C.; Di Cesare, A.; Telesca, A.; Nigro, D.; Castellano, M.G.; Infanti, S. 2020. Influence of DCCSS Bearings Over-Stroke and breakaway on the seismic response of isolated buildings. Proc. of 17th World Conference on Earthquake Engineering, Sendai, Japan.

Ponzo, F.C.; Di Cesare, A.; Telesca, A.; Pavese, A.; Furinghetti, M. 2021. Advanced Modelling and Risk Analysis of RC Buildings with Sliding Isolation Systems Designed by the Italian Seismic Code. Appl. Sci. 11, 1938. https://doi.org/10.3390/app11041938

Preti M, Bolis V. Masonry infill construction and retrofit technique for the infill-frame interaction mitigation: test results. Eng Struct 2017; 132:597–608.

Priestley MJ (1985), Seismic behaviour of unreinforced masonry walls, Bull. New Zeal. Natl. Soc. Earthq. Eng. 18

Ragni, L., Cardone, D., Conte, N., Dall'Asta, A., Cesare, A.D., Flora, A., Leccese, G., Micozzi, F., Ponzo, C. 2018a. Modelling and Seismic Response Analysis of Italian Code-Conforming Base-Isolated Buildings. Journal of Earthquake Engineering, 1–33. Vol. 22(sup2), 2018, 198-230 https://doi.org/10.1080/13632469.2018.1527263

Ragni, L., Tubaldi, E., Dall'Asta, A., Ahmadi, H., Muhr, A. 2018b. Biaxial shear behaviour of HDNR with Mullins effect and deformation-induced anisotropy. Engineering Structures 154, 78–92. https://doi.org/10.1016/j.engstruct.2017.10.060

ReLUIS-RINTC Workgroup 2018. Results of the 2015-2017 RINTC project. ReLUIS-RINTC report, ReLUIS, Naples, Italy. Available at http://www.reluis.it.

Ricci P, De Luca F, Verderame G (2011) 6th April 2009 L'Aquila earthquake, Italy: reinforced concrete building performance, Bulletin of Earthquake Engineering, vol. 9, no. 1, pp. 285-305

Ricci P, Di Domenico M, Verderame GM (2018a) Experimental assessment of the in-plane/out-of-plane interaction in unreinforced masonry infill walls. Eng Struct. 173:960–978

Ricci P, Di Domenico M, Verderame GM (2018b) Experimental investigation of the influence of slenderness ratio and of the in-plane/out-of-plane interaction on the out-of-plane strength of URM infill walls, Construction and Building Materials 191:505-522. doi: 10.1016/j.conbuildmat.2018.10.011.

Ricci P, Di Domenico M, Verderame GM [2018c]. Empirical-based out-of-plane URM infill wall model accounting for the interaction with in-plane demand. Earthquake Engineering and Structural Dynamics, 47.3:802-827.

Ricci P, Di Domenico M, Verderame GM, 2022. Effects of the in-plane/out-of-plane interaction in URM infills on the seismic performance of RC buildings designed to Eurocodes. Journal of Earthquake Engineering.

Ricci P., Manfredi V., Noto F., Terrenzi M., Petrone C., Celano F., De Risi M.T., Camata G., Franchin., Magliulo G., Masi A., Mollaioli F., Spacone E., Verderame G.M., [2018a] "Modeling and Seismic Response Analysis of Italian Code-Conforming Reinforced Concrete Buildings", Journal of Earthquake Engineering, 22 (NO.S2), 105–139, 2018a (doi: 10.1080/13632469.2018.1527733).

Ricci P., Verderame G. M. and Manfredi G. (2011). Analytical Investigation of Elastic Period of Infilled RC MRF "Buildings," Engineering Structures, vol. 33, pp. 308-319.

Ricci, P., Manfredi, V., Noto, F., Terrenzi, M., De Risi, M.T., Di Domenico, M., Camata, G., Franchin, P., Masi, A., Mollaioli, F., Spacone, E., Verderame, G.M. 2019. RINTC-e: towards seismic risk assessment of existing residential reinforced concrete buildings in italy, in: Proceedings of the 7th International Conference on Computational Methods in Structural Dynamics and Earthquake Engineering (COMPDYN 2019), Crete, Greece, pp. 554–576. https://doi.org/10.7712/120119.6939.20040

Ricci, P., Manfredi, V., Noto, F., Terrenzi, M., Petrone, C., Celano, F., De Risi, M.T., Camata, G., Franchin, P., Magliulo, G., Masi, A., Mollaioli, F., Spacone, E., Verderame, G.M. 2018. Modeling and Seismic Response Analysis of Italian Code-Conforming Reinforced Concrete Buildings. Journal of Earthquake Engineering 22, 105–139. https://doi.org/10.1080/13632469.2018.1527733

Rossetto T, Elnashai A (2003) Derivation of vulnerability functions for European-type RC structures based on observational data. Eng Struct.; 25(10):1241-1263

S. Hak , P. Morandi , G. Magenes & T. J. Sullivan (2012) Damage Control for Clay Masonry Infills in the Design of RC Frame Structures, Journal of Earthquake Engineering, 16:sup1, 1-35, DOI: 10.1080/13632469.2012.670575

Sassun K, Sullivan TJ, Morandi P, Cardone D (2016) Characterising the in-plane seismic performance of infill masonry. Bulletin of the New Zealand Society for Earthquake Engineering, 49(1),100-117

Sezen H, Moehle JP (2004) Shear Strength Model for Lightly Reinforced Concrete Columns, Journal of Structural Engineering, 130(11): 1692-1703

Silva L, Vasconcelos G, Lourenço P, Akhoundi F. Experimental evaluation of a constructive system for earthquake resisting masonry enclosure walls. In Proceedings of the 16th International Brick and Block Masonry Conference (IBMAC 2016), 2016, Padova, Italy.

Smyrou E, C. Blandon, S. Antoniou, R. Pinho, F. Crisafulli (2011) Implementation and verifcation of a masonry panel model for nonlinear dynamic analysis of inflled RC frames. Bull Earthq Eng 9(5):1519–1534.

Spillatura A (2017) From Record Selection to Risk Targeted Spectra for Risk based Assessment and Design (Thesis), IUSS Pavia, Italy

Stafford-Smith B (1962) Lateral stiffness of infilled frames, J. Struct.Div., 88 (6), 183–199

Stafford-Smith, B. Behavior of square infilled frames. ASCE J. Struct. Div. 1966, 92, 381–403.

Taghavi S, Miranda E (2002) Seismic performance and loss assesment of nonstructural building components, in: Proceeding 7th Natl. Conf. Earthq. Eng., 2002: pp. 21–25

Takaoka, E., Takenaka, Y., Nimura, A. 2011. Shaking table test and analysis method on ultimate behavior of slender base-isolated structure supported by laminated rubber bearings. Earthquake Engng. Struct. Dyn. 40, 551–570. https://doi.org/10.1002/eqe.1048

Tasligedik, A. S. (2014). Damage mitigation strategies for non-structural infill walls. PhD thesis. Civil and Natural Resources Engineering Department. University of Can-terbury, Christhurch/New Zealand, pp. 304.

Tubaldi, E., Ragni, L., Dall'Asta, A., Ahmadi, H., Muhr, A. 2017. Stress softening behaviour of HDNR bearings: modelling and influence on the seismic response of isolated structures: Stress Softening Behaviour of HDNR Bearings. Earthquake Engineering & Structural Dynamics. https://doi.org/10.1002/eqe.2897

Valluzzi, M. R., Da Porto, F., Garbin, E., & Panizza, M. (2014). Out-of-plane behaviour of infill masonry panels strengthened with composite materials. *Materials and structures*, *47*(12), 2131-2145.

Vamvatsikos D (2014) Accurate application and second-order improvement of SAC/FEMA probabilistic formats forseismic performance assessment. ASCE Journal of Structural Engineering,140(2), 04013058. DOI: 10.1061/(ASCE)ST.1943-541X.0000774.

Varum H, Dumaru R, Furtado A, Barbosa AR, Gautam D, Rodrigues H (2018) Chapter 3 - Seismic Performance of Buildings in Nepal After the Gorkha Earthquake, in Impacts and Insights of the Gorkha Earthquake, D. Gautam and H. Rodrigues, Eds.: Elsevier pp. 47-63

Verderame GM, Manfredi G, Frunzio G (2001a) The mechanical properties of the steels used in reinforced concrete structures built in the 1960s. X Congresso Nazionale ANIDIS, 2001, Italy (in Italian)

Verderame GM, Manfredi G, Frunzio G (2001b) The mechanical properties of the concrete used in reinforced concrete structures built in the 1960s. X Congresso Nazionale ANIDIS, Italy (in Italian)

Verlato N, Guidi G, da Porto F, Modena C. Innovative systems for masonry infill walls based on the use of deformable joints: combined in-plane/out-of-plane tests. In Proceedings of the 16th International Brick and Block Masonry Conference, 2016, Padova, Italy.

Vicente RS, Rodrigues H, Varum H, Costa A, Mendes da Silva JAR (2012) Performance of masonry enclosure walls: lessons learned from recent earthquakes. Earthq Eng Eng Vib 11(1):23–34

Wada A, Hirose K. 1987. Building frames subjected to 2D earthquake motion. Proceedings, Structures Congress ’89, ASCE, San Francisco, CA, 388–397.

Warn, G. P. 2006. The coupled horizontal-vertical response of elastomeric and lead rubber seismic isolation bearings. Ph.D. Dissertation. Buffalo: The State University of New York at Buffalo.